Steel space frames built by tubular elements with thin-wall circular cross-section are regularly employed in engineering practice. The aim of the research is to formulate and develop an algorithm for layout and connections optimization of steel tubular space frames subject to multiple load cases and displacement, minimum element length and stress constraints, in order to provide minimization of manufacturing costs related to material and connections. The manufacturing objective function has connections cost proportional to the material cost, as a quadratic variation between the costs of pinned and fully rigid connections. The finite element formulation is developed by the direct approach, assuming a linear model of connections with two rotational springs at each end acting on the bending planes. Considering the theory of von Mises, a failure criterion is proposed specifically for the previously defined cross-sectional type, forming an expression that accounts for the effect of shear forces and allows the determination of the most critical point in cross-sections of elements with variable length. As the numerical optimization is performed by a gradient-based method, the analytical sensitivity analysis is performed, being validated by central finite differences. Despite the high number of design variables, the proposed optimization problem is able to find optimal solutions that simultaneously account for the lowest manufacturing cost, based on the best cost-benefit between material and connections cost, providing the necessary mechanical strength and complying with local stiffness demands.

Advisor: Pablo Andrés Muñoz-Rojas

Joinville, 2019

YEAR
2019

FELIPE AUGUSTO CARVALHO DE FARIA | LAYOUT AND CONNECTIONS OPTIMIZATION OF STEEL TUBULAR SPACE FRAMES CONSIDERING MANUFACTURING COSTS

UDESC

SANTA CATARINA STATE UNIVERSITY – UDESC
COLLEGE OF TECHNOLOGICAL SCIENCE – CCT
MECHANICAL ENGINEERING GRADUATE PROGRAM

MASTER THESIS

LAYOUT AND CONNECTIONS OPTIMIZATION OF STEEL TUBULAR SPACE FRAMES CONSIDERING MANUFACTURING COSTS

FELIPE AUGUSTO CARVALHO DE FARIA

JOINVILLE, 2019

FELIPE AUGUSTO CARVALHO DE FARIA

LAYOUT AND CONNECTIONS OPTIMIZATION OF STEEL TUBULAR SPACE FRAMES CONSIDERING MANUFACTURING COSTS

Master thesis submitted to the Mechanical Engineering Department at the College of Technological Science of Santa Catarina State University in fulfillment of the partial requirement for the Master's degree in Mechanical Engineering.

Advisor: Dr. Pablo Andrés Muñoz-Rojas

JOINVILLE - SC

2019

Ficha catalográfica elaborada pelo programa de geração automática da
Biblioteca Setorial do CCT/UDESC,
com os dados fornecidos pelo(a) autor(a)

Faria, Felipe Augusto Carvalho de
Layout and Connections Optimization of Steel Tubular Space Frames Considering Manufacturing Costs / Felipe Augusto Carvalho de Faria. -- 2019.
187 p.

Orientador: Pablo Andrés Muñoz-Rojas
Dissertação (mestrado) -- Universidade do Estado de Santa Catarina, Centro de Ciências Tecnológicas, Programa de Pós-Graduação em Engenharia Mecânica, Joinville, 2019.

1. Optimization. 2. Steel space frames. 3. Manufacturing costs. 4. Linear model of connections. 5. Failure criterion. I. Muñoz-Rojas, Pablo Andrés. II. Universidade do Estado de Santa Catarina, Centro de Ciências Tecnológicas, Programa de Pós-Graduação em Engenharia Mecânica. III. Título.

Layout and Connections Optimization of Steel Tubular Space Frames Considering Manufacturing Costs

por

Felipe Augusto Carvalho de Faria

Esta dissertação foi julgada adequada para obtenção do título de

MESTRE EM ENGENHARIA MECÂNICA

Área de concentração em "Modelagem e Simulação Numérica"
e aprovada em sua forma final pelo

CURSO DE MESTRADO ACADÊMICO EM ENGENHARIA MECÂNICA
DO CENTRO DE CIÊNCIAS TECNOLÓGICAS DA
UNIVERSIDADE DO ESTADO DE SANTA CATARINA.

Banca Examinadora:

Prof. Dr. Pablo Andrés Muñoz-Rojas
CCT/UDESC (Orientador/Presidente)

Prof. Dr. Eduardo Lenz Cardoso
CCT/UDESC

VÍDEO CONFERÊNCIA

Prof. Dr. Thiago André Carniel
UNOCHAPECÓ

Joinville,SC, 25 de setembro de 2019.

ACKNOWLEDGMENTS

The author would like to express the following acknowledgments.

To my advisor Prof. Dr. Pablo Andrés Muñoz-Rojas for the continuous support given during the development of this research work, always available to share his immense knowledge about the research area.

To the professors Dr. Eduardo Lenz Cardoso and Dr. Ricardo de Medeiros for contributing to my academic formation, with helpful classes and technical support whenever needed.

To my father Gustavo, my mother Giovanna and my sister Ana Beatriz, for the support, patience, education, advices and love, always believing in my competence and encouraging me for never give up on my dreams. You are my essence and together we will always be the best.

To Gessica for the unconditional love, patience and support, always by my side providing me emotional health to face and overcome my personal challenges. None of this would have been possible without your presence.

To all the colleagues of the “Laboratório de Mecânica Computacional” (LAMEC), without exception, who helped me a lot at the beginning of the journey and are also responsible for my progress due to all the discussions, sharing of ideas, knowledge, experiences and the friendship.

Finally, to Santa Catarina State University (UDESC), “Fundação de Amparo à Pesquisa e Inovação do Estado de Santa Catarina” (FAPESC 2019TR000779) and “Programa de Bolsas de Monitoria de Pós-Graduação” (PROMOP) for the high quality education provided and the financial support.

"On a given day, a given circumstance, you think you have a limit. And you then go for this limit and you touch this limit, and you think, 'Okay, this is the limit.' As soon as you touch this limit, something happens and you suddenly can go a little bit further. With your mind power, your determination, your instinct, and the experience as well, you can fly very high."

Ayrton Senna

ABSTRACT

Steel space frames built by tubular elements with thin-wall circular cross-section are regularly employed in engineering practice. The aim of the research is to formulate and develop an algorithm for layout and connections optimization of steel tubular space frames subject to multiple load cases and displacement, minimum element length and stress constraints, in order to provide minimization of manufacturing costs related to material and connections. The manufacturing objective function has connections cost proportional to the material cost, as a quadratic variation between the costs of pinned and fully rigid connections. The finite element formulation is developed by the direct approach, assuming a linear model of connections with two rotational springs at each end acting on the bending planes. Considering the theory of von Mises, a failure criterion is proposed specifically for the previously defined cross-sectional type, forming an expression that accounts for the effect of shear forces and allows the determination of the most critical point in cross-sections of elements with variable length. As the numerical optimization is performed by a gradient-based method, the analytical sensitivity analysis is performed, being validated by central finite differences. Despite the high number of design variables, the proposed optimization problem is able to find optimal solutions that simultaneously account for the lowest manufacturing cost, based on the best cost-benefit between material and connections cost, providing the necessary mechanical strength and complying with local stiffness demands.

Key-words: Optimization, steel space frames, manufacturing costs, linear model of connections, failure criterion, gradient-based method.

RESUMO

Pórticos espaciais de aço construídos por elementos tubulares com seção transversal circular de parede fina são estruturas regularmente empregadas na prática de engenharia. O objetivo de pesquisa é formular e desenvolver um algoritmo para otimizar layout e conexões de pórticos espaciais de aço sujeitos à múltiplos casos de carregamento e restrições de deslocamento, comprimento mínimo de elemento e tensão, visando possibilitar a minimização de custos de manufatura relativos aos custos de material e conexões. A função objetivo de manufatura possui custo de conexões proporcional ao custo de material, baseado em variação quadrática entre os custos de conexão rotulada e conexão totalmente rígida. A formulação do elemento finito é desenvolvida pelo método direto, assumindo um modelo linear para as conexões com duas molas rotacionais em cada extremidade, atuantes nos planos de flexão. Considerando a teoria de von Mises, um critério de falha é desenvolvido especificamente para o tipo de seção transversal previamente definido, contabilizando o efeito dos esforços cortantes e possibilitando a determinação do ponto mais crítico em seções de elementos com comprimento variável. Como a otimização é realizada por um método baseado em gradientes, a análise de sensibilidade analítica é desenvolvida, sendo validada por diferenças finitas centrais. Apesar da quantidade elevada de variáveis de projeto, o problema de otimização proposto possibilita o encontro de soluções ótimas capazes de simultaneamente agregar o menor custo de manufatura baseado no melhor custo-benefício entre custos de material e conexões, fornecendo a resistência mecânica necessária e suprindo demandas locais de rigidez.

Palavras-chave: Otimização, pórticos espaciais de aço, custos de manufatura, modelo linear de conexões, critério de falha, método baseado em gradientes.

List of Figures

List of Tables

List of Abbreviations

LP	Linear programming
FEM	Finite element method
GSM	Ground structure method
SLP	Sequential linear programming
SQP	Sequential quadratic programming
FEA	Finite element analysis
DOF	Degree of freedom
AISC	American Institute of Steel Construction
GC	Global connector
LO	Layout optimization
SCO	Sizing and connections optimization
LCO	Layout and connections optimization
LU	Matrix decomposition
CFD	Central finite difference
IMSL	Numerical library
DDLPRS	Fortran subroutine to solve LP problems available on the IMSL Numerical Library
NLPQLP	Fortran subroutine for the SQP method developed and provided by Schittkowski (2001)

List of Symbols

a	Generic term of the element stiffness matrix
A	Cross-section area
$\bar{A}'$	Cross-section area above the z'-axis (arc)
AC	Percentage of additional cost of connections
AC_p	Percentage of additional cost of a pinned connection
AC_r	Percentage of additional cost of a fully rigid connection
b	Generic term of the element stiffness matrix
B	Generic term for any function of the optimization problem
c	Index of rotational springs in a given element
$\bar{c}$	Perpendicular distance of M_R to the angular position θ
C_1 and C_2	Unknown variables of the elastic line $v(\tilde{x})$
c_M	Cost per material
c_S	Cost per connection
d	Index for displacement constraints
d'	Index for the expressions f_c
E	Young's modulus
EI	Beam stiffness
$\boldsymbol{F}$	Load vector
F_1, F_2, F_3, F_4 and F_5	Different types of loads
$f(\theta)$	von Mises stress calculation
f_c	Expressions as a function of the fixity factors of the element stiffness matrix
G	Shear modulus
GJ	Beam torsional stiffness
i	Index for elements
$iter$	Total number of iterations
I	Inertia moment
I_y	Inertia moment around $\tilde{y}$-axis
I_z	Inertia moment around $\tilde{z}$-axis

j	Index for design variables
J	Polar moment of inertia
k	Index of cross-sections along the element length
$k_{a,b}$	Generic term of the element stiffness matrix
$\mathbf{K}$	Global stiffness matrix
$\mathbf{K_{bo}}$	Global stiffness matrix of fully rigid 3D frame elements
$\mathbf{K_G}$	Global stiffness matrix of the element
$\mathbf{K_L}$	Local stiffness matrix of the element
$\mathbf{K_s}$	Overall contribution of the rotational stiffness of all joints
K_R	Rotational stiffness
K_{r_y}	Rotational stiffness of the rotational spring in $\tilde{x}\tilde{z}$-plane
K_{r_z}	Rotational stiffness of the rotational spring in $\tilde{x}\tilde{y}$-plane
LC	Index related to the number of load cases
l_m	Negligible length of rotational springs
L	Element length
L_{cr}	Critical length
L_L	Lower bound for constrained element lengths
$l_{o\tilde{x}}$, $m_{o\tilde{x}}$ and $n_{o\tilde{x}}$	Direction cosines of the local $\tilde{x}$-axis
$l_{o\tilde{y}}$, $m_{o\tilde{y}}$ and $n_{o\tilde{y}}$	Direction cosines of the local $\tilde{y}$-axis
$l_{o\tilde{z}}$, $m_{o\tilde{z}}$ and $n_{o\tilde{z}}$	Direction cosines of the local $\tilde{z}$-axis
m	Index for elements connected to a same node
$M(\tilde{x})$	Generic term for the distribution of internal bending moment along the element length
$M_{oy}(\tilde{x})$	Distribution of internal bending moment M_y along the element length
$M_{oz}(\tilde{x})$	Distribution of internal bending moment M_z along the element length
M_{2y}	Term of the sum of the bending moments around node 2 in $\tilde{x}\tilde{z}$-plane
M_{2z}	Term of the sum of the bending moments around node 2 in $\tilde{x}\tilde{y}$-plane
M_x	Torsion
$M_{x_{alw}}$	Allowable value of torsion
M_y	Bending moment in $\tilde{x}\tilde{z}$-plane
M_{y_1}	Bending moment in $\tilde{x}\tilde{z}$-plane of node 1
M_{y_2}	Bending moment in $\tilde{x}\tilde{z}$-plane of node 2

$M_{y_{alw}}$	Allowable value of bending moment in $\tilde{x}\tilde{z}$-plane
M_z	Bending moment in $\tilde{x}\tilde{y}$-plane
M_{z_1}	Bending moment in $\tilde{x}\tilde{y}$-plane of node 1
M_{z_2}	Bending moment in $\tilde{x}\tilde{y}$-plane of node 2
$M_{z_{alw}}$	Allowable value of bending moment in $\tilde{x}\tilde{y}$-plane
M_R	Resulting bending moment
n	Index for iterations
ndv	Total number of design variables
nec	Total number of elements that have a given nodal coordinate
nel	Total number of elements
$\mathbf{N}$	Matrix of interpolation functions
$N^{v_{xoz}}$	Interpolation functions in $\tilde{x}\tilde{z}$-plane (four terms)
$N^{v_{xoy}}$	Interpolation functions in $\tilde{x}\tilde{y}$-plane (four terms)
N^{b_x}	Interpolation functions of translation in $\tilde{x}$-axis (two terms)
N^{t_x}	Interpolation functions of rotation in $\tilde{y}\tilde{z}$-plane (two terms)
N_x	Axial force
$N_{x_{alw}}$	Allowable value of axial force
o	Generic term of the element stiffness matrix
$\boldsymbol{P}$	Vector of expression that represent any load distribution
$\boldsymbol{p_E}$	Vector of consistent nodal loads in the local reference system
$\boldsymbol{p_{EG}}$	Vector of consistent nodal loads in the global reference system
pe	Perturbation factor of the CFD
Q	Static moment
R	Outer radius
R_m	Midline radius
t	Thin-wall thickness
$\mathbf{T}$	Transformation matrix
u	Translation in x-axis
u_1	Translation in $\tilde{x}$-axis of node 1
u_2	Translation in $\tilde{x}$-axis of node 2
$\boldsymbol{u}$	Nodal displacements in the local reference system
$\boldsymbol{U}$	Global nodal displacements
$\boldsymbol{U^a}$	Vector of approximate displacements

${U^a}_{b_x}$	Approximation of translation in $\tilde{x}$-axis
${U^a}_{v_{xoy}}$	Approximation of translation in $\tilde{y}$-axis
${U^a}_{v_{xoz}}$	Approximation of translation in $\tilde{z}$-axis
${U^a}_{t_x}$	Approximation of rotation in $\tilde{y}\tilde{z}$-plane
$\boldsymbol{u_{b_x}}$	Vector with local axial displacements of the nodes
$\boldsymbol{u_{t_x}}$	Vector with local rotations in $\tilde{y}\tilde{z}$-plane of the nodes
$\boldsymbol{u_{v_{xoy}}}$	Vector with local translation displacements in $\tilde{y}$-axis of the nodes
$\boldsymbol{u_{v_{xoz}}}$	Vector with local translation displacements in $\tilde{z}$-axis of the nodes
U_L and U_U	Lower and upper bounds for constrained displacements
v	Translation in y-axis
v_1	Translation in $\tilde{y}$-axis of node 1
v_2	Translation in $\tilde{y}$-axis of node 2
$v(\tilde{x})$	Distribution of translation in $\tilde{y}$-axis along the element length (elastic line)
$\boldsymbol{v_p}$	Vector of design variables
${v_p}_L$ and ${v_p}_U$	Lower and upper bounds of a given design variable
V_0, V_1 and V_2	Coefficients of linear and quadratic variation of connections cost
V_y	Shear force in $\tilde{y}$-direction
V_z	Shear force in $\tilde{z}$-direction
${V_y}_1$	Shear force in $\tilde{y}$-direction of node 1
${V_y}_2$	Shear force in $\tilde{y}$-direction of node 2
${V_z}_1$	Shear force in $\tilde{z}$-direction of node 1
${V_z}_2$	Shear force in $\tilde{z}$-direction of node 2
$V_y(\tilde{x})$	Distribution of internal shear force V_y along the element length
$V_z(\tilde{x})$	Distribution of internal shear force V_z along the element length
V_R	Resulting shear force
${V_R}^{y'}$	Component of V_R in the auxiliary reference system (y')
${V_R}^{z'}$	Component of V_R in the auxiliary reference system (z')
${V_y}_{alw}$	Allowable value of shear force in $\tilde{y}$-direction
${V_z}_{alw}$	Allowable value of shear force in $\tilde{z}$-direction
w	Translation in z-axis
w_1	Translation in $\tilde{z}$-axis of node 1

w_2	Translation in $\tilde{z}$-axis of node 2
$w(\tilde{x})$	Distribution of translation in $\tilde{z}$-axis along the element length (elastic line)
w'	Magnitude of a generic uniformly load distribution
$w_{\tilde{y}}$	Magnitude of the uniformly load distribution in $\tilde{y}$-direction
$w_{\tilde{z}}$	Magnitude of the uniformly load distribution in $\tilde{z}$-direction
W	Manufacturing objective function (cost)
W_{SF}	Initial manufacturing cost
W_1	Material cost
W_2	Connections cost
X^*	Generic representation of joint positions
X, Y and Z	Global nodal coordinates of joints
$\tilde{x}$, $\tilde{y}$ and $\tilde{z}$	Coordinates related to the local reference system
x, y and z	Coordinates related to the global reference system
$\tilde{x}\tilde{y}$ and $\tilde{x}\tilde{z}$	Bending planes
$\tilde{y}\tilde{z}$	Torsional plane
$\bar{y}'$	Distance of the z'-axis to the centroid of the arc
0	Index for current design point
θ	Angular position in the outer radius of a circular thin-wall cross-section
θ_x	Rotation in $\tilde{y}\tilde{z}$-plane
θ_y	Rotation in $\tilde{x}\tilde{z}$-plane
θ_z	Rotation in $\tilde{x}\tilde{y}$-plane
$\theta_z(\tilde{x})$	Distribution of internal rotation in $\tilde{x}\tilde{y}$-plane along the element length
θ_{1x}	Rotation in $\tilde{y}\tilde{z}$-plane of node 1
θ_{2x}	Rotation in $\tilde{y}\tilde{z}$-plane of node 2
θ_{1y}	Rotation in $\tilde{x}\tilde{z}$-plane of node 1
θ_{2y}	Rotation in $\tilde{x}\tilde{z}$-plane of node 2
θ_{1z}	Rotation in $\tilde{x}\tilde{y}$-plane of node 1
θ_{2z}	Rotation in $\tilde{x}\tilde{y}$-plane of node 2
θ_C	Column rotation
θ_F	Frame rotation
ϕ	Rotation due to connection flexibility
ϕ_1, ϕ_2, ϕ_3 and ϕ_4	Rotation due to connection flexibility of case 1 for the formulation of the element stiffness matrix

ϕ_5, ϕ_6, ϕ_7 and ϕ_8	Rotation due to connection flexibility of case 2 for the formulation of the element stiffness matrix
ϕ_9, ϕ_{10}, ϕ_{11} and ϕ_{12}	Rotation due to connection flexibility of case 3 for the formulation of the element stiffness matrix
ϕ_{13}, ϕ_{14}, ϕ_{15} and ϕ_{16}	Rotation due to connection flexibility of case 4 for the formulation of the element stiffness matrix
γ_{yz}	Angular deformation
γ_M	Angle between the bending moments M_y and M_z
γ_V	Angle between the shear forces V_y and V_z
σ	Multiaxial stress state
σ_e	Yield stress
σ_{eq}	von Mises equivalent stress
σ_{xx}, σ_{yy} and σ_{zz}	Components of normal stress
$\sigma_{xx_{máx}}$	Maximum normal stress
σ_{N_x}	Normal stress produced by the axial force
σ_{M_y}	Normal stress produced by the bending moment in $\tilde{x}\tilde{z}$-plane
σ_{M_z}	Normal stress produced by the bending moment in $\tilde{x}\tilde{y}$-plane
σ_{M_R}	Normal stress produced by M_R
τ_{xy}, τ_{xz} and τ_{yz}	Components of shear stress
$\tau_{yz_{máx}}$	Maximum shear stress
τ_{M_x}	Shear stress produced by the torsion
τ_{V_z}	Shear stress produced by the shear force in $\tilde{z}$-direction
τ_{V_y}	Shear stress produced by the shear force in $\tilde{y}$-direction
τ_{V_R}	Shear stress produced by V_R
$\tau_{{V_R}^{y'}}$	Shear stress produced by ${V_R}^{y'}$
$\tau_{{V_R}^{z'}}$	Shear stress produced by ${V_R}^{z'}$
ζ	Correction factor to impose the shear effect in deflection
ζ_y	Correction factor to impose the shear effect in the deflection of $\tilde{x}\tilde{z}$-plane
ζ_z	Correction factor to impose the shear effect in the deflection of $\tilde{x}\tilde{y}$-plane
α	Fixity factor
ρ	Specific mass

$\mathbf{\Omega}$	Sub-matrix of the direction cosines
ε_{xy}	Axial strain
φ	Angle between M_R and the outer radius line which pass though θ
λ	Angle related to the auxiliary reference system $y'z'$
Δv_p	Stepsize of a given design variable
ξ	Percentage of the relationship between $\sigma_{xx_{máx}}$ and $\tau_{yz_{máx}}$
μ	Parameter of the active set strategy on constraints

Table of Contents

Chapter 1

Introduction

Over the years, due to the scarcity of natural resources and the increased competitiveness of the global market, engineers have been showing concern and facing the challenge of designing reliable structures with the lowest manufacturing cost (SANT'ANNA *et. al.*, 2001).

Historically, the interest in structural optimization began in the mid-19th century with the study of Maxwell (1870) and years later, at the beginning of the 20th century with Michell (1904). Both studies investigate analytically the optimal layout of structures, subject to a given load case, in order to provide the lowest material volume.

From there, the development of structural design has become an engineering activity that has been progressively improved by the use of mathematical tools, integrated to the computational environment, capable of automating the repetitive alteration of the available design parameters to define the best technical specification.

In 50's decade, Livesley (1956) introduced the linear programming (LP) technique on design of frames, a numerical method applicable on problems which the objective and design constraints functions appear as linear functions of the design variables (RAO, 2009). Schmit (1960 apud Muñoz-Rojas, 2013) presented the procedure of coupling non-linear optimization techniques with the structural analysis using the finite element method (FEM), providing the possibility to find optimal solutions in structural problems with a complexity not treated until then. Thereafter, structural optimization procedures have been extensively developed and investigated, due to the increasing demand for structures that respect design requirements having feasible costs.

In the context of sizing, where cross-section areas are design variables, Dorn *et. al.* (1964) developed the ground structure method (GSM), a topology optimization method that aims to minimize the material cost from a dense initial mesh (discrete model) that fills the space in which the structure may exist.

Since layout is a constructive aspect that influences the mechanical behavior of a structure, Pedersen (1972) proposed the possibility to optimize layout of structures through a gradient-based method called by sequential linear programming (SLP), using cross-section areas and joint positions as design variables. More recently, also using a gradient-based method, Sergeyev and Pedersen (1996) presented the layout optimization of steel space frames with tubular thin-wall elements subject to multiple load cases and displacement and stress constraints.

The civil construction makes use of tubular thin-wall elements in several types of steel space frames such as industrial sheds, catwalks, offshore structures and flat roof of stadiums, road terminals and airports. The automotive industry also applies this type of structural element, usually in chassis and protective cages of auto racing vehicles such as kart and Nascar. The Fig. 1.1 shows some of these applications.

Figure 1.1 – Examples of (a) flat roof of a supermarket and (b) kart chassis.

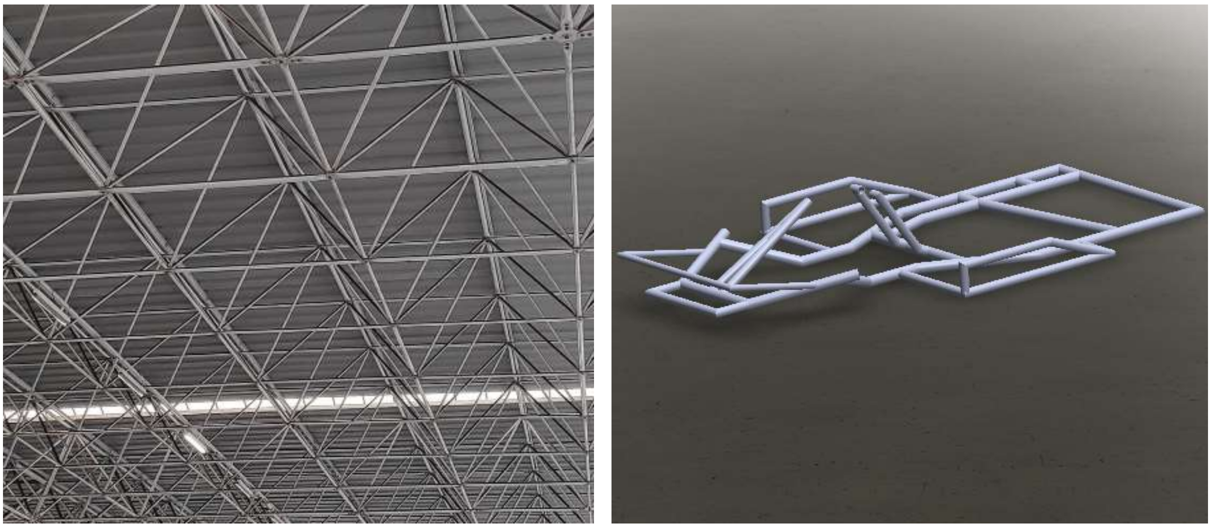

(a) (b)

Source: Author's production.

At these engineering sectors, the typical static design requirements are structural integrity and stiffness. In addition, another design requirement of extreme importance to ensure that a structure does not present catastrophic failure is the structural stability. In this context, layout optimization is a useful procedure for finding optimal solutions that ensure these requirements with manufacturing cost savings. However, local and global buckling can occur not only due to the reduction of cross-sectional size but also to the appearance of long elements (slender ratio).

Generally, according to Santos (1977), designers applying tubular elements because of their aesthetic shape and the mechanical advantage of building joints between two or more elements. This type of element also provides other mechanical advantages such as high torsion resistance, higher natural frequency and less wind resistance. However, there is a downside due to the cost being higher than the cost of rolled sections.

A common practice adopted in most cases of design of frames is to neglect the effect of the shear forces. However, when layout optimization is performed, it is important to have a failure criterion suitable not only to the cross-sectional type but also considering the slender ratio of the element. The joint positions change can produce elements with short length, in which case this negligence may not be acceptable.

Sergeyev and Pedersen (1996) proposed a stress calculation based on the distribution of normal and shear stresses as a function of all the internal forces of the 3D frame element. However, since the location of the critical point of equivalent stress depends on both the cross-sectional local coordinates and the local longitudinal coordinate, this process can be computationally intensive.

To avoid complexity and computational cost, Carniel *et. al.* (2008) also optimized layout of steel tubular space frames and proposed an alternative failure criterion given by the normalization of the internal forces in relation to the respective maximum forces. However, the criterion assumes the worst case of a combined request of internal forces, where the effect of all the stresses produced intensifies. The conservatism of this strategy can cause an oversizing of the structure. Thus, it is evident the need to combine computational efficiency and effectiveness in a stress-based failure criterion to optimize layout of this type of structure.

Returning to the scope of costs, although extensively investigated, optimization procedures that counts only on the mass minimization may be insufficient for certain applications. Two optimal structures with the same mass may present layouts with different levels of complexity and mainly distinct manufacturing costs. The number of joints, elements and layout complexity are particularities capable of making the structure unfeasible not only due to the cost required for the manufacture procedure related to the connections, but also because of the difficulty and consequent time required for manufacturing (ASADPOURE *et. al.*, 2015).

Recently, Asadpoure *et. al.* (2015) proposed a topology optimization process in discrete models where the objective function incorporates the minimization of two independent types of manufacturing cost: material and connections costs. By varying the difference between these two types of cost, the study showed that the approach enables the determination of compromise solutions through the controlled removal of elements (and consequently connections). The higher the cost of connections, the greater the removal of elements/connections and the lower the final complexity of the structure.

On the construction point of view, it is well known that bolted and welded connections are widely used in joints of tubular elements. As can be seen in Vigh and Dunai (2004), several types of connections can be used, and there are cases where bolts and welds are used together through secondary components, which makes it difficult to characterize their structural behavior. The cost of any connection is directly related to the type and quantity of material and the manufacturing process required. Figs. 1.2(a-b) show some practical examples of joints.

Figure 1.2 – (a) Example of tubular joints with (1,2) bolted endplates, (3a) pinned connection by earplates, (4) gusset plate, (5) coverplate and (b) a pinned connection between four elements.

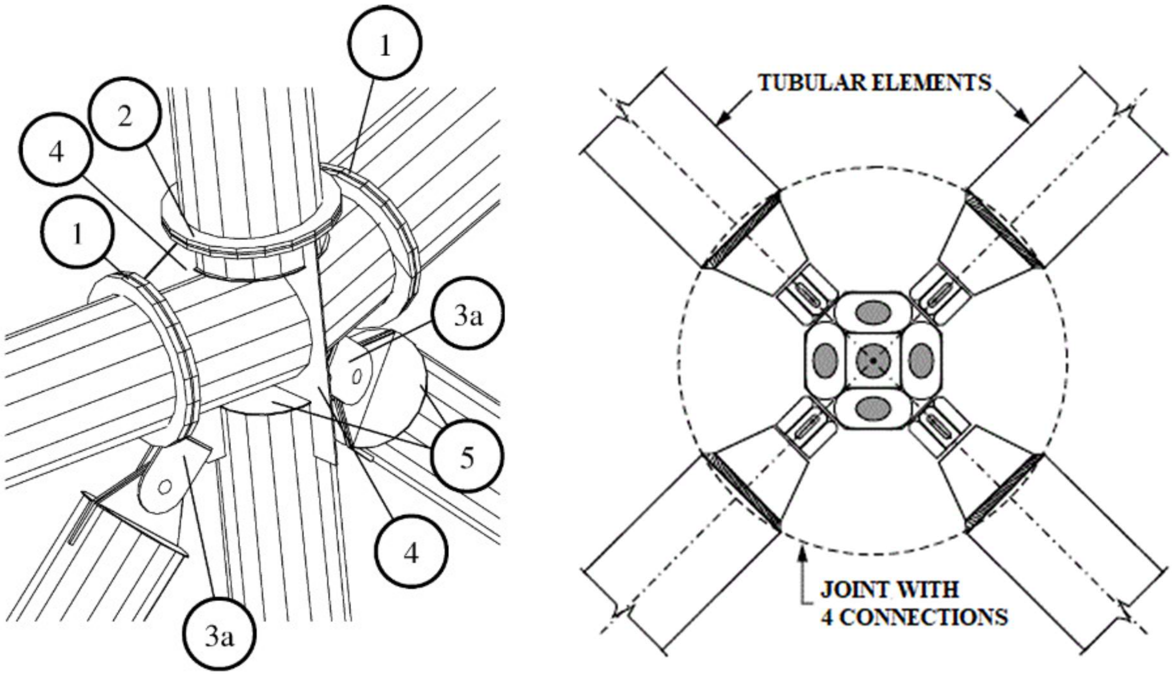

(a) (b)

Source: Vigh and Dunai (2004) and Ghasemi *et. al.* (2010).

In preliminary stages of structural design, in order to simplify the finite element analysis (FEA), another common practice is to idealize that all the connections between column-base, beam-to-column or beam-to-beam members are either perfectly pinned or fully rigid. However, as already commented, this is not an appropriate approach because each type of connection has its own mechanical behavior. Also, several experimental investigations proved that pinned connections have rotational stiffness and fully rigid connections show some degree of flexibility

(CHEN, 2000). Thus, to avoid an inconsistent prediction of structural responses, it is important to develop and apply a physical and mathematical model for connections.

Monforton (1962) developed a formulation for 3D frame elements accounting the effect of semi-rigid connections through a model with rotational springs within the two bending planes. The torsional flexibility was also addressed, but through a different approach. However, none of the case studies evaluated by the author consider more than one element with semi-rigid connection at the same joint. In fact, during the development of this research, only in Kartal *et. al.* (2010) was found an investigation about the constructive concept of two or more elements connected to the same joint, but within a case study of planar frame (i.e. coplanar elements).

Xu and Grierson (1993) and Simões (1996) investigated the effects caused by the imposition of semi-rigid connections as design variables in structural optimization of planar frames. The objective functions stated by the authors also accounts for material and connection costs, but different from what is proposed in Asadpoure *et. al.* (2015), the connections cost of a given element is related to their stiffness and is proportional to the material cost. Comparing with processes where fixed fully rigid connections were assumed, these authors demonstrated that better optimal solutions can be found when semi-rigid connections are considered. Xu and Grierson (1993) also observed different performances of cost minimization when structures are subjected to displacement constraints and external loads from different directions. However, again no research found has addressed case studies with two or more elements connected to the same joint.

Most researches about optimization of frames with semi-rigid connections has focused on procedures based on heuristic methods (exploratory search to found the optimal solution), with sizing optimization of planar frames through discrete design variables consistent with cross-section areas of commercial profiles and experimentally characterized connections. To the author's knowledge, no research deals with thin-wall tubular elements and the constructive concept of two or more non-coplanar elements connected to the same joint. Therefore, an important contribution of this research work is precisely to enable simultaneous optimization of layout and connections of steel tubular space frames with more complex joints through any gradient-based method.

Taking into account gradient-based methods, none of the research found addresses optimization of space frames with semi-rigid connections. Thus, through own procedure to impose the effect of semi-rigid connections at 3D frame elements, this work aims to extend the two-dimensional formulation of the objective function proposed by Simões (1996). Despite having developed a formulation for 3D frame element with rotational stiffness in the three planes of rotation, Monforton (1962) states that in practice it is feasible to assume infinite stiffness for the torsional degree of freedom (DOF). Therefore, the formulation of this work focuses only in the semi-rigidity of the two orthogonal bending planes, while the torsional stiffness is assumed as fully rigid.

Based on steel buildings with commercial profiles different of tubular elements, in the proposals of Xu and Grierson (1993) and Simões (1996) the additional cost of a pinned connection is always lower than that of a fully rigid connection, and the cost of an intermediate semi-rigid connection is given by linear and quadratic variations between these two connection cost, respectively. The extreme costs of pinned and fully rigid connections are based on published data's (not found). For simplicity, this work also assumes this type of range of connections cost, but proposing a mathematical procedure to determine a behaved curve for the quadratic variation. However, it should be noted that the cost of any connection depends not only on the type of the cross-section of the connected elements, but also on the amount of material required and the complexity of the manufacturing process. Therefore, perhaps this assumption does not cover very well connections of tubular elements and different types of space frames constructions. Unfortunately, no published data was found for tubular elements.

Solution techniques based on gradient-based methods have been considered not very efficient for later technical specifications of large scale structures (HAYALIOGLU; DEGERTEKIN, 2005). A discrete solution can be generated from the continuous solution by approximation techniques (HAVELIA, 2016), but Camp *et. al.* (1998) observed that optimizing with continuous design variables can cause optimal solutions with less quality or even infeasible due to construction constraints found in regulatory standards. Despite the potential decrease on the quality of the optimal solution, an advantage of deal with structures build by steel tubular elements is that the optimal continuous solution is easily extrapolated to a very close discrete solution, being important only to check later that the extrapolated solution continues to respect all the design constraints.

1.1 Objectives

The main objective of this research work is to propose a new approach to optimize layout and connections of steel tubular space frames through any gradient-based method. The optimization problem aims to minimize manufacturing costs related to material and connections, with cross-section areas, joint positions and connections stiffness as design variables, subject to multiple load cases and respecting displacement, minimum element length and stress constraints.

The optimization procedure must be capable of identifying competitive design solutions with continuous design variables that can be later extrapolated to a technical specification, simultaneously evaluating stiffness, mechanical strength and manufacturing costs without neglect the effect of connections and transverse shear stresses and releasing the existence of joints with more complex constructive concept.

Based on the von Mises theory, the goal is to develop a new procedure to evaluate stress in 3D frame elements with thin-wall circular cross-section area and variable length as a function of the internal forces and geometric properties, accounting the transverse shear effect and determining the critical point of each cross-section analyzed.

Layout optimization might lead to slender elements subject to the occurrence of local and global buckling failures. For this reason, to apply stability constraints is essential to ensure structural reliability at the optimal solutions. However, as a primary approach, this aspect is not included in the scope of the research.

1.2 Outline

The research work consists of seven chapters organized as follows:

- **Chapter 1 (Introduction)**: after a briefly contextualization of the research field and motivations, the objectives and limitations of the research proposal are presented.
- **Chapter 2 (Literature Review)**: this chapter presents the main contributions correlated with structural optimization of structures, application of semi-rigid connections in FEA and optimization problems and, finally, failure criteria, providing the basis for the further formulations and implementation to be developed. Also, it is important for the understanding of the environment in which the desired contribution is inserted.
- **Chapter 3 (Formulation of the Semi-Rigid Frame Element)**: in order to add the effect of semi-rigid connections, the stiffness matrix of the 3D frame element is formulated using the direct method, considering connections with rotational springs

with respect to two orthogonal bending planes. Then, the procedure to calculate the internal forces is presented.

- **Chapter 4 (Failure Criterion)**: this section presents one of the central contributions of this work. A novel procedure for calculating the von Mises failure criterion taking into consideration the usually neglected transverse shear contributions is developed for tubular elements. This way the criterion can be applied not only to long elements but also to moderately short ones.
- **Chapter 5 (Optimization Problem)**: the proposed optimization problem to minimize manufacturing costs is stated, providing a new approach for simultaneously optimizing layout and connections of steel space frames. Then, the most pertinent features and details about the iterative process of the chosen gradient-based method are presented. Thereafter, the sensitivity analysis of the objective function and design constraints is performed analytically. As the length of the elements varies during the optimization process, the failure criterion developed in Chapter 4 becomes important.
- **Chapter 6 (Results and Discussion)**: investigations are carried out regarding the structural behavior and the optimal solutions obtained by space frames with semi-rigid connections, comparisons between different optimization procedures and the specific failure criterion.
- **Chapter 7 (Conclusions)**: recalling the objectives, developed formulations and obtained results, final conclusions regarding the contribution achieved and suggestions for future works are presented.

Chapter 2

Literature Review

The field of structural optimization in discrete models can be decomposed into three categories: sizing, shape and topology optimization. While sizing optimization deals with geometric parameters of the elements (usually cross-section areas), shape optimization of structures deals with the location of joints and topology optimization modifies the quantity and connectivity of the elements (KICINGER *et. al.*, 2005). In order to clarify the term used throughout this research work, layout optimization incorporates sizing and shape optimization, i.e. cross-section areas and joint positions as design variables. Furthermore, when semi-rigid connections are available, parameters associated with the rotational stiffness level of the connections may be introduced as design variables.

Basically, the sequence of engineering activities related to the design of a structure is given by: definition of the topology based on functional requirements, technical experience and predicted architecture, definition of the layout concept and calculation of dimensional parameters. Analyzing individually, while the first two activities of topology and layout influence significantly in the structural behavior, the sizing is the one that least impacts (HAVELIA, 2016). However, it is important to note that both categories of optimization are highly interdependent. When topology and/or layout changes are made, the distribution of internal forces also changes, which impacts on the later sizing (ROZVANY, 1992).

Proceeding separately with the different types of optimizations facilitates the numerical process but generally achieves sub-optimal solutions (ROZVANY *et. al.*, 1995). When compared to layout or topology optimization, sizing optimization produces less impact on final cost and structural performance (LEE *et. al.*, 2014).

In the next sections, studies that show different types of costs to build a structure are presented. Then, contributions in the area of topology optimization are presented, since the researches aggregates aspects related to minimization of manufacturing costs, use and behavior of different types of approaches (sizing and layout) inside topology optimization, characteristics of optimal solutions and the effect of applying stability constraints.

2.1 Costs for Building Structures

Optimization problems for mass minimization of structures subject to displacement and stress constraints has been extensively investigated since a long time, mainly through the application of gradient-based methods within sizing or layout approaches. For example, see the works of Moses and Onoda (1969), Pedersen (1972), Pedersen and Jøgersen (1984), Yoshida and Vanderplaats (1988), Sergeyev and Pedersen (1996) and Sergeyev and Mróz (2000), Pedersen and Nielsen (2003), Sant'Anna *et. al.* (2001) and Carniel *et. al.* (2008). However, this procedure is a useful procedure to be applied only at initial stages of design, since there are other factors that directly influence in the final cost to build any structure (LIVESLEY, 1956).

In recent decades, while material cost has remained almost constant, other types of costs in terms of manufacturing and erection processes of the elements and their connections have increased (STEENHUIS *et. al.*, 1997).

The total cost can be measured from the material acquisition, depending on the type and size of the cross-section area, quantity of material required (related to the element size) and market conditions (HAVELIA, 2016), up to costs that vary according to the quantity of connections and even the complexity of the layout, which can make the manufacturing process more difficult and expensive (ASADPOURE *et. al.*, 2015).

Depending on construction features related to the type, size and geometry of the elements, the connections cost can vary significantly. For example, according to Havelia (2016), is common to see steel frames that have column members with continuous length through joints related to beam connections, i.e. it is not necessary to account the connections between the column members in FEA and optimization.

In this context, an accurate cost estimation is fundamental to design economical structures (ALI *et. al.*, 2009). Ali *et. al.* (2009) and Havelia (2016), for example, assume several factors and sub-costs related to the costs of material, manufacturing, foundation and erection procedures. A similar concerning can be seen in Hasançebi (2017), where the objective function was formulated as a summation of five items: the material of elements, material and manufacturing of semi-rigid connections, transportation, erection and extra costs. Regarding manufacturing of connections, they included the costs of necessary materials for welding, bolting, stiffeners and plates and costs of welding and hole forming process. The extra costs may be painting, flange aligning, surface preparation, among others.

2.2 Topology Optimization of Discrete Structures

The GSM proposed by Dorn *et. al.* (1964) was the beginning for the application of the procedure of removing elements from a dense and discrete mesh of line elements. Removing an element from a given structure does not only reduce the cost of material but also the quantity and cost of the required connections.

After the initial sizing optimization, the procedure of the GSM consists of removing elements that have cross-sectional area value below a pre-set removal value and reapply the optimization with the new topology as a starting point (ASADPOURE *et. al.*, 2015). According to Hagishita and Ohsaki (2009), the initial mesh density and the nodes location influence the quality of the solution. Case studies presented in Bendsøe *et. al.* (1994), see Fig. 2.1, also demonstrate that there is a tendency to produce optimal solutions with considerably complex layouts (TORII *et. al.*, 2016).

Figure 2.1 – Layout complexity of an optimal solution found by GSM approach.

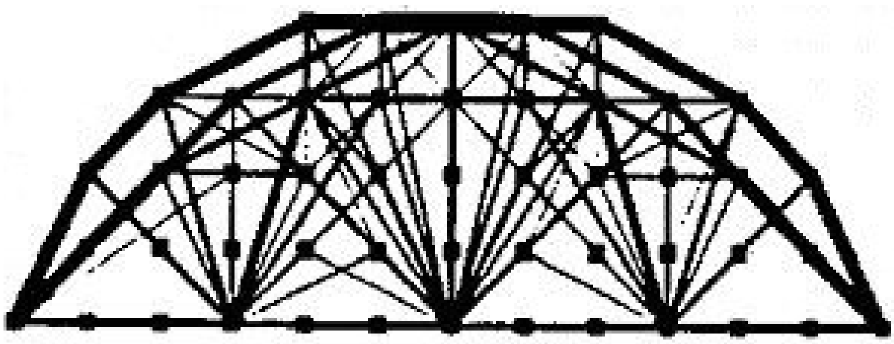

Source: Bendsøe *et. al.* (1994).

Since the GSM formulation, several researches developed and investigated topology optimization of discrete structures based on sizing and layout approaches, such as Achtziger (2007), Hagishita and Ohsaki (2009), Asadpoure *et. al.* (2015), Havelia (2016), Torii *et. al.* (2016) and Tejani *et. al.* (2018). The main concern was the obtention of solutions with layout too complex for practical purposes, since this complexity impacts in several manufacturing costs of the final structure.

A simple procedure commented by Bendsøe *et. al.* (1994) to avoid complex structural designs is to limit intuitively the domain of the design space through the connectivity, i.e. only neighboring nodes are connected. Unfortunately, the performance of this strategy depends heavily on the designer's experience.

Another procedure addressed in Bendsøe *et. al.* (1994), Achtziger (2007) and He and Gilbert (2015), is to use layout optimization into the topology optimization. Considering cross-section areas and joint positions as continuous design variables, Achtziger (2007) demonstrated that this proposal can provide good optimal solutions for problems of moderate size, i.e. without the need to deal with many elements. Also, they observed a tendency to produce unsymmetric trusses as optimal solutions, see Fig. 2.2, even with a symmetric load condition, fact directly related to the use of a non-global optimization algorithm (any gradient-based method), the occurence of a flat objective function and the no imposition of symmetry by additional constraints.

Figure 2.2 – Unsymmetrical truss as optimal solution found in Achtziger (2007).

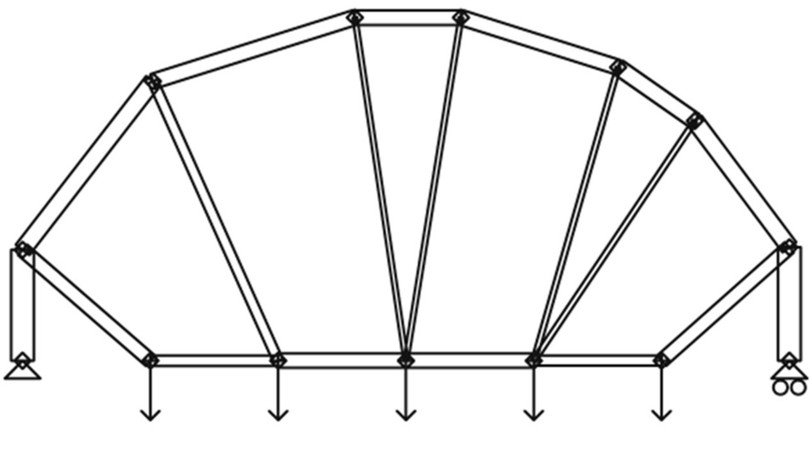

Source: Achtziger (2007).

About the fact that layout optimization induces computational difficulties, Achtziger (2007) proposed the strategy where a feasible starting point is calculated with the fixed layout before proceeding with the layout optimization. This separate optimization process was also adopted in the first strategy discussed in He and Gilbert (2015). This strategy simplifies the optimization process, but can lead to sub-optimal solutions, as Rozvany *et. al.* (1995) identified in some studies performed by sequential optimization of topology and sizing.

Hagishita and Ohsaki (2009) have proposed and obtained satisfactory results with strategies dedicated to adding and removing elements and nodes within layout optimization on trusses subject to static (single or multiple) loading. The authors deal with melting of joints, remove of overlapping elements and initial meshes do not need to have a high number of elements. To illustrate, a particular case studied and the optimal layout achieved is presented in Fig. 2.3.

Figure 2.3 – Problem with overlapping elements in Hagishita and Ohsaki (2009).

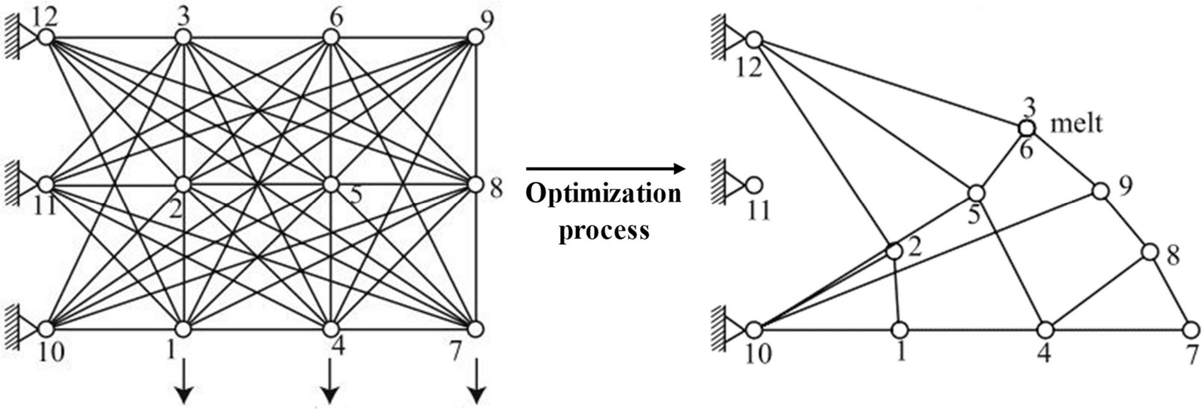

Source: Adapted from Hagishita and Ohsaki (2009).

It is well known that structural optimization problems may have singular optimal solutions that cannot be reached from an arbitrary starting point (SVED; GINOS, 1968). Therefore, an important result achieved by Hagishita and Ohsaki (2009) is that singular optimum solutions can be found for small trusses with stress constraints.

Asadpoure *et. al.* (2015) proposed a formulation to optimize the topology of trusses using normalized areas as design variables and a continuous approximation of the Heaviside function applied in the normalized areas. The formulation enables a process that identifies the optimal solution by analyzing the manufacturing cost-benefit relationship between costs of material and connections (two connections for each element), controlling the layout complexity of the final structure.

The approximation of the Heaviside function is continuous and differentiable, which enables the application of any gradient-based method. The results obtained by Asadpoure *et. al.* (2015) have shown that, according to the adoption of different magnitudes for material (c_M) and connections (c_S) costs, different final layouts are achieved due to the ability to identify "non-structural" elements automatically, reducing the dependence on "artificial" removal factors and the computational cost within the optimization process. As can be seen in Fig. 2.4, the higher the connections cost of the element, the greater is the element removal and consequently lower layout complexity is achieved. Consider L as element length.

Figure 2.4 – A study reproduced by Asadpoure *et. al.* (2015).

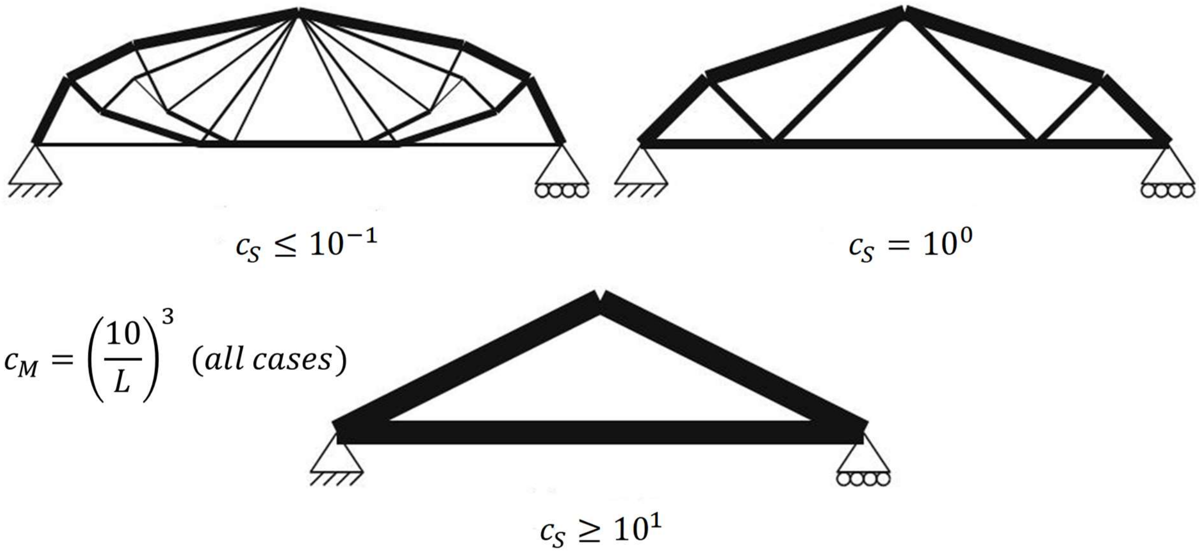

Source: Adapted from Asadpoure *et. al.* (2015).

Torii *et. al.* (2016) also noticed that previous works are capable to reduce layout complexity, but are not able to set a combined level between design complexity and structural performance desired by the designer. Therefore, the authors presented another efficient method to control layout complexity in sizing optimization of truss through any gradient-based method.

Based on two continuous and differentiable functions that measure the number of nodes and elements, both are employed in the optimization process as a penalty into the objective function. The penalization factor is responsible to enforce the desired level of complexity. Torii *et. al.* (2016) observed the existence of local optimal solutions in some examples due to the non-convexity characteristic of the measure functions.

Taking into account a frame structure, Havelia (2016) proposes a topology optimization scheme that has discrete cross-section areas as design variables, connection costs associated with construction features and a technique that recognizes continuity on desired elements, minimizing material, manufacturing and erection cost. After calculating the maximum internal stress and the total cost related to each element, it is produced a ranking that highlights the elements that have a high cost and are not useful to the mechanical strength of the structure (i.e. can be removed).

Havelia (2016) optimized a structure subject to lateral loads with mass and manufacturing cost minimization procedures, see Fig. 2.5. When manufacturing and erection costs are included in the optimization process, the author observed that the columns tend to be heavier compared to the same in the optimal solution related to only mass minimization.

Figure 2.5 – Case study developed by Havelia (2016).

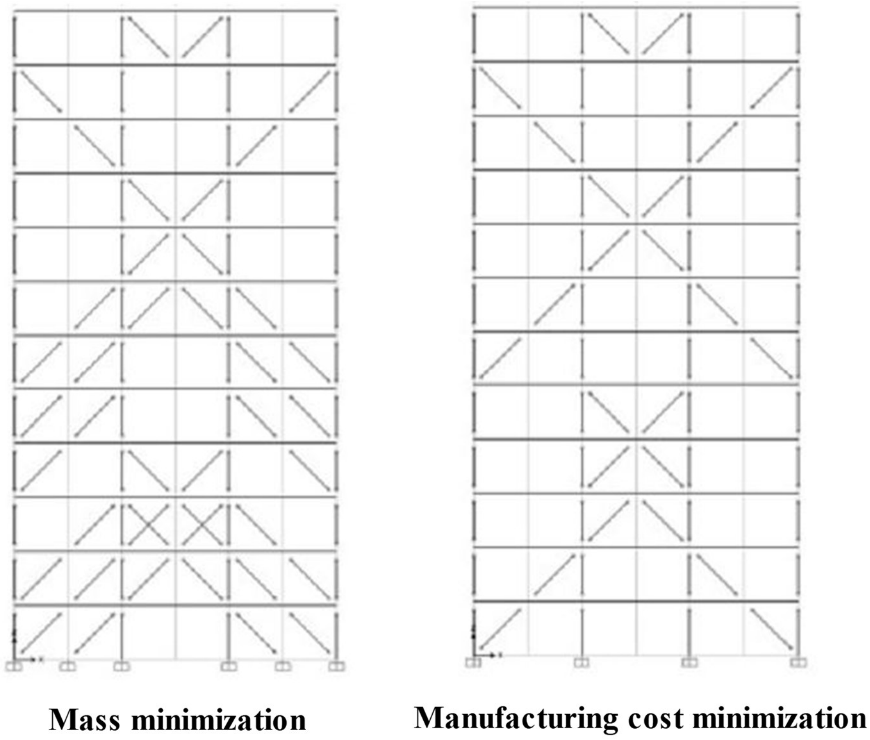

Source: Adapted from Havelia (2016).

This increase of mass in the columns happens because brace elements (see Fig. 2.5, the diagonal elements), which are mechanical efficiently in terms of mass minimization, are removed from the initial topology, decreasing the capacity of resistance to lateral loads. On the construction point of view, it is preferable to have fewer connections and consequently more easy manufacturing and erection procedures.

More recently, Tugilimana *et. al.* (2018) worked with sizing and topology optimization of steel space trusses made of tubular thin-wall elements, such as the large-scale truss dome visualized in Fig. 2.6. Elements with cross-section areas that reach a lower bound are removed from the initial topology.

Including global stability and local buckling constraints, the authors noted that some previous optimization problems treated without these constraints produced unstable structures, due to elements with small cross-sections in compression. In the optimal solution achieved for the truss dome of Fig. 2.6, bracing elements appear and cross-section areas of elements at the bottom are increased to ensure stability. For this case, the optimal design with stability constraints has approximately 10X the total volume of the optimal design that not accounts stability.

Figure 2.6 – Steel space truss investigated in Tugilimana *et. al.* (2018).

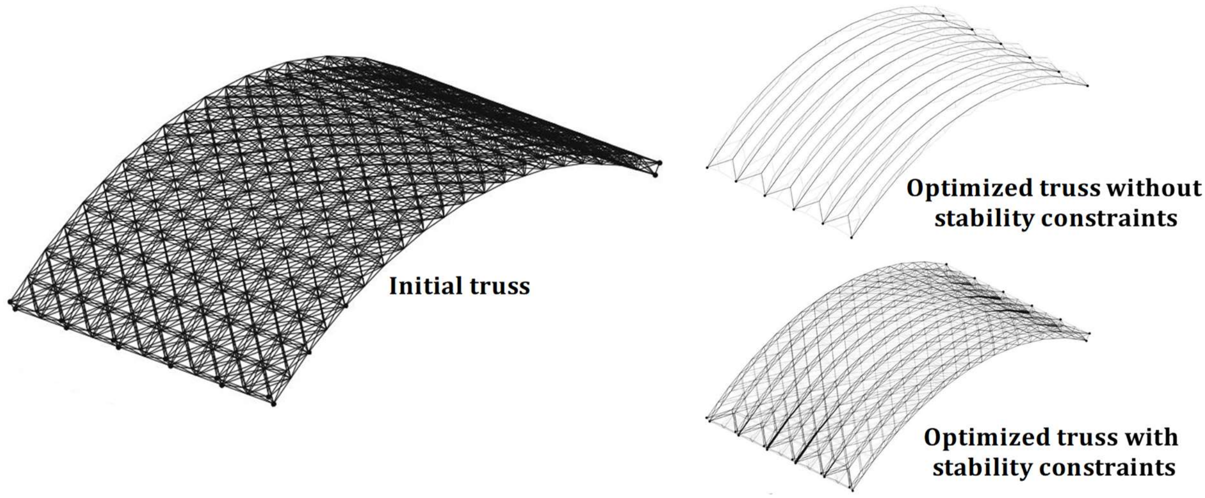

Source: Adapted from Tugilimana *et. al.* (2018).

Despite the knowledge that stability constraints are important to ensure truly secure optimal solutions, this type of constraint typically has a high level of non-linearity that produces difficulties at the optimization process (ROZVANY *et. al.*, 1995). In the research of Wildemann and Muñoz-Rojas (2004), the layout and topology optimization of space trusses is performed by a gradient-based method, and several case studies were analyzed with and without local buckling constraints, through the critical Euler load. The authors not only observed different optimal solutions, but also noted that the optimization process encounters more numerical difficulty for convergence when this type of stability constraint is considered, sometimes falling into unfeasible regions.

Tejani *et. al.* (2018) also treated space trusses and presented a study with layout and topology optimization through a heuristic method, mass minimization and subject to stress, displacement and kinematic stability (no generation of a mechanism due to the topology) constraints. For the removal of elements, they use a simple strategy for existence measure, which is directly multiplied in the objective function. The strategy assumes discrete values 0-1 based on a conditional that evaluates whether the cross-section area is smaller or larger than a critical value.

Deb and Gulati (2001) performed the same strategy in two case studies, one of them presented in Fig. 2.7. Developing two topology optimizations with layout and sizing approaches, the authors compared the obtained results of mass minimization and observed that the optimum solution of the layout optimization is 3% smaller than the optimum solution of the sizing optimization.

Figure 2.7 – Case study developed by Deb and Gulati (2001).

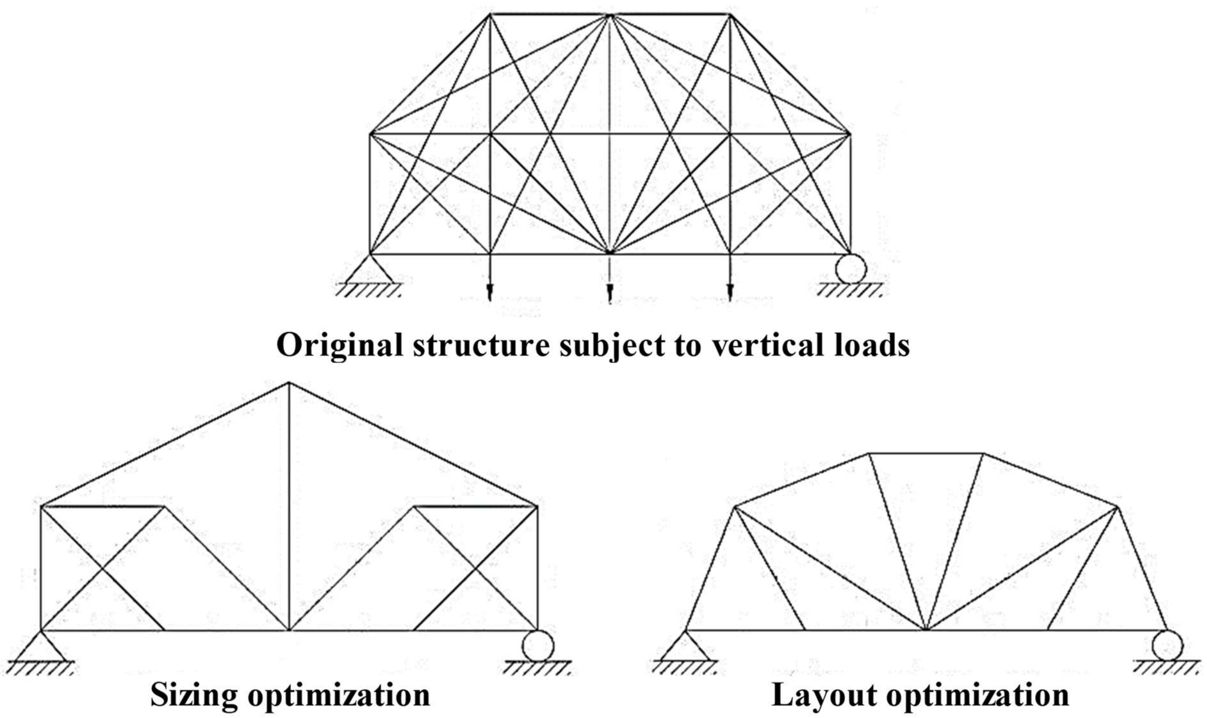

Source: Adapted from Deb and Gulati (2001).

In this research work, manufacturing costs will be evaluated without application of topology optimization, but rather with the use of layout and connections optimization. When layout optimization is performed, slender elements can be subject to compressive load and, consequently, may exhibit structural failure due to local or global buckling. The effect produced in the optimization process and optimum solutions when stability constraints are applied it is extremely important, as verified in Tugilimana *et. al.* (2018). However, according to research such as Rozvany *et. al.* (1995) and Wildemann and Muñoz-Rojas (2004), this type of constraint presents a high level of non-linearity that produces difficulties at the optimization process and would require more time to investigate it. For this reason, stability constraints are not in the scope of research.

Hereafter, contributions related to modeling of connections, objective function proposals to minimize manufacturing costs with connections as design variables and the effects caused by the addition of rotational stiffness in the structural response and optimization are presented.

2.3 Semi-Rigid Connections

Traditionally, to simplify the preliminary analysis and design of a steel frame, it is a common procedure to idealize connections with pinned or fully rigid behavior. However, as already commented, several experimental investigations demonstrated that pinned connections have rotational stiffness and fully rigid connections show some degree of flexibility (CHEN, 2000). Furthermore, according to Pinheiro (2003) and Del Savio (2004), experiments with several types of connections used in practice exhibited non-linear behavior due to the gradual plasticity of components such as plates and bolts.

In this scenario, to neglect the rotational stiffness of connections avoids realistic predictions of responses, such as displacements and internal forces distribution acting on the elements of the structure, and consequently the design reliability (SAGIROGLU; AYDIN, 2015). Studies and analytical models have been developed for non-linear analysis of frames that have several types of semi-rigid connections. In these models, among the various parameters to be determined by empirical expressions, obtained by experimental investigations allied to curve fitting techniques and to the steel connection database, is the initial rotational stiffness (K_r) of the connection (SEKULOVIC; SALATIC, 2001).

At initial stages of frame design, using a linear mathematical model to represent the bending moment-rotation relation curve (M-ϕ) is useful, see Fig. 2.8, since the initial stiffness of any type of connection is constant (PINHEIRO, 2003). Besides, when the goal is to analyze frames with small displacements and strains, the linear model can be applied without major problems, being the initial rotational stiffness the only parameter necessary to define the connection stiffness during the FEA and/or structural optimization processes. Therefore, iterative updating of this stiffness is not necessary as in non-linear models (PINHEIRO; SILVEIRA, 2005).

For linear-elastic model, there are several formulations to incorporate the semi-rigidity behavior of connections, for example Monforton (1962), McGuire *et. al.* (2000), Chan and Chui (2000), Hairil Mohd *et. al.* (2016), among others presented at the master thesis of Pinheiro (2003). The approaches are mentioned in Table 2.1.

Figure 2.8 – Linear mathematical model *vs.* experimental curve of typical connections applied in the engineering practice.

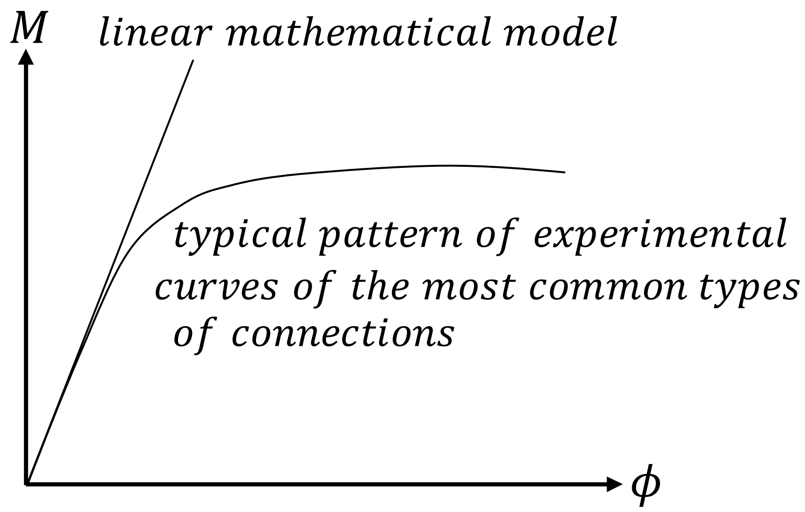

Source: Adapted from Pinheiro (2003).

Table 2.1 – Author's and method's formulations.

	Authors	**Method**
Formulations	Monforton (1962)	Conjugate beam
	McGuire *et. al.* (2000) Chan and Chui (2000)	Hybrid element composed by a frame element and rotational springs at the extremities
	Hairil Mohd *et. al.* (2016)	Potential energy approach

Source: Author's production.

Based on linear-models, several researchers investigated the behavior and structural optimization of frames with semi-rigid connections, such as Xu and Grierson (1993), Heringer (1996), Simões (1996), Csébfalvi (2007), Kartal *et. al.* (2010) and Artal and Daloglu (2018).

According to Sekulovic and Salatic (2001) and Del Savio (2004), in most steel structures the effects of axial and shear forces on the deformation of the connections are insignificant when compared to the effect caused by bending moments. At this context, a simple way of modeling semi-rigid connections of a 2D frame element is to impose rotational flexibility through rotational springs of negligible length l_m and rotational stiffness K_r at the two joints (nodes 1 and 2) of intersection between columns and beam members. This physical model is visualized in Fig. 2.9.

Figure 2.9 – Linear mathematical model for semi-rigid connections.

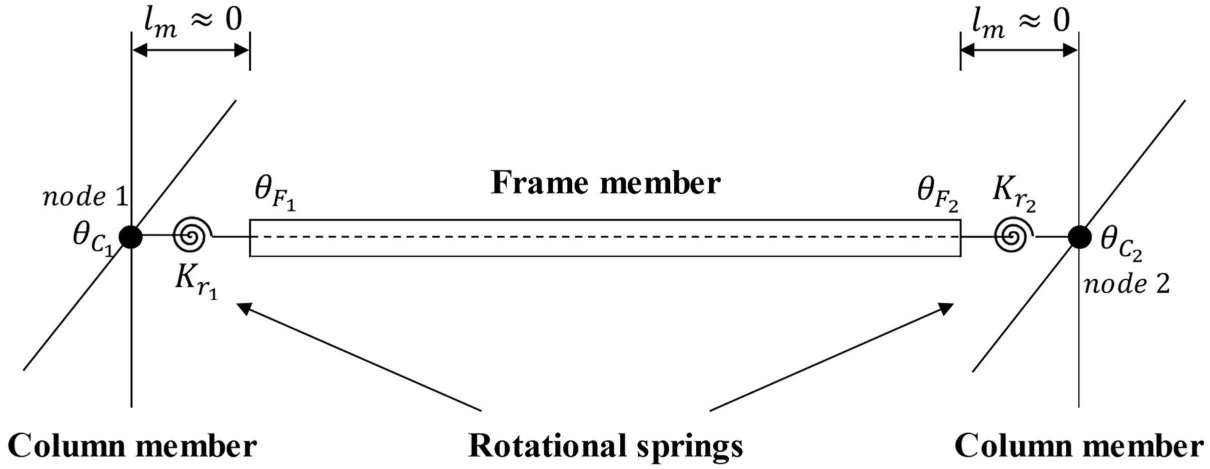

Source: Adapted from Chan and Chui (2000).

Two distinct rotations in the connection region coexist: a column rotation, θ_C, and a frame rotation, θ_F, both shown in Fig. 2.10. Assuming that two elements are connected to the same column, θ_C is the combined rotation that guarantees the compatibility of the global nodal displacements in FEM. However, depending on the internal bending moments transmitted, the elements may have different rotations θ_F.

Figure 2.10 – Difference between the column rotation and the rotation presented by the frame element at the connection.

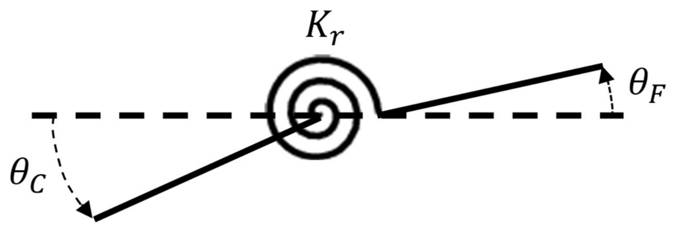

Source: Adapted from Chan and Chui (2000).

By the infinite stiffness hypothesis, when the column has any rotation θ_C the frame element accompanies this rotation as shown in Fig. 2.11(a). However, due to the rotational flexibility of the connection, a rotation ϕ of the frame element at the point of clamping occurs in relation to the line orthogonal to the inclined column, exposed in Fig. 2.11(b).

Figure 2.11 – (a) Fully rigid *vs.* (b) semi-rigid connection.

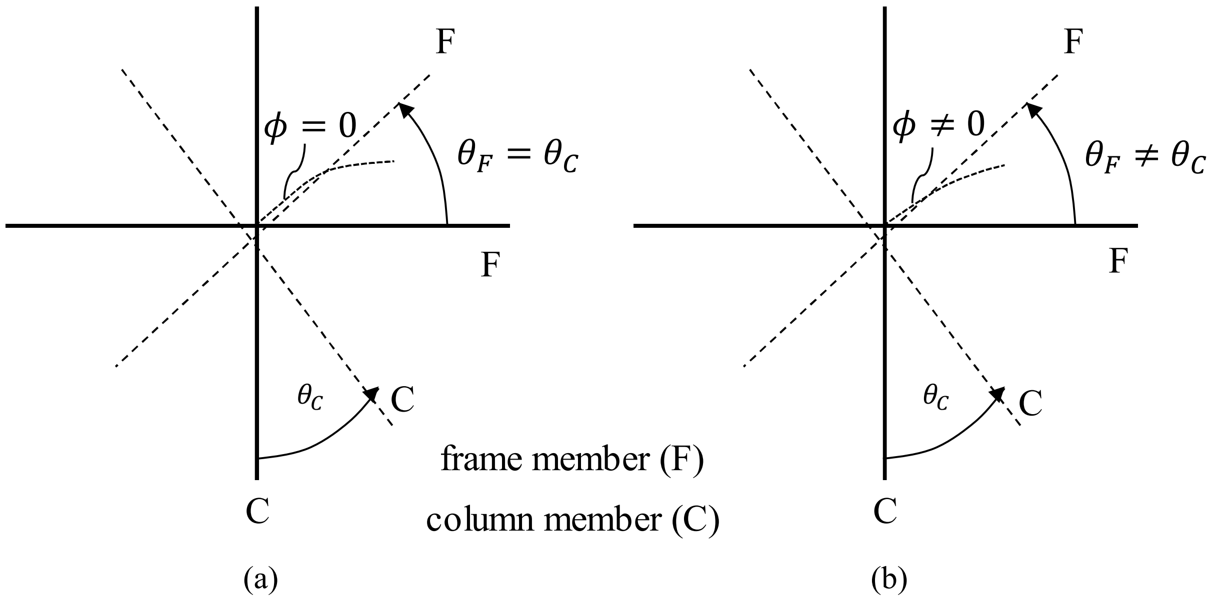

Source: Adapted from Kartal *et. al.* (2010).

The rotation of the 3D frame element at the connection, adopting the linear-elastic model, is defined by the relation of

$$\phi = \frac{M}{K_r}, \tag{2.1}$$

where M is the concentrated bending moment acting in the connection. Hence, the real rotation that the frame element will presents in the connection is

$$\theta_F = \theta_C - \phi. \tag{2.2}$$

According to Chen *et. al.* (2011), the AISC (American Institute of Steel Construction, 2005) considers that semi-rigid connections have rotational stiffness in the range of

$$\frac{2EI}{L} \leq K_r \leq \frac{20EI}{L}, \tag{2.3}$$

where E, I and L represent, respectively, the Young's modulus, the inertia moment and the length of the element. Below and above these limit values, connections are considered pinned and fully rigid, respectively. In addition, it is noteworthy that this information may vary according to the standard in use. Under the Brazilian standard ABNT NBR 8800 (2008), a connection with $\frac{\mathrm{EI}}{2\mathrm{L}}$ or less can be considered as pinned, whereas with $\frac{25\mathrm{EI}}{\mathrm{L}}$ or more can be considered as fully rigid.

Several researches such as Sekulovic and Salatic (2001), Cabrero and Bayo (2005) and Kartal *et. al.* (2010) used an initial rotational stiffness of semi-rigid connections defined as a function of the beam stiffness (EI) and a parameter called by fixity factor (α), which measures the connections stiffness in the range (0,1]. Thus,

$$K_r = \left(\frac{\alpha}{1-\alpha}\right)\frac{3EI}{L}, \tag{2.4}$$

where for pinned connections the fixity factor value is zero (K_r = 0) and for fully rigid connections the value is unitary ($K_r \to \infty$).

The relation between the rotational stiffness and the fixity factor was deduced through the formulation developed by Monforton (1962), based on the conjugate beam method. Basically, the physical meaning of the fixity factors is given by the quotient between the frame element and column rotations, i.e. θ_F and θ_C represented in Fig. 2.12, due to an unitary bending moment. Typically, according to Chen (2000), planar frames present connections with evaluated fixity factors between the range of 0.77 and 0.94.

Figure 2.12 – Physical meaning of the fixity factor.

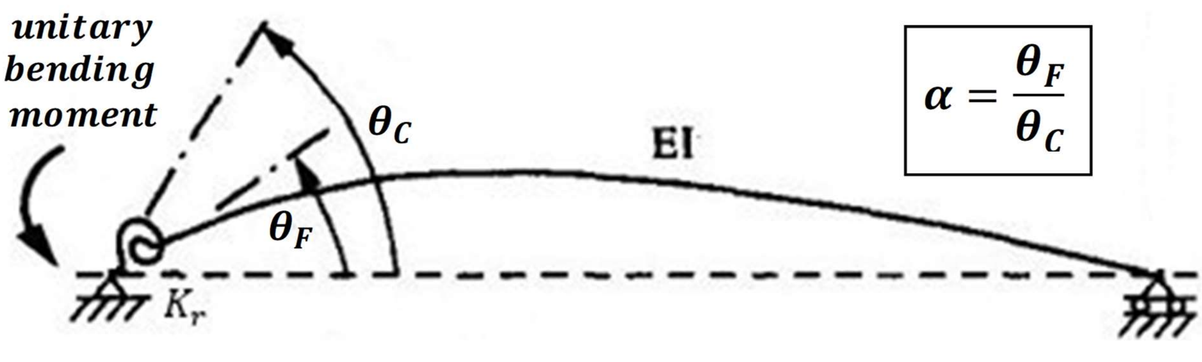

Source: Adapted from Simões (1996).

Manipulating equation (2.4) to investigate and understand some aspects related to the relation between the fixity factor and the rotational stiffness,

$$\frac{K_r L}{EI} = \frac{3\alpha}{(1-\alpha)}, \tag{2.5}$$

and knowing that $\frac{K_r L}{EI}$ presents values in the range of 10.0 and 50.0 at design of frames (GERSTLE, 1988), the graph visualized in Fig. 2.13 is plotted. Note that the relationship between α e K_r is non-linear, especially in the region with α values above 0.5, where a small increase in the fixity factor would correspond to an exaggerated increase in the rotational stiffness (CHEN, 2000). In the graph, Y$'$correspond to $\frac{K_r L}{EI}$.

Figure 2.13 – Non-linear relationship between rotational stiffness and the fixity factor.

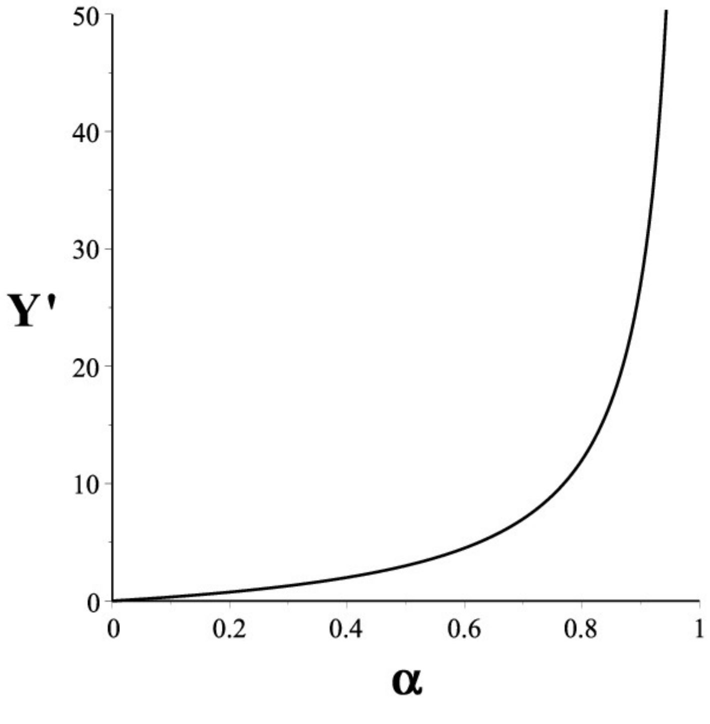

Source: Adapted from Chen (2000).

At the engineering practice, the introduction of the fixity factors is beneficial for the static analysis of frames, since it allows previous investigations of structural responses coupled with the physical notion of the level of rotational stiffness in the connections, as opposed to the fictitious infinite stiffness (CHEN, 2000).

According to Monforton (1962), up to the mid-1960s there were few theoretical and experimental investigations about the structural behavior related to connection rotations around $\tilde{x}$ ($\tilde{y}\tilde{z}$ plane) and in the $\tilde{x}\tilde{z}$ plane on space frames, i.e. torsion and bending DOF (in this work, the index "~" refers to the local reference system). The author states that most types of semi-rigid connections exhibit fully rigid behavior in torsion and pinned behavior in rotation at the $\tilde{x}\tilde{z}$ plane. The main displacements in frames are rotations at the same plane of application of the external loads (HERINGER, 1996).

With respect to the torsional DOF, in the study of Monforton (1962) the torsional flexibility in the plane $\tilde{y}\tilde{z}$ is given by fixity factors directly proportional to the torsional stiffness (GJ) of the 3D frame element (G is the shear modulus and J is the polar moment of inertia). However, the author informs that connections between 3D frame elements can be considered fully rigid in torsion.

2.4 Optimization of Frames with Semi-Rigid Connections

In the field of structural optimization, linear models of semi-rigid connections have also been extensively applied and investigated in planar and space frames, with different optimization methods.

Lui and Chen (1986) develop a study about connections flexibility in frames and concluded that, generally, fully rigid idealization underestimate the displacements and overestimate the strength. On the other hand, assuming pinned connection provides overdesign of beam members and underdesign of columns.

Xu and Grierson (1993) present a procedure to minimize the combined cost of elements and semi-rigid connections of planar frames. Using discrete American standard steel sections and continuous rotational stiffness as design variables, a continuous-discrete optimization algorithm is applied based on a gradient-based method, with stress and displacement constraints. Thus, the objective function W is given by

$$W = \sum_{i=1}^{nel}\left(c_{M_i}\rho_i A_i L_i + \left(\sum_{c=1}^{2}\left(V_0 + V_1 K_{r_c}\right)\right)_i c_{M_i}\rho_i A_i L_i\right), \tag{2.6}$$

where ρ is the specific mass and A is the cross-section area. The indexes i and nel represent the sum of elements, c is related to each rotational spring of a given element and V_0 and V_1 are parameters that control the additional cost of the connections of each element, which is directly related to the material cost. Also, remember that c_M represent the material cost $\left[\frac{\$}{kg}\right]$.

The objective function of equation (2.6) verifies the cost of each connection based on its rotational stiffness. Recently, Junior and Falcón (2019) also used this same expression to minimize costs of planar frames with geometric non-linearity, but adapted to account separately for the manufacturing costs of columns (material only) and beams (material and connections).

Xu and Grierson (1993) define the parameters V_0 and V_1 in such a way that the connection cost are limited by pinned and fully rigid cases, the cost of a pinned connection being lower than a fully rigid connection. By the polinomial degree characteristic, the connections cost has linear dependence on the material cost. In an example, for W-sections, Xu and Grierson (1993) assumed a suggestion informed by a published data (does not encountered) for the linear range of the additional connection cost, given by

$$0.25\rho_i A_i L_i \leq \left(\sum_{c=1}^{2}\left(V_0 + V_1 K_{r_c}\right)\right)_i \rho_i A_i L_i \leq 0.70\rho_i A_i L_i, \tag{2.7}$$

the cost of each element is increased by 25% if it is pinned and by 70% if it is fully rigid connected. Fig. 2.14 shows the linear variation of this additional cost, where AC is the percentage of additional cost of connections.

Figure 2.14 – Linear variation of the connections cost.

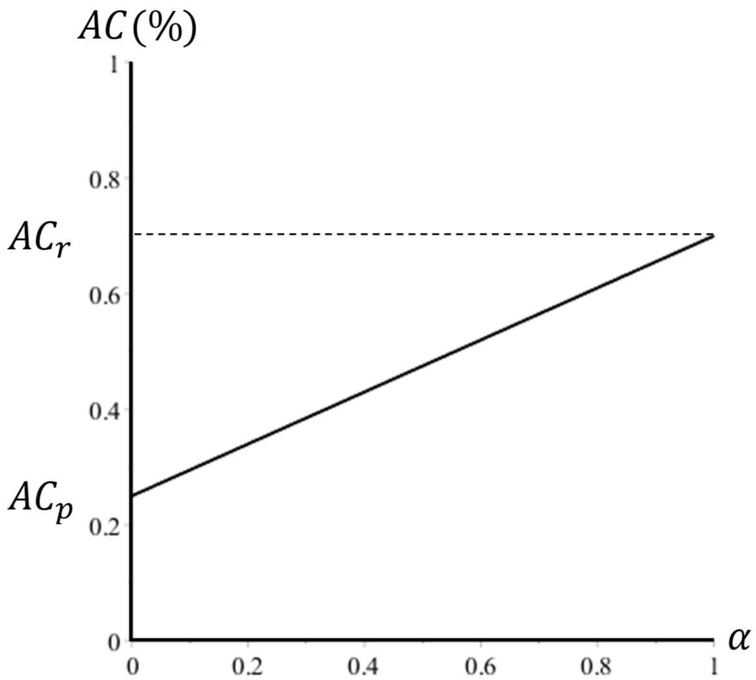

Source: Author's production.

Compared to rigid frames, Xu and Grierson (1993) observed that greater material cost minimization is sometimes achieved when considering semi-rigid connections, especially when vertical loadings imposed (external or self-weight) predominate, as the study presented in Fig. 2.15(a). This behavior is due to the reduction of the magnitude of the internal bending moment distribution caused by the flexibility of the connection.

Figure 2.15 – Structural problems treated by Xu and Grierson (1993): (a) a frame with recommended semi-rigid connections and (b) a frame with rigid connections as the best solution for minimal cost.

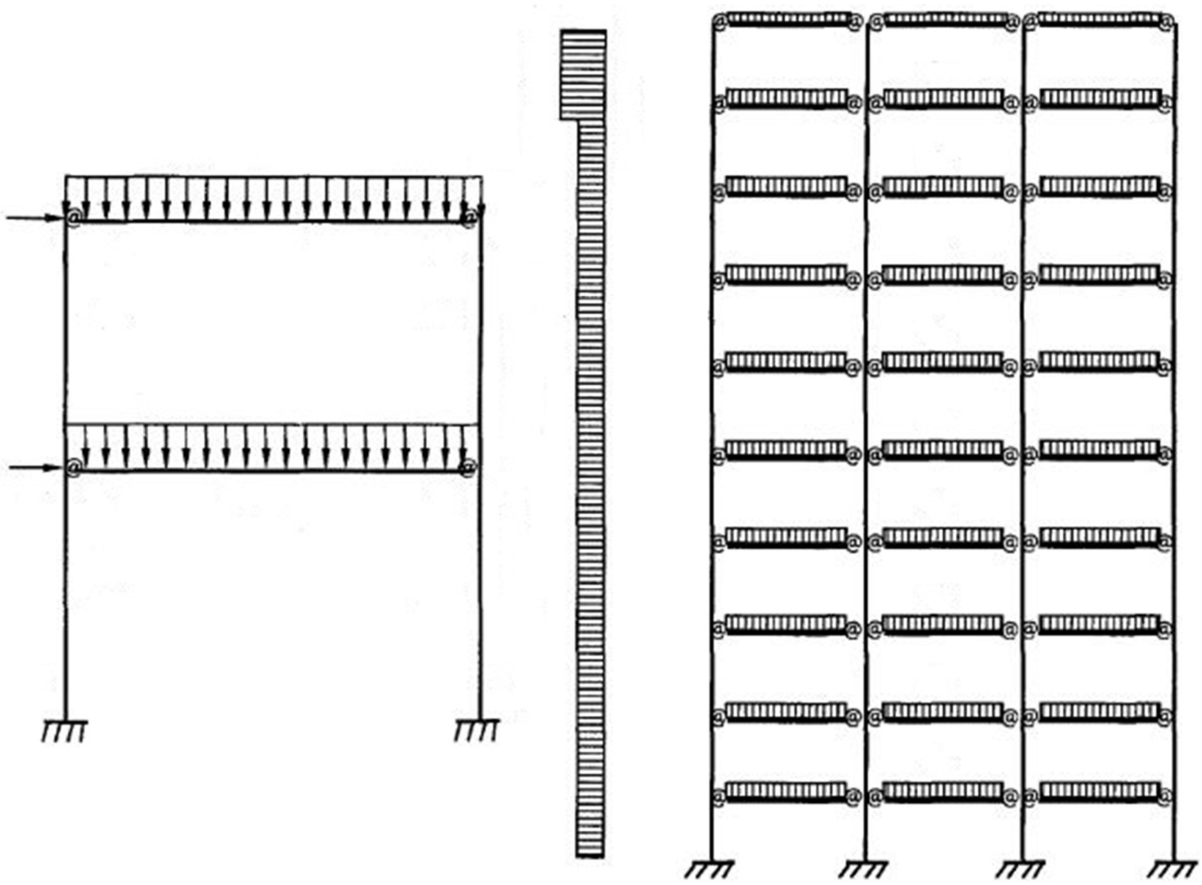

(a) (b)

Source: Adapted from Xu and Grierson (1993).

On the other hand, when a lateral load of considerable magnitude and lateral displacements constraints are assumed, as in the structure of Fig. 2.15(b), fully rigid connections are more recommended to provide greater lateral stiffness, especially in the sizing of the columns. As can be seen in Heringer (1996), semi-rigid connections tend to have larger horizontal displacements.

Csébfalvi (2007) dealt only with material cost minimization of planar frames, using discrete cross-section as design variables and displacement and stress constraints. Optimizing with distinct magnitudes of rotational stiffness, he noted a different effect in optimal solutions of different structural problems. While in one case rigid connections were recommended, in another case a better solution was achieved by semi-rigid connections. Both problems had lateral and vertical loads. Therefore, Csébfalvi (2007) concluded that the optimal solution may have a dependence on the fixed structural layout coupled with the load condition assumed.

Recently, the influence of semi-rigid connections is also investigated in Krystosik (2018), on structures subject to both vertical and lateral loads. The results obtained are compared with the results of a rigid frame. The author verified reduction of the internal bending moment distribution and critical buckling load in the columns but an increase in the lateral displacements of beam members.

Using different levels of fixity factors, Kartal *et. al.* (2010) analyzed planar frames with a distinct layout, semi-rigid connections and load aspects. First, assuming a frame with semi-rigid connections only at the foundations and subject to lateral and vertical loads, the authors evaluated the variation of lateral displacements, bending moment, shear and axial forces in the frame system. In this case, they noted that connections that are more rigid increased the bending moment in the columns of foundations, while the shear presented no variation. The axial forces also presented variation only at the bottom of the structure, with higher magnitudes when pinned connections are assumed. At the top of the frame, greater lateral displacement was observed for pinned connections.

In the second frame, semi-rigid connections are considered only in beam-to-column joints and lateral loads are applied. With pinned connections, the clamping region has the highest bending moments and the lowest axial forces. On the other hand, with fully rigid connections, this region is subject to the highest axial forces.

In the third case, a frame containing additional (related to the second frame) X-braced elements with semi-rigid connections presented an interesting result: no changes in the variations of the analyzed forces and lateral displacement, that is, the global structural behavior does not present variations although different stiffness levels of semi-rigid connections are assumed.

The last case study, shown in Fig. 2.16, consists of a truss system with semi-rigid connections between all the elements and subject to vertical and lateral loads. To the author's knowledge, this is the only work that investigated a case study with two or more elements connected to the same node. The results obtained demonstrate no change in the axial forces.

However, greater connections stiffness provided a decrease in vertical displacements and increases in the bending moment and shear force diagrams.

Figure 2.16 – Fourth case studied by Kartal *et. al.* (2010).

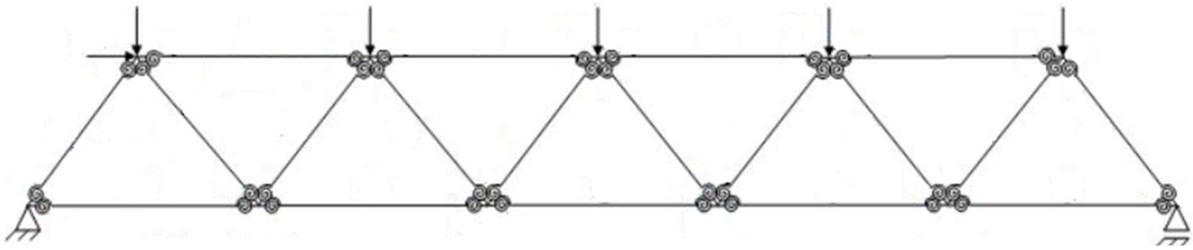

Source: Adapted from Kartal *et. al.* (2010).

Artar and Daloglu (2018) presented optimizations studies performed by a heuristic method coupled to a FEM software of space frames, with discrete W-sections as design variables and subject to lateral wind loads (see examples in Fig. 2.17). Each optimization process is developed with fixed and distinct semi-rigid connections, similar to the approach applied by Csébfalvi (2007).

Figure 2.17 – Space frames investigated by Artar and Daloglu (2018).

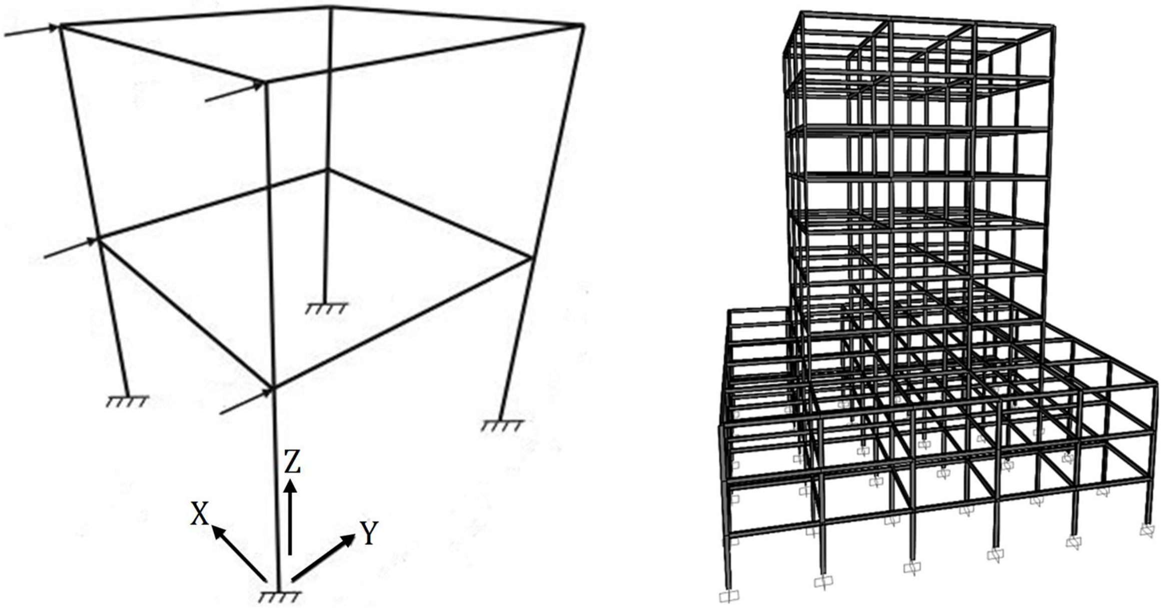

Source: Adapted from Artar and Daloglu (2018).

According to the results obtained, the structures with semi-rigid connections obtained less material cost minimization mainly due to the increase of the lateral displacements of the structure, caused by the reduction of the lateral stiffness. Consequently, the cross-section profiles are increased to overcome the absence of the lateral stiffness.

Simões (1996) developed a study similar to Xu and Grierson (1993), but modified the previous objective function formulation of the equation (2.6) to

$$W = \sum_{i=1}^{nel} \left(c_{M_i} \rho_i A_i L_i + \left(\sum_{c=1}^{2} (V_0 + V_1 \alpha_c + V_2 {\alpha_c}^2) \right)_i c_{M_i} \rho_i A_i L_i \right), \tag{2.8}$$

using fixity factors as continuous design variables and imposing the parameter V_2 to assume additional connections cost with quadratic dependence on the material cost.

Considering IPE cross-sections for the beams, Simões (1996) assumed that the cost is increased by 20% for pinned connections and 60% for fully rigid connections, that is

$$0.20 \rho_i A_i L_i \leq \left(\sum_{c=1}^{2} (V_0 + V_1 \alpha_c + V_2 {\alpha_c}^2) \right)_i \rho_i A_i L_i \leq 0.60 \rho_i A_i L_i. \tag{2.9}$$

As Xu and Grierson (1993), Simões (1996) also assumed the cost of a pinned connection being lower than a fully rigid connection. To the author's knowledge, this is the only research that proposes the use of quadratic variation of the connections cost. Simões (1996) argues that the adoption of this type of variation provides greater accuracy on the prediction of the additional cost of connections. However, there is no standard procedure described for defining the constant coefficients.

Analyzing mathematically, it was possible to note that the quadratic variation adopted by Simões (1996) has the pattern visualized in Fig. 2.18. With this convex configuration, Simões (1996) assumes that the cost of semi-rigid connections of up to 0.60 is less than the cost of pinned or fully rigid connections. Therefore, as expected, the results obtained by the author in two case studies show optimal semi-rigid connections with intermediate values of this interval, since not only do these semi-rigid connections offer greater lateral stiffness so that the structures do not violate the imposed displacement constraints, but also by the lower cost associated. The author does not justify this proposal for additional costs.

Developing these two case studies, which had vertical and lateral loads and lateral displacement and stress constraints, Simões (1996) noted that optimal solutions that account for semi-rigid connections are lighter than the optimal solutions achieved by frames with fixed fully rigid connections. However, in this case, as already evidenced, this is directly related to the curve adopted for the variation of the connections cost.

Figure 2.18 – Specific quadratic variation adopted by Simões (1996).

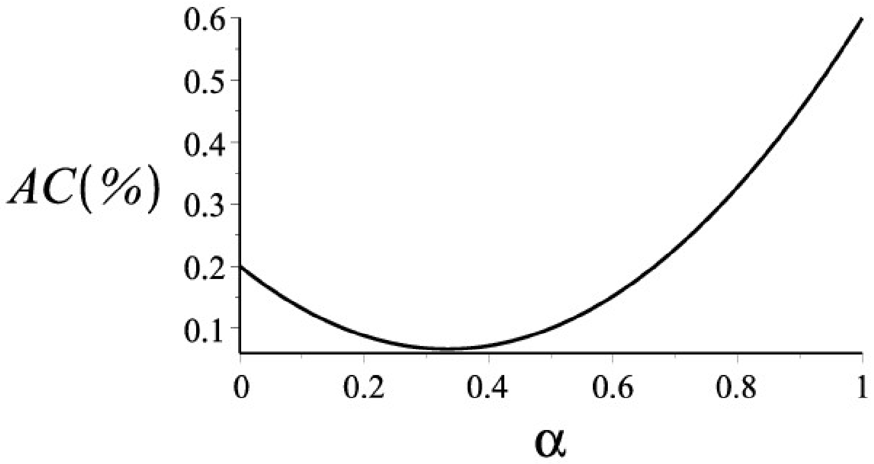

Source: Author’s production.

Returning to the context of the studies developed by Csébfalvi (2007) and Artar and Daloglu (2018), note that the conflicting result achieved by Simões (1996) – lightweight structures with semi-rigid connections even with lateral loads and displacement constraints – may depend on the range and variation of the connections cost and the type of problem analyzed, relative to the different geometric properties of the cross-sections assumed, the fixed structural layout or even the magnitude ratio between the lateral and vertical loads applied. Also, it may be related to how design variables represent the semi-rigid connections (continuous or discrete values, fixity factors or rotational stiffness).

Interesting results were also obtained by researchers that used nonlinear models for the connections, about the effect of semi-rigid connections on the structural behavior.

Sekulovic and Salatic (2001) studied the effects of flexible connections in planar frames with geometric nonlinearity, adopting a nonlinear connection model. The authors observed that with increased stiffness on the connections, the lateral displacement at beam members and the bending moment at the column-base are reduced. In a particular case developed without geometric nonlinearity, the structural behavior was similar for different load levels. Considering another nonlinear connection model, Pinheiro and Silveira (2005) investigated the same structural problems and achieved similar results.

Cabrero and Bayo (2005) developed a methodology to elastic and plastic practical design of semi-rigid frames. Through this procedure, the authors observed that the cost estimation of semi-rigid frames is smaller compared to frames with pinned or fully rigid connections.

Hayalioglu and Degertekin (2005) used genetic algorithm and the same approach of Xu and Grierson (1993) for the connections cost dependence with material cost, but semi-rigid connections of beam-to-column and column-base were treated separately in the objective function. Only discrete W-sections are assumed as design variables. With lateral displacement and stress constraints of standard specifications and structures subject to vertical and lateral loads, the authors reached the same behavior of lateral displacement and cost minimization observed by Xu and Grierson (1993).

Also based on a genetic algorithm, Ali *et. al.* (2009) formulated an optimization problem configured with discrete cross-sections, beam-to-column and column-base connections as design variables. As mentioned in the beginning of this chapter, a different objective function was assumed by these authors, containing four types of costs: material, manufacturing, erection and foundation costs.

Compared to traditional frame design, frames with semi-rigid connections in the approach of Ali *et. al.* (2009) have a greater cost reduction, mainly obtained in manufacturing and erection costs. In addition, the better distribution of internal bending moments decreases the cost related to the foundation and less structural weight is achieved. Besides, the authors noted that connections cost may represent more than 20% of the total cost of a steel frame.

Truong *et. al.* (2017) optimized space frame using discrete cross-section areas and semi-rigid connections as design variables. As well as in Artar and Daloglu (2018), it became evident the need to increase the cross-section profiles to provide lateral stiffness when lateral loads are considered. In addition, comparing optimization processes that used only one type of semi-rigid connection with a process that used mixed semi-rigid connections, all constant during the processes, Truong *et. al.* (2017) also observed that the space frame with mixed connections had better performance in mass minimization. However, on a construction point of view, the authors concluded that it is more prudent to use only one type of semi-rigid connection.

All these contributions show that, in structural optimization, is extremely important to take into consideration that with a connection model that poorly represents the physical phenomenon, perhaps the final optimal solution will not be able to realistically respect the imposed design constraints.

While the 3D frame element formulation procedure is presented in Chapter 3, the formulation of the optimization problem is found in Chapter 5. The results obtained are presented and discussed in Chapter 6. In the next section, after presenting different failure criteria already developed and applied in structural optimization surveys, specific failure criteria for tubular elements are displayed and analyzed.

2.5 Failure Criteria

Considering truss or frame elements, as explained in Vanderplaats and Salajegheh (1989), it is preferable to treat stress as a function of internal forces, in order to ease the necessary derivation to apply stress constraints within gradient-based methods. As the internal forces can be approximated with respect to section properties and other parameters that can be design variables, the authors demonstrated that this procedure provides computational efficiency within the optimization process, due to the reduction in the level of nonlinearity of the stress functions. In addition, the use of section properties is a technical advantage since most of them are physical variables commonly treated in the engineering practice.

Researchers such as Sheu and Schmit Jr. (1971), Saka (1990), Sant'Anna *et. al.* (2001) and Pedersen and Nielsen (2003) adopted the axial stress failure criterion as design constraint in truss optimization. On the topology optimization field, Hagishita and Ohsaki (2009) and He and Gilbert (2015) used this strategy directly in the tensile and compressive forces.

Pedersen and Nielsen (2003) inserted the axial stress constraint using Danish standards for specific cross-section profiles and adding buckling constraint. Saka (1990) developed a similar treatment, adhering to the United States and German standards specific to steel trusses. Most countries have standards which specify the allowable stress level that needs to be satisfied in structural design (PEDERSEN; NIELSEN, 2003).

While bar elements have mechanical resistance evaluated simply through the transmitted axial stress component at each element, frame elements have stresses associated to axial, bending, shear and torsion internal forces, with different distributions and critical cross-section points. Therefore, in order to determine the point that has the highest equivalent stress in a frame element, it is recommended to perform a detailed analysis of the stress state at several points of a given cross-section along the longitudinal axis of each element (CARNIEL *et. al.*, 2008).

Moses and Onoda (1969) studied frames composed by beam members subject to concentrated and distributed loads, assuming the bending stress as design constraint based in the British standard. Xu and Grierson (1993) used the same approach but considering bending moments affected by the effect of semi-rigid connections.

Pedersen e Jørgensen (1984) also disregarded the shear effects and defined a failure criterion based on the calculation of von Mises stress in the one-dimensional stress state, considering only the normal stresses produced by axial forces N_x and bending moments M_z ($\tilde{x}\tilde{y}$ plane) and specifically at the top and bottom extremities of the desirable cross-sections. Simões (1996) assumed the same failure criterion, but in IPE sections and, just as Xu and Grierson (1993), imposing the effect of semi-rigid connections. Csébfalvi (2007) also used a similar approach, but both normal stresses related to N_x and M_z are divided by an allowable stress and the sum cannot exceed a unitary value. In Havelia (2016), the normal stress produced by the bending moment M_y ($\tilde{x}\tilde{z}$ plane) is also computed and the extreme case is considered, where the three normal stresses are summed.

In the context of space frames, Hayalioglu and Degertekin (2005) and Artar and Daloglu (2018) respect requirements defined by the manual of steel construction developed by the AISC. Sagiroglu and Aydin (2015) design space frames based on combined stress constraints detailed in the Turkish Building Code for Steel Structures.

In the research of Yoshida and Vanderplaats (1988) four extremities points in rectangular and I-profiles, at the ends of the elements, are evaluated by the von Mises equivalent stress measured by normal and shear stresses associated with all the internal forces of a 3D frame element. However, more detailed information is not available, since the authors make use of "black-box" (designation used by the authors) in FEA and optimization.

Specific for 3D tubular thin-wall elements subject to any combination of all possible internal forces, Sergeyev and Pedersen (1996) also presented a failure criterion based on equivalent stress σ_{eq}. The criterion is given by the stress calculation referring to the hypotheses of Tresca ($S = 4$) or von Mises ($S = 3$) in the form

$$\sigma_{eq_{i,k}}(\tilde{x}, \tilde{y}, \tilde{z}) = \sqrt{{\sigma_{xx}}_{i,k}^{\;2} + S{\tau_{yz}}_{i,k}^{\;2}}, \tag{2.10}$$

where σ_{xx} and τ_{yz} represent the normal and shear stresses, respectively, and the index k represent any cross-section along the element length. Note that the stress calculation is dependent of the three local coordinates $\tilde{x}, \tilde{y}$ and $\tilde{z}$ of the element. This criterion was also used by Sergeyev and Mróz (2000). It is observed that when considering the normal stresses together with the shear stresses, is necessary to determine the location of the most critical point, both along the longitudinal $\tilde{x}$-axis and in the cross-section plane $\tilde{y}\tilde{z}$. This process can be computationally intensive.

To reduce complexity and computational cost in layout optimization, Carniel *et. al.* (2008) have proposed an alternative failure criterion that does not investigate the stress state and is given by

$$\left|\frac{N_{x_{i,k}}}{N_{x_{alw}}}\right| + \left|\frac{V_{y_{i,k}}}{V_{y_{alw}}}\right| + \left|\frac{V_{z_{i,k}}}{V_{z_{alw}}}\right| + \left|\frac{M_{x_{i,k}}}{M_{x_{alw}}}\right| + \left|\frac{M_{y_{i,k}}}{M_{y_{alw}}}\right| + \left|\frac{M_{z_{i,k}}}{M_{z_{alw}}}\right| \leq 1, \tag{2.11}$$

where V_y and V_z are the shear forces in $\tilde{y}$ and $\tilde{z}$ directions, M_x is the torsion in the $\tilde{y}\tilde{z}$ plane and $N_{x_{alw}}$, $M_{y_{alw}}$, $M_{z_{alw}}$, $V_{y_{alw}}$, $V_{z_{alw}}$ and $M_{x_{alw}}$ are allowable values for, respectively, the axial force, the bending moments, the shear forces and torsion, which cause failure in a given cross-section of the element when acting individually. As design constraint, the criterion is applied at the ends and the center of the element length.

The failure criterion of Carniel *et. al.* (2008) assumes the worst case of a combined solicitation, where all stresses intensify. The conservatism of this strategy may decrease the effectiveness of the design constraint.

In the Brazilian standard ABNT NBR 8800 (2008), there is a specific section for tubular elements with circular cross-section. When the torsion is greater than 20% of the allowable torsion, the following equation is recommended

$$\left(\frac{N_{x_{i,k}}}{N_{x_{alw}}} + \frac{M_{y_{i,k}}}{M_{y_{alw}}} + \frac{M_{z_{i,k}}}{M_{z_{alw}}}\right) + \left(\frac{V_{y_{i,k}}}{V_{y_{alw}}} + \frac{V_{z_{i,k}}}{V_{z_{alw}}} + \frac{M_{x_{i,k}}}{M_{x_{alw}}}\right)^2 \leq 1. \tag{2.12}$$

Note that the failure criterion of equation (2.12) is slightly less conservative than the criterion of Carniel *et. al.* (2008), enabling combinations of internal forces with higher magnitudes, positive or negative (different signals, i.e. directions). Greater weight is given to the internal forces that produce normal stresses. However, when internal forces that produce the same type of stress (normal or shear) have the same signals, it still allows only one internal force with magnitude of the respective critical internal force.

Using the reference system shown in Fig. 2.19, Irles and Irles (2001) presented elastic interaction diagrams for the case where the cross-section is submitted simultaneously to shear, bending and torsion internal forces.

Figure 2.19 – Reference system of Irles and Irles (2001).

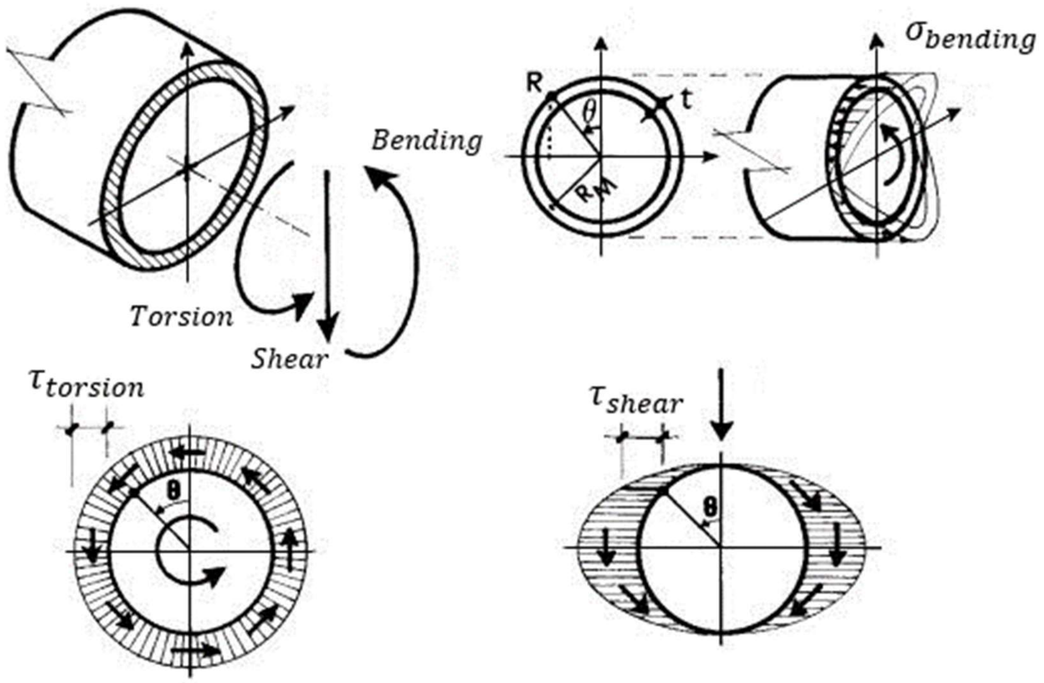

Source: Adapted from Irles and Irles (2001).

As the critical equivalent stress in this type of cross-section is encountered necessarily in the outer radius, Irles and Irles (2001) characterized the stress distributions associated with each internal force as a function of the angular position θ. Then, they used the von Mises failure criterion to formulate the stress calculation $f(\theta)$ and the subsequent global surfaces of elastic interaction. Therefore,

$$\sigma_{M_{y\,i,k}} = \frac{M_{y\,i,k} R_i \cos\theta_{i,k}}{I_i}, \qquad \tau_{V_{z\,i,k}} = \frac{V_{z\,i,k} {R_{m}}_i^{\,2} \sin\theta_{i,k}}{I_i}, \qquad \tau_{M_{x\,i,k}} = \frac{M_{x\,i,k} R_i}{J_i}, \tag{2.13}$$

$$f(\theta)_{i,k} = \sqrt{{\sigma_{M_{y\,i,k}}}^2 + 3\left(\tau_{V_{z\,i,k}} + \tau_{M_{x\,i,k}}\right)^2}, \tag{2.14}$$

$$f(\theta)_{i,k} \leq \sigma_e, \tag{2.15}$$

where R is the outer radius, R_m is the midline radius, σ_e is the yield stress (allowable), σ_{M_y} is the normal bending stress at the local $\tilde{y}$-axis, τ_{V_z} and τ_{M_x} are shear stresses of the shear force V_z and torsion M_x, respectively. Both shear stresses are tangential to the outer radius and therefore can be summed.

After developing the elastic interaction diagrams, Irles and Irles (2001) identified that it is possible to determine the critical stress point when the bending moment and the shear force coexist in the cross-section.

As the works of Sergeyev and Pedersen (1996) and Carniel *et. al.* (2008) proved the need to combine computational efficiency and effectiveness in a stress-based failure criterion to optimize layout of space frames, the von Mises stress evaluation strategy developed by Irles and Irles (2001) can be beneficial to solve these limitations. Thus, it will be explored in Chapter 4, where the new procedure to calculate the von Mises failure criterion of tubular elements is presented. Hereafter, the case studies presented in Chapter 6 demonstrate the importance of considering this failure criterion as a stress constraint within the layout optimization.

Chapter 3

Formulation of the Semi-Rigid Frame Element

This chapter presents all the formulations developed to comply with the scope of the research. To begin, the following initial hypotheses were assumed:

- Space frames subject to small displacements and strains;
- Each element has two connections, one at each end, and the connections have rotational stiffness in the $\tilde{x}\tilde{y}$ and $\tilde{x}\tilde{z}$ (local) planes of bending.

Initially, the 3D frame finite element with semi-rigid connections is formulated using the direct method, determining the interpolation functions and the local stiffness matrix of the element. Then, applying the interpolation functions, the consistent nodal loads are determined in the case of a uniformly distributed load over the length of a given element. Finally, the calculation procedure of the internal forces is presented.

3.1 3D Frame Finite Element

The initial procedure for calculating nodal displacements $\boldsymbol{U}$ of a structure is given by the numerical resolution of the equilibrium equation,

$$\mathbf{K}\boldsymbol{U} = \boldsymbol{F}, \tag{3.1}$$

where $\mathbf{K}$ is the global stiffness matrix and $\boldsymbol{F}$ is the load vector.

Once the global displacements are known, internal forces and stresses can be determined by formulations that will be presented.

Unlike trusses which have pinned connections between the structural components, frames are characterized by having a union of the components by welded and bolted connections. When subjected to any external loads, these types of connections are responsible not only for the transmission of axial force between the components but also bending moments, shear forces and torsion.

Extrapolating the above concept to FEM, the 3D frame element is a line finite element that has two nodes and contains six DOF per node, associated to three translational and three rotational, which are: u, v and w (translation) and θ_x, θ_y and θ_z (rotation) in global x, y and z axes, respectively. Each node has six internal forces, being an axial (N_x) and a torsion (M_x) on the $\tilde{x}$-axis and two shears (V_y and V_z) and two bending moments (M_y and M_z) on the $\tilde{y}$ and $\tilde{z}$ axes, respectively. All these nodal parameters are shown in Fig. 3.1.

Figure 3.1 – Nodal parameters of a 3D frame element.

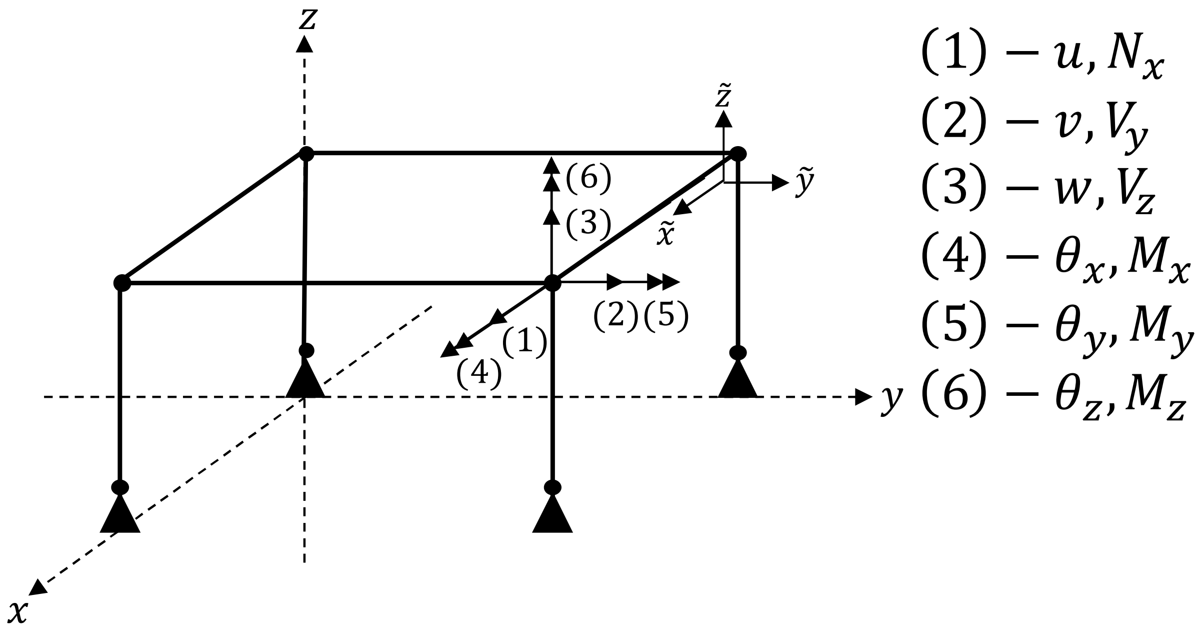

Source: Author's production.

According to the number of DOF, the element stiffness matrix $\mathbf{K_L}$ in the local reference system has a $12x12$ dimension. To represent it in the global reference system, i.e. $\mathbf{K_G}$, the transformation matrix **T** is applied, which has the same dimension and is constructed through the sub-matrix $\mathbf{\Omega}$ referring to the direction cosines of the arbitrary local reference system in relation to the global reference system. Thus,

$$\boldsymbol{\Omega} = \begin{bmatrix} l_{o\tilde{x}} & m_{o\tilde{x}} & n_{o\tilde{x}} \\ l_{o\tilde{y}} & m_{o\tilde{y}} & n_{o\tilde{y}} \\ l_{o\tilde{z}} & m_{o\tilde{z}} & n_{o\tilde{z}} \end{bmatrix}, \qquad \mathbf{T} = \begin{bmatrix} \boldsymbol{\Omega} & 0 & 0 & 0 \\ 0 & \boldsymbol{\Omega} & 0 & 0 \\ 0 & 0 & \boldsymbol{\Omega} & 0 \\ 0 & 0 & 0 & \boldsymbol{\Omega} \end{bmatrix}, \tag{3.2}$$

$$\mathbf{K_G} = \mathbf{T}^{\mathrm{T}}\mathbf{K_L}\mathbf{T}, \tag{3.3}$$

where $l_{o\tilde{x}}$, $m_{o\tilde{x}}$ e $n_{o\tilde{x}}$ represent the direction cosines of the local $\tilde{x}$-axis of the element in relation to the global coordinate system. The same is valid for the local $\tilde{y}$ and $\tilde{z}$ axes. Details about the direction cosines can be found in Chandrupatla and Belegundu (2002).

To formulate the 3D frame finite element, the linear mathematical model is adopted. As can be seen in Fig. 3.2, the model is extended to space frames adding two rotational springs at each connection, related to the two planes $\tilde{x}\tilde{y}$ (K_{r_z}) and $\tilde{x}\tilde{z}$ (K_{r_y}) that have the bending moments M_z and M_y and the rotations θ_z and θ_y, respectively.

Figure 3.2 – 3D frame element with semi-rigid connections.

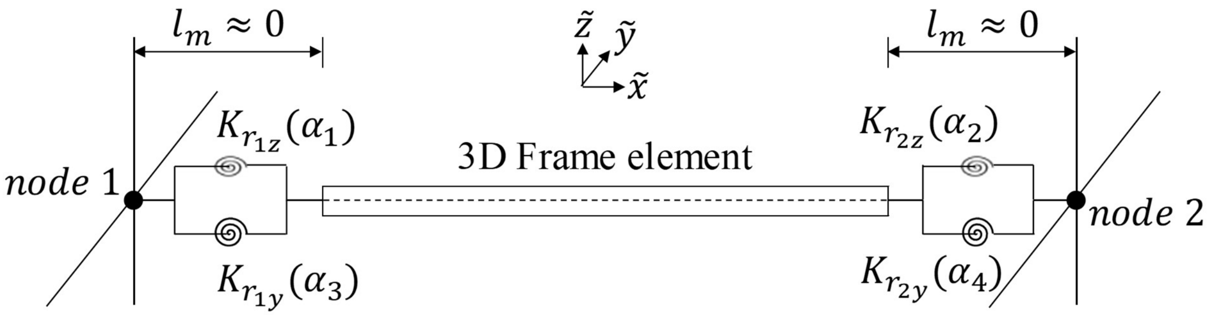

Source: Adapted from Chan and Chui (2000).

The formulation is valid for any type of connection, i.e. beam-to-column, beam-to-beam and column-base. Also, to facilitate the representation of the semi-rigid connections, both springs having rotational stiffness in the $\tilde{x}\tilde{y}$ and $\tilde{x}\tilde{z}$ planes are represented by the symbol of a single spring (see Fig. 3.3).

Figure 3.3 – Spring for both rotational stiffness in $\tilde{x}\tilde{y}$ and $\tilde{x}\tilde{z}$ planes.

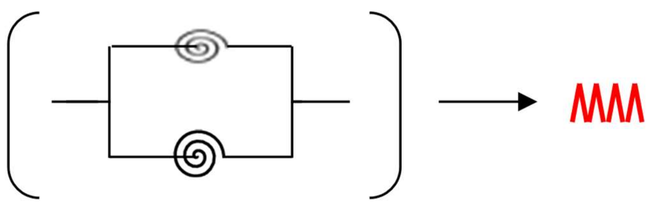

Source: Author's production.

To begin the procedure to formulate the one-dimensional finite element, consider the 3D frame element with semi-rigid connections shown in Fig. 3.2. According to Figs. 3.4 and 3.5, respectively, the element has length L and translations and rotations in in $\tilde{x}\tilde{y}$ and $\tilde{x}\tilde{z}$ planes. The free body diagrams of Figs. 3.4 and 3.5 also demonstrate the signal convention of the local reference system adopted for the DOF and internal forces, consistent with Fig. 3.1.

Figure 3.4 – Signal convention for the local reference system, the DOF and internal forces in $\tilde{x}\tilde{y}$ plane.

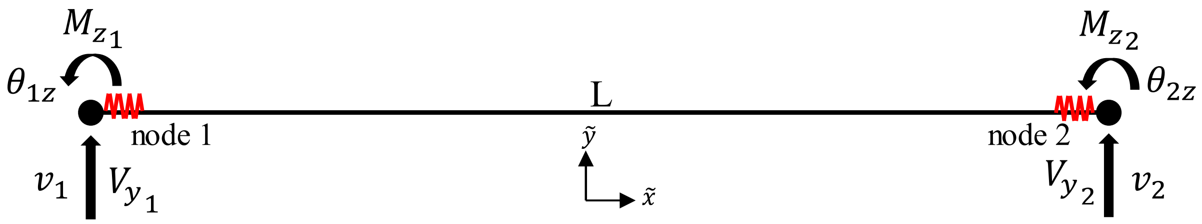

Source: Author’s production.

Figure 3.5 – Signal convention for the local reference system, the DOF and internal forces in $\tilde{x}\tilde{z}$ plane.

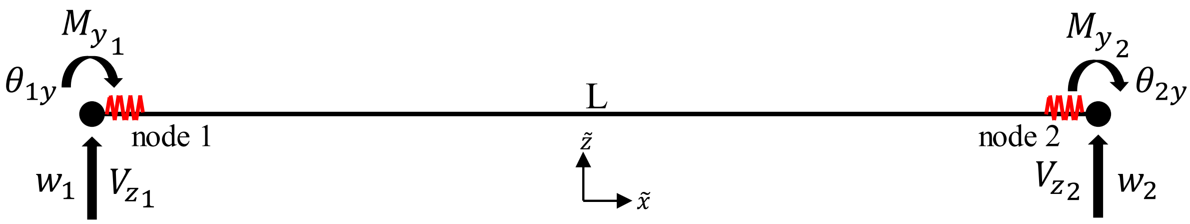

Source: Author’s production.

The thin-wall circular cross-section is considered, allowing simplification by the symmetry of the moments of inertia around the y and z axes (I_y and I_z) for the moment of inertia around the neutral line (I).

Based on the direct method, the terms $k_{a,b}$ of the stiffness matrix of any finite element can be physically interpreted as the necessary force in the DOF "a" to promote a unitary displacement in the DOF "b".

By making a cut in any place within the length of the element, it is known that the expression of the internal bending moments in $\tilde{x}\tilde{y}$ and $\tilde{x}\tilde{z}$ planes, as a function of a local coordinate $\tilde{x}$ along the length, as can be seen in Figs. 3.6(a-b), are represented by

$$(a)\sum M_{oz} = 0\ (\curvearrowleft +), \qquad (b)\sum M_{oy} = 0\ (\curvearrowleft +), \tag{3.4}$$

$$M_{oz}(\tilde{x}) + M_{z_1} - V_{y_1}\tilde{x} = 0, \qquad M_{oy}(\tilde{x}) - M_{y_1} - V_{z_1}\tilde{x} = 0, \tag{3.5}$$

$$M_{oz}(\tilde{x}) = -M_{z_1} + V_{y_1}\tilde{x}, \qquad M_{oy}(\tilde{x}) = M_{y_1} + V_{z_1}\tilde{x}. \tag{3.6}$$

Figure 3.6 – Internal bending moments in the (a) $\tilde{x}\tilde{y}$ and (b) $\tilde{x}\tilde{z}$ planes.

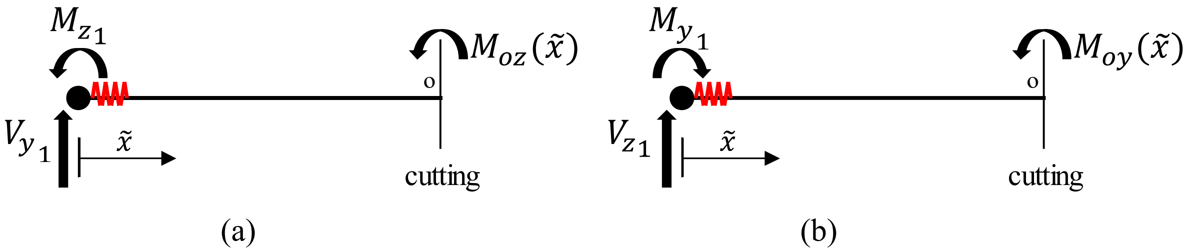

Source: Author's production.

Then, by static equilibrium,

$$(a)\sum M_{2z} = 0\ (\curvearrowleft +), \qquad (b)\sum M_{2y} = 0\ (\curvearrowright +), \tag{3.7}$$

$$M_{z_1} + M_{z_2} - V_{y_1}L = 0, \qquad M_{y_1} + M_{y_2} + V_{z_1}L = 0. \tag{3.8}$$

$$(a)\sum V_y = 0\ (\uparrow +), \qquad (b)\sum V_z = 0\ (\uparrow +), \tag{3.9}$$

$$V_{y_1} + V_{y_2} = 0, \qquad V_{z_1} + V_{z_2} = 0. \tag{3.10}$$

Considering that the beam stiffness EI is constant throughout the length, the two expressions given by equation (3.6a) and equation (3.6b) are applied in equation (3.11) of the Euler-Bernoulli model,

$$\frac{d^2v(\tilde{x})}{d\tilde{x}^2} = \frac{M(\tilde{x})}{EI}, \tag{3.11}$$

and defining the boundary conditions that separately represent the four possible cases of unitary displacements in the DOF of each plane, we can define the necessary internal forces to produce such displacements. Therefore, by analogy of the direct method, the terms of the stiffness matrix of the element are defined. It is noteworthy that the rotations ϕ, and consequently the resulting fixity factors, are always aligned with local axes of the element.

The four cases of the $\tilde{x}\tilde{y}$ plane are characterized in Fig. 3.7 and Tables 3.1 and 3.2 represent the four cases of the $\tilde{x}\tilde{y}$ and $\tilde{x}\tilde{z}$ planes. Note that the procedure is done separately for each plane, and each curve represents the interpolation functions $N^{v_{xoy}}$ and $N^{v_{xoz}}$. The rotations ϕ in all cases are represented by the equation (2.1), with the associated rotational stiffness and bending moment, and the signal is related to the local reference system.

Figure 3.7 – Cases to define the $k_{a,b}$ terms in the $\tilde{x}\tilde{y}$ plane.

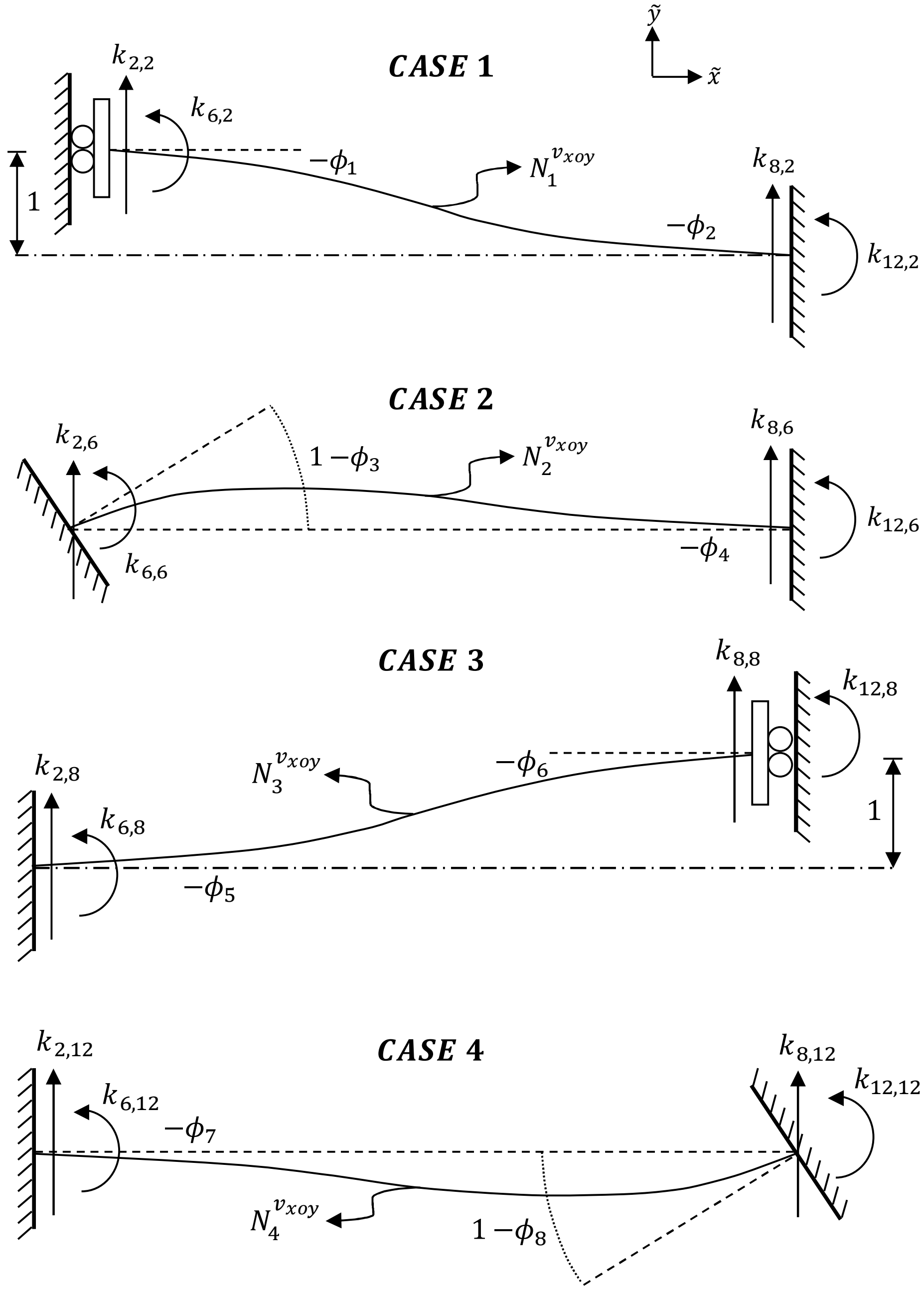

Source: Author’s production.

Table 3.1 – Necessary boundary conditions in $\tilde{x}\tilde{y}$ plane.

Boundary conditions:	Case 1 $v_1 = 1$	Case 2 $\theta_{1z} = 1$	Case 3 $v_2 = 1$	Case 4 $\theta_{2z} = 1$
$\boldsymbol{\theta_{1z}(\tilde{x} = 0)}$	$0 - \phi_1$	$1 - \phi_3$	$0 - \phi_5$	$0 - \phi_7$
$\boldsymbol{\theta_{2z}(\tilde{x} = L)}$	$0 - \phi_2$	$0 - \phi_4$	$0 - \phi_6$	$1 - \phi_8$
$\boldsymbol{v_1(\tilde{x} = 0)}$	1	0	0	0
$\boldsymbol{v_2(\tilde{x} = L)}$	0	0	1	0

Source: Author's production.

Table 3.2 – Necessary boundary conditions in $\tilde{x}\tilde{z}$ plane.

Boundary conditions:	Case 5 $w_1 = 1$	Case 6 $\theta_{1y} = -1$	Case 7 $w_2 = 1$	Case 8 $\theta_{2y} = -1$
$\boldsymbol{\theta_{1y}(\tilde{x} = 0)}$	$0 + \phi_9$	$-1 + \phi_{11}$	$0 + \phi_{13}$	$0 + \phi_{15}$
$\boldsymbol{\theta_{2y}(\tilde{x} = L)}$	$0 + \phi_{10}$	$0 + \phi_{12}$	$0 + \phi_{14}$	$-1 + \phi_{16}$
$\boldsymbol{w_1(\tilde{x} = 0)}$	1	0	0	0
$\boldsymbol{w_2(\tilde{x} = L)}$	0	0	1	0

Source: Author's production.

To illustrate, the calculation procedure for case 1 described in Table 3.1 is demonstrated. The other cases are solved by a similar treatment.

Applying the Euler-Bernoulli model of equation (3.11) in equation (3.6a) and integrating twice,

$$\theta_z(\tilde{x}) = \frac{1}{EI}\left(\frac{V_{y_1}\tilde{x}^2}{2} - M_{z_1}\tilde{x} + C_1\right), \tag{3.12}$$

$$v(\tilde{x}) = N_1{}^{v_{xoy}} = \frac{1}{EI}\left(\frac{V_{y_1}\tilde{x}^3}{6} - \frac{M_{z_1}\tilde{x}^2}{2} + C_1\tilde{x} + C_2\right), \tag{3.13}$$

we find the equations representing the rotation $\theta_z(\tilde{x})$ and the vertical translation $v(\tilde{x})$ in any arbitrary point $\tilde{x}$ along the element length. Moreover, after the determination of the expressions of the unknown variables V_{y_1}, M_{z_1}, C_1 and C_2, equation (3.13) represents the interpolation function $N_1{}^{v_{xoy}}$ of the case 1. The other interpolation functions are found analogously.

With equations (3.12) and (3.13) of the rotation and elastic line, and equations (3.8a) and (3.10a) of static equilibrium, there are six unknowns in the problem: the four internal forces of the extremities and the constants C_1 and C_2. Recalling expression (2.1) for the rotations ϕ

and equation (2.4) for the rotational stiffness K_r at the extremities of the element, the boundary conditions of case 1 are imposed in equations (3.12) and (3.13). By making possible simplifications,

$$\begin{gathered}
\left(\frac{(1-\alpha_1)L}{3EI\alpha_1}\right)M_{z_1}+\left(\frac{1}{EI}\right)C_1=0,\\
\left(\frac{L^2}{2EI}\right)V_{y_1}+\left(-\frac{L}{EI}\right)M_{z_1}+\left(\frac{(1-\alpha_2)L}{3EI\alpha_2}\right)M_{z_2}+\left(\frac{1}{EI}\right)C_1=0,\\
\left(\frac{1}{EI}\right)C_2=1,\\
\left(\frac{L^3}{6EI}\right)V_{y_1}+\left(-\frac{L^2}{2EI}\right)M_{z_1}+\left(\frac{L}{EI}\right)C_1+\left(\frac{1}{EI}\right)C_2=0.
\end{gathered} \tag{3.14}$$

Grouping the system of equation (3.14) with the equations (3.8a) and (3.10a) of static equilibrium, the result is a linear system with six unknowns and the same amount of equations, given as follows

$$\begin{gathered}
(0)V_{y_1}+(0)V_{y_2}+\left(\frac{(1-\alpha_1)L}{3EI\alpha_1}\right)M_{z_1}+(0)M_{z_2}+\left(\frac{1}{EI}\right)C_1+(0)C_2=0,\\
\left(\frac{L^2}{2EI}\right)V_{y_1}+(0)V_{y_2}+\left(-\frac{L}{EI}\right)M_{z_1}+\left(\frac{(1-\alpha_2)L}{3EI\alpha_2}\right)M_{z_2}+\left(\frac{1}{EI}\right)C_1+(0)C_2=0,\\
(0)V_{y_1}+(0)V_{y_2}+(0)M_{z_1}+(0)M_{z_2}+(0)C_1+\left(\frac{1}{EI}\right)C_2=1,\\
\left(\frac{L^3}{6EI}\right)V_{y_1}+(0)V_{y_2}+\left(-\frac{L^2}{2EI}\right)M_{z_1}+(0)M_{z_2}+\left(\frac{L}{EI}\right)C_1+\left(\frac{1}{EI}\right)C_2=0,\\
(-L)V_{y_1}+(0)V_{y_2}+M_{z_1}+M_{z_2}+(0)C_1+(0)C_2=0,\\
V_{y_1}+V_{y_2}+(0)M_{z_1}+(0)M_{z_2}+(0)C_1+(0)C_2=0.
\end{gathered} \tag{3.15}$$

Solving the linear system (3.15),

$$\begin{aligned} V_{y_1} = k_{2,2} &= \frac{12EI}{L^3}\left(\frac{\alpha_1+\alpha_2+\alpha_1\alpha_2}{4-\alpha_1\alpha_2}\right), \\ M_{z_1} = k_{6,2} &= \frac{6EI}{L^2}\left(\frac{2\alpha_1+\alpha_1\alpha_2}{4-\alpha_1\alpha_2}\right), \\ V_{y_2} = k_{8,2} &= -\frac{12EI}{L^3}\left(\frac{\alpha_1+\alpha_2+\alpha_1\alpha_2}{4-\alpha_1\alpha_2}\right), \\ M_{z_2} = k_{12,2} &= \frac{6EI}{L^2}\left(\frac{2\alpha_2+\alpha_1\alpha_2}{4-\alpha_1\alpha_2}\right), \\ C_1 &= \frac{2EI}{L}\left(\frac{2\alpha_1-\alpha_2+\alpha_1\alpha_2-2}{4-\alpha_1\alpha_2}\right), \\ C_2 &= EI, \end{aligned} \tag{3.16}$$

fours terms $k_{a,b}$ are defined. Developing an analogous procedure for the other cases, all the terms related to beam DOF at the $\tilde{x}\tilde{y}$ and $\tilde{x}\tilde{z}$ planes can be found.

Improving the Euler-Bernoulli model with Timoshenko's theory, consider that ζ_y and ζ_z are correction factors to impose the shear effect in deflection of the $\tilde{x}\tilde{y}$ and $\tilde{x}\tilde{z}$ planes. The correction factors depend on the type of cross-section considered and the effective shear areas in both directions. For circular sections, these two factors can be simplified to a single factor ζ because the effective area will be the same. More details about the inclusion of these factors on the stiffness matrix can be found in Filho (2000).

The bar and shaft elements formulations, described in Cardoso *et. al.* (2007), are inserted by superposition to add the DOF of translation and rotation in the $\tilde{x}$-axis into the stiffness matrix of the 3D frame element. Therefore, returning with the indexes, considering the following terms

$$a_i = \frac{E_i A_i}{L_i}, \qquad o_i = \frac{G_i J_i}{L_i}, \qquad b_i = \frac{E_i I_i}{{L_i}^3}\left(\frac{1}{(1+\zeta_i)}\right), \tag{3.17}$$

and the ${f_c}^{d'}$ expressions

$${f_c}^1{}_i = \frac{\alpha_{1_i}+\alpha_{2_i}+\alpha_{1_i}\alpha_{2_i}}{4-\alpha_{1_i}\alpha_{2_i}}, \quad {f_c}^2{}_i = \frac{\alpha_{3_i}+\alpha_{4_i}+\alpha_{3_i}\alpha_{4_i}}{4-\alpha_{3_i}\alpha_{4_i}}, \quad {f_c}^3{}_i = \frac{2\alpha_{1_i}+\alpha_{1_i}\alpha_{2_i}}{4-\alpha_{1_i}\alpha_{2_i}}, \tag{3.18}$$

$${f_c}^4{}_i = \frac{2\alpha_{2_i}+\alpha_{1_i}\alpha_{2_i}}{4-\alpha_{1_i}\alpha_{2_i}}, \quad {f_c}^5{}_i = \frac{2\alpha_{3_i}+\alpha_{3_i}\alpha_{4_i}}{4-\alpha_{3_i}\alpha_{4_i}}, \quad {f_c}^6{}_i = \frac{2\alpha_{4_i}+\alpha_{3_i}\alpha_{4_i}}{4-\alpha_{3_i}\alpha_{4_i}}, \tag{3.19}$$

$${f_c}^7{}_i = \frac{3\alpha_{1_i}\alpha_{2_i}}{4-\alpha_{1_i}\alpha_{2_i}}, \quad {f_c}^8{}_i = \frac{3\alpha_{3_i}\alpha_{4_i}}{4-\alpha_{3_i}\alpha_{4_i}}, \quad {f_c}^9{}_i = \frac{3\alpha_{1_i}}{4-\alpha_{1_i}\alpha_{2_i}}, \tag{3.20}$$

$$f_c{}^{10}{}_i = \frac{3\alpha_{2_i}}{4 - \alpha_{1_i}\alpha_{2_i}}, \qquad f_c{}^{11}{}_i = \frac{3\alpha_{3_i}}{4 - \alpha_{3_i}\alpha_{4_i}}, \quad f_c{}^{12}{}_i = \frac{3\alpha_{4_i}}{4 - \alpha_{3_i}\alpha_{4_i}}, \tag{3.21}$$

the stiffness matrix $\mathbf{K_L}$ of the 3D frame element is assembled by equation (3.22).

$$\mathbf{K}_{\mathbf{L}_i} = \begin{bmatrix} a_i & 0 & 0 & 0 & 0 & 0 & -a_i & 0 & 0 & 0 & 0 & 0 \\ 0 & 12b_i{f_c}^{1}{}_{i} & 0 & 0 & 0 & 6b_iL_i{f_c}^{3}{}_{i} & 0 & -12b_i{f_c}^{1}{}_{i} & 0 & 0 & 0 & 6b_iL_i{f_c}^{4}{}_{i} \\ 0 & 0 & 12b_i{f_c}^{2}{}_{i} & 0 & -6b_iL_i{f_c}^{5}{}_{i} & 0 & 0 & 0 & -12b_i{f_c}^{2}{}_{i} & 0 & -6b_iL_i{f_c}^{6}{}_{i} & 0 \\ 0 & 0 & 0 & o_i & 0 & 0 & 0 & 0 & 0 & -o_i & 0 & 0 \\ 0 & 0 & -6b_iL_i{f_c}^{5}{}_{i} & 0 & (4+\zeta_i)b_i{L_i}^2{f_c}^{11}{}_{i} & 0 & 0 & 0 & 6b_iL_i{f_c}^{5}{}_{i} & 0 & (2-\zeta_i)b_i{L_i}^2{f_c}^{8}{}_{i} & 0 \\ 0 & 6b_iL_i{f_c}^{3}{}_{i} & 0 & 0 & 0 & (4+\zeta_i)b_i{L_i}^2{f_c}^{9}{}_{i} & 0 & -6b_iL_i{f_c}^{3}{}_{i} & 0 & 0 & 0 & (2-\zeta_i)b_i{L_i}^2{f_c}^{7}{}_{i} \\ -a_i & 0 & 0 & 0 & 0 & 0 & a_i & 0 & 0 & 0 & 0 & 0 \\ 0 & -12b_i{f_c}^{1}{}_{i} & 0 & 0 & 0 & -6b_iL_i{f_c}^{3}{}_{i} & 0 & 12b_i{f_c}^{1}{}_{i} & 0 & 0 & 0 & -6b_iL_i{f_c}^{4}{}_{i} \\ 0 & 0 & -12b_i{f_c}^{2}{}_{i} & 0 & 6b_iL_i{f_c}^{5}{}_{i} & 0 & 0 & 0 & 12b_i{f_c}^{2}{}_{i} & 0 & 6b_iL_i{f_c}^{6}{}_{i} & 0 \\ 0 & 0 & 0 & -o_i & 0 & 0 & 0 & 0 & 0 & o_i & 0 & 0 \\ 0 & 0 & -6b_iL_i{f_c}^{6}{}_{i} & 0 & (2-\zeta_i)b_i{L_i}^2{f_c}^{8}{}_{i} & 0 & 0 & 0 & 6b_iL_i{f_c}^{6}{}_{i} & 0 & (4+\zeta_i)b_i{L_i}^2{f_c}^{12}{}_{i} & 0 \\ 0 & 6b_iL_i{f_c}^{4}{}_{i} & 0 & 0 & 0 & (2-\zeta_i)b_i{L_i}^2{f_c}^{7}{}_{i} & 0 & -6b_iL_i{f_c}^{4}{}_{i} & 0 & 0 & 0 & (4+\zeta_i)b_i{L_i}^2{f_c}^{10}{}_{i} \end{bmatrix}. \quad (3.22)$$

Formally, a distributed load on the length L of any i-element is decomposed into consistent nodal loads through the following standard expression

$$\int_0^{L_i} \mathbf{N}_i^{\mathrm{T}} \boldsymbol{P}_i \, d\tilde{x}, \tag{3.23}$$

remembering that **N** is the matrix that contains the interpolation functions and $\boldsymbol{P}$ is the vector with the mathematical expressions that represent the distribution of the load, which can be uniform, linear and quadratic, for example.

If there is a uniformly distributed load on the length, either in $\tilde{y}$ or $\tilde{z}$ directions with magnitudes $w_{\tilde{y}}$ and $w_{\tilde{z}}$ of the local reference system, Chandrupatla and Belegundu (2002) show that it can be decomposed into consistent nodal loads as

$$\boldsymbol{p}_{\boldsymbol{E}_i} = \begin{bmatrix} 0 & \frac{w_{\tilde{y}_i} L_i}{2} & \frac{w_{\tilde{z}_i} L_i}{2} & 0 & -\frac{w_{\tilde{z}_i} {L_i}^2}{12} & \frac{w_{\tilde{y}_i} {L_i}^2}{12} & 0 & \frac{w_{\tilde{y}_i} L_i}{2} & \frac{w_{\tilde{z}_i} L_i}{2} & 0 & \frac{w_{\tilde{z}_i} {L_i}^2}{12} & -\frac{w_{\tilde{y}_i} {L_i}^2}{12} \end{bmatrix}^{\mathrm{T}}, \tag{3.24}$$

for the frame element with connections of infinite stiffness. The signal of $w_{\tilde{y}}$ and $w_{\tilde{z}}$ must be consistent with the local reference system adopted, see Figure 3.8.

Figure 3.8 – Signal convention of the distributed load and consistent nodal loads.

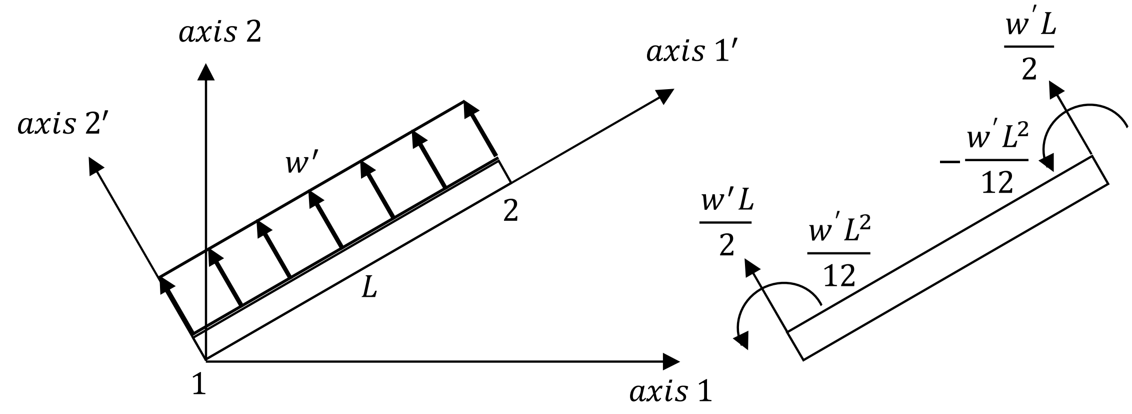

Source: Adapted from Chandrupatla e Belegundu (2002).

Then, to represent the consistent nodal loads in the global reference system ($\boldsymbol{P}_{\boldsymbol{EG}}$), $\boldsymbol{p}_{\boldsymbol{E}}$ is multiplied by the transposed transformation matrix **T**

$$\boldsymbol{p}_{\boldsymbol{EG}_i} = \mathbf{T}_i^{\mathrm{T}} \boldsymbol{p}_{\boldsymbol{E}_i}. \tag{3.25}$$

If the element has semi-rigid connections, the bending moments of the ends must be corrected due to the effect of the existing rotational stiffness. Therefore, using the interpolation functions, considering loadings in the $\tilde{x}\tilde{y}$ and $\tilde{x}\tilde{z}$ planes and integrating,

$$\int_0^{L_i} \left[{N_2}_i^{v_{xoy}} \quad {N_4}_i^{v_{xoy}} \right]^{\mathbf{T}} w_{\tilde{z}_i} d\tilde{x}, \tag{3.26}$$

$$\int_0^{L_i} \left[{N_2}_i^{v_{xoz}} \quad {N_4}_i^{v_{xoz}} \right]^{\mathbf{T}} w_{\tilde{y}_i} d\tilde{x}, \tag{3.27}$$

we arrive at the following correction expressions for the bending moments, which need to be replaced in equation (3.24).

$$M_{z_{1_i}} = \frac{w_{\tilde{y}_i} {L_i}^2}{12} \left(\frac{3\alpha_{1_i}(2 - \alpha_{2_i})}{4 - \alpha_{1_i}\alpha_{2_i}} \right) \quad and \quad M_{z_{2_i}} = -\frac{w_{\tilde{y}_i} {L_i}^2}{12} \left(\frac{3\alpha_{2_i}(2 - \alpha_{1_i})}{4 - \alpha_{1_i}\alpha_{2_i}} \right), \tag{3.28}$$

$$M_{y_{1_i}} = -\frac{w_{\tilde{z}_i} {L_i}^2}{12} \left(\frac{3\alpha_{3_i}(2 - \alpha_{4_i})}{4 - \alpha_{3_i}\alpha_{4_i}} \right) \quad and \quad M_{y_{2_i}} = \frac{w_{\tilde{z}_i} {L_i}^2}{12} \left(\frac{3\alpha_{4_i}(2 - \alpha_{3_i})}{4 - \alpha_{3_i}\alpha_{4_i}} \right). \tag{3.29}$$

Semi-rigid connections with characteristic close to the pinned connection condition in the $\tilde{x}\tilde{y}$ and $\tilde{x}\tilde{z}$ planes are possible through fixity factors with values close to null. On the other hand, fully rigid connections imply infinite stiffness which is not achievable and obtained only approximately. Most of the reviewed works study planar frames have only beam-to-column and/or column-base connections, which will always have a rigid part (column or base). In this context, the procedure to constraint the nullity and the unity of fixity factors is not uncommon, since values near the extremes are also physically interpretable as pinned and fully rigid connections. Kartal *et. al.* (2010), for example, investigate four planar frames with semi-rigid connections which have fixity factors within the range of 0.01 and 0.99.

Usually, steel space frames have two or m-elements neighborhood of connectivity, as can be seen in Fig. 3.9, and consequently a given joint can have $2m$-rotational springs referring to the connected elements.

Figure 3.9 – Node with m-elements connected.

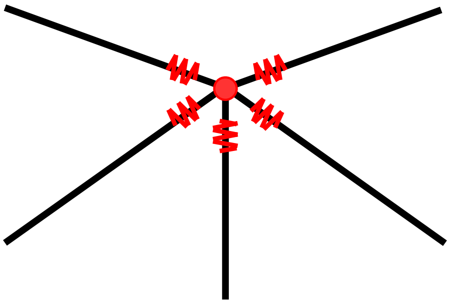

Source: Author's production.

In this situation, the structural behavior of all the joints can be understood through the stiffness matrix. Since $\mathbf{K_{bo}}$ refers to the global stiffness matrix produced by 3D frame elements with fully rigid connections, the overall contribution $\mathbf{K_s}$ of the rotational stiffness of all joints can be calculated by

$$\mathbf{K_s} = \mathbf{K} - \mathbf{K_{bo}}, \tag{3.30}$$

that is, with the addition of the fixity factors in the 3D frame element formulation, each joint becomes an additional element of the structure, having all the necessary rotational stiffness portions.

Disregarding manufacturing and assembly difficulties, the connection between m-elements can be represented by the constructive scheme of Fig. 3.10. The local rotational stiffness of each element are absorbed by a "global connector" (GC) which is rigid. The GC is illustrated as a cube and in the node 2 it has only two elements connected to him. If more elements are connected in a non-coplanar form, each element must be connected with the local longitudinal axis $\tilde{x}$ orthogonal to a given surface of the GC.

Figure 3.10 – The constructive scheme for the connection between m-elements.

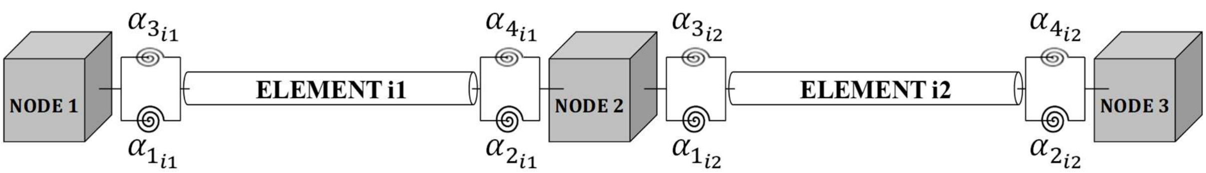

Source: Author's production.

To understand the constructive concept of Fig. 3.10, look at the particular case depicted in Fig. 3.11, where the pair of fixity factors $\alpha_{2_{i1}}$ and $\alpha_{4_{i1}}$ are null and the pair $\alpha_{1_{i2}}$ and $\alpha_{3_{i2}}$ have a certain degree of rotational stiffness at node 2.

Figure 3.11 – A particular case of m-elements connected to the same joint.

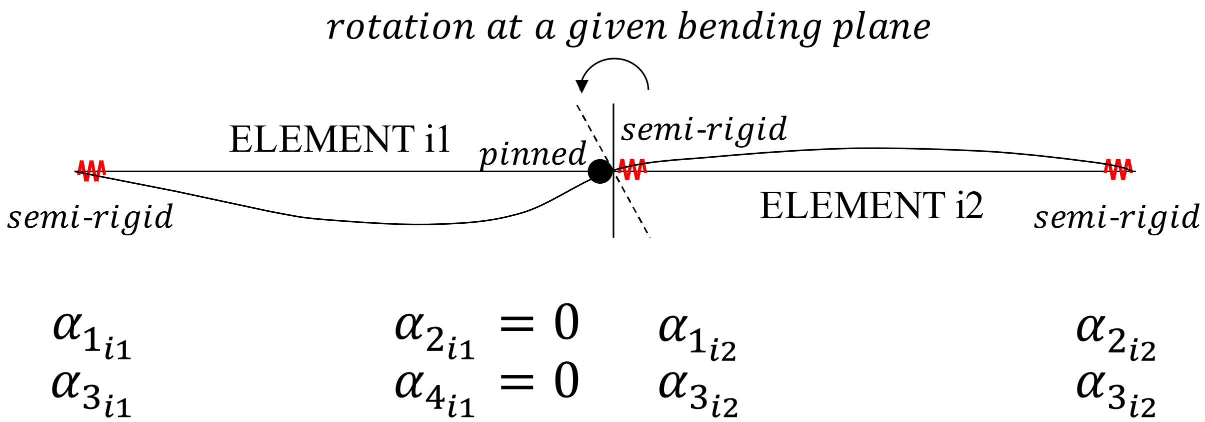

Source: Author's production.

If any rotation occurs at node 2, acting on either of the bending planes, the element 2 provides portions of rotational stiffness related to both end rotational springs and to the element itself, and bending moment transmission occurs along the element length. On the other hand, while the left connection of the element 1 offers rotational stiffness, the connection in the right side offers no resistance to the rotation. Even so, the element 1 will also presents bending moments, since the left connection is semi-rigid (except in the labeled local, where the bending moment will be null).

3.2 Calculation of Internal Forces

In order to calculate the internal forces – axial force, shear forces, bending moments and torsion – in any cross-section, it is necessary to use the interpolation functions assumed in the element formulation, to define the displacement field along the length of the element. Thus, it is possible to predict local displacements at any point $\tilde{x}$.

The displacement field is given by an approximation directly related to the local nodal displacements and to the polynomial degree of the interpolation functions. Local nodal displacements are determined by the global displacements mapped and rotated by the transformation matrix **T**.

As can be seen in equations (3.31)-(3.39), linear interpolation functions are adopted to the translation and rotation in the $\tilde{x}$-axis, while cubic interpolation functions characterize the translation in y and z axes, related to the cases exhibited in the Tables 3.1 and 3.2. Therefore,

$$N_1{}^{b_x} = N_1{}^{t_x} = 1 - \frac{\tilde{x}}{L_i}, \qquad N_2{}^{b_x} = N_2{}^{t_x} = \frac{\tilde{x}}{L_i}, \tag{3.31}$$

are the interpolation functions of translation (N^{b_x}) and rotation (N^{t_x}) in $\tilde{x}$-axis,

$$N_1{}^{v_{xoy}} = \frac{2}{L_i{}^3}\left(\frac{\alpha_{1_i} + \alpha_{2_i} + \alpha_{1_i}\alpha_{2_i}}{4 - \alpha_{1_i}\alpha_{2_i}}\right)\tilde{x}^3 - \frac{3}{L_i{}^2}\left(\frac{2\alpha_{1_i} + \alpha_{1_i}\alpha_{2_i}}{4 - \alpha_{1_i}\alpha_{2_i}}\right)\tilde{x}^2 + \frac{2}{L_i}\left(\frac{2\alpha_{1_i} - \alpha_{2_i} + \alpha_{1_i}\alpha_{2_i} - 2}{4 - \alpha_{1_i}\alpha_{2_i}}\right)\tilde{x} + 1, \tag{3.32}$$

$$N_2{}^{v_{xoy}} = \frac{1}{L_i{}^2}\left(\frac{2\alpha_{1_i} + \alpha_{1_i}\alpha_{2_i}}{4 - \alpha_{1_i}\alpha_{2_i}}\right)\tilde{x}^3 - \frac{6}{L_i}\left(\frac{\alpha_{1_i}}{4 - \alpha_{1_i}\alpha_{2_i}}\right)\tilde{x}^2 - \left(\frac{\alpha_{1_i}\alpha_{2_i} - 4\alpha_{1_i}}{4 - \alpha_{1_i}\alpha_{2_i}}\right)\tilde{x}, \tag{3.33}$$

$$N_3{}^{v_{xoy}} = -\frac{2}{L_i{}^3}\left(\frac{\alpha_{1_i} + \alpha_{2_i} + \alpha_{1_i}\alpha_{2_i}}{4 - \alpha_{1_i}\alpha_{2_i}}\right)\tilde{x}^3 + \frac{3}{L_i{}^2}\left(\frac{2\alpha_{1_i} + \alpha_{1_i}\alpha_{2_i}}{4 - \alpha_{1_i}\alpha_{2_i}}\right)\tilde{x}^2 - \frac{2}{L_i}\left(\frac{2\alpha_{1_i} - \alpha_{2_i} + \alpha_{1_i}\alpha_{2_i} - 2}{4 - \alpha_{1_i}\alpha_{2_i}}\right)\tilde{x}, \tag{3.34}$$

$$N_4{}^{v_{xoy}} = \frac{1}{L_i{}^2}\left(\frac{2\alpha_{2_i} + \alpha_{1_i}\alpha_{2_i}}{4 - \alpha_{1_i}\alpha_{2_i}}\right)\tilde{x}^3 - \frac{3}{L_i}\left(\frac{\alpha_{1_i}\alpha_{2_i}}{4 - \alpha_{1_i}\alpha_{2_i}}\right)\tilde{x}^2 + 2\left(\frac{\alpha_{1_i}\alpha_{2_i} - \alpha_{2_i}}{4 - \alpha_{1_i}\alpha_{2_i}}\right)\tilde{x}, \tag{3.35}$$

are the interpolation functions of the displacements in plane $\tilde{x}\tilde{y}$ ($N^{v_{xoy}}$) and

$$N_1{}^{v_{xoz}} = \frac{2}{L_i{}^3}\left(\frac{\alpha_{3_i} + \alpha_{4_i} + \alpha_{3_i}\alpha_{4_i}}{4 - \alpha_{3_i}\alpha_{4_i}}\right)\tilde{x}^3 - \frac{3}{L_i{}^2}\left(\frac{2\alpha_{3_i} + \alpha_{3_i}\alpha_{4_i}}{4 - \alpha_{3_i}\alpha_{4_i}}\right)\tilde{x}^2 + \frac{2}{L_i}\left(\frac{2\alpha_{3_i} - \alpha_{4_i} + \alpha_{3_i}\alpha_{4_i} - 2}{4 - \alpha_{3_i}\alpha_{4_i}}\right)\tilde{x} + 1, \tag{3.36}$$

$$N_2{}^{v_{xoz}} = -\frac{1}{L_i{}^2}\left(\frac{2\alpha_{3_i} + \alpha_{3_i}\alpha_{4_i}}{4 - \alpha_{3_i}\alpha_{4_i}}\right)\tilde{x}^3 + \frac{6}{L_i}\left(\frac{\alpha_{3_i}}{4 - \alpha_{3_i}\alpha_{4_i}}\right)\tilde{x}^2 + \left(\frac{\alpha_{3_i}\alpha_{4_i} - 4\alpha_{3_i}}{4 - \alpha_{3_i}\alpha_{4_i}}\right)\tilde{x}, \tag{3.37}$$

$$N_3{}^{v_{xoz}} = -\frac{2}{L_i{}^3}\left(\frac{\alpha_{3_i} + \alpha_{4_i} + \alpha_{3_i}\alpha_{4_i}}{4 - \alpha_{3_i}\alpha_{4_i}}\right)\tilde{x}^3 + \frac{3}{L_i{}^2}\left(\frac{2\alpha_{3_i} + \alpha_{3_i}\alpha_{4_i}}{4 - \alpha_{3_i}\alpha_{4_i}}\right)\tilde{x}^2 - \frac{2}{L_i}\left(\frac{2\alpha_{3_i} - \alpha_{4_i} + \alpha_{3_i}\alpha_{4_i} - 2}{4 - \alpha_{3_i}\alpha_{4_i}}\right)\tilde{x}, \tag{3.38}$$

$$N_4{}^{v_{xoz}} = -\frac{1}{L_i{}^2}\left(\frac{2\alpha_{4_i} + \alpha_{3_i}\alpha_{4_i}}{4 - \alpha_{3_i}\alpha_{4_i}}\right)\tilde{x}^3 + \frac{3}{L_i}\left(\frac{\alpha_{3_i}\alpha_{4_i}}{4 - \alpha_{3_i}\alpha_{4_i}}\right)\tilde{x}^2 - 2\left(\frac{\alpha_{3_i}\alpha_{4_i} - \alpha_{4_i}}{4 - \alpha_{3_i}\alpha_{4_i}}\right)\tilde{x}, \tag{3.39}$$

are the interpolation functions of the displacements in plane $\tilde{x}\tilde{z}$ ($N^{v_{xoz}}$). As already mentioned, the interpolation functions $N^{v_{xoy}}$ and $N^{v_{xoz}}$ are determinated by the procedure explained in equation (3.13).

Considering these interpolation functions, the distributions of the translational displacements on the three cartesian axes (U_{b_x}, $U_{v_{xoy}}$ and $U_{v_{xoz}}$) and the rotation around the $\tilde{x}$-axis (U_{t_x}), along the length of the element, can be approximated ($U^a{}_{b_x}$, $U^a{}_{v_{xoy}}$, $U^a{}_{v_{xoz}}$ and $U^a{}_{t_x}$, respectively) as follows

$$U^{a}{}_{b_{x_i}} = N_1{}^{b_x} u_{1_i} + N_2{}^{b_x} u_{2_i}, \tag{3.40}$$

$$U^{a}{}_{v_{xoy_i}} = N_1{}^{v_{xoy}} v_{1_i} + N_2{}^{v_{xoy}} \theta_{1z_i} + N_3{}^{v_{xoy}} v_{2_i} + N_4{}^{v_{xoy}} \theta_{2z_i}, \tag{3.41}$$

$$U^{a}{}_{v_{xoz_i}} = N_1{}^{v_{xoz}} w_{1_i} + N_2{}^{v_{xoz}} \theta_{1y_i} + N_3{}^{v_{xoz}} w_{2_i} + N_4{}^{v_{xoz}} \theta_{2y_i}, \tag{3.42}$$

$$U^{a}{}_{t_{x_i}} = N_1{}^{t_x} \theta_{1x_i} + N_2{}^{t_x} \theta_{2x_i}. \tag{3.43}$$

In matrix form, the set of equations (3.40)-(3.43) is described by the linear combination

$$\boldsymbol{U^{a}}_i = \mathbf{N}_i \boldsymbol{u}_i, \tag{3.44}$$

where $\boldsymbol{U^a}$ is the vector of aproximate displacements at the i-element, $\mathbf{N}$ is the matrix of the interpolation functions and $\boldsymbol{u}$ is the vector of nodal displacements in the local reference system.

The procedure to calculate the internal forces is analogous to the procedure presented in Carniel *et. al.* (2008), only with distinct interpolation functions that incorporate the effect of the semi-rigid connections.

Returning with the index k for a given cross-section and based on the definitions of the axial strain ε_{xy}, the Hooke's law and the basic equation to calculate the normal stress σ_{xx} produced by an axial force,

$$\varepsilon_{xy_i} = \frac{dU^{a}{}_{b_{x_i}}}{d\tilde{x}}, \tag{3.45}$$

$$\sigma_{xx_{i,k}} = E_i \varepsilon_{xy_i} \tag{3.46}$$

$$\sigma_{xx_{i,k}} = \frac{N_{x_{i,k}}}{A_i}, \tag{3.47}$$

differentiating equation (3.45) with respect to equation (3.40) and replacing equations (3.45) and (3.47) in equation (3.46), the calculation of axial forces N_x is performed as follows

$$N_{x_{i,k}} = \left(\frac{E_i A_i}{L_i}\right) [-1 \quad 1] \left\{\boldsymbol{u}_{\boldsymbol{b}_{x_i}}\right\}, \tag{3.48}$$

where $\boldsymbol{u}_{\boldsymbol{b}_x}$ is the vector with the local axial displacements of nodes 1 and 2.

Considering the known relationship between the shear and bending moments,

$$M_{oz}(\tilde{x})_i = E_i I_i \frac{d^2 v(\tilde{x})_i}{d\tilde{x}^2}, \qquad V_y(\tilde{x})_i = -\frac{dM_{oz}(\tilde{x})_i}{d\tilde{x}}, \tag{3.49}$$

$$M_{oy}(\tilde{x})_i = E_i I_i \frac{d^2 w(\tilde{x})_i}{d\tilde{x}^2}, \qquad V_z(\tilde{x})_i = -\frac{dM_{oy}(\tilde{x})_i}{d\tilde{x}}, \tag{3.50}$$

being the translations in $\tilde{y}$ and $\tilde{z}$ axes approximated by equations (3.41) and (3.42) and using the second and third derivatives of the interpolation functions viewed in equations (3.32)-(3.39), given by

$$\begin{aligned}
&\frac{d^2 N_1{}^{v_{xoy}}}{d\tilde{x}^2} = \frac{12}{L_i{}^3}\left(\frac{\alpha_{1_i} + \alpha_{2_i} + \alpha_{1_i}\alpha_{2_i}}{4 - \alpha_{1_i}\alpha_{2_i}}\right)\tilde{x} - \frac{6}{L_i{}^2}\left(\frac{2\alpha_{1_i} + \alpha_{1_i}\alpha_{2_i}}{4 - \alpha_{1_i}\alpha_{2_i}}\right), &&\frac{d^3 N_1{}^{v_{xoy}}}{d\tilde{x}^3} = \frac{12}{L_i{}^3}\left(\frac{\alpha_{1_i} + \alpha_{2_i} + \alpha_{1_i}\alpha_{2_i}}{4 - \alpha_{1_i}\alpha_{2_i}}\right),\\
&\frac{d^2 N_2{}^{v_{xoy}}}{d\tilde{x}^2} = \frac{6}{L_i{}^2}\left(\frac{2\alpha_{1_i} + \alpha_{1_i}\alpha_{2_i}}{4 - \alpha_{1_i}\alpha_{2_i}}\right)\tilde{x} - \frac{12}{L_i}\left(\frac{\alpha_{1_i}}{4 - \alpha_{1_i}\alpha_{2_i}}\right), &&\frac{d^3 N_2{}^{v_{xoy}}}{d\tilde{x}^3} = \frac{6}{L_i{}^2}\left(\frac{2\alpha_{1_i} + \alpha_{1_i}\alpha_{2_i}}{4 - \alpha_{1_i}\alpha_{2_i}}\right),\\
&\frac{d^2 N_3{}^{v_{xoy}}}{d\tilde{x}^2} = -\frac{12}{L_i{}^3}\left(\frac{\alpha_{1_i} + \alpha_{2_i} + \alpha_{1_i}\alpha_{2_i}}{4 - \alpha_{1_i}\alpha_{2_i}}\right)\tilde{x} + \frac{6}{L_i{}^2}\left(\frac{2\alpha_{1_i} + \alpha_{1_i}\alpha_{2_i}}{4 - \alpha_{1_i}\alpha_{2_i}}\right), &&\frac{d^3 N_3{}^{v_{xoy}}}{d\tilde{x}^3} = -\frac{12}{L_i{}^3}\left(\frac{\alpha_{1_i} + \alpha_{2_i} + \alpha_{1_i}\alpha_{2_i}}{4 - \alpha_{1_i}\alpha_{2_i}}\right),\\
&\frac{d^2 N_4{}^{v_{xoy}}}{d\tilde{x}^2} = \frac{6}{L_i{}^2}\left(\frac{2\alpha_{2_i} + \alpha_{1_i}\alpha_{2_i}}{4 - \alpha_{1_i}\alpha_{2_i}}\right)\tilde{x} - \frac{6}{L_i}\left(\frac{\alpha_{1_i}\alpha_{2_i}}{4 - \alpha_{1_i}\alpha_{2_i}}\right), &&\frac{d^3 N_4{}^{v_{xoy}}}{d\tilde{x}^3} = \frac{6}{L_i{}^2}\left(\frac{2\alpha_{2_i} + \alpha_{1_i}\alpha_{2_i}}{4 - \alpha_{1_i}\alpha_{2_i}}\right),\\
&\frac{d^2 N_1{}^{v_{xoz}}}{d\tilde{x}^2} = \frac{12}{L_i{}^3}\left(\frac{\alpha_{3_i} + \alpha_{4_i} + \alpha_{3_i}\alpha_{4_i}}{4 - \alpha_{3_i}\alpha_{4_i}}\right)\tilde{x} - \frac{6}{L_i{}^2}\left(\frac{2\alpha_{3_i} + \alpha_{3_i}\alpha_{4_i}}{4 - \alpha_{3_i}\alpha_{4_i}}\right), &&\frac{d^3 N_1{}^{v_{xoz}}}{d\tilde{x}^3} = \frac{12}{L_i{}^3}\left(\frac{\alpha_{3_i} + \alpha_{4_i} + \alpha_{3_i}\alpha_{4_i}}{4 - \alpha_{3_i}\alpha_{4_i}}\right),\\
&\frac{d^2 N_2{}^{v_{xoz}}}{d\tilde{x}^2} = -\frac{6}{L_i{}^2}\left(\frac{2\alpha_{3_i} + \alpha_{3_i}\alpha_{4_i}}{4 - \alpha_{3_i}\alpha_{4_i}}\right)\tilde{x} + \frac{12}{L_i}\left(\frac{\alpha_{3_i}}{4 - \alpha_{3_i}\alpha_{4_i}}\right), &&\frac{d^3 N_2{}^{v_{xoz}}}{d\tilde{x}^3} = -\frac{6}{L_i{}^2}\left(\frac{2\alpha_{3_i} + \alpha_{3_i}\alpha_{4_i}}{4 - \alpha_{3_i}\alpha_{4_i}}\right),\\
&\frac{d^2 N_3{}^{v_{xoz}}}{d\tilde{x}^2} = -\frac{12}{L_i{}^3}\left(\frac{\alpha_{3_i} + \alpha_{4_i} + \alpha_{3_i}\alpha_{4_i}}{4 - \alpha_{3_i}\alpha_{4_i}}\right)\tilde{x} + \frac{6}{L_i{}^2}\left(\frac{2\alpha_{3_i} + \alpha_{3_i}\alpha_{4_i}}{4 - \alpha_{3_i}\alpha_{4_i}}\right), &&\frac{d^3 N_3{}^{v_{xoz}}}{d\tilde{x}^3} = -\frac{12}{L_i{}^3}\left(\frac{\alpha_{3_i} + \alpha_{4_i} + \alpha_{3_i}\alpha_{4_i}}{4 - \alpha_{3_i}\alpha_{4_i}}\right),\\
&\frac{d^2 N_4{}^{v_{xoz}}}{d\tilde{x}^2} = -\frac{6}{L_i{}^2}\left(\frac{2\alpha_{4_i} + \alpha_{3_i}\alpha_{4_i}}{4 - \alpha_{3_i}\alpha_{4_i}}\right)\tilde{x} + \frac{6}{L_i}\left(\frac{\alpha_{3_i}\alpha_{4_i}}{4 - \alpha_{3_i}\alpha_{4_i}}\right), &&\frac{d^3 N_4{}^{v_{xoz}}}{d\tilde{x}^3} = -\frac{6}{L_i{}^2}\left(\frac{2\alpha_{4_i} + \alpha_{3_i}\alpha_{4_i}}{4 - \alpha_{3_i}\alpha_{4_i}}\right),
\end{aligned} \tag{3.51}$$

the internal bending moments (M_y and M_z) and shear forces (V_y and V_z) are defined by the following expressions

$$M_{z_{i,k}} = (E_i I_i)\left[\frac{d^2 \mathbf{N}^{v_{xoy}}{}_k}{d\tilde{x}^2}\right]\left\{\boldsymbol{u}_{v_{xoy_i}}\right\}, \tag{3.52}$$

$$V_{y_{i,k}} = (-E_i I_i)\left[\frac{d^3 \mathbf{N}^{v_{xoy}}{}_k}{d\tilde{x}^3}\right]\left\{\boldsymbol{u}_{v_{xoy_i}}\right\}, \tag{3.53}$$

$$M_{y_{i,k}} = (E_i I_i)\left[\frac{d^2 \mathbf{N}^{v_{xoz}}{}_k}{d\tilde{x}^2}\right]\left\{\boldsymbol{u}_{v_{xoz_i}}\right\}, \tag{3.54}$$

$$V_{z_{i,k}} = (-E_i I_i)\left[\frac{d^3 \mathbf{N}^{v_{xoz}}{}_k}{d\tilde{x}^3}\right]\left\{\boldsymbol{u}_{v_{xoz_i}}\right\}, \tag{3.55}$$

where $\boldsymbol{u}_{v_{xoy}}$ and $\boldsymbol{u}_{v_{xoz}}$ are vectors with the local translation of the nodes in $\tilde{y}$ and $\tilde{z}$ axes.

Starting from the same procedure which was described for the axial force, we have

$$\gamma_{yz_i} = R_i \frac{dU^a{}_{t_{x_i}}}{d\tilde{x}}, \tag{3.56}$$

$$\tau_{yz_{i,k}} = G_i \gamma_{yz_i}, \tag{3.57}$$

$$\tau_{yz_{i,k}} = \frac{M_{x_{i,k}} R_i}{J_i}, \tag{3.58}$$

where γ_{yz} is the angular deformation and, at this case, τ_{yz} is a shear stress produced by torsion. Replacing equation (3.58) into equation (3.57),

$$\frac{M_{x_{i,k}} R_i}{J_i} = G_i \gamma_{yz_i}, \tag{3.59}$$

and then equation (3.56) into equation (3.59), after differentiating equation (3.43), the torsion M_x can be determined by

$$M_{x_{i,k}} = \left(\frac{G_i J_i}{L_i}\right) [-1 \quad 1] \left\{\boldsymbol{u}_{t_{x_i}}\right\}. \tag{3.60}$$

Analyzing the equations of the six internal forces, it is seen that the distributions of the axial force and torsion are constant along the length of the element since the derivative is applied in linear interpolation functions. On the other hand, while the shear forces also have constant magnitude along the length, due to the third derivatives of the cubic interpolation functions, the bending moments can have different magnitudes according to the arbitrary point $\tilde{x}$, since the resulting second derivatives are linear.

Chapter 4

Failure Criterion

The formulation of the new failure criterion for tubular elements with circular cross-section and variable length is grounded on the von Mises theory and based on the stress calculation strategy proposed by Irles and Irles (2000). The reference system adopted for internal forces, stress distributions and angular location θ in the outer radius is shown in Fig. 4.1.

Figure 4.1 – Reference system adopted for the failure criterion formulation.

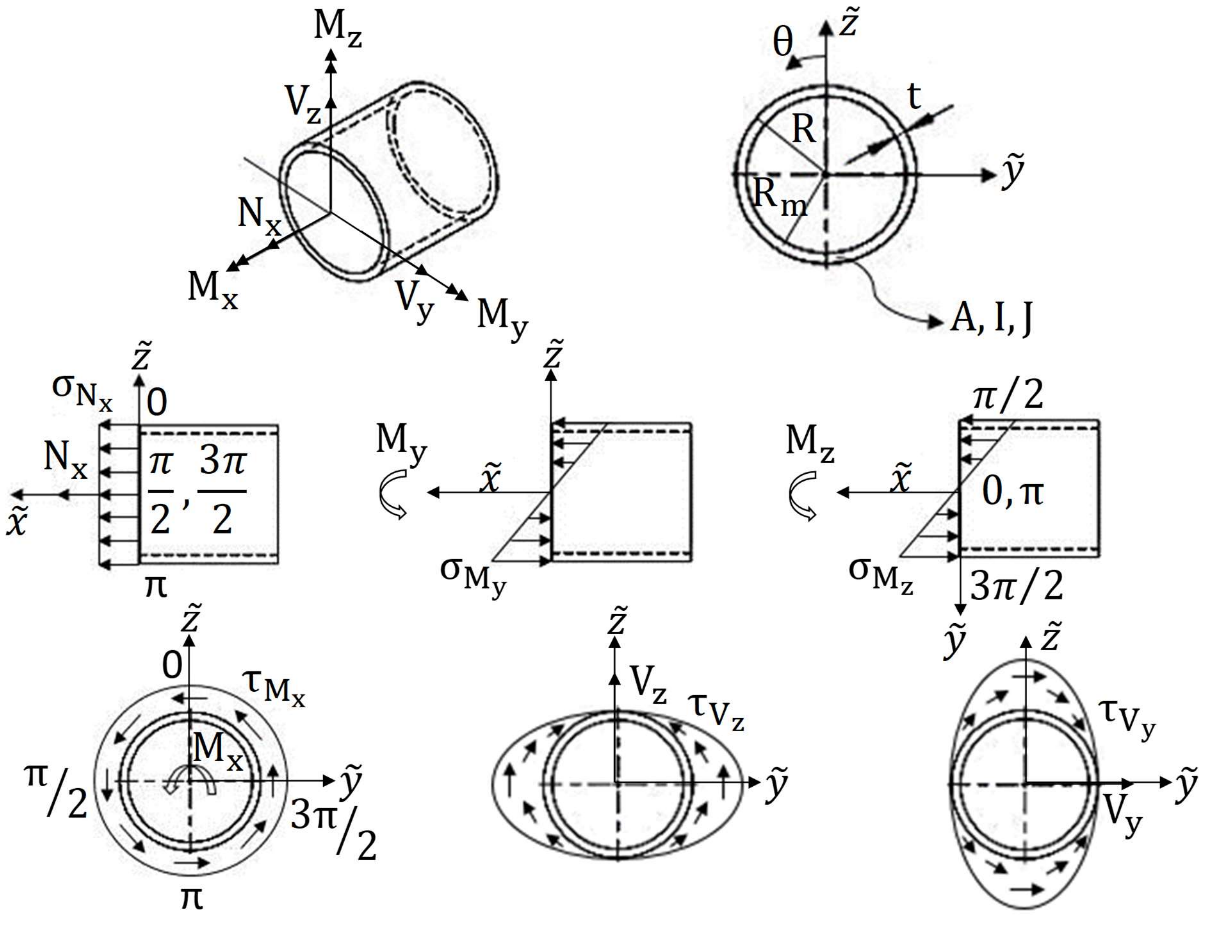

Source: Author’s production.

For the development of the formulation the following hypotheses are considered:

I. Element with symmetrical and prismatic cross-sectional area along the longitudinal $\tilde{x}$-axis;
II. Ductile, homogeneous and isotropic material;
III. Concentrations and residual stresses are neglected;
IV. Normal and shear stresses, shown in Fig. 4.1, distributed according to the internal forces reference system coupled to the angular reference system θ;
V. Constant distribution for the normal stress of the axial force, linear distribution of the normal stress of the bending moments, linear distribution of the shear stress resulting from the torsion and parabolic distribution of the shear stresses related to the shear forces;
VI. In the outline of the outer radius, the shear stresses of shear forces and torsion are both tangential;
VII. Cross-section remains flat during the deformation of the axial stress;
VIII. Distortion of the cross-section is insignificant and the thin-wall thickness (t) is small enough to assume that there is no variation of the shear stresses along the thickness;
IX. Small torsion angles where the length and the outer radius of the element remain unchanged;
X. The critical point of mechanical solicitation localized in the outer radius and dependent only on the angular position θ, inserted in the fixed range of $[0,2\pi]$ and assumed from the local $\tilde{z}$-axis.

The von Mises failure criterion for a point under a multiaxial stress state σ is

$$\sigma^2 = \frac{1}{2}\left[\left(\sigma_{xx} - \sigma_{yy}\right)^2 + \left(\sigma_{yy} - \sigma_{zz}\right)^2 + (\sigma_{zz} - \sigma_{xx})^2\right] + 3\left({\tau_{xy}}^2 + {\tau_{yz}}^2 + {\tau_{zx}}^2\right), \quad (4.1)$$

where σ_{xx}, σ_{yy} e σ_{zz} are normal stresses and τ_{xy}, τ_{yz} e τ_{zx} are shear stresses.

While the normal stress σ_{N_x} of the axial force is uniform throughout the area, the shear stress τ_{M_x} of the torsion is maximal at any point θ. That is,

$$\sigma_{N_{x\,i,k}} = \frac{N_{x\,i,k}}{A_i} \qquad and \qquad \tau_{M_{x\,i,k}} = \frac{M_{x\,i,k} R_i}{J_i}. \quad (4.2)$$

However, the locations of the maximum normal and shear stresses of the resulting bending moment and shear force depend on θ, and therefore, it is necessary to deduce these terms properly.

Considering that the cross-section of Fig. 4.2 is subjected to the bending moments M_y and M_z, the resulting bending moment M_R and the angle γ_M are known as

$$M_{R_{i,k}} = \sqrt{{M_{y_{i,k}}}^2 + {M_{z_{i,k}}}^2} \quad and \quad \gamma_{M_{i,k}} = \tan^{-1}\left(\frac{M_{z_{i,k}}}{M_{y_{i,k}}}\right). \tag{4.3}$$

Figure 4.2 – Cross-section properties used in the deduction of the normal stress from the bending moments.

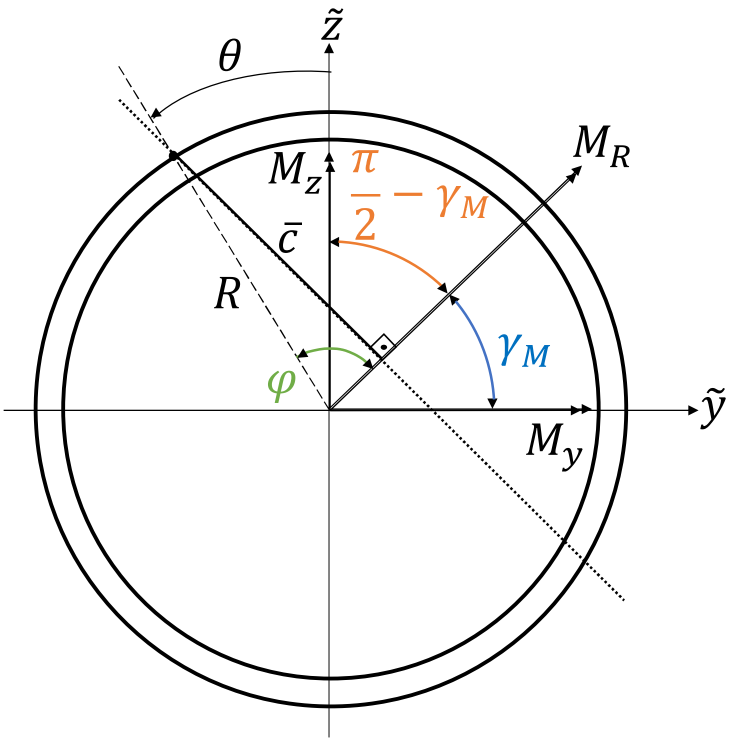

Source: Author's production.

The normal stress depends on the distance $\bar{c}$ (perpendicular to M_R) between the line of action of the vector of M_R and the point θ. Also, the angle between M_R and the $\tilde{z}$-axis is known, since it is the complement of γ_M for form the $\frac{\pi}{2}$ angle between the $\tilde{y}$ and $\tilde{z}$ axes.

By making the relation between the angles,

$$\bar{c}_{i,k} = R_i \sin(\varphi_{i,k}), \qquad \varphi_{i,k} = \theta_{i,k} + \left(\frac{\pi}{2} - \gamma_{M_{i,k}}\right), \tag{4.4}$$

it is possible to determine the normal stress σ_{M_R} of the resulting bending moment as a function of θ

$$\sigma_{M_{R\,i,k}} = \frac{M_{R\,i,k}\bar{c}_{i,k}}{I_i}. \tag{4.5}$$

To define the shear stress expression of the resulting shear forces V_y and V_z as a function of the angle θ, consider the cross-section of Fig. 4.3.

Figure 4.3 – Cross-section properties used in the deduction of the shear stress produced by the shear forces.

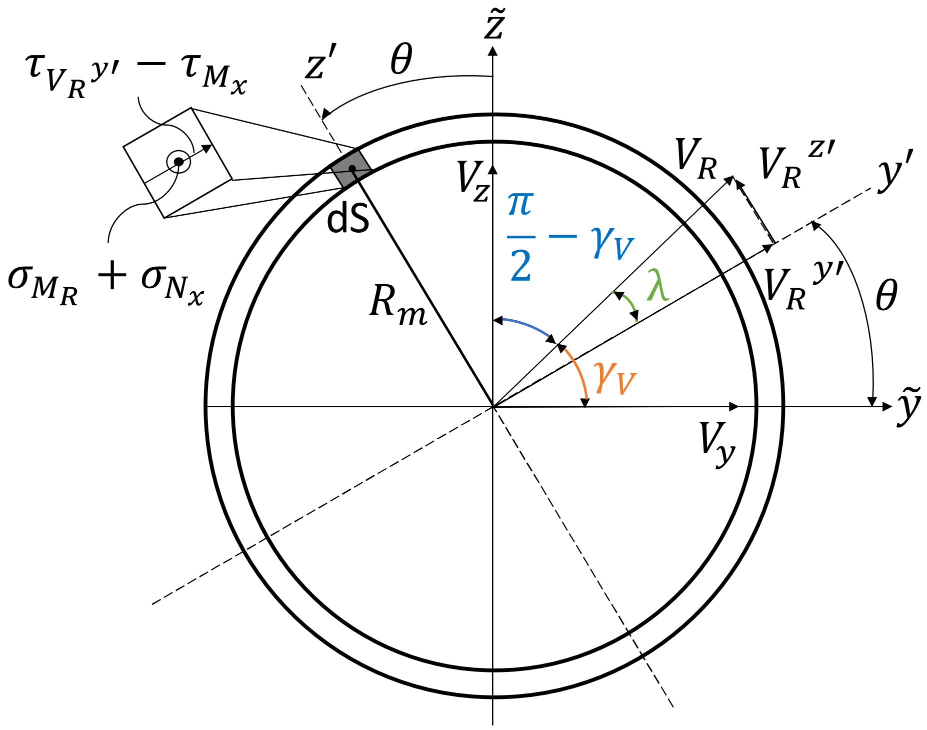

Source: Author's production.

By analogous procedure,

$$V_{R\,i,k} = \sqrt{V_{y\,i,k}{}^2 + V_{z\,i,k}{}^2} \quad and \quad \gamma_{V\,i,k} = \tan^{-1}\left(\frac{V_{z\,i,k}}{V_{y\,i,k}}\right). \tag{4.6}$$

After the definition of V_R and using the angle λ given by

$$\lambda_{i,k} = \gamma_{V\,i,k} - \theta_{i,k}, \tag{4.7}$$

V_R is decomposed in the auxiliary reference system $y'z'$ by the components $V_R{}^{y'}$ and $V_R{}^{z'}$

$$V_R{}^{y'}{}_{i,k} = V_{R\,i,k}\cos(\lambda_{i,k}) \quad and \quad V_R{}^{z'}{}_{i,k} = V_{R\,i,k}\sin(\lambda_{i,k}). \tag{4.8}$$

Based on the characteristic of the stress distribution, while the shear stress of $V_R{}^{z'}$ is zero in θ, the shear force $V_R{}^{y'}$ produces maximum shear stress in θ. As this shear stress is tangential to the outer contour, as well as the shear stress of the torsion, it becomes possible to add these two portions of shear stresses.

The shear stress from $V_R{}^{y'}$ at the arbitrary point θ depends on the static moment Q, calculated with respect to the area $\bar{A}'$ of the arc above the z'-axis and to the distance $\bar{y}'$ of the z'-axis to the centroid of this arc. Therefore, knowing that R_m is the midline radius of the cross-section, we have the following geometric properties

$$\bar{y}'_i = \frac{4t_i}{3\pi}, \qquad \bar{A}_i{}' = \pi R_{m_i} t_i, \qquad Q_i = \bar{y}'_i \bar{A}_i{}' = \frac{4{t_i}^2 R_{m_i}}{3}, \tag{4.9}$$

and the expression for the shear stress $\tau_{V_R{}^{y'}}$ is determined as

$$\tau_{V_R{}^{y'}{}_{i,k}} = \frac{V_R{}^{y'}{}_{i,k} Q_i}{I_i t_i}. \tag{4.10}$$

Returning to equation (4.1), considering that the stresses σ_{yy}, τ_{xy} e τ_{zx} are zero, the outer radius, midline radius, inertia moment and the polar inertia moment can be represented as a function of the cross-section area and the thin-wall thickness

$$R_i = \frac{1}{2}\left(\frac{A_i + \pi {t_i}^2}{\pi t_i}\right), \qquad R_{m_i} = R_i - \frac{t_i}{2}, \qquad I_i = \pi {R_{m_i}}^3 t_i, \qquad J_i = 2I_i, \tag{4.11}$$

and adopting σ_e as the allowable stress, the failure criterion is established by

$$f(\theta)_{i,k} \le {\sigma_e}^2, \tag{4.12}$$

$$f(\theta)_{i,k} = \left(\frac{N_{x_{i,k}}}{A_i} + \frac{M_{R_{i,k}}\bar{c}_{i,k}}{I_i}\right)^2 + 3\left(\frac{M_{x_{i,k}}R_i}{2I_i} - \frac{V_R{}^{y'}{}_{i,k}Q_i}{I_i t_i}\right)^2. \tag{4.13}$$

According to the allowable stress and geometric properties, the failure criterion evaluates the mechanical strength of the cross-sections through the von Mises stress, calculated by $f(\theta)$ in terms of the internal forces acting on the cross-section and only at the critical point defined by an adequate sweep within the range of $[0,2\pi]$. The sweep procedure is adopted due to the simplicity of $f(\theta)$ and ease of implementation, however it is noteworthy that any unconstrained optimization method could be applied to find the critical point without major problems.

In addition to the internal forces, note that the failure criterion is dependent on only three more geometric parameters: the cross-section area A, the thin-wall thickness t and the critical point θ. While the cross-section area is a design variable of the optimization process, it is important to note that the critical point and the thin-wall thickness are constant parameters, the first one being defined by the mentioned sweep and the adjacent is an input data kept fixed.

It is worth note that this failure criterion can be easily adapted for elements with a massive circular section, being necessary to assume $t = R$ and to modify the tabulated equations for the calculation of the static moment Q. Therefore, the adaptation would require small changes in the failure criterion and in its sensitivity analysis.

To justify the development and use of this failure criterion, an analytical investigation about a particular case and a 2D optimization problem are detailed in the beginning of Chapter 6. Hereafter, the importance of the failure criterion is confirmed by the results obtained in the developed case studies.

Chapter 5

Optimization Problem

In the context of this research work, the manufacturing cost of a steel tubular space frame consists on the sum of costs related to material and connections of each element. Thus, the definition of the total cost found in Simões (1996) can be extended to space frames as follows

$$W = \sum_{i=1}^{nel} \left(c_{M_i} \rho_i A_i L_i + c_{S_i} \right), \tag{5.1}$$

$$c_{S_i} = \left(\sum_{c=1}^{4} \left(V_0 + V_1 \alpha_c + V_2 {\alpha_c}^2 \right) \right)_i c_{M_i} \rho_i A_i L_i, \tag{5.2}$$

remembering that c_M is the monetary material cost per mass $\left[\frac{\$}{kg}\right]$, c_S is the monetary connections cost and now the index c represents the four fixity factors related to the four rotational springs of the i-elements.

According to Eurocode 3 (2013), in relation to structures designed for the civil construction sector, the connections cost that only have components like plates and bolts is not high. However, when it is desired to increase the stiffness in connections, the welding process is required and this process increases the cost (operation and inspection of the welds). Therefore, to analyze the cost-benefit relationship between increased stiffness and its associated cost, the additional cost of the connections is inserted into the objective function W, being proportional to material cost.

The coefficients V_0, V_1 and V_2 define the quadratic variation for the range of the additional cost of the connections, delimited by pinned (AC_p) and fully rigid (AC_r) connections costs, as can be seen at Simões (1996). In mathematical form,

$$(AC^p)_i c_{M_i} \rho_i A_i L_i \le \left(\sum_{c=1}^{4} (V_0 + V_1 \alpha_c + V_2 {\alpha_c}^2)\right)_i c_{M_i} \rho_i A_i L_i \le (AC^r)_i c_{M_i} \rho_i A_i L_i, \quad (5.3)$$

$$0 \le AC^p, AC^r \le 100\ (\%).$$

For connections between steel tubular members, no published data was found with suggestions concerning the percentage cost increase referred to this type of connection. Therefore, representative values will be derived to AC^p and AC^r.

Since no method in the literature or even a technical publication on regulatory standards was found to define the constant coefficients of this quadratic variation, in the following is presented a generic mathematical procedure proposed to standardize the definition of these coefficients, to be applied in the development of case studies that evaluate and analyze different costs of pinned and fully rigid connections. In other case studies, it is not necessary to apply this procedure: the coefficients can be determinated based on graphical verification, ensuring that the costs of pinned and fully rigid connections are the minimum and maximum extreme costs.

Basically, a quadratic curve can be determinated knowing three distinct informations, which can be three points or even two points and a derivative at any point. In this work, the second procedure is adopted, due to its mathematical simplicity and the guarantee of a well behaved curve.

For better visualization, consider only the quadratic variation AC given by

$$AC_i = \sum_{c=1}^{4} (V_0 + V_1 \alpha_c + V_2 {\alpha_c}^2), \quad (5.4)$$

$$AC_i = 4V_0 + V_1(\alpha_1 + \alpha_2 + \alpha_3 + \alpha_4) + V_2({\alpha_1}^2 + {\alpha_2}^2 + {\alpha_3}^2 + {\alpha_4}^2), \quad (5.5)$$

being equation (5.5) the complete expression for the quadratic variation.

Since the percentages of the additional costs of pinned and fully rigid connections are input data, the constant coefficient V_0 is easily defined as follows

$$\alpha_1, \alpha_2, \alpha_3, \alpha_4 \approx 0 \ \rightarrow \ AC_i = AC_p, \quad (5.6)$$

$$4V_0 = AC_p, \quad (5.7)$$

$$V_0 = \frac{AC_p}{4}. \quad (5.8)$$

Then, for the curve to be always well behaved, with the concavity located at the initial point of the additional cost of pinned connections, the mathematical condition of an inflection point must be imposed. That is,

$$\left.\frac{\partial AC_i}{\partial \alpha_c}\right|_{\alpha_c \approx 0} = 0. \tag{5.9}$$

Applying the derivative of equation (5.9), it is defined that the constant coefficient V_1 is null, as can be seen in equations (5.10)-(5.12).

$$\sum_{c=1}^{4} \left.\frac{\partial AC_i}{\partial \alpha_c}\right|_{\alpha_c \approx 0} (V_0 + V_1\alpha_c + V_2{\alpha_c}^2) = 0, \tag{5.10}$$

$$0 = \sum_{c=1}^{4} (V_1 + 2V_2\alpha_c), \tag{5.11}$$

$$V_1 = 0. \tag{5.12}$$

Finally, with two coefficients already defined, the constant coefficient V_2 is easily obtained by checking the equation (5.5) at the extreme point of the additional cost of fully rigid connections. Therefore,

$$\alpha_1, \alpha_2, \alpha_3, \alpha_4 \approx 1 \;\; \rightarrow \;\; AC_i = AC_r, \tag{5.13}$$

$$4V_0 + 4V_1 + 4V_2 = AC_r, \tag{5.14}$$

$$V_2 = \frac{1}{4}\left(AC_r - AC_p\right). \tag{5.15}$$

Considering the presented procedure, the imposed quadratic variations will always have the characteristic shown in Fig. 5.1.

Figure 5.1 – Mathematical pattern defined for the quadratic variations.

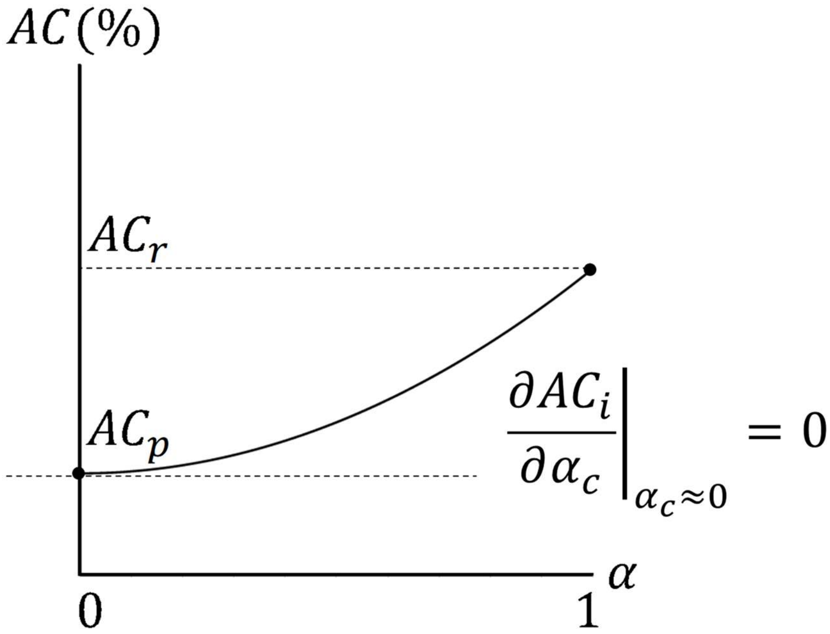

Source: Author's production.

Based on the purpose of this research, the optimization problem can be stated as finding a set of continuous design variables $\boldsymbol{v_p}$ – cross-section areas, joint positions and fixity factors – that minimize the manufacturing costs W of a steel tubular space frame subject to LC-load cases and displacement, stress and minimum length as design constraints. In the standard form,

$$Minimize_{\ \boldsymbol{v_p} \rightarrow \boldsymbol{A,X,Y,Z,\alpha}} \qquad \frac{W\left(v_{p_j}\right)}{W_{SF}}, \tag{5.16}$$

$$respecting \qquad \mathbf{K}\boldsymbol{U}^{LC} = \boldsymbol{F}^{LC}, \tag{5.17}$$

$$subject\ to \qquad \frac{{U_d}^{LC}}{\left|U_{L_d}\right|} + 1.0 \geq 0, \tag{5.18}$$

$$-\frac{{U_d}^{LC}}{U_{U_d}} + 1.0 \geq 0, \tag{5.19}$$

$$-\frac{{f(\theta)_{i,k}}^{LC}}{{\sigma_e}^2} + 1.0 \geq 0, \tag{5.20}$$

$$\frac{L_i}{L_L} - 1.0 \geq 0, \tag{5.21}$$

where W_{SF} is the value of the objective function at the starting point, U_{L_d} and U_{U_d} are the lower and upper bounds for a constrained displacement and L_L is the minimum length acceptable to all the elements. The index j is related to the design variables, while d refer to the displacement constraints.

Note that the objective function and constraints are normalized to avoid poor conditioning of the optimization problem. The constraints that exist in the proposed problem have very different orders of magnitude, and in the original condition the optimization process could suffer serious difficulty in judging the severity of possible constraints violations (ARORA, 2011).

The displacement constraints were dismembered, all design constraints were adapted to type " $\geq$ " and the optimization problem can be solved by any gradient-based method. In this work, maintaining the format of the original code developed by Cardoso *et. al.* (2007) and Carniel *et. al.* (2008), the SLP method was chosen. The method is described in the next section.

As performed by Carniel *et. al.* (2008), the failure criterion will be evaluated and applied as a stress constraint at the cross-sections localized at the extremities and center of each element. Therefore,

$$\tilde{x}_i = 0_{\,(k=1)}, \qquad \tilde{x}_i = 0.5L_{i\,(k=2)} \qquad and \qquad \tilde{x}_i = L_{i\,(k=3)}. \tag{5.22}$$

For the convergence of the optimization processes, stopping criteria with prescribed tolerances are adopted to ensure the stabilization not only of the objective function, but also of all design variables.

Following the content of AISC (2005) and Chen (2000), in engineering practice pinned connections always have some stiffness and fully rigid connections have some flexibility, therefore fixity factors with 0-1 is only theoretical. Furthermore, as can be seen in Fig. 5.2, pinned and fully rigid connections can be characterized by wider regions. Therefore, to facilitate the physical interpretation of any optimal solution, connections will be considered pinned for $\alpha < 0.1$ and fully rigid when $\alpha > 0.9$. However, it is worth mentioning that the term "pinned connection" should not be taken literally, because an element with theorically pinned connections would have only translational DOF, and remember that 3D frame elements always have the torsional DOF. Thus, in this work, pinned connections is always related to the bending planes.

Figure 5.2 – Ranges of pinned and fully rigid connections.

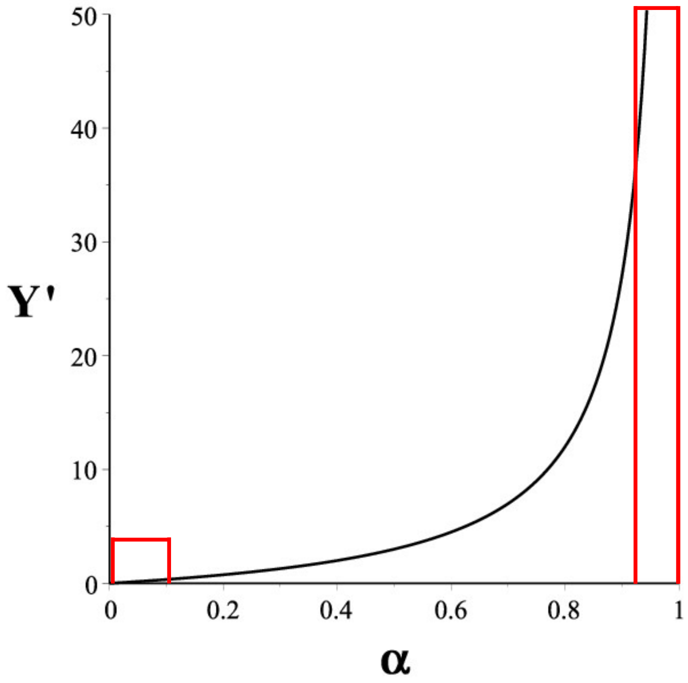

Source: Adapted from Chen (2000).

5.1 The Gradient-Based Method

In the numerical field of optimization, among the most distinct types of methods that exist, two classes stand out: gradient-based methods and derivative free methods.

Gradient-based methods are specifically applicable to continuous problems, continuously differentiable and with accurate first-order derivative calculation. They fit very well with smooth nonlinear optimization problems that have available gradient information. The iterative process is performed based on the information of the functions, the gradients and even the Hessian of the problem. Although they only guarantee convergence to local minima, due to the nature of the information used (local, around the current design point), the gradient-based methods present a good computational gain compared to the nature-inspired methods, since they decrease the amount of evaluation of the functions of the problem (ARORA, 2011).

The SLP is a gradient-based method widely used in complex situations, converting any nonlinear problem into a sequence of linear problems that can be solved iteratively by any LP method, such as the simplex method (CHOI; KIM, 2005). Despite the existence of several methods, the simplex remains the most used because of its efficiency in finding feasible basic solutions within the feasible domain. As the objective function and constraints are expressed as a linear combination of the design variables, an LP method always finds a solution located in the boundary of the design domain, at the intersection between constraints (RAO, 2009).

Pedersen (1972) and Pedersen and Jøgersen (1984) demonstrated in detail the formulation and use of the SLP method integrated with FEA. Each LP problem can be generated by linear approximations of all the functions of the problem around the current design point, using the Taylor series expansion truncated at the first order term. Thus, after the development of a sensitivity analysis, the optimization problem stated by equations (5.16)-(5.21) can be assembled in the LP format as

$$\text{Minimize} \qquad \sum_{j=1}^{ndv} \left(\frac{\partial}{\partial v_{p_j}} \left(\frac{W}{W_{SF}} \right) \right) \Bigg|_0 v_{p_j}, \tag{5.23}$$

$$\text{subject to} \quad \sum_{j=1}^{ndv} \left(\frac{\partial}{\partial v_{p_j}} \left(\frac{{U_d}^{LC}}{|U_{L_d}|} \right) \right) \Bigg|_0 v_{p_j} \geq -1.0 - \frac{{U_d}^{LC}{}_0}{|U_{L_d}|} + \sum_{j=1}^{ndv} \left(\frac{\partial}{\partial v_{p_j}} \left(\frac{{U_d}^{LC}}{|U_{L_d}|} \right) \right) \Bigg|_0 v_{p_{j_0}}, \tag{5.24}$$

$$\sum_{j=1}^{ndv} \left(\frac{\partial}{\partial v_{p_j}} \left(-\frac{{U_d}^{LC}}{U_{U_d}} \right) \right) \Bigg|_0 v_{p_j} \geq -1.0 + \frac{{U_d}^{LC}{}_0}{U_{U_d}} + \sum_{j=1}^{ndv} \left(\frac{\partial}{\partial v_{p_j}} \left(-\frac{{U_d}^{LC}}{U_{U_d}} \right) \right) \Bigg|_0 v_{p_{j_0}}, \tag{5.25}$$

$$\sum_{j=1}^{ndv} \left(\frac{\partial}{\partial v_{p_j}} \left(-\frac{{f(\theta)_{i,k}}^{LC}}{{\sigma_e}^2} \right) \right) \Bigg|_0 v_{p_j} \geq -1.0 + \frac{{f(\theta)_{i,k}}^{LC}{}_0}{{\sigma_e}^2} + \sum_{j=1}^{ndv} \left(\frac{\partial}{\partial v_{p_j}} \left(-\frac{{f(\theta)_{i,k}}^{LC}}{{\sigma_e}^2} \right) \right) \Bigg|_0 v_{p_{j_0}}, \tag{5.26}$$

$$\sum_{j=1}^{ndv} \left(\frac{\partial}{\partial v_{p_j}} \left(\frac{L_i}{L_L} \right) \right) \Bigg|_0 v_{p_j} \geq 1.0 - \frac{L_{i_0}}{L_L} - \sum_{j=1}^{ndv} \left(\frac{\partial}{\partial v_{p_j}} \left(\frac{L_i}{L_L} \right) \right) \Bigg|_0 v_{p_{j_0}}, \tag{5.27}$$

$$v_{p_{j_L}} \leq v_{p_j} \leq v_{p_{j_U}}, \tag{5.28}$$

$$i = 1, 2, \ldots, nel.$$

$$j = 1, 2, \ldots, ndv.$$

$$k = 1, 2 \text{ and } 3.$$

where ndv represent the number of design variables, 0 is the index for the previous iteration (current design point) and $v_{p_{j_L}}$ and $v_{p_{j_U}}$ are lower and upper bounds for the design variables. The design variables v_{p_j} are the constant coefficients of the LP problem. Thus, the development of the iterative procedure is supported by

$${v_{p_j}}^{n+1} = v_{p_{j_0}} + \Delta {v_{p_j}}^{n+1}, \tag{5.29}$$

$$n = 1, 2, \ldots, iter.$$

being Δv_{p_j} the stepsize of the design variables, n the index for iterations and $iter$ the total number of iterations. The LP problems are solved in n-iterations until the convergence criteria are satisfied.

Move limits on the side constraint of the design variables are applied and responsible for limiting the step at the $n\text{-}th$ iteration, avoiding the application of a line search and making the linearized sub problems bounded. Therefore, the SLP method may not converge to the precise minimum, since no descent function is defined (ARORA, 2011). In addition, both efficacy and computational efficiency of the optimization process are affected by the move limits (VANDERPLAATS, 1999).

Since linear approximations of the problem functions are used, the design changes Δv_{p_j} should not be large in the minimization direction, that is, the move limits cannot be excessively large. Usually, move limits are determined through fractions related to the design variable, ranging from 1 to 100% (ARORA, 2011). According to Pedersen (1972) and Pedersen and Jøgersen (1984), it is interesting to give large steps in the first iterations and tightethen as the optimal solution is approached. In the work of Yoshida and Vanderplaats (1988), the move limits were critical only in the early design stages. Therefore, the SLP method should not be used as a black box, because the user needs to understand how to select and update correctly the move limits.

The choice for a gradient-based method is supported by the fact that any nature-inspired method would present an exorbitant computational cost, since the amount of FEA required would be much higher, especially for the high number of design variables involved. Thus, after the definition of the optimization problem and the numerical optimization method, a computational code was developed in Fortran 90 language. Its iterative process follows the flowchart presented in Fig. 5.3. If desirable, detailed information about the working principle is presented in the Appendix A. Reading this appendix is not mandatory to understand the research.

For the development of the case studies of Chapter 6, as there is no guarantee of finding the optimal global solution in this optimization problem, a multistart strategy is assumed, being the structural problems optimized with different initial design variables and move limits. Then, the best configuration is established.

Figure 5.3 – The iterative optimization process of the algorithm.

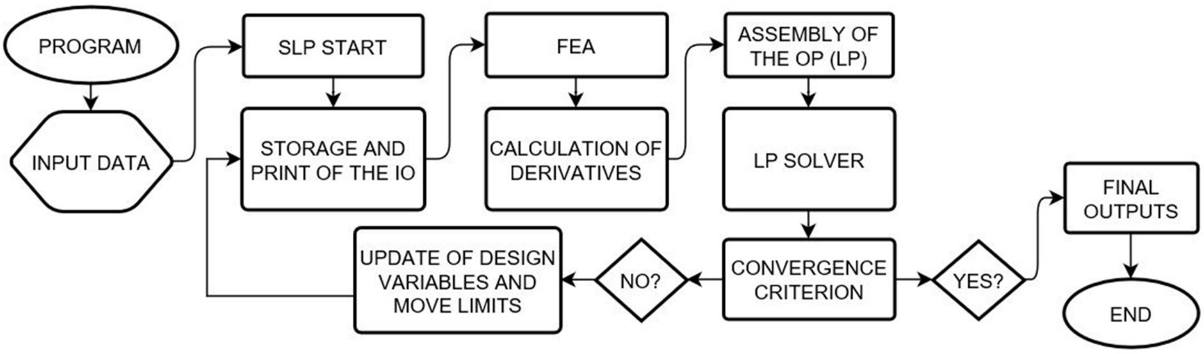

LEGEND: IO - ITERATIVE OUTPUTS
OP - OPTIMIZATION PROBLEM

Source: Author's production.

5.2 Analytical Sensitivity Analysis

To apply any gradient-based method in the structural optimization problem stated in equations (5.16)-(5.21), it is necessary to compute the gradient of the objective function and all the design constraints related to all the design variables.

The analytical sensitivity analysis is an important tool to allow the computation of the gradients at each iteration and to evaluate how the problem equations behave under any modification in the design variables (SERGEYEV; PEDERSEN, 1996). Despite some difficulty of finding the analytic expressions, this procedure allows the efficient and inexpensive use of mathematical programming (SANT'ANNA *et. al.*, 2001).

From now on, for simplicity, X^* represents generically the joint positions X, Y e Z as design variables.

5.2.1 Objective function

Directly, the gradient of the objective function defined in equation (5.1), referring to the design variables, can be defined as

$$\frac{\partial W}{\partial A_j} = c_{M\,j}\rho_j \frac{\partial A_j}{\partial A_j} L_j + \frac{\partial c_{S\,j}}{\partial A_j}, \tag{5.30}$$

$$\frac{\partial W}{\partial X^*} = c_{M\,j}\rho_j A_j \frac{\partial L_j}{\partial {X^*}_j} + \frac{\partial c_{S\,j}}{\partial X^*}, \tag{5.31}$$

$$\frac{\partial W}{\partial \alpha_j} = \frac{\partial c_{S_j}}{\partial \alpha_j}, \tag{5.32}$$

and after algebraic manipulations and simplifications, computed by

$$\frac{\partial W}{\partial A_j} = c_{M_j}\rho_j L_j \left(1 + \left(\sum_{c=1}^{4} (V_0 + V_1\alpha_c + V_2{\alpha_c}^2) \right)_j \right), \tag{5.33}$$

$$\frac{\partial W}{\partial {X_j}^*} = \sum_{m=1}^{nec} c_{M_m}\rho_m A_m \left(1 + \left(\sum_{c=1}^{4} (V_0 + V_1\alpha_c + V_2{\alpha_c}^2) \right)_m \right) \frac{\partial L_m}{\partial {X^*}_j}, \tag{5.34}$$

$$\frac{\partial W}{\partial \alpha_j} = c_{M_j}\rho_j A_j L_j \big(V_1 + 2V_2\alpha_j\big). \tag{5.35}$$

$$m = 1, 2, \dots, nec.$$

where m and nec are counters related to the elements that have the node coordinate X_j.

Note that while the cross-section areas and the fixity factors are parameters related only to the element that incorporate them, in the sensitivity relative to joint positions it is necessary to analyze the connectivity of the structure, since any modification in a given nodal coordinate, see Fig. 5.4, can affect the length of m-elements connected to the joint.

Figure 5.4 – Sensitivity of m-elements length related to iterative modifications in a given nodal coordinate X^*.

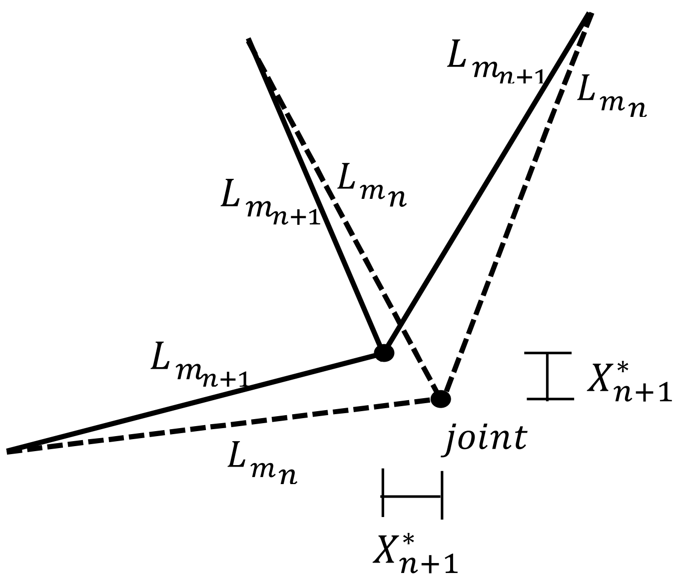

Source: Author’s production.

5.2.2 Displacement constraint

To compute the sensitivity of displacements relative to any design variable, the equilibrium equation (5.17) is differentiated and the sensitivity is defined by the linear system as follows

$$\mathbf{K}\frac{\partial \boldsymbol{U}^{LC}}{\partial v_{p_j}} = \left(\frac{\partial \boldsymbol{F}^{LC}}{\partial v_{p_j}} - \frac{\partial \mathbf{K}}{\partial v_{p_j}}\boldsymbol{U}^{LC}\right), \tag{5.36}$$

where the sensitivity of $\boldsymbol{F}$ depends on the nature of the load (distributed loads have sensitivity related to joint positions and fixity factors that must be accounted for) and the sensitivity of $\mathbf{K}$ is given by the sensitivity of $\mathbf{K_G}$ with respect to v_{p_j}. Thus, remembering,

$$\mathbf{K_G} = \mathbf{T}^{\mathrm{T}}\mathbf{K_L}\mathbf{T}, \tag{5.37}$$

and differentiating equation (5.37), we arrive at

$$\frac{\partial \mathbf{K_G}_i}{\partial v_{p_j}} = \frac{\partial \mathbf{T}_i{}^{\mathrm{T}}}{\partial v_{p_j}}\mathbf{K_L}_i\mathbf{T}_i + \mathbf{T}_i{}^{\mathrm{T}}\frac{\partial \mathbf{K_L}_i}{\partial v_{p_j}}\mathbf{T}_i + \mathbf{T}_i{}^{\mathrm{T}}\mathbf{K_L}_i\frac{\partial \mathbf{T}_i}{\partial v_{p_j}}. \tag{5.38}$$

Note that for cross-section areas and fixity factors, the first and third terms of the expressions are zero. The transformation matrix has only sensitivity related to the joint positions and the development of this sensitivity it is not trivial. Details about this sensitivity analysis are found in the report of Cardoso *et. al.* (2007). Also, the sensitivity of the elements length in relation to the joint positions can be easily identified at this development. Details about the analytical sensitivities of the element stiffness matrix $\mathbf{K_L}$ and consistent nodal loads of distributed loads are also described in the report of Faria and Muñoz-Rojas (2019).

5.2.3 Stress constraint

In order to impose stress constraints at each i-element, first is required to compute the sensitivity of the local nodal displacements, due to the sensitivity of the internal forces. To this end, it is necessary to map the sensitivity of the respective global nodal displacements, calculated in equation (5.36), and rotate to the local reference system.

Since the allowable stress σ_e is a constant parameter, the sensitivity analyzes are developed considering $f(\theta)$, but the final sensitivity is normalized. By manipulating equation (4.13),

$$f(\theta)_{i,k} = \frac{{N_x}_{i,k}^{\ 2}}{A_i^{\ 2}} + 2\left(\frac{\bar{c}_{i,k}{N_x}_{i,k}{M_R}_{i,k}}{A_i I_i}\right) + \frac{\bar{c}_{i,k}^{\ 2}{M_R}_{i,k}^{\ 2}}{I_i^{\ 2}} + \frac{3}{4}\left(\frac{{M_x}_{i,k}^{\ 2}R_i^{\ 2}}{I^2}\right) - \frac{3}{t_i}\left(\frac{R_i Q_i {M_x}_{i,k}{V_R}^{y'}{}_{i,k}}{I_i^{\ 2}}\right) + \frac{3}{t_i^{\ 2}}\left(\frac{Q_i^{\ 2}{V_R}^{y'}{}_{i,k}^{\ 2}}{I_i^{\ 2}}\right), \tag{5.39}$$

the sensitivity of the failure criterion can be computed for any design variable as

$$\begin{aligned}
\frac{\partial}{\partial {v_p}_j}\left(f(\theta)_{i,k}\right) = {}& {N_x}_{i,k}^{\ 2}\frac{\partial}{\partial {v_p}_j}\left(\frac{1}{A_i^{\ 2}}\right) + \frac{1}{A_i^{\ 2}}\frac{\partial}{\partial {v_p}_j}\left({N_x}_{i,k}^{\ 2}\right) + 2\left(\frac{{N_x}_{i,k}{M_R}_{i,k}}{A_i I_i}\right)\frac{\partial}{\partial {v_p}_j}\left(\bar{c}_{i,k}\right) \\
& + 2\left(\frac{\bar{c}_{i,k}{N_x}_{i,k}{M_R}_{i,k}}{I_i}\right)\frac{\partial}{\partial {v_p}_j}\left(\frac{1}{A_i}\right) + 2\left(\frac{\bar{c}_{i,k}{N_x}_{i,k}{M_R}_{i,k}}{A_i}\right)\frac{\partial}{\partial {v_p}_j}\left(\frac{1}{I_i}\right) \\
& + 2\left(\frac{\bar{c}_{i,k}{M_R}_{i,k}}{A_i I_i}\right)\frac{\partial}{\partial {v_p}_j}\left({N_x}_{i,k}\right) + 2\left(\frac{\bar{c}_{i,k}{N_x}_{i,k}}{A_i I_i}\right)\frac{\partial}{\partial {v_p}_j}\left({M_R}_{i,k}\right) + \frac{{M_R}_{i,k}^{\ 2}}{I_i^{\ 2}}\frac{\partial}{\partial {v_p}_j}\left(\bar{c}_{i,k}^{\ 2}\right) \\
& + \bar{c}_{i,k}^{\ 2}{M_R}_{i,k}^{\ 2}\frac{\partial}{\partial {v_p}_j}\left(\frac{1}{I_i^{\ 2}}\right) + \frac{\bar{c}_{i,k}^{\ 2}}{I_i^{\ 2}}\frac{\partial}{\partial {v_p}_j}\left({M_R}_{i,k}^{\ 2}\right) + \frac{3}{4}\left(\frac{{M_x}_{i,k}^{\ 2}}{I_i^{\ 2}}\right)\frac{\partial}{\partial {v_p}_j}\left(R_i^{\ 2}\right) \\
& + \frac{3}{4}\left(R_i^{\ 2}{M_x}_{i,k}^{\ 2}\right)\frac{\partial}{\partial {v_p}_j}\left(\frac{1}{I_i^{\ 2}}\right) + \frac{3}{4}\left(\frac{R_i^{\ 2}}{I_i^{\ 2}}\right)\frac{\partial}{\partial {v_p}_j}\left({M_x}_{i,k}^{\ 2}\right) \\
& - \frac{3}{t_i}\left(\frac{Q_i{M_x}_{i,k}{V_R}^{y'}{}_{i,k}}{I_i^{\ 2}}\right)\frac{\partial}{\partial {v_p}_j}\left(R_i\right) - \frac{3}{t_i}\left(\frac{R_i{M_x}_{i,k}{V_R}^{y'}{}_{i,k}}{I_i^{\ 2}}\right)\frac{\partial}{\partial {v_p}_j}\left(Q_i\right) \\
& - \frac{3}{t_i}\left(R_iQ_i{M_x}_{i,k}{V_R}^{y'}{}_{i,k}\right)\frac{\partial}{\partial {v_p}_j}\left(\frac{1}{I_i^{\ 2}}\right) - \frac{3}{t_i}\left(\frac{R_iQ_i{V_R}^{y'}{}_{i,k}}{I_i^{\ 2}}\right)\frac{\partial}{\partial {v_p}_j}\left({M_x}_{i,k}\right) \\
& - \frac{3}{t_i}\left(\frac{R_iQ_i{M_x}_{i,k}}{I_i^{\ 2}}\right)\frac{\partial}{\partial {v_p}_j}\left({V_R}^{y'}{}_{i,k}\right) + \frac{3}{t_i^{\ 2}}\left(\frac{{V_R}^{y'}{}_{i,k}^{\ 2}}{I_i^{\ 2}}\right)\frac{\partial}{\partial {v_p}_j}\left(Q_i^{\ 2}\right) \\
& + \frac{3}{t_i^{\ 2}}\left(Q_i^{\ 2}{V_R}^{y'}{}_{i,k}^{\ 2}\right)\frac{\partial}{\partial {v_p}_j}\left(\frac{1}{I_i^{\ 2}}\right) + \frac{3}{t_i^{\ 2}}\left(\frac{Q_i^{\ 2}}{I_i^{\ 2}}\right)\frac{\partial}{\partial {v_p}_j}\left({V_R}^{y'}{}_{i,k}^{\ 2}\right).
\end{aligned} \tag{5.40}$$

The differentiation of equation (5.40) required many algebraic operations and investigations, due to mathematical indeterminancy ($\frac{0}{0}$) related to different nullity combinations of the pairs of internal forces (V_y, V_z) and (M_y, M_z). This equation is recapture from the Appendix B with respect to the cross-sections areas, remembering that the thin-wall thickness and the critical point are constant terms and, therefore, do not present sensitivity to any design variable of the optimization process. Further details of the analytic development considering joint positions and fixity factors are available in the report of Faria and Muñoz-Rojas (2019).

Chapter 6

Results and Discussion

The purpose of this chapter is to develop, analyze and discuss the proposed structural optimization problem. First, an analytical study and a simple 2D optimization problem is presented, mainly to justify the applicability of the failure criterion in the scope of layout optimization. The mechanical effects of semi-rigid connections on FEA and structural optimization of space frames are analyzed. Through three case studies, special focus will be given to the comparison between layout optimization (LO), sizing and connections optimization (SCO) and layout and connections optimization (LCO) – "LO x LCO" and "SCO x LCO". The efficacy and computational efficiency of the processes will be compared by analyzing, respectively, the optimal solutions and the relative time of processing required. As will be seen, many other quantitative and qualitative features are also analyzed.

6.1 Failure Criterion Analysis

6.1.1 Analytical study

Optimizing space frame layout required a failure criterion that is able to correctly evaluate the mechanical strength of elements with variable lengths, due to the iterative modification in the joint positions. Thus, it is important to account the shear effect when calculating von Mises stresses. To prove this statement, consider the particular case of Fig. 6.1, a clamped beam of length L and circular thin-wall cross-section area, subjected to the concentrated load F at the free end.

Based on the imposed boundary conditions, only two type of stress can coexist in the cross-sections along the length of the element: the normal stress due to the bending moment and the shear stress due to the shear force. Analytically, considering the clamping point at node 1, the maximum stresses ${\sigma_{xx}}_{máx}$ e ${\tau_{yz}}_{máx}$ can be calculated as follows,

$$\sigma_{xx_{máx}} = \frac{FLR}{I} \quad e \quad \tau_{yz_{máx}} = \frac{FQ}{It}. \tag{6.1}$$

Figure 6.1 – Clamped beam.

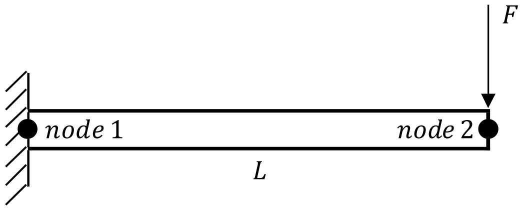

Source: Author's production.

To correctly measure the magnitude of the shear effect on the cross-section, the following expression is described

$$\tau_{yz_{máx}} = \xi\sigma_{xx_{máx}} \quad \rightarrow \quad \frac{FQ}{It} = \xi\frac{FL_{cr}R}{I}, \tag{6.2}$$

where $\xi(\%)$ is the percentage that characterizes the relationship between the magnitude of the maximum stresses and L_{cr} is the critical length necessary for the equality to occur. Thus, for any ξ, knowing the static moment Q by the equation given in the expression (4.9) and simplifying equation (6.2),

$$\frac{4tR_m}{3} = \xi L_{cr}R. \tag{6.3}$$

Observing equation (6.3), it is noted that the analysis depends only on geometric parameter belonging to the element. Remembering the equation of the midline radius R_m

$$R_m = R - \frac{t}{2}, \tag{6.4}$$

replacing equation (6.4) in equation (6.3) and applying the possible simplifications,

$$L_{cr} = \xi^{-1}\left(\frac{4t}{3}\left(1 - \frac{t}{2R}\right)\right), \tag{6.5}$$

$$L_{cr} = \xi^{-1}g(R, t). \tag{6.6}$$

Depending on the percentage ξ adopted, the expression $g(R,t)$ indicates the length L_{cr} that an element must have to presents a shear stress of relevant magnitude ($\xi\sigma_{xx_{máx}}$). As an example, in the hypothetical case where and expressive shear stress value with magnitude in the order of 10% of the normal stress is considered, $\xi = 0{,}1$, L_{cr} is $10x$ greater than the original value of $g(R,t)$.

Assuming a set of distinct lengths, concentrated load of $50\ kN$ (negative) and geometric properties referring to a commercial circular section ($\emptyset 141.3\ mm$ and $t = 12.70\ mm$) taken from Grupo Açotubo (2019), the equivalent stresses are calculated in the cross-section located in the clamping of the beam shown in Fig. 6.1. Considering $\xi = 1$ in equation (6.5), the critical length L_{cr} is approximately $15\ mm$.

Remembering that the failure criterion provides a greater weight ($\sqrt{3}$) for the shear stresses, according to the von Mises theory, and evaluates the stress at the critical point θ, the graph of Fig. 6.2 compares the code results (dashed lines) with the respective results obtained considering the analytical solution (solid line) without the shear effect of the resulting shear force. Only the range $0 - 100\ mm$ is shown, but longer lengths have been tested.

Figure 6.2 – Numerical results (with the transverse shear stress) *vs.* analytical results (without the transverse shear stress).

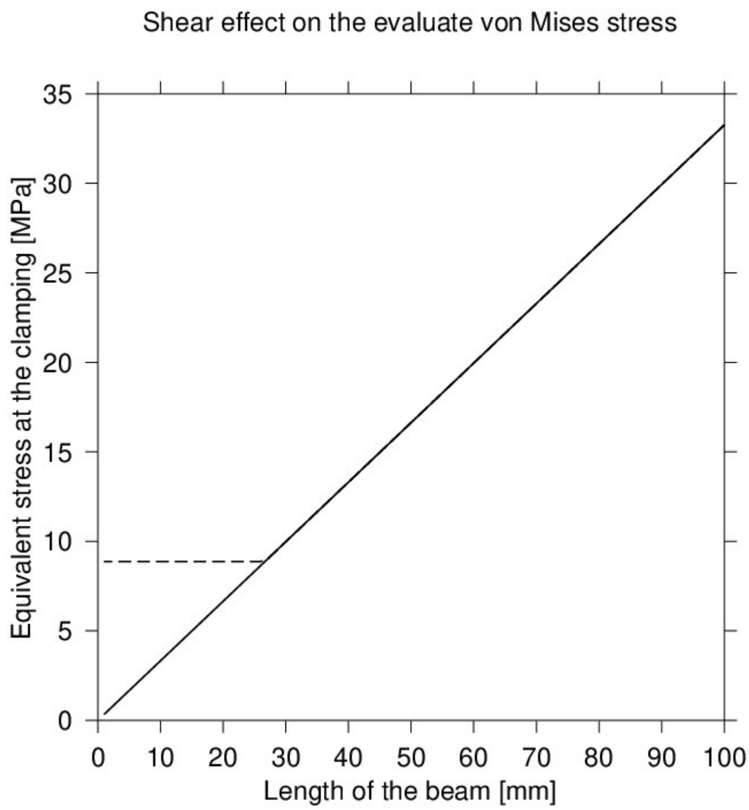

Source: Author's production.

Note that the numerical and analytical equivalent stresses coincide until a visible separation region, approximately $L \approx 25\ mm$ $(\sqrt{3} * (15)\ mm)$, where the shear stress of the resulting shear force cannot be neglected. As a consequence, due to the combination of normal and shear stresses, the critical point is changed from $\frac{\pi}{2}$ to 0, consistent with the reference system adopted for the stresses distribution at Fig. 4.1 (remember that θ is evaluated from the local $\tilde{z}$-axis). According to the formulation, equation (6.7) mathematically demonstrates this combination of stresses and, additionally, Figs. 6.3(a-b) show the modification of the critical point.

$$\sigma_{eq} = \sqrt{\left(\frac{FLR\sin(\theta)}{I}\right)^2 + 3\left(-\frac{4tR_mF\cos(\theta)}{3I}\right)^2}. \tag{6.7}$$

Figure 6.3 – Normal, shear and equivalent stresses for lengths of (a) $20\ mm$ and (b) $40\ mm$.

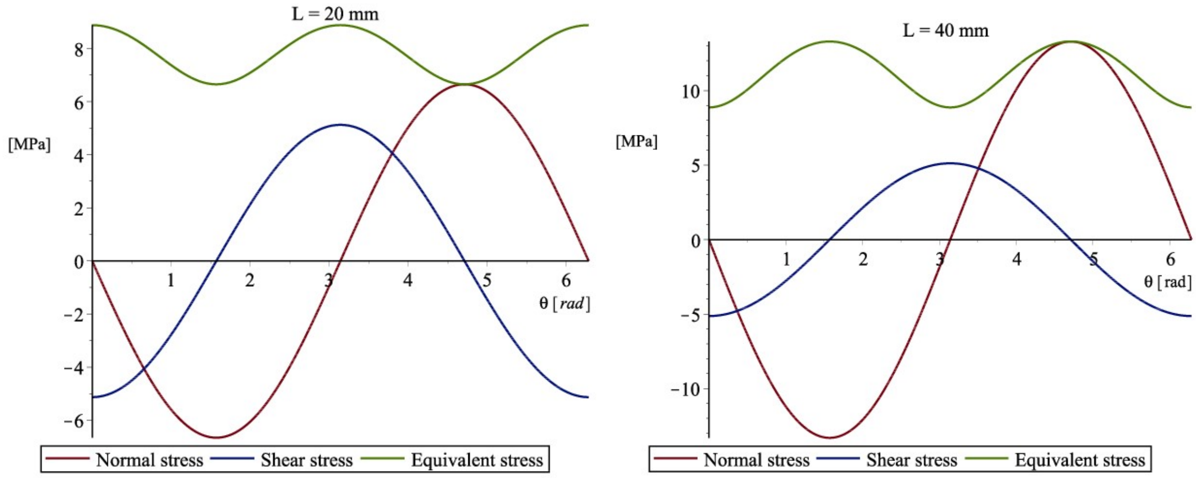

(a) (b)

Source: Author's production.

When $L \approx 25\ mm$, the shear stress of approximately 9 MPa that would be neglected is significant. The case of clamped beam is very particular, where only the bending moment and the shear force of the $\tilde{x}\tilde{y}$ plane are considered. In 3D frame elements, combination of six internal forces may arise and the shear stresses from the shear forces V_y and V_z may be determinant for the correct judgment of the mechanical strength.

6.1.2 Power transmission tower

To illustrate the applicability of the failure criterion, consider the planar frame shown in Fig. 6.4. Layout optimization with stress constraints ($\sigma_e = 147\ MPa$) and minimum element length ($5\ mm$) is developed. The power transmission tower is clamped and subjected to two load cases (remember the index LC) that correspond to weight and wind forces, both transmitted by the cables connected at the top end nodes (orthogonal to the plane of the structure). Details about mechanical properties, boundary conditions and connectivity are omitted as they are not relevant to the context of the present study.

Figure 6.4 – The 2D optimization problem developed and highlight of the short element with the highest shear stress τ_{V_R}.

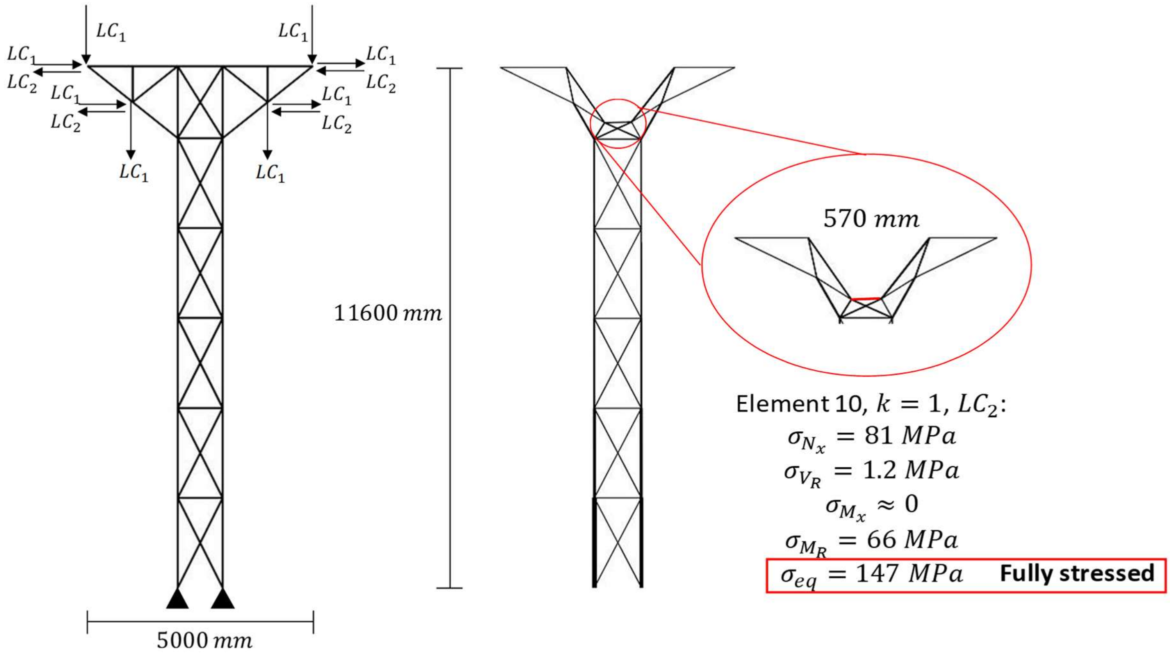

Source: Author's production.

All elements had their respective areas optimized, while layout changes were allowed only at the top of the structure. For this reason, note that the optimization process produced short elements in the middle region, see the optimal solution in Fig. 6.4. In addition, as seen in Achtziger (2007), the optimal solution is not perfectly symmetrical.

The optimal structure has several elements with shear stress τ_{V_R} in the order of magnitude of 0.1-1.0 MPa. However, special attention must be paid to element 10 (highlighted in red, see Fig. 6.4): it has one of the shortest lengths ($570\ mm$, being larger than just two diagonal elements connected to its ends) and shear stresses τ_{V_R} of $1.2\ MPa$ in the two load cases.

The emphasis given to the element 10 stems from the fact that it is fully stressed under both load conditions. Even knowing that the bending moment stresses of this same element have magnitudes ranging between 30-$70\ MPa$ (and the other axial and torsional stresses added up) along the length, realize that if the optimization process had not taken into account the effect of shear forces at the shear stress, the optimal solution would probably be incorrectly sized and all elements which are in similar situation would have shear section failure.

This example demonstrates the importance of optimizing structural layout by accounting for the effect of shear forces within shear stresses.

6.2 Semi-Rigid Connections within FEA and Optimization

Before presenting the case studies developed, it is important to clarify the procedure adopted for the post processing of optimal solutions. Through a code developed in Maple, the elements that reach the area removal factor (a minimum value of area at the side constraint previously set) are removed from the initial topology. Moreover, elements with cross-section areas that closely approximate the lower bound and have no structural function are also removed. The non-structural elements are those that are not transmitting internal forces and, consequently, are not aiding in the global mechanical strength of the structure. Then, to ensure that the solution does not violate the imposed constraints, an additional optimization process is performed with the optimal solution as a starting point, providing an ajustment of the optimal solution with the modified topology.

It is worth mentioning that none of the case studies will take into account the effects of shear on deflections, hence $\zeta = 0$. Additionally, to simplify, all the case studies consider that the material cost $[\frac{\$}{kg}]$ is unitary.

6.2.1 Frame dome

As the original data of the mesh was not found, the frame dome shown in Fig. 6.5 is an approximation with own choices of joint positions of the structure, which was firstly investigated by Pedersen (1973) and contains 52 elements and 21 nodes. Following Pedersen

(1973), all the elements have circular thin-wall cross-sections with constant thickness of 8 mm, initial cross-section areas $A = 30.10^3\ mm^2$, Young's modulus $E = 200.10^3\ MPa$, shear modulus $G = 80\ MPa$, yield strength $\sigma_e = 147\ MPa$ and specific mass $\rho = 7.799E^{-6}\ kg/mm^3$. The structure is clamped at the nodes of the external contour. The connectivity is presented in Table 6.1. Whit this data, the initial structure has approximately $70000\ kg$ of mass.

Figure 6.5 – Frame dome of Pedersen (1973).

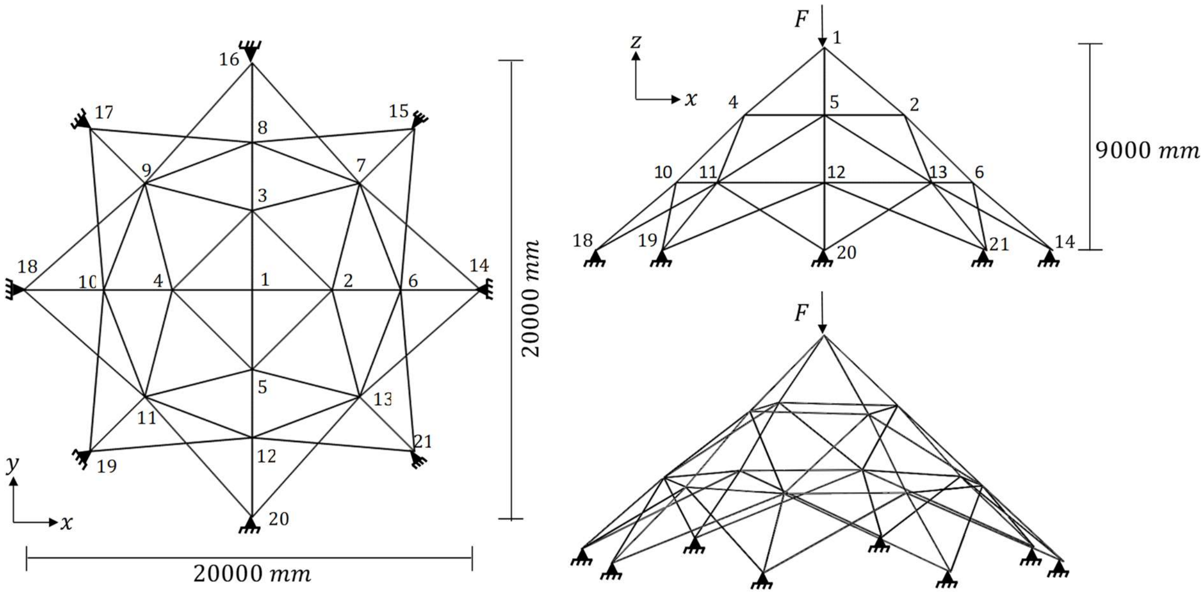

Source: Author's production based on Sergeyev and Pedersen (1996).

Table 6.1 – Connectivity of the structure.

Elements	**1**	**2**	**3**	**4**	**5**	**6**	**7**	**8**	**9**	**10**	**11**	**12**	**13**	**14**	**15**	**16**	**17**	**18**
Nodes	*14*	*7*	*16*	*9*	*18*	*11*	*20*	*13*	*15*	*8*	*17*	*10*	*19*	*12*	*21*	*6*	*6*	*7*
	7	*16*	*9*	*18*	*11*	*20*	*13*	*14*	*8*	*17*	*10*	*19*	*12*	*21*	*6*	*15*	*7*	*8*
Elements	**19**	**20**	**21**	**22**	**23**	**24**	**25**	**26**	**27**	**28**	**29**	**30**	**31**	**32**	**33**	**34**	**35**	**36**
Nodes	*8*	*9*	*10*	*11*	*12*	*13*	*2*	*7*	*3*	*9*	*4*	*11*	*5*	*13*	*2*	*3*	*4*	*5*
	9	*10*	*11*	*12*	*13*	*6*	*7*	*3*	*9*	*4*	*11*	*5*	*13*	*2*	*3*	*4*	*5*	*2*
Elements	**37**	**38**	**39**	**40**	**41**	**42**	**43**	**44**	**45**	**46**	**47**	**48**	**49**	**50**	**51**	**52**		
Nodes	*14*	*6*	*2*	*18*	*10*	*4*	*20*	*12*	*5*	*16*	*8*	*3*	*15*	*17*	*19*	*21*		
	6	*2*	*1*	*10*	*4*	*1*	*12*	*5*	*1*	*8*	*3*	*1*	*7*	*9*	*11*	*13*		

Source: Author's production.

The optimization processes takes into account a single load case $F = 632745\ N$, without self-weight and with a unique load acting in the negative z-axis, see Fig. 6.5.

Aiming to compare the results obtained, the analysis will be developed as follows:

- Layout optimization with fixed fully rigid connections and semi-rigid connections with 75%, 50%, 25% and 1% of rotational stiffness;
- Layout and connections optimization.

The design variables adopted are the same for all the studies of the frame dome: all the cross-section areas, the joint positions X and Y of nodes 6, 7, 8, 9, 10, 11, 12 and 13, and the joint positions Z of nodes 2, 3, 4 and 5. The design variables are not linked and there is no explicit side constraints on the joint positions. Constraints on the von Mises stress and on the minimum length (5 mm) of each element are applied.

In the LCO process, all possible fixity factors are also added as design variables, with initial rotational stiffness of 75%. The clamped elements have fixed fully rigid connections (i.e. are not design variables). The additional cost of connections is within the range of 20-60%. To analyze the behavior of the LCO process from the perspective of a design constraint related to the flexibility of the structure, displacement constraints on nodes 2, 3, 4 and 5 are also imposed. All these features are shown in Fig. 6.6.

Figure 6.6 – Design variables and displacement constraints applied in LCO process.

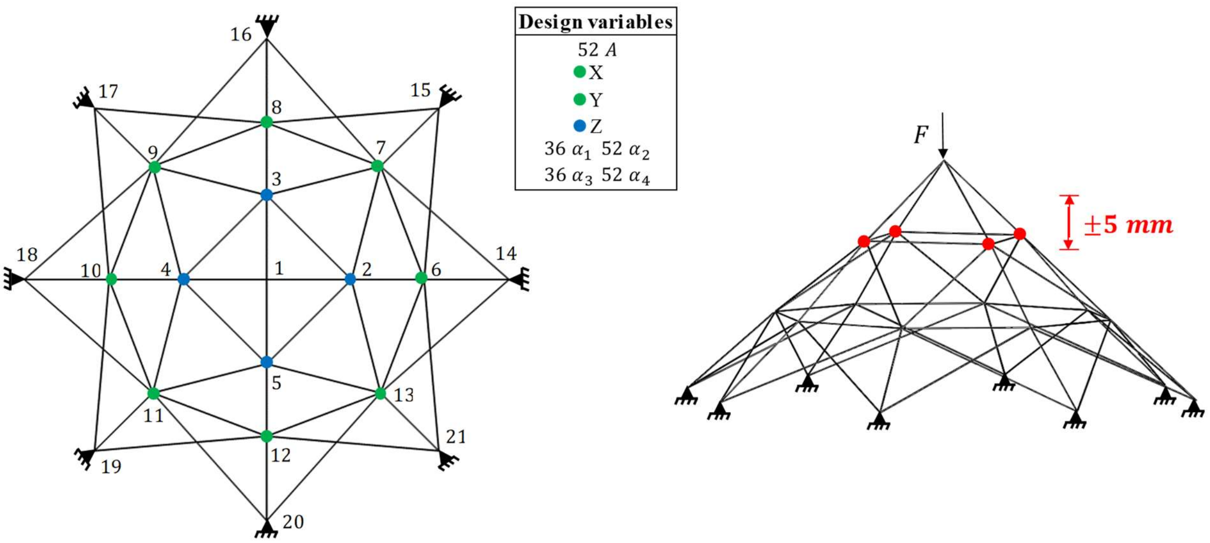

Source: Author's production.

The critical point of each cross-section area and its von Mises stress are determined after a sweep of 0 to 2π. The stepsize was chosen by a previous convergence study, visualized in Figs. 6.7(a-b). After identifying an element and cross-section area in which it has the highest von Mises stress, at the last iteration, several sweeps are performed on it with different stepsizes. Observing Fig. 6.7(a), it is possible to note that since the maximum stress at this point is always found at π, the sweep may even be considered unnecessary. However, some elements present maximum stress at different points, not multiples of 0 or π, due to different combinations of the internal forces, a fact that proves the usefulness of the failure criterion formulated.

Figure 6.7 – Convergence analysis of the stress calculation at (a) the element 39, cross-section 1, and (b) the element 22, cross-section 3.

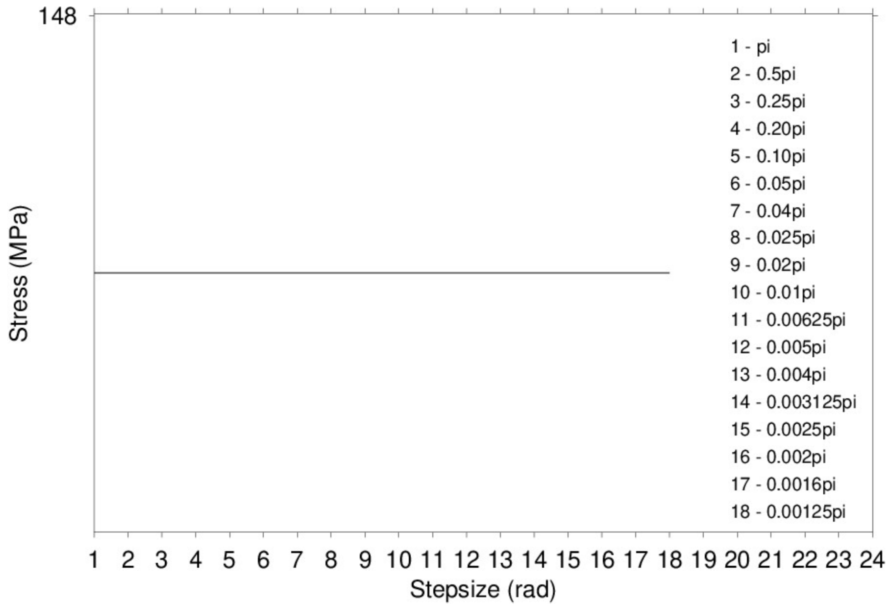

(a)

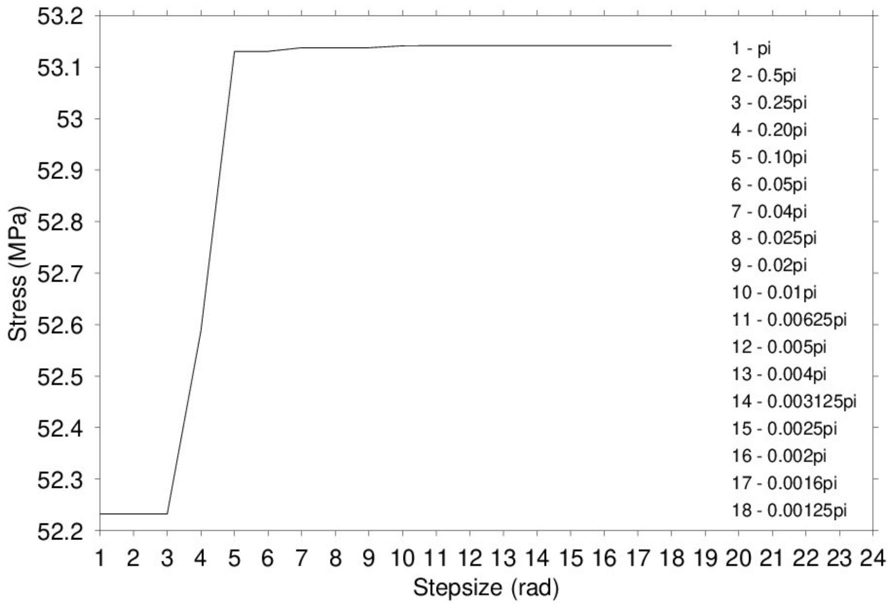

(b)

Source: Author's production.

Thus, another convergence study was developed, as can be seen in Fig. 6.7(b). The stress calculation converges and the stepsize of 0.00625π could be assumed without major problems. As the computational cost practically does not increase, the stepsize of 0.002π was chosen, in order to ensure a good accuracy.

6.2.1.1 Layout optimization with fixed (A) fully rigid connections and fixed semi-rigid connections with (B) 75%, (C) 50%, (D) 25% and (E) 1% of rotational stiffness

After 244 iterations, the optimal solution of (A) is found through the process exposed in Fig. 6.8(a). Also, Fig. 6.8(b) shows the 16 fully stressed elements, of the 24 that remained in the topology. As seen in Fig. 6.8(b) and in the other case studies, note that the different thicknesses of the elements represent the magnitude of their areas.

Figure 6.8 – (a) The optimization process and final solution and (b) the fully stressed (red) elements of study (A).

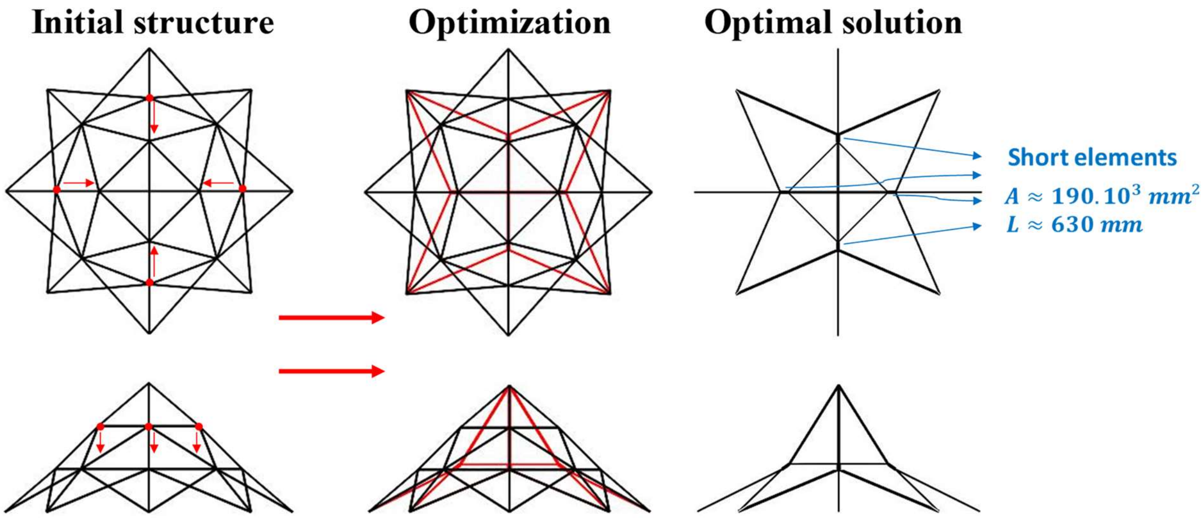

(a)

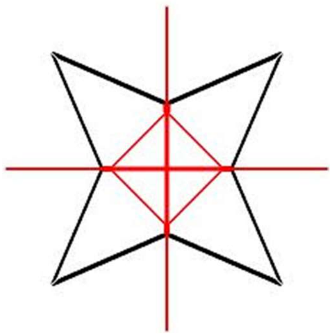

(b)

Source: Author’s production.

To minimize the objective function and resist to the imposed loading, see Fig. 6.8(a), the optimization process chooses to act as follows: gradually, decreases the areas of all the elements connected to nodes 7, 9, 11 and 13, until they can be removed, redirecting the transmission of internal forces to the other elements. Simultaneously, by descending the upper nodes 2, 3, 4 and 5 at negative z-direction and approaching nodes 6, 7, 8, 9, 10, 11, 12 and 13 at x and y directions to the center of the structure, the process shortens and offers the largest areas (compared to the others) to four elements (38, 41, 44 and 47), aiming to supply the absence of the non-structural elements. It is interesting to note that since all elements connected to the nodes 7, 9, 11 and 13 are removed, the nodes themselves disappear from the topology of the structure.

The optimization starts the stabilization process after iteration 220, see Fig. 6.9(a), and the final cost of the optimized structure is \$$1946$, being \$$1216$ of material cost and \$$729$ of connections cost. The graph of Fig. 6.9(b) represents the most stressed element at each iteration. Note that until iteration 130 there was no fully stressed element.

Figure 6.9 – Results about (a) convergence diagram of the objective function and (b) diagram of the most stressed element at each iteration.

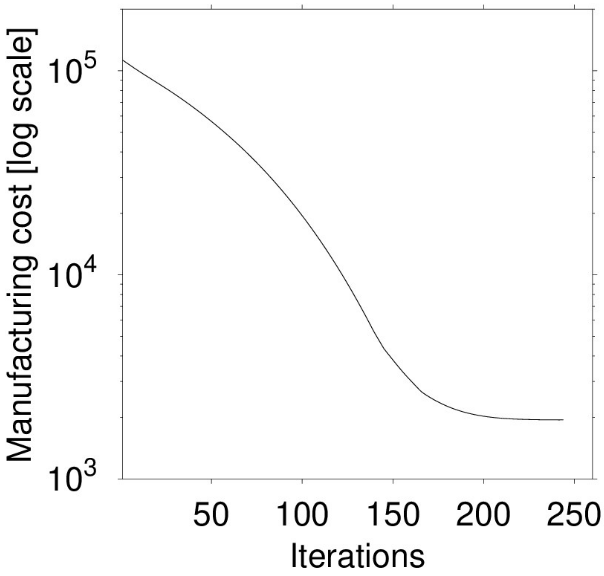

(a)

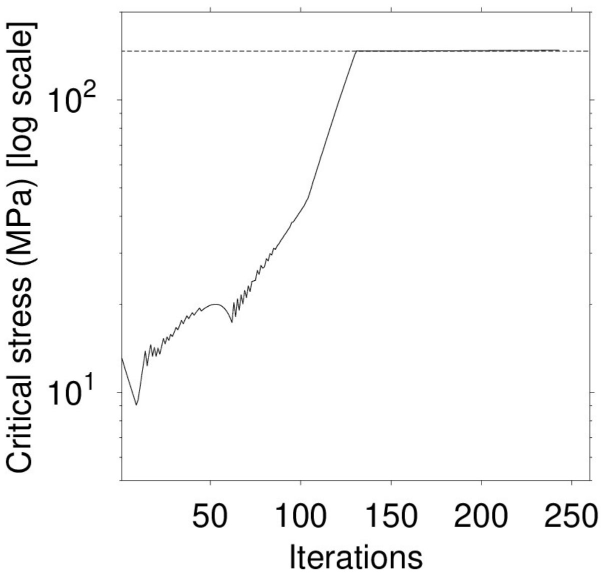

(b)

Source: Author’s production.

The four elements with the smallest lengths have the highest shear forces ($10^3 \gg 10^0$ magnitudes) of all structure. However, the respective shear stresses computed have the magnitude of $0.02\ MPa$, which is not significant.

From the global point of view, it was observed that this new layout greatly reduces the magnitude of all the internal forces, especially the bending moments, but also the shear forces and torsion. All elements have axial forces and consequently normal stresses that are much greater compared to all other internal forces and their respective stresses.

Thereafter, all the case studies with fixed semi-rigid connections are developed and analyzed analogously to the previous one. With exception of study (E), the layout and topology of the optimal solutions does not change (so the representations are omitted). The short elements of all studies continue to have negligible shear stresses produced by the resulting shear force and the same elements are fully stressed in studies (A-D). A comparison of convergence graphs is demonstrated in Fig. 6.10, where W_1 and W_2 are the material and connections costs, respectively.

Figure 6.10 – Comparison between the convergence of the objective function.

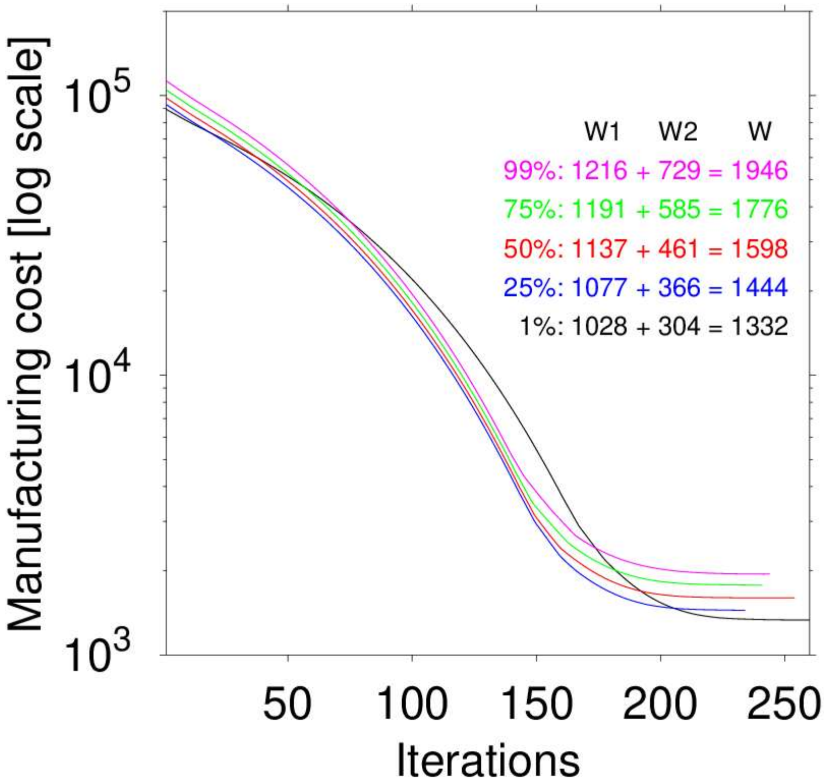

Source: Author's production.

As can be seen in Fig. 6.11, in study (E) a different optimal solution is found, with 36 fully stressed elements. Note that the layout and topology are not symmetrical. Also, instability was faced during this optimization process, requiring several additional testing on the move limits to find a configuration that could converge to some optimal solution.

Figure 6.11 – The optimal solution when all connections are pinned, study (E), with the 36 fully stressed elements.

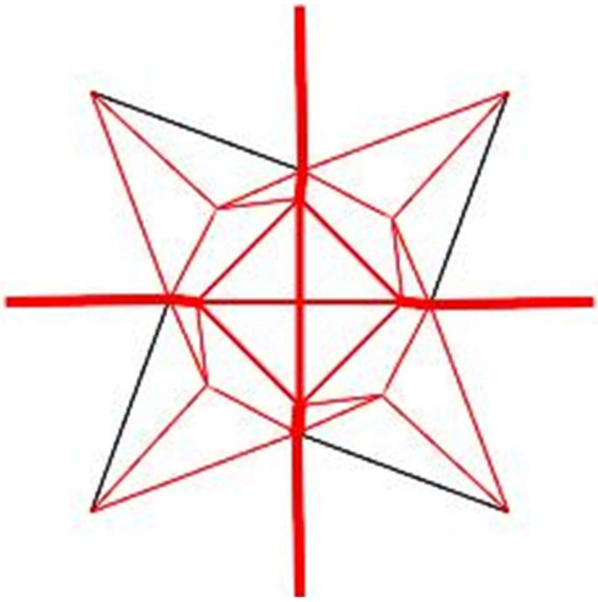

Source: Author's production.

By reducing the rotational stiffness of the connections, all studies showed the expected reduction in the magnitude of bending moments and the increase in nodal displacements. In study (B), for example, when compared to the study where the connections are rigid (25% less rotational stiffness), the bending moments decreased within the range of 15 to 30%. On the other hand, the increase in displacements is within the range of 1 to 70%, being the largest increase due to the rotations. In study (E) we find the largest translational displacements ($23\ mm$ at the z-direction) and, although not considered at first, this exaggerated flexibility could be a future problem. Without the application of displacement constraints, there is a possibility that the optimal structure presents large displacements and, consequently, the linear model for the connections becomes invalid.

According to Fig. 6.10, the greater the reduction in rotational stiffness of the connections, the greater the manufacturing cost minimization. As the bending moments decrease, the von Mises stresses also decrease and this allows larger area reductions and, consequently, greater material savings. As the cost of connections is not only directly related to the level of rotational stiffness but also proportional to the material cost, this cost also reduces. Thus, according to the results obtained until here for this structural optimization problem (stress and minimum length constraints), it is economically feasible to manufacture the structure with only pinned connections. The optimal solution of the study (E) has 31% less manufacturing cost than the optimal fully rigid structure.

In addition, note that the optimal solutions of studies (A-D) are structures for this single load case. However, if the real structure presents any different loading, all these solutions become mechanisms. This proves the importance of analyzing and optimizing structures considering multiple load cases.

6.2.1.2 Layout and connections optimization

After 264 iterations, the optimal solution is presented in Fig. 6.12. Note that the solution (layout and topology) of the structure is equal to the solution of study (E). The short elements have a much larger length (1067 mm, almost double) than previous studies (A-D). Only 12 elements are removed, but 36 elements are fully stressed, see the previous Fig 6.11.

Figure 6.12 – The physical behavior of the optimization process.

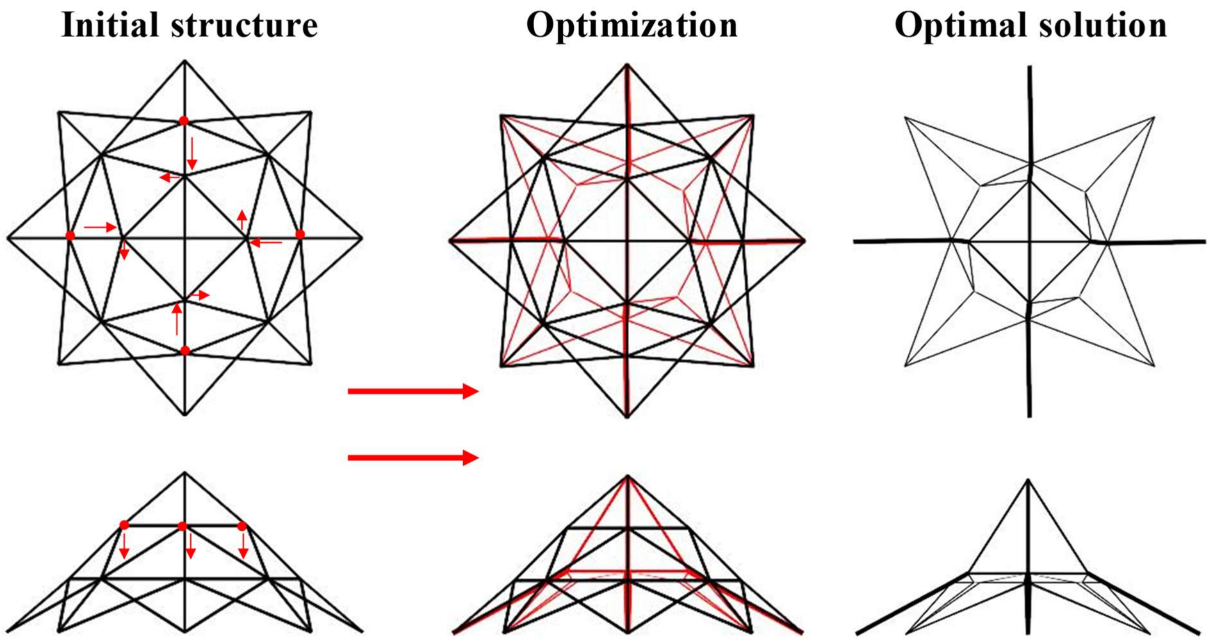

Source: Author's production.

The optimization faced a path, see Fig. 6.12, not yet seen during the iterative process:

1) Move the upper nodes 2, 3, 4 and 5 downwards;
2) Approach nodes 6, 8, 10 and 12 to the center of the structure;
3) Reduce the rotational stiffness of all connections until they become pinned;
4) Allowing the existence for more elements and finally moving the nodes 6, 8, 10 and 12, but now non-symmetrically.

Table 6.2 shows the optimal joint positions and, for convenience, the optimal areas are presented later, when this LCO process is compared to another LCO process.

Table 6.2 – Optimal joint positions.

Nodes	**6**	**7**	**8**	**9**	**10**	**11**	**12**	**13**
$\boldsymbol{X}$ **[mm]**	14443	13161	10092	7207	5556	6838	9907	12792
$\boldsymbol{Y}$ **[mm]**	9907	12792	14443	13161	10092	7207	5556	6838
Nodes	2	3	4	5				
$\boldsymbol{Z}$ **[mm]**	3537	3524	3537	3524				

Source: Author's production.

The optimal solution has only pinned connections and non-symmetrical layout and topology, a fact already faced in the research of Achtziger (2007), but theoretically unexpected since the structural problem is symmetric. Therefore, it is a local solution. Since the SLP method linearizes the optimization problem in each iteration, a small numerical error in the rounding of the design variables can cause a perturbation on the linearization, which can modify the minimization direction and cause the process to fall in a local minima. As commented in Achtziger (2007), this could be avoided by using a global optimization algorithm or applying additional constraints that impose symmetry.

This sensitivity of the linearization is associated with the small degree of approximation of the functions in the optimization process. The optimal structure of Fig. 6.12 was tested with the inverted non-symmetry. By the results obtained, the structure not only guarantees the non-violation of the constraints, but also presents the same objective function. Therefore, it can be concluded that they are local solutions.

Since the addition of fixity factors as design variables represents an addition of 176 variables, and no information about convexity is available, the proposed optimization problem increases the possibility of finding local minima. Moreover, it became apparent that the computational cost of processing also increases, not only due to the additional calculation of derivatives, but also by the increase in the size of the LP problems.

Due to a different layout and topology with more elements ($40 > 24$) than previous studies (A-D), in this optimal solution the transmission of internal forces to the clamped points of the structure is smoother. Because of this uniform distribution, most of the axial forces are smaller. While in studies (A-D) the maximum axial forces are in the range of 10^6, here the maximum axial forces are in the range of 10^5.

With this reduction of axial forces, and also of the bending moments (consequence of the pinned connections), the optimization process is able to further reduce the cross-section areas and hence greater material cost savings (and consequently connections cost) is achieved. Another feature that can be seen in Fig. 6.13 is that the elements that make a "+" cross-shape in the optimal solution of this study have larger areas, which allow greater reduction of the areas of the adjacent elements.

Figure 6.13 – Comparison between the optimal solutions of studies (E) and LCO and the optimal solutions of the previous studies (A-D).

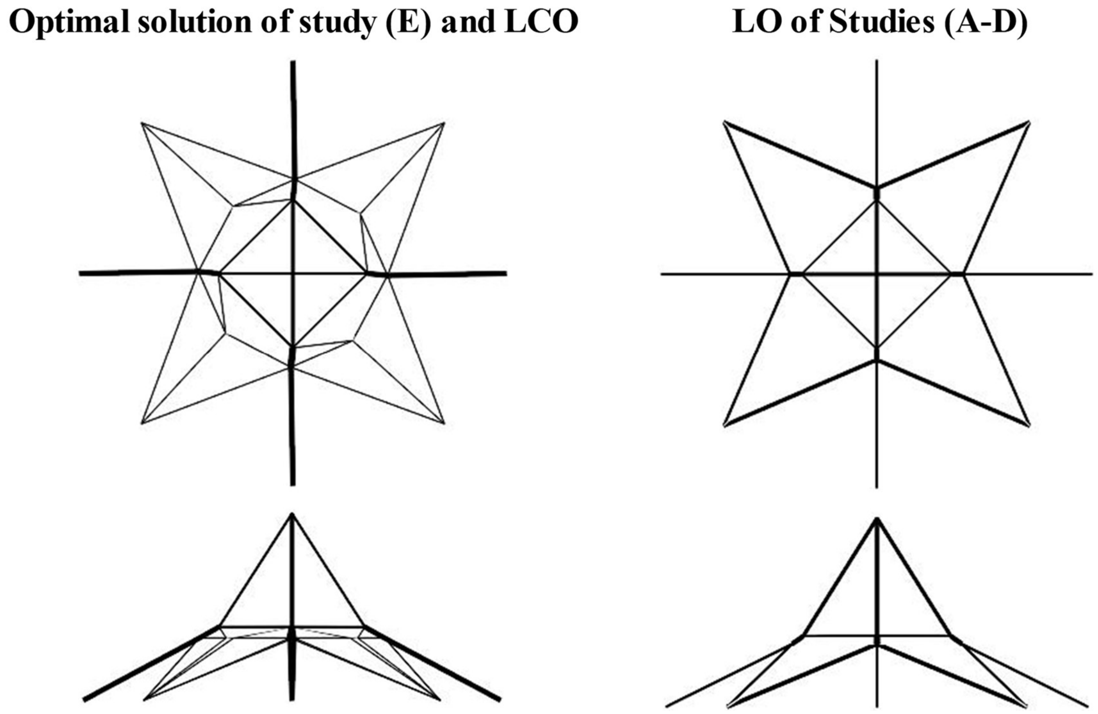

Source: Author’s production.

Analyzing the evolution of the design variables, it was observed that all connections are made to be pinned in a uniform way, with the same step pattern. This is expected since displacement constraints are not imposed and pinned connections have the lowest manufacturing cost.

The optimized structure has \$1331 of total cost, being \$1026 of material cost and \$304 of connections cost, is 31% cheaper than the fully rigid structure. Compared to studies (A-D), the most interesting fact is that although less elements are removed, the process achieves a greater reduction of material cost, choosing a minimization path to a local minima where cross-section areas are reduced in a different way. The graph results are presented in Figs. 6.14(a-d).

Figure 6.14 – Results about convergence diagram of the actual study for (a) material cost, (b) connections cost, (c) manufacturing cost and (d) diagram of the most stressed element at each iteration.

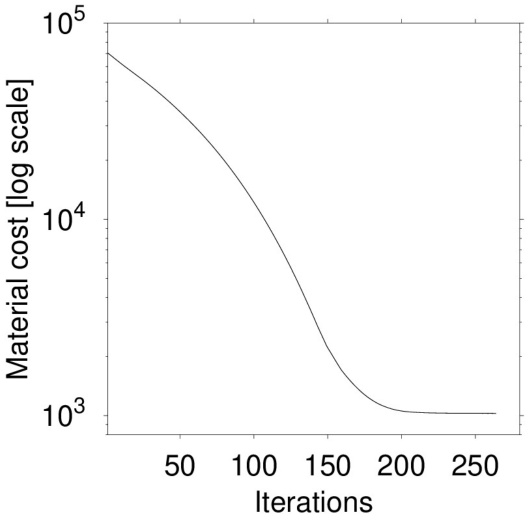

(a)

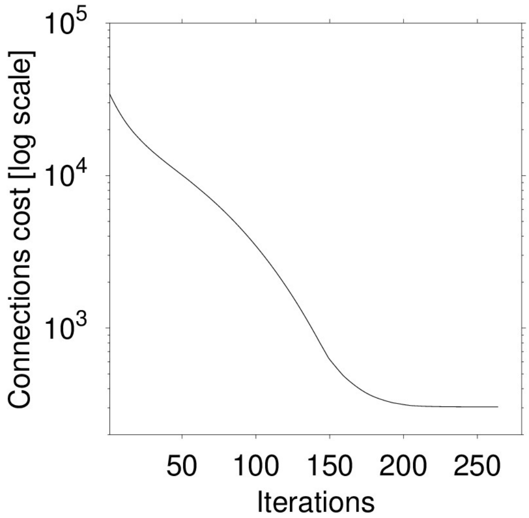

(b)

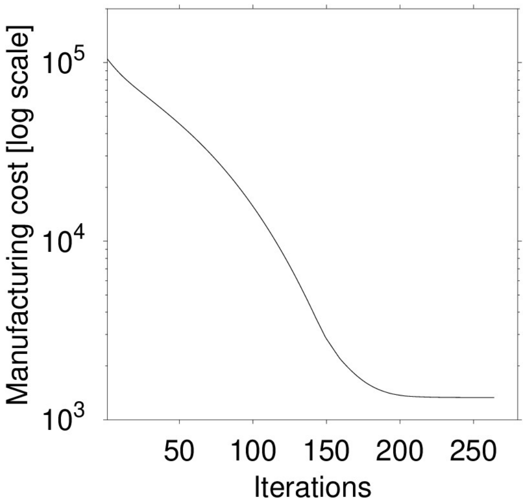

(c)

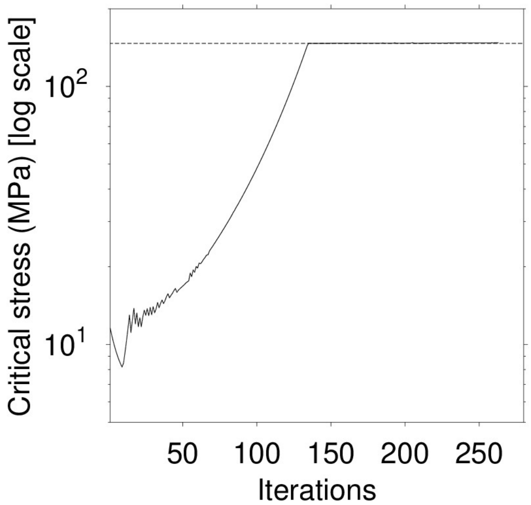

(d)

Source: Author's production.

As expected, it is proven that for this structural optimization problem it is more appropriate to adopt pinned connections, reducing the bending moments and providing more economical projects. Thus, the frame dome would actually be a lattice structure. Note that this conclusion could be drawn due to the application of the proposed optimization procedure, proving the importance of analyzing manufacturing costs with embedded connections as design variables.

The smaller the rotational stiffness adopted for the connections of a given structure, it became evident that the frame elements behave like bar elements, having axial forces that are much larger than other internal forces. Thus, in this problem, the failure criterion was important during the development of the optimization process, but has lost importance on the optimal solution, since the equivalent stresses in almost all elements are uniform throughout the external contour of the cross-section.

As mentioned before, the optimal structure has several elements that are fully stressed, all with normal stresses produced by axial forces. Among these elements, many are fully stressed in compression. Since there is no buckling constraint within the proposed optimization problem, it is evident that further study is necessary to verify if it is a stable structure, mainly the last four elements (49, 50, 51 and 52), since they have the smallest areas and relatively large lengths ($\approx 6500\ mm$).

To analyze the behavior of this type of optimization under a different condition, the additional imposition of displacement constraints is performed. After 261 iterations, the optimal solution and the elements and nodes which have semi-rigid connections are highlighted and presented in Fig. 6.15(a). Again, the optimal solution has non-symmetry related to layout and connections, but only the four elements at the top of the structure are fully stressed, see Fig. 6.15(b). Since the optimal layout of this optimal solution is similar to the previous study without displacement constraints, the length of the smallest elements is the same (and the previous Table 6.2 also applies to this optimal solution).

Figure 6.15 – (a) The optimal solution and the highlight of elements and specific locals with semi-rigid connections (listed for further analysis) and (b) the fully stressed elements.

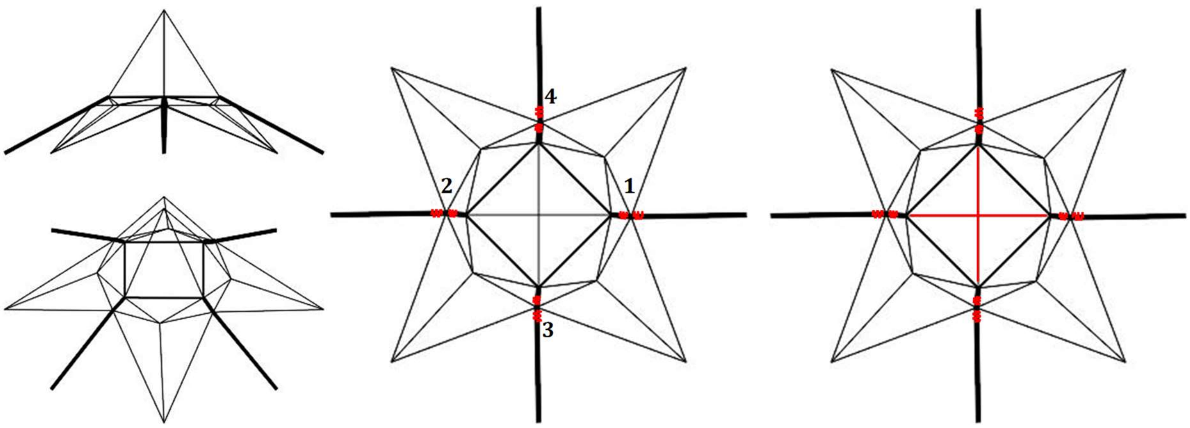

(a) (b)

Source: Author's production.

Initially, in order to ensure stiffness, the optimization process is placed in a structural problem where there is an oversizing of areas and connections of high rotational stiffness.

Therefore, knowing that large areas result in a high material cost and that fully rigid connections not only have a higher manufacturing cost but also produce greater bending moments, the process obviously decides to reduce the areas and rotational stiffness of the connections. Until iteration 60, this is what it does, while also looking for a new layout.

After iteration 60, all connections are pinned (except the clamped region) and the process continues through the design space. Upon reaching iteration 162, due to the linearization of the problem, the design variables deviate slightly and induce a non-symmetry to the structure. Consequently, the distribution of internal forces becomes non symmetric, and each region of the structure becomes more flexible at different planes. Also, the constrained nodes already present the maximum allowable displacement in the z-direction, and the largest magnitudes of internal forces are seen in the axial forces (10^6).

Taking into account the above information, the process understands that it is more feasible to reduce the material cost and proceed as follows: to reduce the areas but, to continue providing the necessary stiffness at the z-direction of the constrained nodes, it induces the appearence of semi-rigid connections. However, this procedure is developed strategically: the addition of rotational stiffness for the chosen connections acts in the plane in which there is the greatest flexibility (and consequently the smaller bending moments), avoiding the faster increase of the stresses.

With more rigid connections, the bending moments increase, but there is also a reduction of axial forces, and thus the process can continue to reduce areas and consequently the material cost. It is a compromise solution, where the optimization process chooses the path in which the gain (minimization of the total cost from the material cost) is greater than the loss (increase of the connection cost), while ensuring that the constraints are not violated.

The optimization features can be seen in Figs. 6.16(a-e). Stress and displacement constraints are active, and the optimized structure has $\$3462$ of total cost, being $\$2610$ of material cost and $\$851$ of connections cost. Note that on the diagram of all four displacement constraints the curves are overlapped.

Figure 6.16 – Convergence diagram for (a) material cost, (b) connections cost, (c) manufacturing cost, (d) most stressed element and (e) constrained DOF at each iteration.

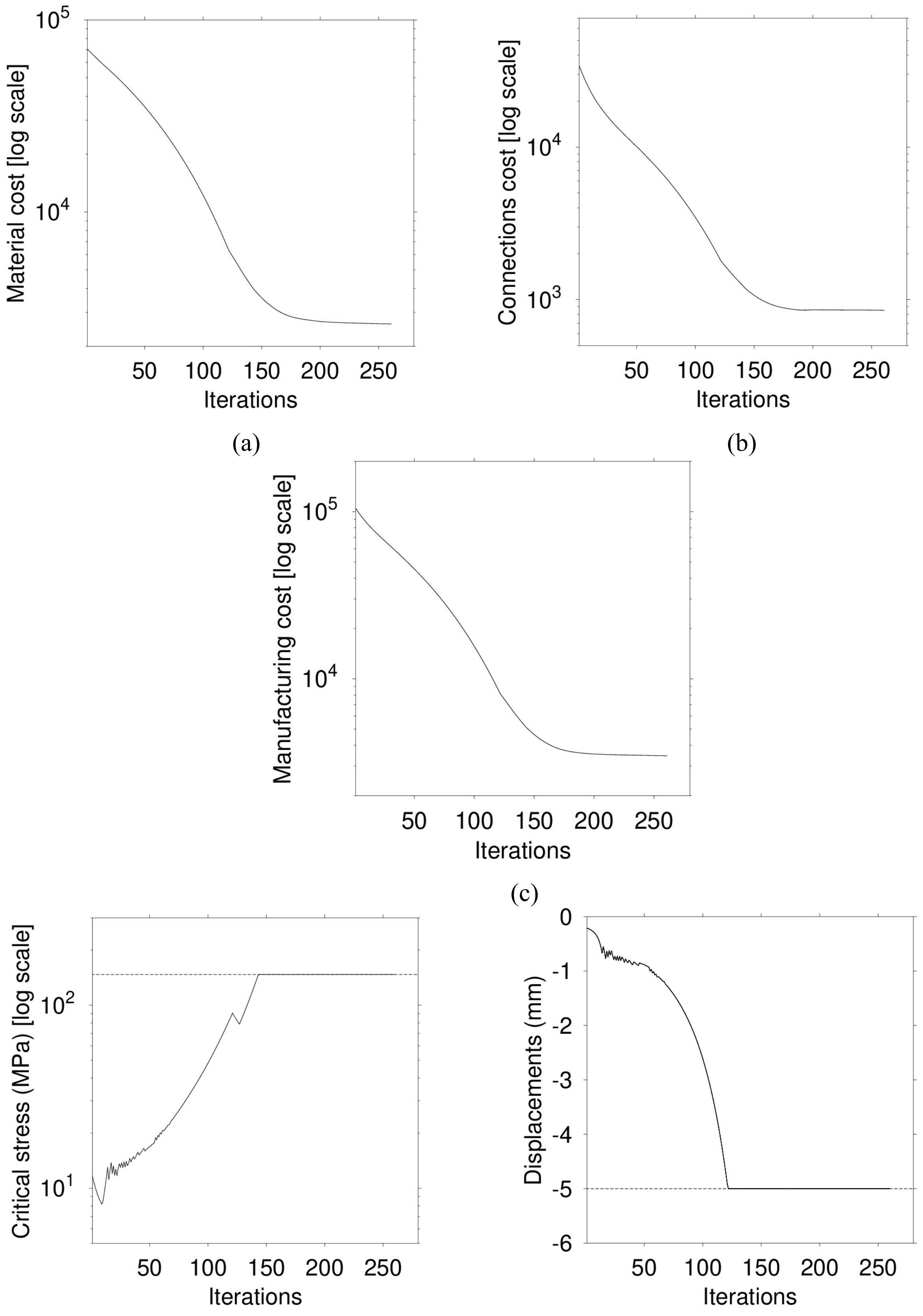

Source: Author’s production.

It is noticeable that the displacement constraints are stronger than the stress constraints, since the final manufacturing cost is considerably higher than the same final cost in the previous case study. The structure needs to have more elements, elements with larger cross-section areas and semi-rigid connections to ensure no violation of any of the displacement constraints imposed, as can be seen in Tables 6.3 and 6.4.

Table 6.3 – Comparison of optimal areas related to the two studies of LCO, without (LCO_1) and with (LCO_2) displacement constraints. The higher cross-section areas are highlighted.

$\mathbf{10^6 mm^2}$	$\mathbf{LCO_1}$	$\mathbf{LCO_2}$	$\mathbf{10^6 mm^2}$	$\mathbf{LCO_1}$	$\mathbf{LCO_2}$	$\mathbf{10^6 mm^2}$	$\mathbf{LCO_1}$	$\mathbf{LCO_2}$
A_9	$0.22E^{-3}$	$0.35E^{-3}$	A_{24}	-	$0.35E^{-4}$	A_{39}	$0.13E^{-2}$	$0.12E^{-2}$
A_{10}	$0.48E^{-4}$	$0.95E^{-4}$	A_{25}	$0.33E^{-3}$	$0.59E^{-3}$	A_{40}	$0.19E^{-2}$	$0.66E^{-2}$
A_{11}	$0.30E^{-3}$	$0.35E^{-3}$	A_{26}	-	$0.60E^{-4}$	A_{41}	$0.21E^{-2}$	$0.74E^{-2}$
A_{12}	$0.39E^{-3}$	$0.15E^{-3}$	A_{27}	$0.39E^{-4}$	$0.45E^{-3}$	A_{42}	$0.13E^{-2}$	$0.12E^{-2}$
A_{13}	$0.22E^{-3}$	$0.30E^{-3}$	A_{28}	-	$0.20E^{-4}$	A_{43}	$0.20E^{-2}$	$0.66E^{-2}$
A_{14}	$0.54E^{-4}$	$0.72E^{-4}$	A_{29}	$0.34E^{-3}$	$0.56E^{-3}$	A_{44}	$0.20E^{-2}$	$0.73E^{-2}$
A_{15}	$0.30E^{-3}$	$0.39E^{-3}$	A_{30}	-	$0.14E^{-4}$	A_{45}	$0.11E^{-2}$	$0.12E^{-2}$
A_{16}	$0.38E^{-3}$	$0.16E^{-3}$	A_{31}	$0.36E^{-4}$	$0.50E^{-3}$	A_{46}	$0.21E^{-2}$	$0.65E^{-2}$
A_{17}	$0.24E^{-3}$	$0.44E^{-3}$	A_{32}	-	$0.10E^{-4}$	A_{47}	$0.20E^{-2}$	$0.73E^{-2}$
A_{18}	$0.26E^{-4}$	$0.95E^{-4}$	A_{33}	$0.69E^{-3}$	$0.34E^{-2}$	A_{48}	$0.11E^{-2}$	$0.12E^{-2}$
A_{19}	$0.29E^{-4}$	$0.34E^{-3}$	A_{34}	$0.88E^{-3}$	$0.35E^{-2}$	A_{49}	$0.13E^{-3}$	$0.20E^{-3}$
A_{20}	-	$0.44E^{-4}$	A_{35}	$0.68E^{-3}$	$0.34E^{-2}$	A_{50}	$0.15E^{-4}$	$0.16E^{-3}$
A_{21}	$0.25E^{-3}$	$0.41E^{-3}$	A_{36}	$0.88E^{-3}$	$0.35E^{-2}$	A_{51}	$0.14E^{-3}$	$0.20E^{-3}$
A_{22}	$0.26E^{-4}$	$0.54E^{-4}$	A_{37}	$0.19E^{-2}$	$0.65E^{-2}$	A_{52}	$0.14E^{-4}$	$0.18E^{-3}$
A_{23}	$0.27E^{-4}$	$0.38E^{-3}$	A_{38}	$0.21E^{-2}$	$0.74E^{-2}$			

Source: Author's production.

With the appearance of semi-rigid connections at some elements, and also due to the fact that the structure is clamped at six points, relevant levels of bending moments and shear forces also arise. Then, several combinations of internal forces are faced, justifying the use of the new failure criterion as stress constraint. Despite the stresses resulting from bending moments and shear forces are not so high at this case study, it was observed that some elements have critical points related to these internal forces ($0, \frac{\pi}{2}, \pi$ and $\frac{3\pi}{2}$). The largest normal stress from a resulting bending moment recorded is $15\ MPa$, while the highest shear stress of a resulting shear is only $0.11\ MPa$.

Table 6.4 – Semi-rigid connections of the optimal solution.

Joint Connections	Elements	Fixity Factors			
		Node 1		Node 2	
		α_1	α_3	α_2	α_4
1	**37**	fully rigid		0.446	pinned
	38	0.369	pinned	pinned	
2	**40**	fully rigid		pinned	0.468
	41	pinned	0.388	pinned	
3	**43**	fully rigid		0.342	pinned
	44	0.285	pinned	pinned	
4	**46**	fully rigid		pinned	0.264
	47	pinned	0.220	pinned	

Source: Author's production.

The elements with semi-rigid connections are exactly the ones that "interconnect" the clamped joints to the joints where the displacement constraints are imposed, and have the largest cross-section areas. That is, the overall stiffness required in the z-direction of the structure is provided by both features.

According to the arrangement of the optimal fixity factors (Table 6.4), the respective connections would probably not be difficult to build, as they all need to incorporate only two rotational stiffness in each joint, one of each element.

As a preliminary conclusion, it can be said that the LCO proved useful for the frame dome study, not only for evaluating two different types of costs that practically command the total cost at the design of any structure, but also for enabling the optimal solution to have stiffness only in the required places, saving additional costs that would be spent if all connections were considered to be fully rigid. Moreover, it is seen that assuming displacement constraints is not only important to ensure that the structure does not exhibit exaggerated flexibility, but also the fixity factors gain importance within the optimization process. However, in the numerical field, occurs the appearence of a computational cost addition, due to the considerable increase of design variables.

6.2.2 Cantilever beam

The cantilever beam presented in Fig. 6.17 was firstly investigated by Pedersen and Nielsen (2003), containing 36 elements and 13 nodes. All the elements have circular thin-wall cross-section with constant thickness of $8\,mm$, initial cross-section areas $A = 30.10^3\ mm^2$, Young's modulus $E = 210.10^3\ MPa$, shear modulus $G = 80\ MPa$, yield strength $\sigma_e = 355\ MPa$ and specific mass $\rho = 7.799E^{-6}\ kg/mm^3$. The structure is clamped at the nodes 5 and 10 and node 1 has a pinned connection. The connectivity is presented in Table 6.5. Whit this initial data, the structure has approximately $45000\ kg$ of mass.

Figure 6.17 – Cantilever beam of Pedersen and Nielsen (2003).

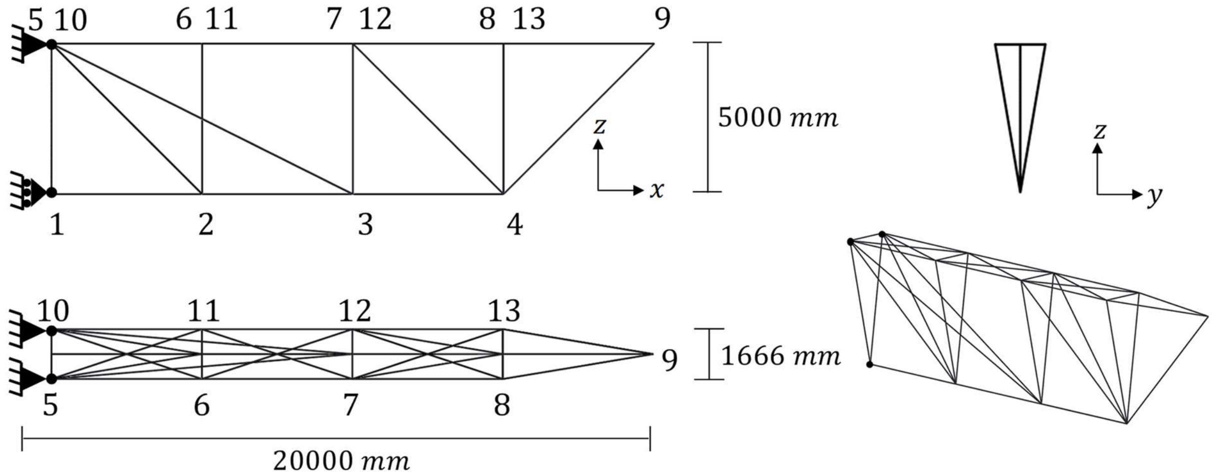

Source: Author’s production based on Pedersen and Nielsen (2003).

Table 6.5 – Connectivity of the structure.

Elements	**1**	**2**	**3**	**4**	**5**	**6**	**7**	**8**	**9**	**10**	**11**	**12**	**13**	**14**	**15**	**16**	**17**	**18**
Nodes	*1*	*2*	*3*	*4*	*5*	*6*	*7*	*8*	*10*	*11*	*12*	*13*	*5*	*6*	*7*	*8*	*5*	*10*
	2	*3*	*4*	*9*	*6*	*7*	*8*	*9*	*11*	*12*	*13*	*9*	*10*	*11*	*12*	*13*	*11*	*6*
Elements	**19**	**20**	**21**	**22**	**23**	**24**	**25**	**26**	**27**	**28**	**29**	**30**	**31**	**32**	**33**	**34**	**35**	**36**
Nodes	*6*	*11*	*7*	*12*	*5*	*10*	*6*	*11*	*7*	*12*	*8*	*13*	*5*	*10*	*5*	*10*	*7*	*12*
	12	*7*	*13*	*8*	*1*	*1*	*2*	*2*	*3*	*3*	*4*	*4*	*2*	*2*	*3*	*3*	*4*	*4*

Source: Author’s production.

The optimization processes will take into account the multiple load condition described in Fig. 6.18 and Table 6.6, referred to a working load (F_1), lift load (F_2) due to the wind load and the wind load (F_3) itself. Differently of Pedersen and Nielsen (2003), the self-weight is neglected.

Figure 6.18 – Load cases.

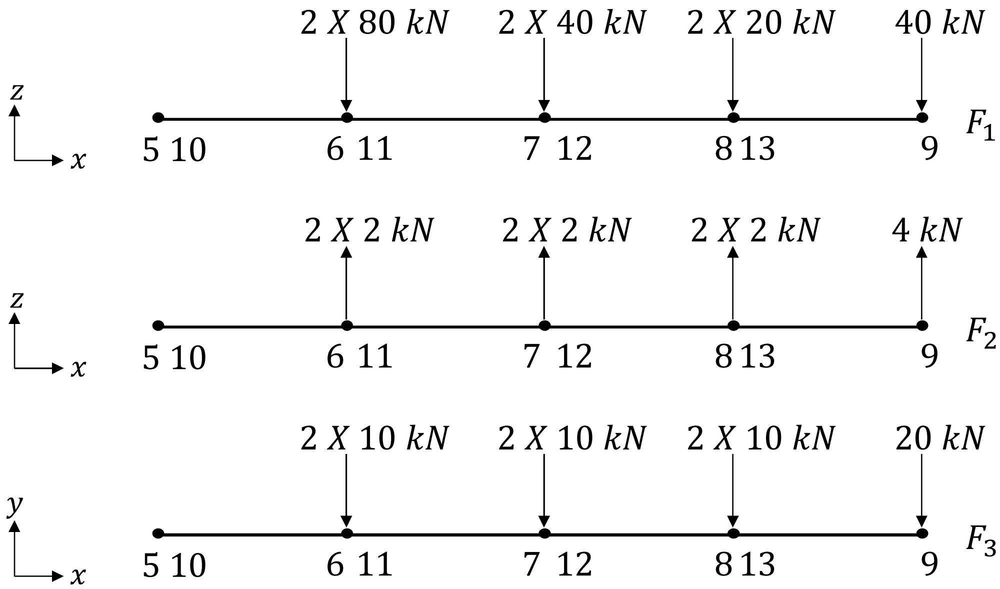

Source: Author's production based on Pedersen and Nielsen (2003).

Table 6.6 – Multiple load condition.

Load cases	**Load condition**
1	F_1
2	$0.5F_1 + F_3$
3	$0.5F_1 - F_3$
4	$F_2 + F_3$
5	$F_2 - F_3$

Source: Author's production.

Constraints on the von Mises stress, the displacement at the z-direction of the node 9 (should have less than 30 mm – see Fig. 6.19) and the minimum length (5 mm) of each element are applied. Similar to the frame dome study, the critical point of each cross-section area and its von Mises stress are determined after a sweep of 0 to 2π, with a stepsize of 0.002π determinated through a previous convergence study.

Aiming to compare the results obtained, the analysis will be developed as follows:

- Sizing and connections optimization (SCO) with cost of connections ranging on 20-60 %;
- LCO with cost of connections ranging on 20-60%;

- LCO with different ranges of additional cost of connections (20-60%, 20-30% and 45-60%).

Figure 6.19 – Design variables and displacement constraint assumed.

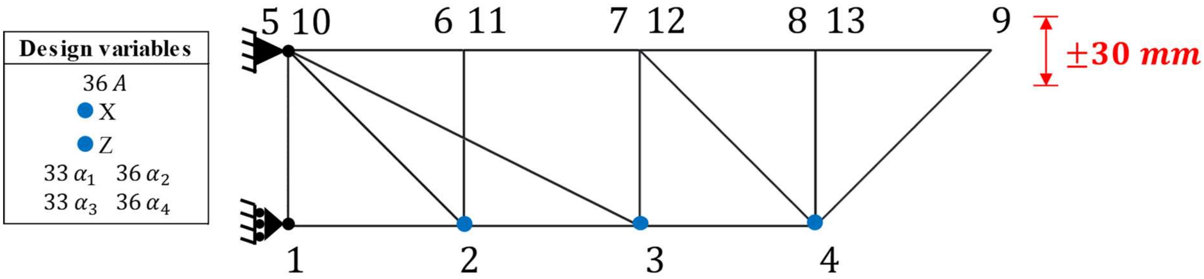

Source: Author’s production.

First of all, a process with sizing and connections optimization (SCO) is performed, being all the cross-section areas, 33 fixity factors α_1/α_3 and 36 fixity factors α_2/α_4 design variables. Initially, all of the fixity factors have rotational stiffness of 90%.

Next, the coordinates X and Z of the nodes 2, 3 and 4 (see Fig. 6.19) are included as design variables and the LCO is developed, allowing the comparison between SCO x LCO, mainly from the point of view of efficacy and computational efficiency. Nodes which are loaded are not free to change positions, their side constraints do not have the imposition of extremes values and none of the design variables are linked.

Moreover, LCO processes with different ranges for the additional cost of connections are performed, aiming to analyze and compare other features about the behavior of the optimized structures and their optimization processes. At these processes, the definition of the constant coefficients related to the quadratic variation of the connections cost is based on the procedure explained in equations (5.4)-(5.15).

Pedersen and Nielsen (2003) used the same SLP algorithm and considered an active set strategy on the stress constraints, when it achieves a critical level of 80% compared to the allowed stress defined. In preliminary tests with the application of this strategy on the case studies developed here, a lot of instability was observed in the optimization processes. Applying the strategy on the minimum length constraints obviously reduced the size of the optimization problem, but was not observed a significant improvement in the computational efficiency. On the other hand, in the stress constraints, the processes began to show a great deal of instability, falling in local solutions of low quality and, in most of the time, falling in unfeasible regions. Due to lack of time to deeply analyze, the use of this strategy was disregarded.

6.2.2.1 SCO with cost of connections of 20-60%

After 243 iterations, the optimal solution is presented in Fig. 6.20(b). Only four elements are removed from the initial topology of Fig. 6.20(a).

Figure 6.20 – (a) Initial structure and (b) optimal solution.

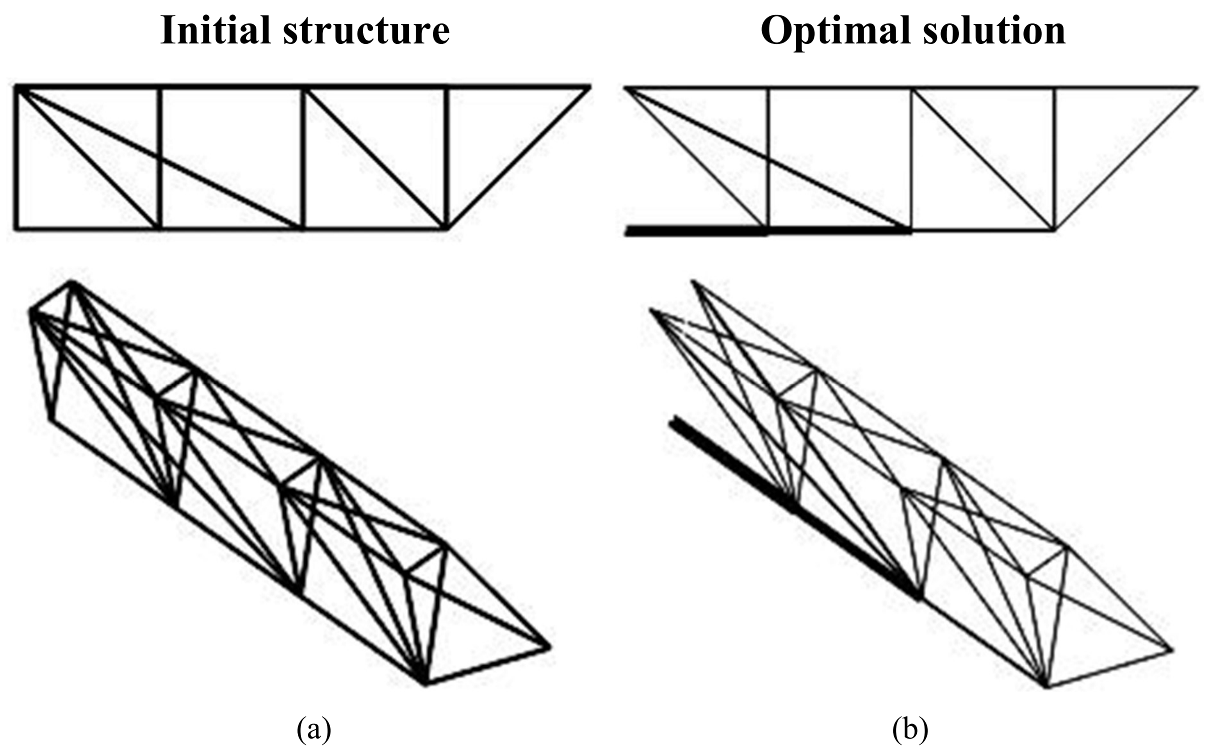

Source: Author's production.

By analyzing the assumed structure and multiple load cases, the structure will always be subject to the global bending around two planes, but mainly in the xz-plane, because the magnitude of the loads applied in this plane are much larger.

At the beginning of the optimization process, all the internal forces are relevant. Since the main load F_1 is at the xz-plane, the elements parallel to this plane have considerable magnitudes of bending moment M_y, and thus all the critical points of these elements are located at 0 or π.

To minimize the objective function, the optimization process basically chooses to produce only pinned connections, i.e. a lattice structure, and decrease the areas of the top elements and the elements farthest from the region where the structure is attached. For convenience, the optimal areas are presented later in Table 6.8, where this solution is compared to the solution of the LCO process. With pinned connections, the process can reduce significantly the large magnitudes of bending moments and shear forces. At the end, almost all the elements of the structure present axial forces of relevant magnitude compared to the other internal forces.

Since the bottom of the structure is supported only by a pinned connection and has larger stresses at the beginning, the process supplies the lack of strength and stiffness at this location with these two elements having larger cross-sectional areas. Therefore, the stresses are softened and four elements (13, 15, 23 and 24) connected to this region are removed from the initial topology, because the internal forces are entirely absorbed mainly by these elements with larger areas.

The optimized structure has \$2560 of total cost, see the convergence diagram of Fig. 6.21(a), being \$2109 of material cost and \$451 of connections cost. According to Fig. 6.21(b), there is a small violation of these stress constraints between 60-70 iterations. Regarding the displacement constraints, Fig. 6.21(c) demonstrates the diagram of all five displacement constraints. Some curves are overlapped and only the constraint applied in load case 1 is active. This load case is critical because has the largest concentrated forces (F_1).

Unlike the frame dome study, the stiffness required to withstand the displacement constraints in the current study of SCO is entirely provided by the distribution of areas, even with the option of more rigid connections. The optimization process understands that is economically more feasible to produce stiffness with areas (material cost) than with connections. With different ranges for the additional cost of connections, this behavior may change.

Figure 6.21 – Results about convergence diagram of the actual study for (a) manufacturing cost, (b) diagram of the most stressed element at each iteration and (c) diagram of the constrained DOF at each iteration.

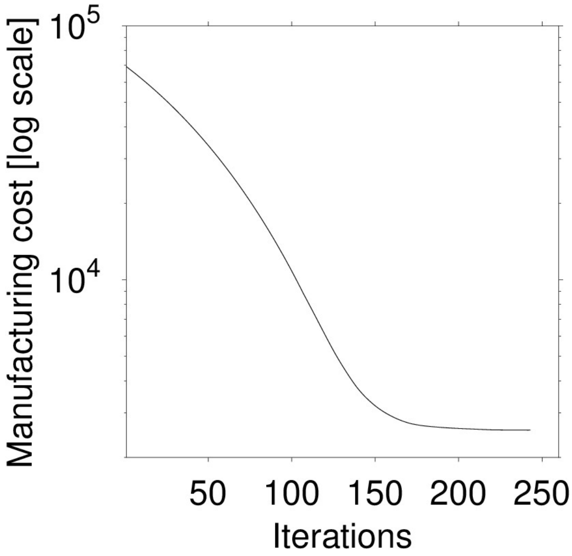

(a)

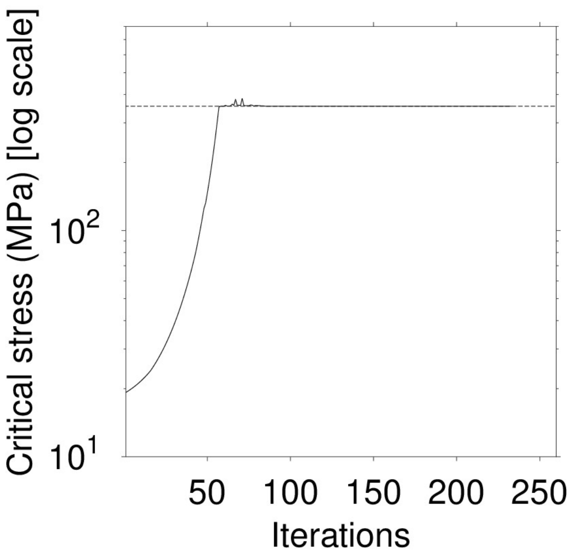

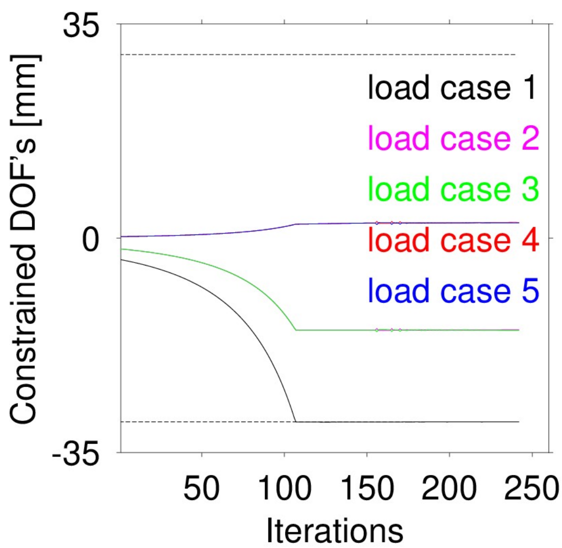

(b) (c)

Source: Author's production.

6.2.2.2 LCO with cost of connections of 20-60%

After 392 iterations, the optimization process of Fig. 6.22(a) found the optimal solution presented in Fig. 6.22(b). The pairs of elements connected between the nodes 7/12 and 3/4 are almost overlapped. However, due to the topology removal, the overlap is suppressed. Five elements can be removed from the initial topology, one more than SCO, and a short element appears due to the approximation of nodes 3 and 4. Also, Fig. 6.22(b) highlighted the element and nodes which have semi-rigid connections.

Figure 6.22 – (a) The behavior of the LCO process and (b) the optimal solution, the short element and the highlight of the element with semi-rigid connections.

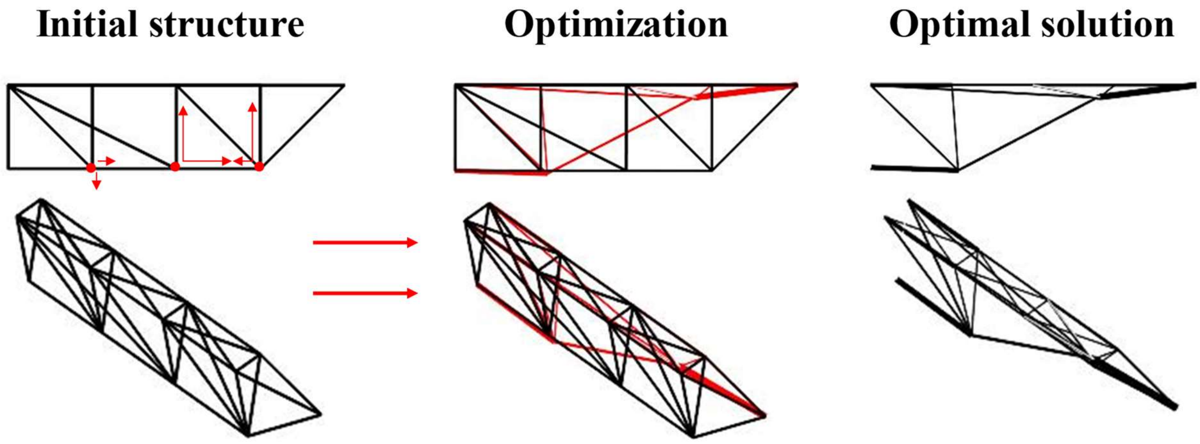

(a)

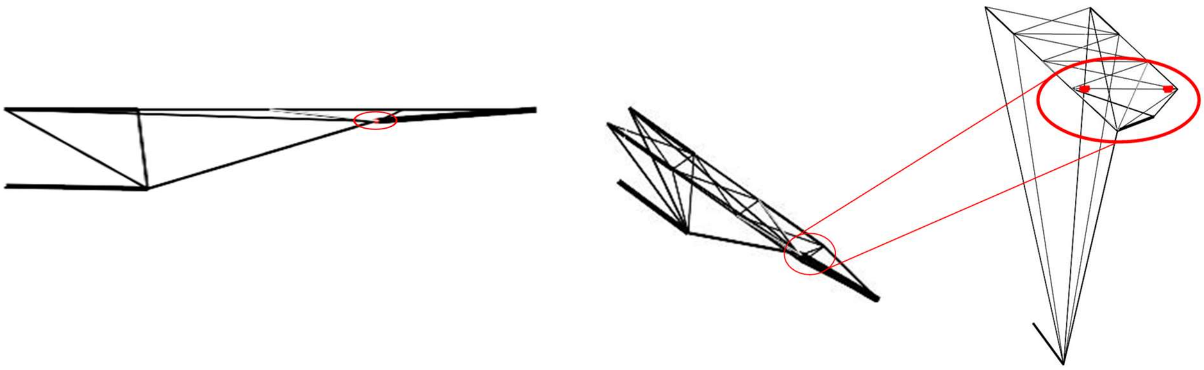

(b)

Source: Author’s production.

The upward movement of nodes 3 and 4 is mainly related to the displacement constraint applied in node 9, since this layout modification allows a greater concentration of stiffness close to this node. The optimal joint positions are shown in Table 6.7, where can be seen that node 2 goes down in the z-direction. Simultaneously, the process provides the largest cross-section area for the element 4 directly connected to the constrained node and semi-rigid connections in the nearby element 16. These connections provide 35% of rotational stiffness in the two bending planes, while all other connections are pinned. From a practical point of view, this symmetry of connections facilitates the construction of the structure. Also, these connections would be simple to build, since the joints 8 and 13 only need two rotational springs and the other elements are pinned.

Table 6.7 – Optimal joint positions.

Nodes	**2**	**3**	**4**
$\boldsymbol{X}$ **[mm]**	5379	13913	14079
$\boldsymbol{Z}$ **[mm]**	−177	4241	4275

Source: Author's production.

Although the short element has not achieved the minimum length constraint, probably the most correct physical interpretation of this optimal solution is the removal of this element and the joining of adjacent elements connected to him. Also, since almost all connections converge to be pinned, the axial forces become more relevant than the other internal forces (as seen in the SCO process).

The distribution of areas to ensure both stiffness and strength for the structure is different from what was seen in the previous study: in the SCO, the elements 1 and 2 have the largest areas. On the other hand, in the LCO there is a slightly more even distribution of areas towards the free end, with the two top elements and the element at the bottom in the attachment region also having large areas (in addition to element 4). Table 6.8 presents the comparison of optimal areas.

Table 6.8 – Comparison of optimal areas related to the SCO and LCO processes. The higher cross-section areas are highlighted.

$\mathbf{10^6 mm^2}$	**SCO**	**LCO**	$\mathbf{10^6 mm^2}$	**SCO**	**LCO**	$\mathbf{10^6 mm^2}$	**SCO**	**LCO**
$\boldsymbol{A_1}$	$0.97E^{-2}$	$0.20E^{-2}$	$\boldsymbol{A_{13}}$	-	-	$\boldsymbol{A_{25}}$	$0.22E^{-3}$	$0.22E^{-3}$
$\boldsymbol{A_2}$	$0.83E^{-2}$	$0.12E^{-2}$	$\boldsymbol{A_{14}}$	$0.90E^{-5}$	$0.31E^{-4}$	$\boldsymbol{A_{26}}$	$0.22E^{-3}$	$0.22E^{-3}$
$\boldsymbol{A_3}$	$0.30E^{-2}$	$0.19E^{-2}$	$\boldsymbol{A_{15}}$	-	$0.87E^{-4}$	$\boldsymbol{A_{27}}$	$0.12E^{-2}$	$0.61E^{-3}$
$\boldsymbol{A_4}$	$0.17E^{-2}$	$0.20E^{-3}$	$\boldsymbol{A_{16}}$	$0.78E^{-4}$	$0.34E^{-3}$	$\boldsymbol{A_{28}}$	$0.12E^{-2}$	$0.61E^{-3}$
$\boldsymbol{A_5}$	$0.16E^{-2}$	$0.16E^{-2}$	$\boldsymbol{A_{17}}$	$0.38E^{-3}$	$0.35E^{-3}$	$\boldsymbol{A_{29}}$	$0.57E^{-4}$	$0.11E^{-3}$
$\boldsymbol{A_6}$	$0.13E^{-2}$	$0.78E^{-3}$	$\boldsymbol{A_{18}}$	$0.38E^{-3}$	$0.35E^{-3}$	$\boldsymbol{A_{30}}$	$0.57E^{-4}$	$0.11E^{-3}$
$\boldsymbol{A_7}$	$0.52E^{-3}$	$0.94E^{-3}$	$\boldsymbol{A_{19}}$	$0.28E^{-3}$	$0.27E^{-3}$	$\boldsymbol{A_{31}}$	$0.32E^{-3}$	$0.65E^{-3}$
$\boldsymbol{A_8}$	$0.63E^{-3}$	$0.10E^{-2}$	$\boldsymbol{A_{20}}$	$0.28E^{-3}$	$0.27E^{-3}$	$\boldsymbol{A_{32}}$	$0.32E^{-3}$	$0.65E^{-3}$
$\boldsymbol{A_9}$	$0.16E^{-2}$	$0.16E^{-2}$	$\boldsymbol{A_{21}}$	$0.18E^{-3}$	$0.22E^{-3}$	$\boldsymbol{A_{33}}$	$0.28E^{-2}$	$0.44E^{-3}$
$\boldsymbol{A_{10}}$	$0.13E^{-2}$	$0.78E^{-3}$	$\boldsymbol{A_{22}}$	$0.18E^{-3}$	$0.22E^{-3}$	$\boldsymbol{A_{34}}$	$0.28E^{-2}$	$0.44E^{-3}$
$\boldsymbol{A_{11}}$	$0.52E^{-3}$	$0.94E^{-3}$	$\boldsymbol{A_{23}}$	-	-	$\boldsymbol{A_{35}}$	$0.12E^{-2}$	-
$\boldsymbol{A_{12}}$	$0.63E^{-3}$	$0.10E^{-2}$	$\boldsymbol{A_{24}}$	-	-	$\boldsymbol{A_{36}}$	$0.12E^{-2}$	-

Source: Author's production.

The optimization starts the stabilization process after iteration 300, see Fig. 6.23(a), and the optimized structure has \$1140 of total cost, being \$927 of material cost and \$212 of connections cost. According to Figs. 6.23(b-c), the stress and displacement constraints are sometimes violated. Compared to SCO, there are more elements fully stressed, and again only the constraint applied in load case 1 is active.

Figure 6.23 – Results about convergence diagram of the actual study for (a) manufacturing cost, (b) diagram of the most stressed element and (c) diagram of the constrained DOF at each iteration.

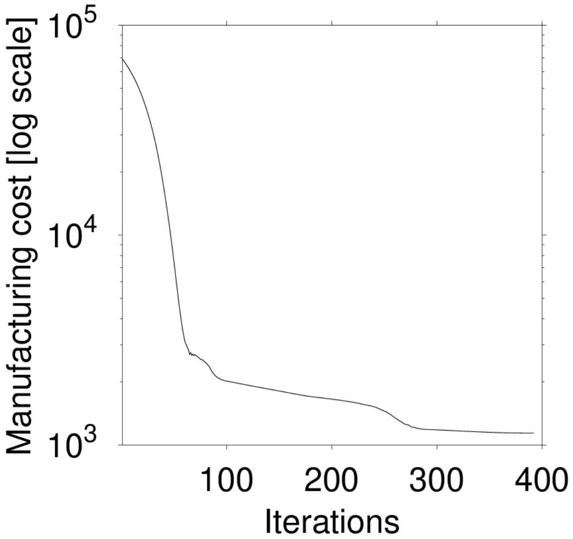

(a)

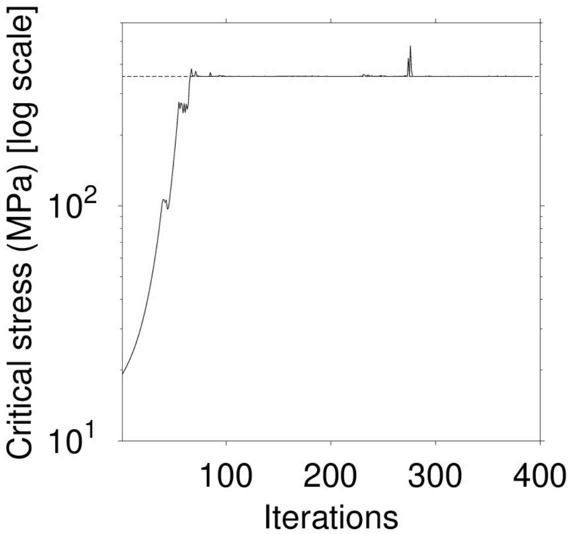

(b)

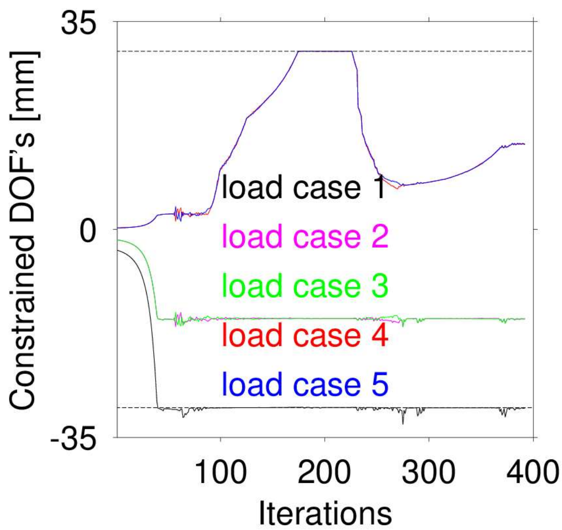

(c)

Source: Author's production.

From the convergence graph of Fig. 6.23(a), it is possible to visualize between the 100-250 iterations that the optimization process almost stabilizes and finds a local solution. Also, during these iterations, the displacement constraints in load cases 4 and 5 become active, because until the moment of being activated, the process is more concerned to ensure that the displacement constraint of the critical load case 1 is not violated.

By simultaneously checking the behavior of displacement constraints and the evolution of design variables, we realize that this region is probably a “flat area” of the objective function. In this interval of iterations, the structure still has only pinned connections. However, after iteration 250, the process is able to bypass this region and begin to impose semi-rigid connections on element 16. At this transition, displacement constraints of load cases 4 and 5 are not active and violations occur in some stress constraints and in the displacement constraint of load case 1.

The preceding analyses show that the LCO provides the required stiffness for the structure for adequate values in the three types of design variables. While in SCO this is accomplished only by areas, the optimal solution of LCO provides greater savings in manufacturing costs (55.4%), being 56% less material cost and 53% less connections cost. This greater saving is mainly obtained due to the better distribution of areas, because this directly reduces the material cost and reduces indirectly the cost of the connections (proportional to the material cost).

Based on quantitative and qualitative results of the cantilever beam study, it is proven that for this structure the LCO reaches a better solution than SCO, with a relative simple layout modification. Since the structure under study has a relatively small amount of DOF, the higher number of iterations (67.5% more) is not a problem because the time spent solving the FEA, calculating the derivatives and the LP at each iteration it is just a little higher. However, for more complex structures, this can be a problem.

Analogous to the frame dome study, this optimal solution also has fully stressed elements with normal stress produced by axial force of compression. Again, to ensure reliability, all the pinned-pinned elements need to have their Euler stress limit calculated and checked as a post-processing procedure.

As can be seen in Fig. 6.24, the element 3 has a considerable small length (170 mm), the highest shear forces in the range of 10^4 and shear stress τ_{V_R} of $-0.74\ MPa$. Element 16 has a fixed length of 1666 mm and a larger magnitude of shear stress τ_{V_R} (2.64 MPa), because its shear forces are also higher (range of 10^3), due to the existence of semi-rigid connections, and the respective cross-section area is smaller compared to the area of element 3.

Figure 6.24 – The elements with the highest shear stresses τ_{V_R} produced by the resulting shear force.

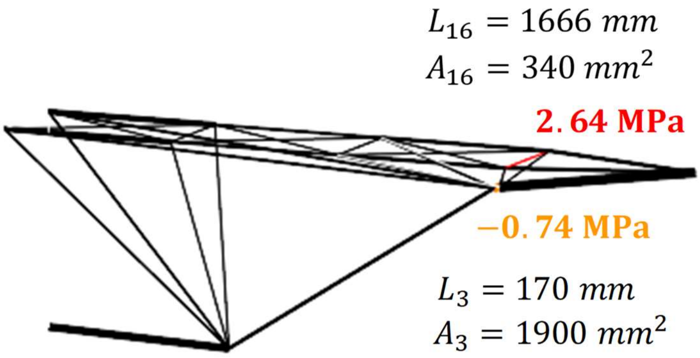

Element	3	16
σ_{N_x} $[MPa]$	-99.9	-23.61
σ_{M_R} $[MPa]$	-1.99	-1.70
τ_{M_x} $[MPa]$	2.13	9.35
τ_{V_R} $[MPa]$	-0.74	2.64

Source: Author's production.

These values of shear stresses seem small compared to the allowable stress – and they really are in this case, since the equivalent stresses are much lower than the allowable stress – but they cannot be neglected because it could happen that these shear stresses, added to the stresses associated to the other five internal forces, lead the cross-section area to collapse. Note that these elements have shear stresses τ_{V_R} with the same range of magnitudes of the normal stresses σ_{M_R} (indeed, in element 16 we see that $\tau_{V_R} > \sigma_{M_R}$).

Being a discrete structure which "simulates" a clamped beam subject to the global bending of the five sub-cases of loads imposed, this situation of non-negligible shear forces and stresses could be expected.

6.2.2.3 LCO with different ranges of connections cost (20-60%, 20-30% and 45-60%)

In this section, the previous LCO study with connections cost of 20-60% is again developed, but with V_0, V_1, and V_2 coefficients adopted for the quadratic variation of the connections cost of all current studies has the same curve behavior.

The Figs. 6.25-6.27 and Tables 6.9-6.11 present, respectively, the results obtained for studies 20-60%, 20-30% and 45-60%. Table 6.12 presents the comparison between these studies.

Figure 6.25 – Summary of results about the convergence diagrams and the optimal solution of 20-60%.

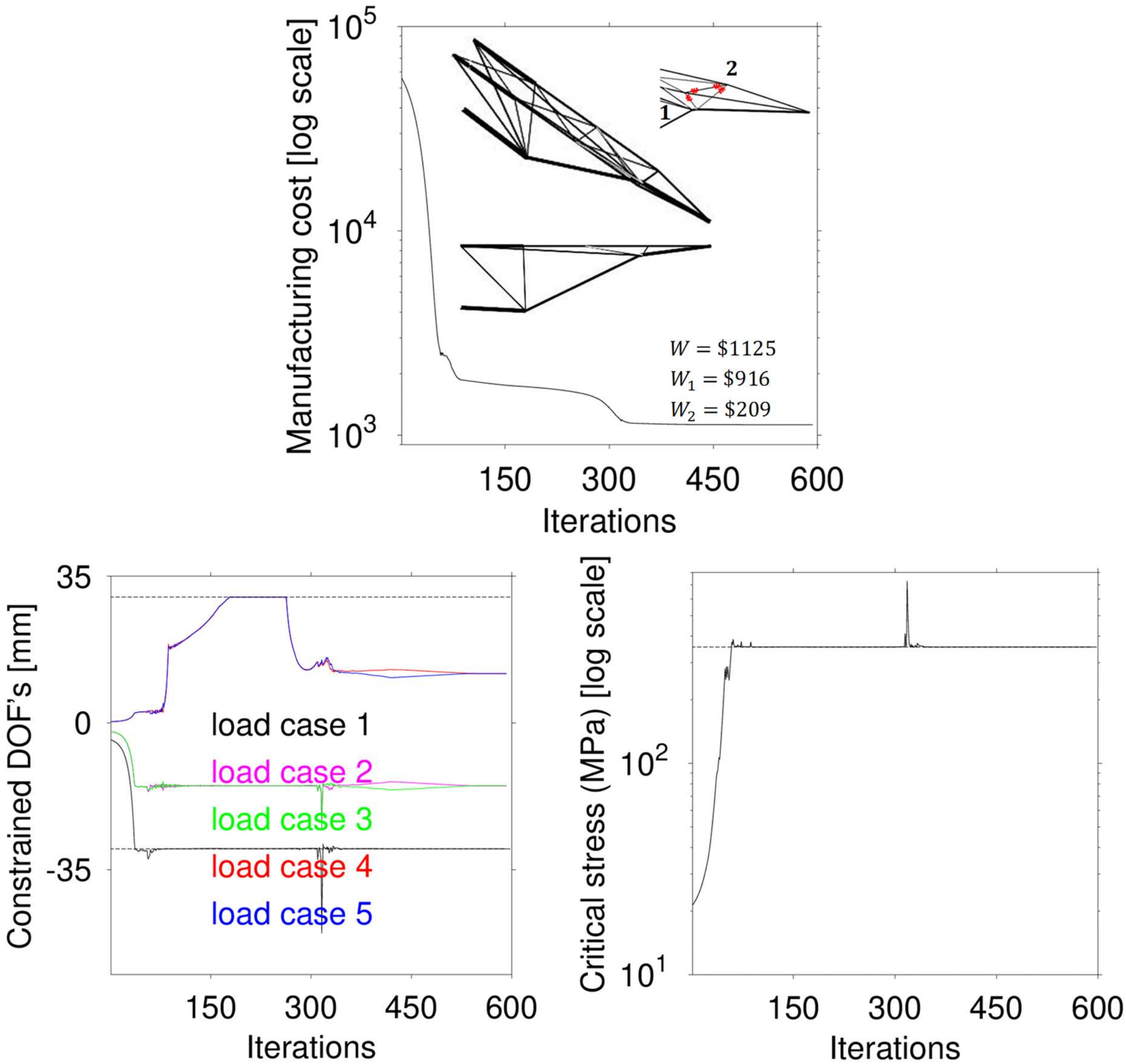

Source: Author's production.

Table 6.9 – Semi-rigid connections of the optimal solution for 20-60%.

Joint Connections	Elements	Fixity Factors			
		Node 1		Node 2	
		α_1	α_3	α_2	α_4
1	**16**	0.472	0.467	0.471	0.467
	29	0.186	pinned	pinned	
2	**16**	0.472	0.467	0.471	0.467
	30	pinned	0.197	pinned	

Source: Author's production.

Figure 6.26 – Summary of results about the convergence diagrams and the optimal solution of 20-30%.

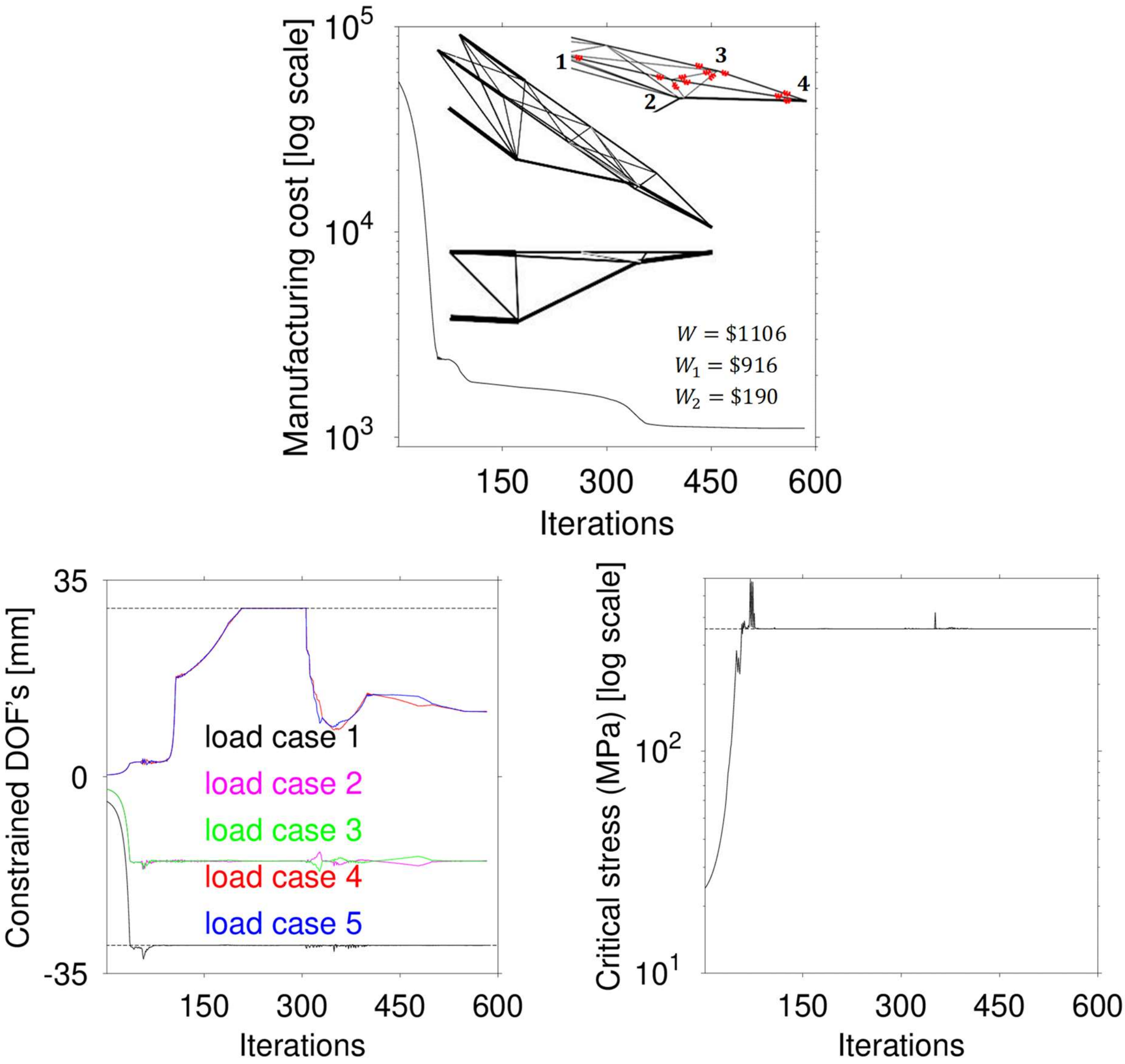

Source: Author's production.

Table 6.10 – Semi-rigid connections of the optimal solution for 20-30%.

Joint Connections	Elements	Fixity Factors			
		Node 1		Node 2	
		α_1	α_3	α_2	α_4
1	4	pinned		0.108	0.100
2	7	0.114	pinned	pinned	0.145
	8	pinned	0.118	0.245	0.323
	16	0.347	0.347	0.343	0.348
	29	0.248	pinned	pinned	

Source: Author's production.

Table 6.10 (Continuation) – Semi-rigid connections of the optimal solution for 20-30%.

Joint Connections	Elements	Fixity Factors			
		Node 1		Node 2	
		α_1	α_3	α_2	α_4
3	**11**	pinned		pinned	0.183
	12	pinned		0.342	0.415
	16	0.347	0.347	0.343	0.348
	30	pinned	0.243	pinned	
4	**4**	pinned		0.108	0.100
	8	pinned	0.118	0.245	0.323
	12	pinned		0.342	0.415

Source: Author's production.

Table 6.11 – Semi-rigid connections of the optimal solution for 45-60%.

Joint Connections	Elements	Fixity Factors			
		Node 1		Node 2	
		α_1	α_3	α_2	α_4
1	**8**	pinned		pinned	0.100
	12	pinned		pinned	0.124
2	**16**	0.547	0.541	0.537	0.537
	29	0.282	pinned	pinned	
3	**16**	0.547	0.541	0.537	0.537
	30	pinned	0.264	pinned	

Source: Author's production.

Figure 6.27 – Summary of results about the convergence diagrams and the optimal solution of 45-60%.

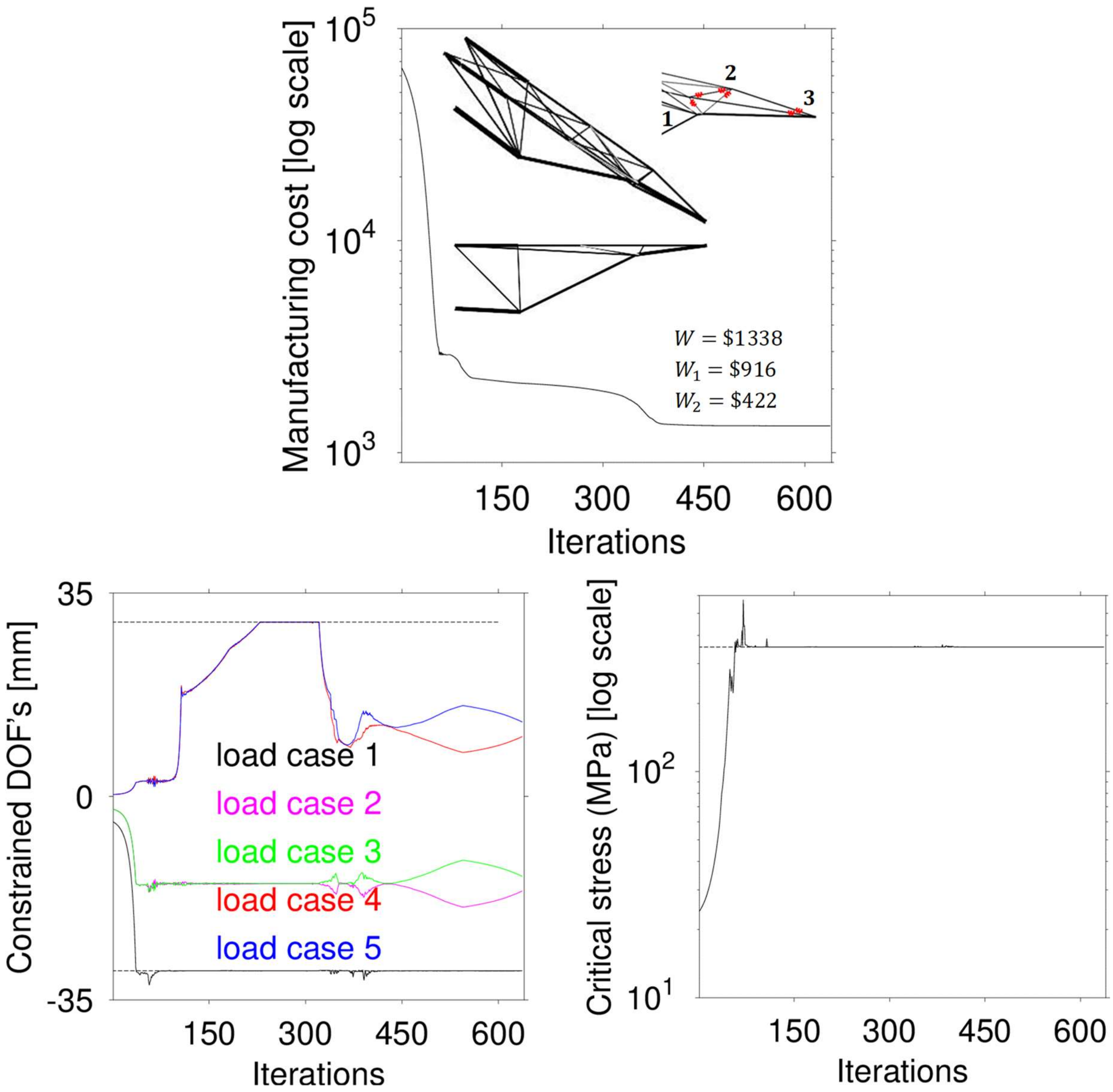

Source: Author's production.

Table 6.12 – Comparison between the costs of the optimal solutions.

	Optimization processes		
Costs (\$)	**20-60%**	**20-30%**	**45-60%**
Manufacturing cost ($\boldsymbol{W}$)	1125	1106	1338
Material cost ($\boldsymbol{W_1}$)	916	916	916
Connections cost ($\boldsymbol{W_2}$)	209	190	422

Source: Author's production.

Both studies have optimal solutions with the same areas and joint positions (presented in Table 6.13) and, therefore, the same layout and final material cost (see Table 6.12). However, these optimal solutions are not equal as they have different numbers of connections with different levels of rotational stiffness. It is noteworthy that the manufacturing costs cannot be directly compared, since different connections cost were evaluated.

Table 6.13 – Optimal areas and joint positions of the three LCO processes.

Cross-section areas						Coordinates	
$\mathbf{10^6 mm^2}$		$10^6\mathrm{mm}^2$		$10^6\mathrm{mm}^2$		mm	
A_1	$0.18E^{-2}$	A_{13}	-	A_{25}	$0.22E^{-3}$	X_2	5176
A_2	$0.11E^{-2}$	A_{14}	$0.45E^{-4}$	A_{26}	$0.22E^{-3}$	Z_2	-266
A_3	$0.15E^{-2}$	A_{15}	$0.93E^{-4}$	A_{27}	$0.66E^{-3}$	X_3	14310
A_4	$0.18E^{-3}$	A_{16}	$0.39E^{-3}$	A_{28}	$0.66E^{-3}$	Z_3	4238.00
A_5	$0.16E^{-2}$	A_{17}	$0.35E^{-3}$	A_{29}	$0.97E^{-4}$	X_4	14538
A_6	$0.83E^{-3}$	A_{18}	$0.35E^{-3}$	A_{30}	$0.97E^{-4}$	Z_4	4292
A_7	$0.74E^{-3}$	A_{19}	$0.27E^{-3}$	A_{31}	$0.65E^{-3}$		
A_8	$0.92E^{-3}$	A_{20}	$0.27E^{-3}$	A_{32}	$0.65E^{-3}$		
A_9	$0.16E^{-2}$	A_{21}	$0.23E^{-3}$	A_{33}	$0.56E^{-3}$		
A_{10}	$0.83E^{-3}$	A_{22}	$0.23E^{-3}$	A_{34}	$0.56E^{-3}$		
A_{11}	$0.74E^{-3}$	A_{23}	-	A_{35}	-		
A_{12}	$0.92E^{-3}$	A_{24}	-	A_{36}	-		

Source: Author's production.

Decreasing the gap between connections costs and the magnitude of the cost of fully rigid connections, the optimization process finds it economically feasible to provide structural stiffness with more semi-rigid connections. Connections appear in the region near the constrained node 9, and in the last two studies there are connections directly connected to this node.

The study with connections cost 20-30% not only has the lowest manufacturing cost and the largest number of semi-rigid connections, but also the largest number of elements with shear stresses produced by shear forces within the range of 0.5-3 MPa. This fact is directly related to the larger number of semi-rigid connections, as this results in a structure that has more bending moments and shear forces being transmitted.

With the need to perform study 20-60% again using recalculated coefficients for the quadratic variation of the connections cost, the current solution of Fig. 6.25 is different from the solution obtained in the first LCO study (Fig. 6.22). The optimization process required more iterations to converge ($593 > 392$), two more connections were added to the structure, as can be seen in Table 6.9, and the material cost is lower ($\$916 < \$927$), due to the different optimal areas shown in Table 6.13.

The study 20-30% has several cases where three or more elements have rotational stiffness connected to the same joint. Although the constructive concept is not complex, it is possible that the variation assumed for the additional connections cost does not faithfully represent the cost of the resulting connections of this study.

Based on the results obtained, it can be concluded that the optimization process is sensitive not only to the interval adopted for the cost of connections, but also to the quadratic variation that is imposed. Therefore, in practical applications, these two requirements must be well defined beforehand, in order for the process to analyze and optimize a given structure with cost information that faithfully reproduces actual manufacturing costs that will be faced.

6.2.3 Mobile crane

The mobile crane presented in Fig. 6.28 was firstly investigated by Apostol *et. al.* (1995) and then by researchers such as Sergeyev and Pedersen (1996) and Sergeyev and Mróz (2000). The structure has 26 elements, 18 nodes, all the elements have circular thin-wall cross-sections with constant thickness of 8 mm, initial cross-section areas $A = 30.10^3\ mm^2$ (except the six columns which have $A = 10.10^3\ mm^2$), Young's modulus $E = 200.10^3\ MPa$, shear modulus $G = 80\ MPa$, yield strength $\sigma_e = 147\ MPa$ and specific mass $\rho = 7.799E^{-6}\ kg/mm^3$. The structure is clamped in the six nodes indicated in Fig. 6.28. The connectivity is presented in Table 6.14. Whit this initial data, the structure has approximately $18448\ kg$ of mass.

The optimization processes of this case study will take into account the multiple load cases presented in Fig. 6.29 and Table 6.15. A vertical load F_1 in the negative z-direction, where all the top nodes are loaded, is combined with four lateral loads of equal magnitudes. The self-weight is not considered.

Figure 6.28 – Mobile crane of Apostol *et. al.* (1995).

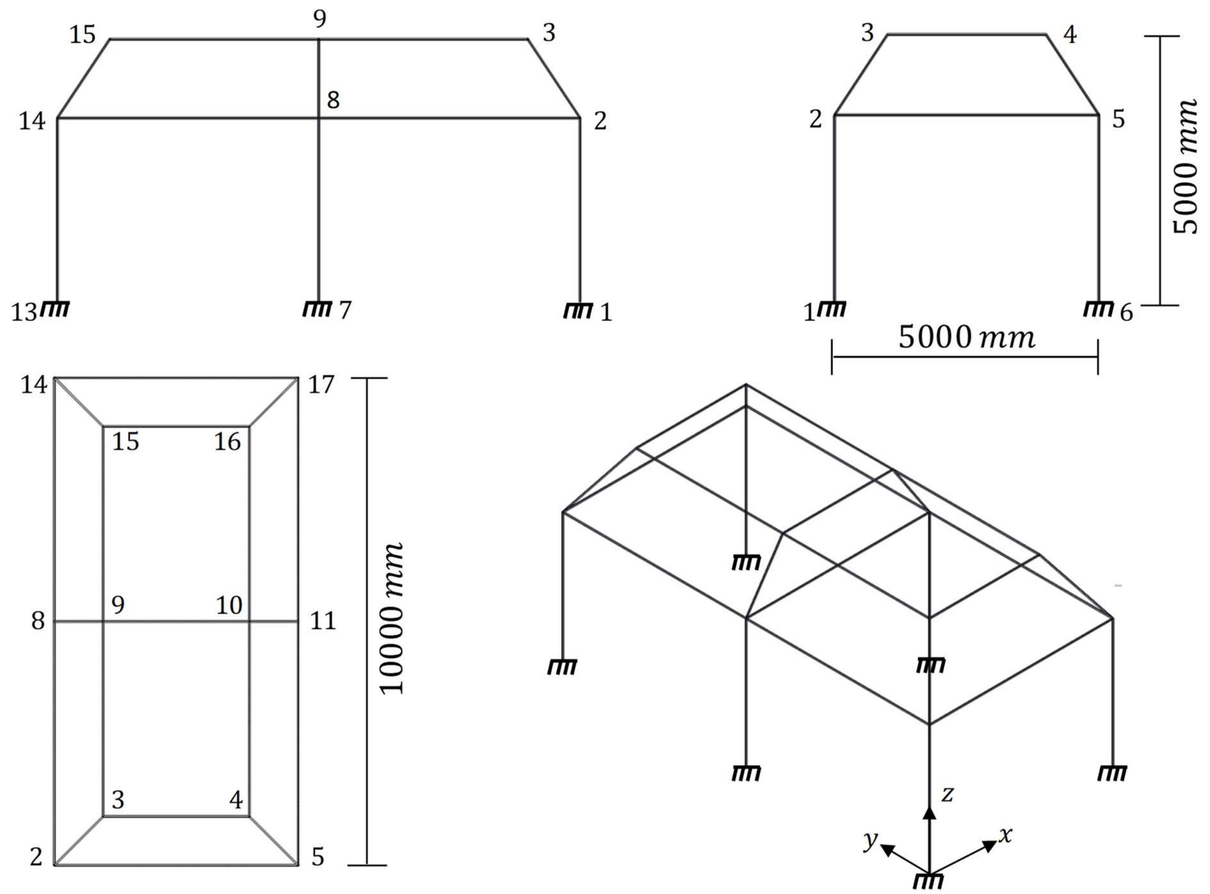

Source: Author's production based on Sergeyev and Pedersen (1996).

Table 6.14 – Connectivity of the structure.

Elements	**1**	**2**	**3**	**4**	**5**	**6**	**7**	**8**	**9**	**10**	**11**	**12**	**13**	**14**	**15**	**16**	**17**	**18**
Nodes	*1*	*2*	*5*	*2*	*3*	*5*	*7*	*8*	*11*	*8*	*9*	*11*	*13*	*14*	*17*	*14*	*15*	*17*
	2	*5*	*6*	*3*	*4*	*4*	*8*	*11*	*12*	*9*	*10*	*10*	*14*	*17*	*18*	*15*	*16*	*16*

Elements	**19**	**20**	**21**	**22**	**23**	**24**	**25**	**26**
Nodes	*2*	*8*	*3*	*9*	*3*	*11*	*4*	*10*
	8	*14*	*9*	*15*	*11*	*17*	*10*	*16*

Source: Author's production.

Table 6.15 – Multiple load cases.

Load cases	**Load condition**
1	$F_1 + F_2$
2	$F_1 + F_3$
3	$F_1 + F_4$
4	$F_1 + F_5$

Source: Author's production.

Figure 6.29 – Multiple load cases.

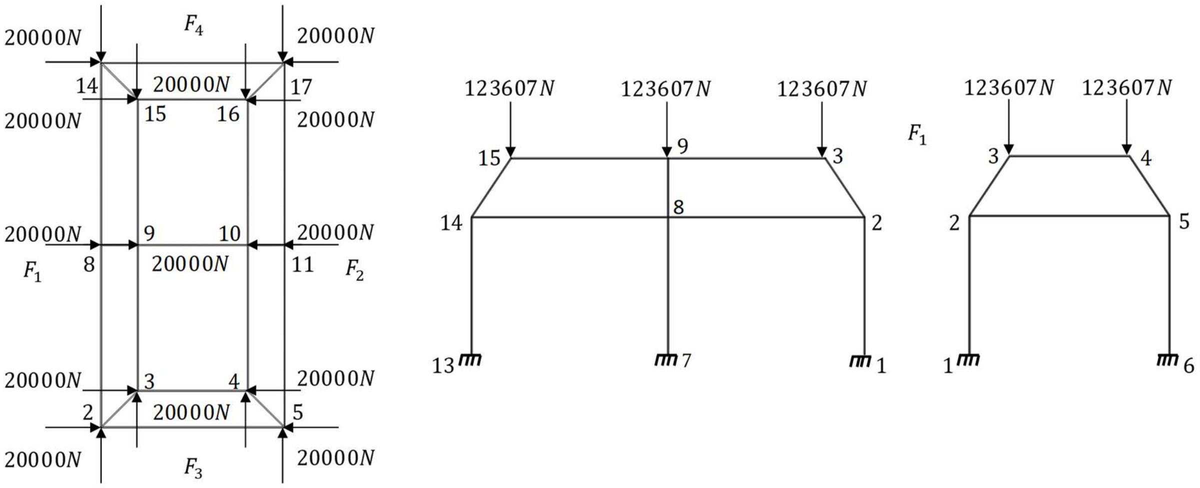

Source: Author's production based on Sergeyev and Pedersen (1996).

As shown in Fig. 6.30, the following design constraints are applied:

- von Mises stress constraints;
- Displacements constraints on the displacements at the x and y direction of the nodes 2, 3, 4, 5, 8, 9, 10, 11, 14, 15, 16 and 17 ($5\ mm$) and at the z-direction of the nodes 3, 4, 9, 10, 15 and 16 ($5\ mm$);
- Minimum element length ($5\ mm$).

Figure 6.30 – Displacements constraints and design variables.

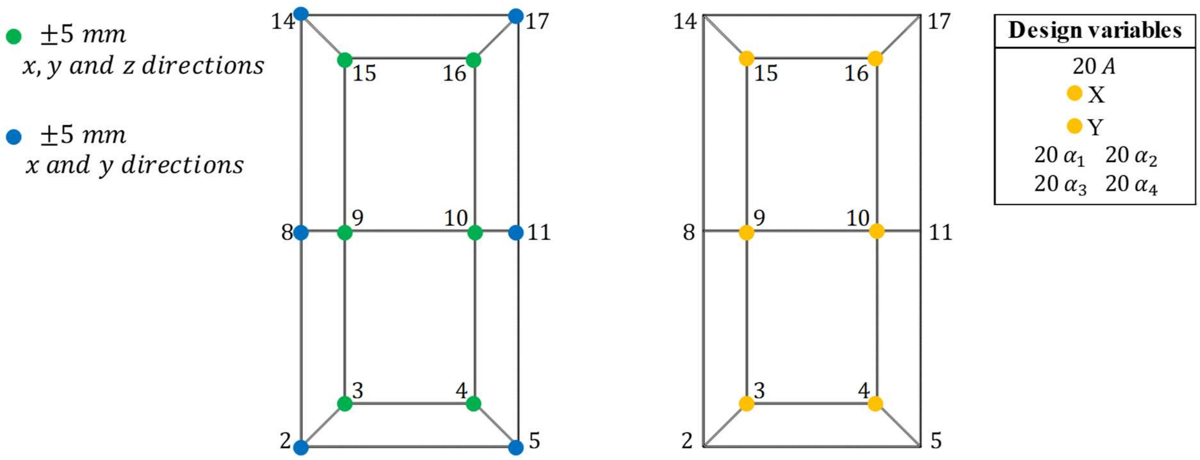

Source: Author's production.

To start, the SCO process is performed, adopting as design variables almost all the cross-section areas (except of the columns which are fixed) and 20 fixity factors $\alpha_1/\alpha_2/\alpha_3/\alpha_4$.

All connections that are design variables start with rotational stiffness of 94%. Then, adding the coordinates X and Y of the nodes 3, 4, 9, 10, 15 and 16 as design variables, the LCO is developed, allowing the comparison between these two procedures, mainly from the point of view of efficacy and computational efficiency. The design variables of areas and joint positions are visualized in Fig. 6.30.

Note that only the roof of the mobile crane is subject to optimization. The column connections are considered to be fixed fully rigid in all processes. The range and quadratic variation of the additional connections cost is the same for both studies, being 20% for pinned and 60% for fully rigid connections.

Some nodes that are loaded are free to change positions in the LCO process. Similar to the previous studies, the critical point of the three cross-section areas and its von Mises stress are determined after a sweep of 0 to 2π, with a step of 0.002π.

6.2.3.1 SCO *vs.* LCO

The optimal solutions and the elements with semi-rigid connections of the SCO and LCO processes are presented in Figs. 6.31(a-b). The topology of the structure does not change in none of the studies. The LCO has a higher time processing cost.

Since the optimization problem has several displacement constraints, both processes provide structural stiffness through various semi-rigid connections, which are shown in Tables 6.16 and 6.17. However, the LCO process requires fewer semi-rigid connections, and consequently has less connections cost, as the layout also works in favor of the global stiffness of the structure. Basically, the LCO avoids the reduction of areas in the central elements and approximates the nodes of the top of the roof, see Table 6.18, causing a concentration of stiffness in the upper center of the structure. Also, note that in both studies again occurs the case where m-elements are connected to the same joint.

Observing Figs. 6.31(a-b) from a sizing point of view, while in the SCO larger areas for the top elements of the roof are established, in the LCO process only the middle elements of the roof have larger areas. So again the LCO turns out better than SCO as it needs less material to ensure no violation of displacement constraints. Moreover, remember that the lower the cost of materials, the lower the cost of the connections. The comparison of optimized areas is shown in Table 6.19.

Table 6.16 – Data of semi-rigid connections of the SCO process.

Joint Connections	Elements	Fixity Factors			
		Node 1		Node 2	
		α_1	α_3	α_2	α_4
1 (in the column)	**16**	0.219	0.833	0.681	0.829
2 (in the column)	**10**	0.399	0.633	fully rigid	0.813
3 (in the column)	**4**	0.813	0.214	0.748	0.801
4	**16**	0.219	0.833	0.681	0.829
	17	fully rigid	fully rigid	fully rigid	fully rigid
	22	fully rigid	fully rigid	fully rigid	fully rigid
5	**10**	0.399	0.633	fully rigid	0.813
	11	fully rigid	fully rigid	fully rigid	fully rigid
	21	fully rigid	fully rigid	fully rigid	fully rigid
	22	fully rigid	fully rigid	fully rigid	fully rigid
6	**4**	0.813	0.214	0.748	0.801
	5	fully rigid	fully rigid	fully rigid	fully rigid
	21	fully rigid	fully rigid	fully rigid	fully rigid
7	**17**	fully rigid	fully rigid	fully rigid	fully rigid
	18	0.823	0.157	0.830	0.742
	26	fully rigid	fully rigid	fully rigid	fully rigid
8	**11**	fully rigid	fully rigid	fully rigid	fully rigid
	12	0.605	0.477	0.802	0.875
	25	fully rigid	fully rigid	0.880	fully rigid
	26	fully rigid	fully rigid	fully rigid	fully rigid
9	**5**	fully rigid	fully rigid	fully rigid	fully rigid
	6	0.503	0.753	0.836	0.630
	25	fully rigid	fully rigid	0.880	fully rigid
10 (in the column)	**18**	0.823	0.157	0.830	0.742
11 (in the column)	**12**	0.605	0.477	0.802	0.875
12 (in the column)	**6**	0.503	0.753	0.836	0.630

Source: Author's production.

Table 6.17 – Data of semi-rigid connections of the LCO process.

Joint Connections	Elements	Fixity Factors			
		Node 1		Node 2	
		α_1	α_3	α_2	α_4
1	8	fully rigid	fully rigid	fully rigid	fully rigid
	10	fully rigid	0.437	fully rigid	0.157
2	8	fully rigid	fully rigid	fully rigid	fully rigid
	12	fully rigid	fully rigid	0.366	0.338
3	5	0.443	pinned	pinned	pinned
	10	fully rigid	0.437	fully rigid	0.157
	11	0.837	0.514	0.864	0.484
	12	fully rigid	fully rigid	0.366	0.338
	17	pinned	0.593	pinned	pinned
	21	pinned	pinned	0.144	0.562
	22	pinned	0.571	pinned	pinned

Source: Author's production.

Table 6.18 – Optimal joint positions of the LCO process.

Node	3	4	9	10	15	16
X [mm]	2499	2505	2505	2505	2505	2505
Y [mm]	4925	4929	5000	4998	5092	5082

Source: Author's production.

Table 6.19 – Comparison of optimal areas related to the SCO and LCO processes. The higher cross-section areas are highlighted.

10^6mm^2	SCO	LCO	10^6mm^2	SCO	LCO	10^6mm^2	SCO	LCO
A_2	$0.96E^{-4}$	$0.48E^{-3}$	A_{12}	$0.12E^{-1}$	$0.81E^{-2}$	A_{21}	$0.61E^{-2}$	$0.38E^{-2}$
A_4	$0.11E^{-1}$	$0.12E^{-2}$	A_{14}	$0.40E^{-4}$	$0.47E^{-3}$	A_{22}	$0.61E^{-2}$	$0.41E^{-2}$
A_5	$0.78E^{-2}$	$0.13E^{-2}$	A_{16}	$0.11E^{-1}$	$0.12E^{-2}$	A_{23}	$0.40E^{-4}$	$0.71E^{-3}$
A_6	$0.11E^{-1}$	$0.12E^{-2}$	A_{17}	$0.77E^{-2}$	$0.14E^{-2}$	A_{24}	$0.40E^{-4}$	$0.65E^{-3}$
A_8	$0.36E^{-3}$	$0.12E^{-1}$	A_{18}	$0.11E^{-1}$	$0.12E^{-2}$	A_{25}	$0.63E^{-2}$	$0.48E^{-4}$
A_{10}	$0.11E^{-1}$	$0.58E^{-2}$	A_{19}	$0.40E^{-4}$	$0.89E^{-3}$	A_{26}	$0.60E^{-2}$	$0.14E^{-3}$
A_{11}	$0.72E^{-2}$	$0.64E^{-2}$	A_{20}	$0.59E^{-4}$	$0.84E^{-3}$			

Source: Author's production.

Figure 6.31 – Optimal solutions and semi-rigid connections of the (a) SCO and (b) LCO processes.

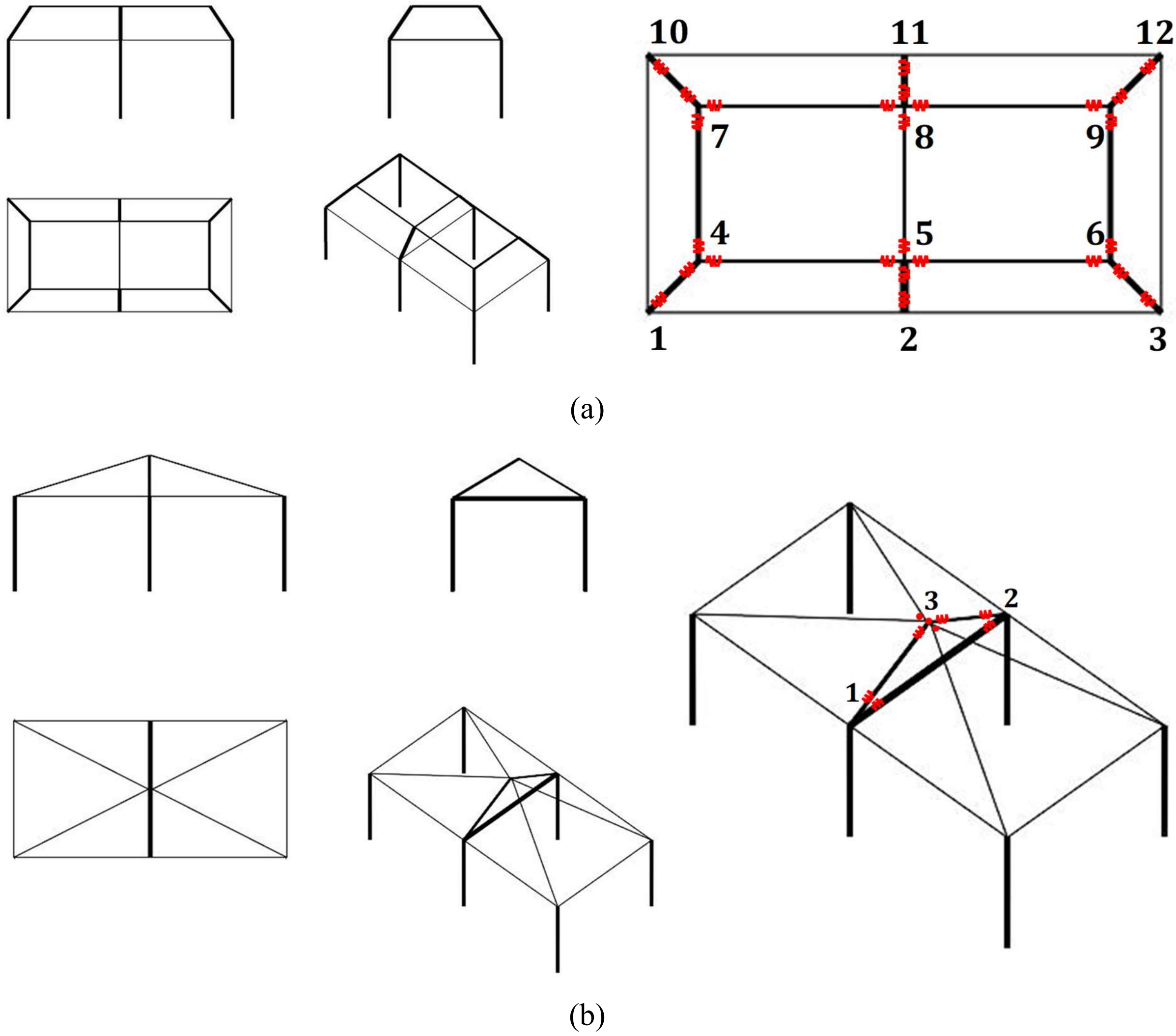

Source: Author's production.

According to the results presented in Table 6.20, the optimal solution of LCO has larger manufacturing cost savings (31.3%), with 30.2% less material cost and 33.2% less connections cost. The convergence diagrams of both studies are depicted in Fig. 6.32(a). While in the SCO there are no fully stressed elements and only eight active displacement constraints, the LCO has some stressed elements since iteration 200 (see Fig. 6.32(b)), eighteen active (and several near activation) displacement constraints and one active minimum length constraint (and others six elements very close to activation). Therefore, the displacement constraints are stronger than the stress constraints.

Despite the higher number of iterations in LCO ($348 > 266$), the optimal solution is found after iteration 210 but took time to converge due to the a delay in the stabilization of the design variables.

Figure 6.32 – Results about the convergence diagram of the SCO and LCO studies for (a) manufacturing cost and (b) diagram of the most stressed element at each iteration.

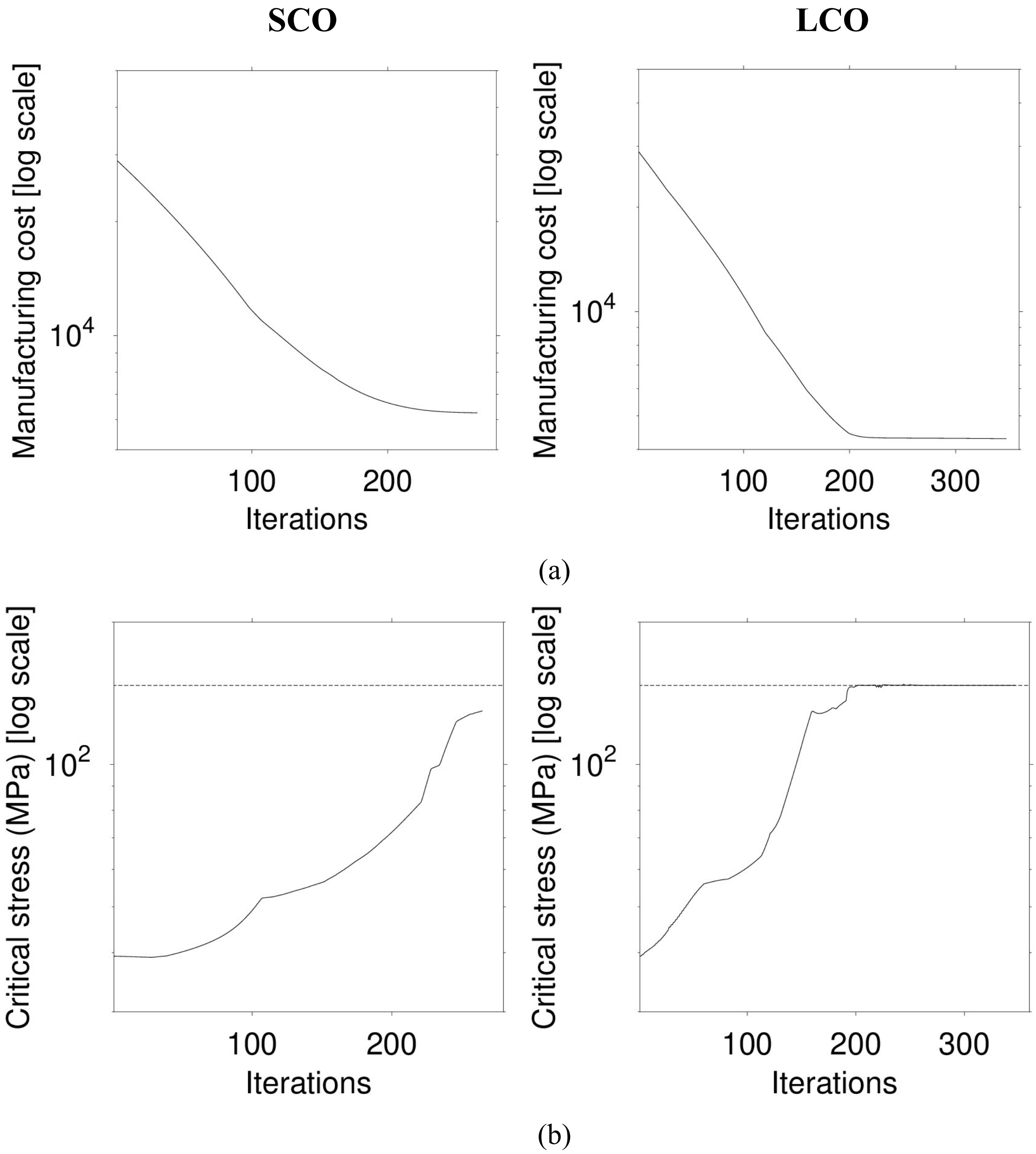

Source: Author’s production.

Table 6.20 – Comparison between the costs of the optimal solutions.

	Optimization processes	
Costs (\$)	**SCO**	**LCO**
Manufacturing cost ($\boldsymbol{W}$)	6254	4297
Material cost ($\boldsymbol{W_1}$)	4036	2816
Connections cost ($\boldsymbol{W_2}$)	2218	1481

Source: Author's production.

According to Fig. 6.33, possibly the optimal solution would be the disappearance of all the seven short elements (5, 11, 17, 21, 22, 25 and 26) and the joining of the adjacent elements at the center of the structure. Analyzing from a practical point of view, it would also be the right decision for the manufacture and assembly of the structure. Also, for this reason, a unique connection is assumed, as can be seen in Table 6.17.

Figure 6.33 – Short elements at the top of the roof.

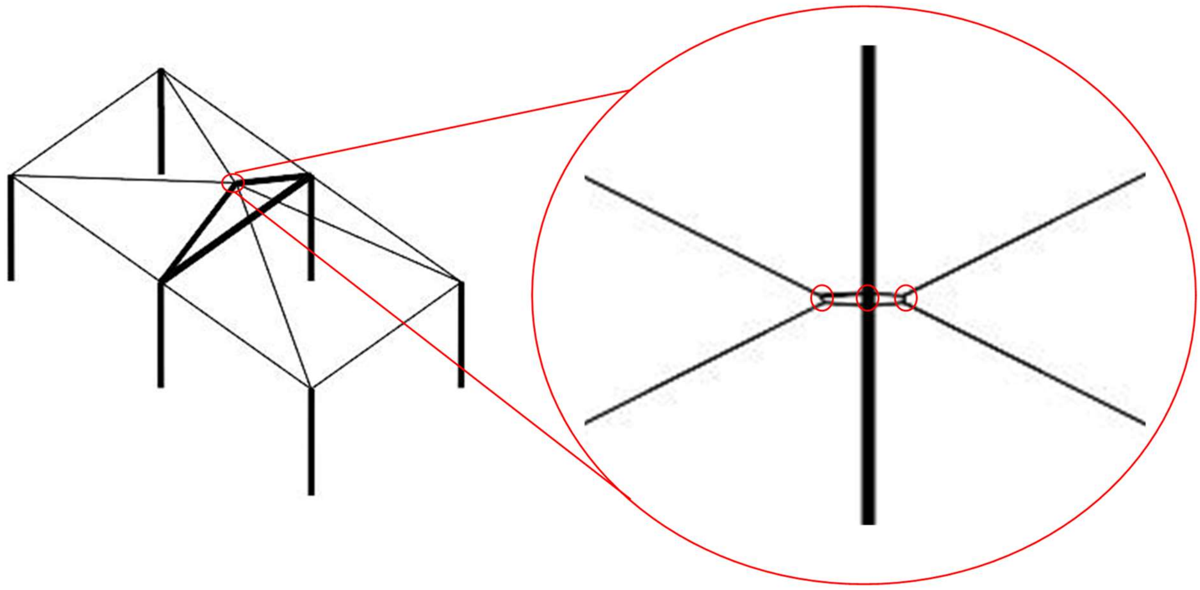

Source: Author's production.

The short elements are practically invisible, with lengths between 5-90 mm, but have cross-section areas of great magnitude (see Table 6.19) and have shear stresses within the range of 10-75 MPa. Although the construction interpretation of the solution can be the removal of these elements, they do not cease to exist in the final topology and it is precisely the elements that are fully stressed, i.e. the failure criterion is useful for the layout optimization process. If the designer choses this final layout, without topology modifications, these elements are well sized, since the shear stresses produced by the resulting shear forces were not neglected and, as we can see, have higher magnitudes.

Unlike previous studies, the optimal solution of the LCO has several elements that have shear stresses τ_{V_R} in the order of 0.1-0.5 MPa, certainly due to the appearance of a considerable amount of more rigid connections. The element 9 (a column), for example, in the load case 1 and in the middle of its length, has a shear stress τ_{V_R} of $0.5\ MPa$, while its normal bending stress σ_{M_R} is $5.0\ MPa$. Note that the magnitudes are not high, but the difference between them is not significant enough to neglect the effect of the shear forces.

In this same element and load case, but in the cross-section $\tilde{x} = L_{(k=3)}$, the shear stress τ_{V_R} remains $0.5\ MPa$, the normal bending stress σ_{M_R} is $-89.0\ MPa$, but the calculated equivalent stress is $129\ MPa$. Therefore, note that this section is almost fully stressed. Although smaller compared to the normal stress of the bending moments, the shear stress τ_{V_R} almost had the potential to cause catastrophic failure if neglected by the calculations.

Confronting the results obtained by SCO and LCO processes, it was concluded that the layout change (joint positions) was an additional tool to provide structural stiffness in the three cartesian axes and therefore it was possible to reduce not only the magnitude of the cross-section areas, but also the quantity and levels of semi-rigid connections. Consequently, greater reduction of manufacturing cost was achieved in the LCO process and therefore, for this structural problem, the LCO process proved to be better than the SCO process. The only misfortune is the longer processing time.

Chapter 7

Conclusions

The introduction of semi-rigid connections in the 3D frame element allowed more realistic prediction and evaluation of the mechanical behavior that a given steel tubular space frame will present in practice. The optimal fixity factors presented in each case study should be treated as a good approximation of the degree of rotational stiffness that each connection on the joints should present at each bending plane. In other words, not necessarily an optimal solution, but a good decision for the structural design.

In the context of structural optimization, the addition of connections within FEA and objective function is a useful tool to make the iterative process able to more accurately predict manufacturing costs and minimize them. Moreover, the first case study of Chapter 6 demonstrates that it is possible to find more economically feasible solutions than solutions given by a process that considers the original formulation for fully rigid frames.

With displacement constraints, the proposed optimization process has the ability to provide optimal solutions that add the best cost-benefit ratio between manufacturing cost and stiffness, providing stiffness only to the required locations and avoiding the expense of unnecessary more rigid connections.

From a numerical point of view, since each element has four fixity factors associated with the rotational stiffness of the two connections, the increase in the amount of design variables is considerable high, causing the computational cost to increase due to the need to compute a greater amount of derivatives. Also, this makes each LP process difficult to solve as it increases the size of the problem, and increases the possibility of finding local optimal solutions or even falling in unfeasible regions. It is noteworthy that these characteristics were observed not only in the small and medium size studies that were presented, but also with one large study that was omitted. This large structure required a lot of processing time not only in the derivatives, but also in the LP solver, and has fallen countless times in unfeasible regions.

Regarding the comparison between the SCO and LCO processes, despite the higher computational processing cost, the LCO seems to be a better option, making it possible to find more economical optimal solutions with not very complex layout. Modifications in joint positions make it possible to improve the distribution of internal forces and, consequently, better sizing and manufacturing cost savings.

Based on the results obtained in all the case studies, it is noticeable that connections between two or more non-coplanar elements in the same joint can occur in optimal solutions. This may be one of the reasons for not finding registered researches (to the author's knowledge) that address this characteristic. Recent research focuses on optimization processes with experimentally characterized discrete connections. Therefore, it is up to future research to develop experimental studies of some constructive concepts reached in the optimal solutions, according to the optimal fixity factors. Additionally, it is noteworthy that maybe the ranges of the connections cost assumed in the case studies are not consistent with the reality that would be faced in these connections manufacturing. The formulation assumed for the range of connections cost is based on research that considered simpler connections, different structural profiles and structures of the construction sector. In automotive structures, for example, the cost of a fully rigid connection may be less than a pinned connection.

Considering that steel tubular space frames are regularly employed in engineering practice, the formulated failure criterion was useful as it is proven that the proposed optimization problem can have fixed small elements or lead to the appearance of moderately short elements, during the optimization process or even in the optimal solution, that have non-negligible shear stresses produced by shear forces.

Another noticeable fact during the development of the case studies was the existence of different critical points, associated with the occurrence of different combinations of internal forces. However, it should be noted that the operation of the failure criterion is intrinsically dependent mainly to the existence of displacement constraints and the assumed range and quadratic variation for the additional cost of connections. If the optimization problem only imposes stress constraints and the cost of more rigid connections is very high, the tendency is for the optimization process to opt for pinned connections only. From a structural point of view, this choice is more efficient because it practically nullifies the transmission of shear forces and bending moments through the structure. Thus, the failure criterion is useful during the optimization process, but in the end the axial forces prevail and there is no need to calculate the critical point of stress and to account the shear effect, because the normal stress produced is uniform throughout the cross-section.

Not applying displacement constraints can also lead to another problem which is the excessive flexibility of the optimal structure. In addition to being mechanically undesirable, the appearance of large displacements also invalidates the mathematical model of the connections adopted and the formulation of the 3D frame element.

After the development of the case studies, it became evident that the appearance of slender elements may indeed occur, being extremely important to apply stability constraints to ensure that the optimal solutions are reliable. However, the limited time established for the conclusion of this master thesis did not allow including this type of design constraint in the scope of research. Thus, this is a limitation of this work.

Finally, based on the literature review and the contributions made, the implementation of the present research allows the development of various future works about the following aspects:

- Adapt the code to develop optimization processes within a discrete design space or with a more robust gradient-based method, to improve numerical performance;
- Carry out more investigation on the performance of the already implemented active set strategy of Pedersen and Nielsen (2003) on the design constraints;
- Investigate if the effects of shear on deflections ($\zeta_y, \zeta_z \neq 0$) can significantly influence the optimal solutions of the case studies developed;
- Implement a solver to eigenvalue and eigenvector problems to impose buckling and frequencies constraints, investigating what happens in the optimal solutions found and providing more reliable solutions regarding structural stability;
- Theoretical and numerical studies about a Heaviside continuous approximation applied to the areas and lengths of the elements, aiming to provide the development of topology optimization within the LCO process;
- Extend the 3D frame element formulation to impose torsional flexibility in $\tilde{y}\tilde{z}$ plane and add the subsequent fixity factors as design variables of the proposed optimization problem;
- Adapt the sensitivities already developed and implement the technique to enable optimization problems with linked design variables, aiming to reduce not only the number of design variables (mainly fixity factors) and the computational cost, but also to provide the possibility to look for optimal solutions with symmetrical constructive concept.

Bibliography

ABNT NBR 8800. **“Projeto de estruturas de aço e de estruturas mistas de aço e concreto de edifícios”**. Design of steel and composite structures for buildings, Brasil, 2008.

ACHTZIGER, W. **On simultaneous optimization of truss geometry and topology**. Struct. Multidisc. Optim., 33(4-5):285-304, 2007.

ALI, N. B. H. SELLAMI, M. CUTTING-DECELLE, AF. MANGIN, JC. **Multi-stage production cost optimization of semi-rigid steel frames using genetic algorithms**. Engineering Structures, Elsevier, 31:2766-2778, 2009.

ARORA, J. S. **Introduction to Optimum Design**. 3th Edition, Elsevier Inc., 2011.

ARTAR, M. DALOGLU, A. T. **Optimum weight design of steel space frames with semi-rigid connections using harmony search and genetic algorithms**. Neural Comput. & Applic., 29:1089-1100, 2018.

ASADPOURE, A. GUEST, J. K. VALDEVIT, L. **Incorporating fabrication cost into topology optimization of discrete structures and lattices**. Struct. Multidisc. Optim., Springer, 51:385-396, 2015.

BENDSØE, M. BEN-TAL, A. ZOWE, J. **Optimization methods for truss geometry and topology design**. Struct. Multidisc. Optim., 7(3):141-159, 1994.

CABRERO, J. M. BAYO, E. **Development of practical design methods for steel structures with semi-rigid connections**. Engineering Structures, Elsevier, 27:1125-1137, 2005.

CAMP, C. PEZESHK, S. CAO, G. **Optimized design of two-dimensional structures using a genetic algorithm**. Journal of Structural Engineering, Vol. 124, 5:551-559, 1998.

CARDOSO, M. R. MUÑOZ-ROJAS, P. A. CARDOSO, E. L. **Otimização topológica de estruturas tridimensionais de barras e pórticos**. Internal report, LAMEC – Laboratory of Computational Mechanics, Department of Mechanical Engineering, Santa Catarina State University, 2008.

CARNIEL, T. A. CARDOSO, M. R. MUÑOZ-ROJAS, P. A. **Otimização do layout de pórticos espaciais**. XXIX CILAMCE - Iberian Latin American Congress on Computational Methods in Engineering, 2008.

CHAN, S. L. CHUI, P. P. T. **Non-Linear Static and Cyclic Analysis of Steel Frames with Semi-Rigid Connections**. Elsevier Science Ltda, 2000.

CHANDRUPATLA, T. R. BELEGUNDU, A. D. **Introduction to Finite Elements in Engineering**. 3rd Edition, Prentice-Hall, 2002.

CHEN, W. F. **Practical Analysis for Semi-Rigid Frame Design**. World Scientific Publishing Co. Pte. Ltd., Singapore, 2000.

CHEN, W. F. KISHI, N. KOMURO, M. **Semi-Rigid Connections Handbook**. J. Ross Publishing, Inc., USA, 2011.

CHOI, K. K. KIM, N. H. **Structural Sensitivity Analysis and Optimization 1**. Mechanical Engineering Series, Springer, 1st Ed, New York, 2005.

CSÉBFALVI, A. **Optimal design of frame structures with semi-rigid joints**. Periodica Polytechnica Civil Engineering, Vol. 51, No. 1, p.9-15, 2007.

DEB, K. GULATI, S. **Design of truss-structures for minimum weight using genetic algorithms**. Finite Elements in Analysis and Design, 37:447-465, 2001.

DEL SAVIO, A. A. **Modelagem computacional de estruturas de aço com ligações semi-rígidas**. Master thesis, Department of Civil Engineering, Pontificia Catholic University of Rio de Janeiro, Rio de Janeiro, 152p., 2004.

DHATT, Gouri; TOUZOT, Gilbert. **The Finite Element Method Displayed**. Chichester: John Wiley & Sons, 1984.

DORN, W. S. GOMORY, R. E. GREENBERG, H. J. **Automatic design of optimal structures**. Journal de Mecanique 3(1):25-52, 1964.

EUROCODE 3. **Joints in Steel Construction: Moment-Resisting Joints to Eurocode 3**. The Steel Construction Institute and The British Constructional Steelwork Association Limited, Publication P398, 2013.

FARIA, F. A. C. MUÑOZ-ROJAS, P. A. **Layout and Connections Optimization of Steel Tubular Space Frames Considering Manufacturing Costs**. Internal Report, LAMEC – Laboratory of Computational Mechanics, Department of Mechanical Engineering, Santa Catarina State University, 2019.

FILHO, A. A. **Elementos Finitos: A Base da Tecnologia CAE**. São Paulo, Érica, 2000.

GHASEMI, M. DAVOODI, M. R. MOSTAFAVIAN, S. A. **Tensile Stiffness of MERO-Type Connector Regarding Bolt Tightness**. Journal of Applied Sciences, 10:724-730, 2010.

GERSTLE, K. H. **Effect of connections on frames**. J. Construct. Steel Research, 10:241-267, 1988.

GRUPO AÇOTUBO. Technical Document. Available at: <https://acotubo.com.br/>. Access: July of 2019.

HAGISHITA, T. OHSAKI, M. **Topology optimization of trusses by growing ground structure method**. Struct. Multidisc. Optim, Springer, 27:377-393, 2009.

HAIRIL MOHD, M. TAHIR, M. M. MOHD YASSIN, A. Y. **Finite element formulation for semi-rigid beam-to-column connections using potential energy approach**. Contemporary Engineering Sciences, Vol. 9, No. 8, 357-375, 2016.

HASANÇEBI, O. **Cost efficiency analyses of steel frameworks for economical design of multi-storey buildings**. Journal of Constructional Steel Research, 128:380-396, 2017.

HAVELIA, P. **A Ground Structure Method to Optimize Topology and Sizing of Steel Frame Structures to Minimize Material, Fabrication and Erection Cost**. Thesis, Department of Civil and Environmental Engineering, Stanford University, 2016.

HAYALIOGLU, M. S. DEGERTEKIN, S. O. **Minimum cost design of steel frames with semi-rigid connections and column bases via genetic optimization**. Computers and Structures Vol. 83, p.1849-1863, 2005.

HE, L. GILBERT, M. **Rationalization of trusses generated via layout optimization**. Struct. Multidisc. Optim., 52;677-694, 2015.

HERINGER, A. A. **Análise de pórticos planos com conexões semi-rígidas através da programação matemática**. Master thesis, Publication E.DM 006A/96, Department of Civil Engineering, Brasília University, Brasília, 1996.

IRLES, R; IRLES, F. **Shear-bending-torsion elastic interaction diagrams in circular steel sections**. International Journal of Solids and Structures, 38, 435-443, 2001.

JUNIOR, S. S. F. FALCÓN, G. A. S. **Dimensionamento ótimo de pórtico de aço com ligações semirrígidas utilizando elementos finitos híbridos**. Steel Structure Review (REA), Brazilian Center of Steel Construction (CBCA), Vol. 8, p. 215-234, 2019.

KARTAL, M. E. BASAGA, H. B. BAYRAKTAR, A. MUVAFIK, M. **Effects of semi-rigid connection on structural responses**. Electronic Journal of Structural Engineering, Vol.10, 22-35, 2010.

KICINGER, R. ARCISZEWSKI, T. JONG, K. D. **Evolutionary computational and structural design: a survey of the state-of-the-art**. Computers & Structures, 83(23-24): p. 1943-1978, 2005.

LEE, D. LEE, J. KIM, J. SRAROSSEK, U. **Investigation on material layouts of structural diagrid frames by using topological optimization**. KSCE Journal of Civil Engineering, 18(2):549-557, 2014.

LIVESLEY, R. K. **The automatic design of structural frames**. Q. J. Me&. Appl. Math. 9(3), 257-278, 1956.

LUI, E. M. CHEN, W. F. **Analysis and behavior of flexibly-jointed frames**. Engng. Struct., Vol. 8, April, 1986.

Math/Library 1991: **User's Manual**, IMSL Inc., 2500 City- West Boulevard, Houston TX 77042.

MAXWELL, J. C. **On reciprocal figures, frames, and diagram of forces**. Transactions of the Royal Society of Edinburgh, vol. 26, issue 01, pp. 1-40, 1870.

MCGUIRE, W. GALLAGHER, R. H. ZIEMIAN, R. D. **Matrix and Structural Analysis**. 2 ed., John Wiley & Sons, Inc., 2 ed., EUA, 2000.

MICHELL, A. G. M. MELBOURNE, M. C. E. **The limits of economy of material in frame-structures**. Philosophical Magazine Series 6, vol. 8, issue 47, pp. 589-597, 1904.

MONFORTON G. R. **Matrix analysis of frames with semi-rigid connections**. Dissertation thesis, Department of Civil Engineering, University of Windsor, Canada, 1962.

MOSES, F. ONODA, S. **Minimum weight design of structures with application to elastic grillages**. International Journal for Numerical Methods in Engineering, Vol. 1, 311-331, 1969.

MUÑOZ-ROJAS, P. A. **Optimization of Structures and Components**. Advanced Structured Materials, Volume 43, Springer, 2013.

PEDERSEN, P. **On the optimal layout of multi-purpose trusses**. Computers and Structures, Vol. 2, pp. 695–712, 1972.

PEDERSEN, P. JØRGENSEN, L. **Minimum mass design of elastic frames subjected to multiple load cases**. Computers & Structures, Vol. 18, No. 1, pp. 147-157, 1984.

PEDERSEN, N. L. NIELSEN, A. K. **Optimization of practical trusses with constraints on eigenfrequencies, displacements, stresses and buckling**. Struct. Multidisc. Optim., 25:436-445, 2003.

PINHEIRO, L. **Análises não-lineares de sistemas estruturais metálicos rotulados e semi-rígidos**. Master thesis, Department of Civil Engineering, Federal University of Ouro Preto, Minas Gerais, 245p., 2003.

PINHEIRO, L. SILVEIRA, R. A. M. **Computational procedures for nonlinear analysis of frames with semi-rigid connections**. Latin American Journal of Solids and Structures, Vol. 2, pp. 339-367, 2005.

RAO, S. S. **Engineering Optimization: Theory and Practice**. 4th Edition, John Wiley & Sons, Inc., New Jersey, 2009.

ROZVANY, G. I. N. **Shape and Layout Optimization of Structural Systems and Optimality Criteria Methods**. CISM Courses and Lectures No. 325, International Center for Mechanical Sciences, Springer, 1992.

ROZVANY, G. I. N. BENDSØE, M. P. KIRSCH, U. **Layout optimization of structures**. Appl. Mech. Rev., 48(2):41-119, 1995.

SAGIROGLU, M. AYDIN, A. C. **Design and analysis of non-linear space frames with semi-rigid connections**. Steel and Composite Structures, Vol. 18, No. 6, pp. 1405-1421, 2015.

SANTOS, A. F. **Estruturas Metálicas: Projeto e Detalhes para Fabricação**. São Paulo, McGraw-Hill, 1977.

SAKA, M. P. **Optimum design of pin-jointed steel structures with practical applications**. ASCE, Journal of Structural Engineering, Vol. 116, No. 10, 1990.

SANT'ANNA, H. M. GUILHERME, C. E. M. FONSECA, J. S. O. MUÑOZ-ROJAS, P. A. **Truss optimization in aerospace structures**. SAE Technical Paper Series, Vol. 1, 2001.

SEKULOVIC, M. SALATIC, R. **Nonlinear analysis of frames with flexible connections**. Computers and Structures, Vol. 79, pp. 1097-1107, 2001.

SERGEYEV, O. MRÓZ, Z. **Sensitivity analysis and optimal design of 3D frame structures for stress and frequency constraints**. Computers & Structures, Vol. 75, pp. 167-185, 2000.

SERGEYEV, O. PEDERSEN, P. **On design of joint positions for minimum mass 3D frames**. Structural Optimization, 11:95-101, 1996.

SHEU, C. Y. SCHMIT JR., L. A. **Minimum weight design of elastic redundant trusses under multiple static loading conditions**. AIAA Journal, ASME 12th Structures, Structural Dynamics and Materials Conference, Vol. 10, No. 2, 155-162, 1971.

SIMÕES, L. M. C. **Optimization of frames with semi-rigid connections**. Computers & Structures, Vol. 60, No. 4, pp. 531-539, 1996.

STEENHUIS, C. M. STARK, J. W. B. GRESNIGT, A. M. **Cost-effective connections**. Progress in Structural Engineering and Materials, Vol. 1, pp. 18-24, 1997.

SVED, G. GINOS, Z. **Structural optimization under multiple loading**. Int. J. Mech. Sci., Pergamon Press., Vol. 10, pp. 803-805, 1968.

TEJANI, G. G. SAVSANI, V. J. PATEL, V. K. SAVSANI, P. V. **Size, shape and topology optimization of planar and space trusses using mutation-based improved metaheuristics**. Journal of Computational Design and Engineering, 5:198-214, 2018.

TORII, A. J. LOPEZ, R. H. MIGUEL, L. F. F. **Design complexity control in truss optimization**. Struct. Multidisc. Optim., 54:289-299, 2016.

TRUONG, V. H. NGUYEN, P. C. KIM, S. E. **An efficient method for optimizing space steel frames with semi-rigid joints using practical advanced analysis and the micro-genetic algorithm**. Journal of Constructional Steel Research, 128:416-427, 2017.

TUGILIMANA, A. COELHO, R. F. THRALL, A. P. **Including global stability in truss layout optimization for the conceptual design of large-scale applications**. Struct. Multidisc. Optim., 57:1213-1232, 2018.

VANDERPLAATS, G. N. **Numerical Optimization Techniques for Engineering Design**. Vanderplaats Research & Development, Inc. Colorado Springs, 3th Edition, 1999.

VANDERPLAATS, G. N. SALAJEGHEH, E. **New approximation method for stress constraints in structural synthesis**. AIAA Journal, Vol. 27, pp. 352-358, 1989.

VIGH, L. G. DUNAI, L. **Finite element modelling and analysis of bolted joints of 3D tubular structures**. Computers and Structures, Vol. 82, pp. 2173-2187, 2004.

WILDEMANN, F. MUÑOZ-ROJAS, P. A. **Otimização de topologia/layout de treliças espaciais com restrições de tensão, deslocamentos e estabilidade local**. Academic Day – UDESC, Florianópolis, 2004.

XU, L. GRIERSON, D. E. **Computer-automated design of semi-rigid steel frameworks**. J. Struct. Eng., 119(6), p.1740-1760, 1993.

YOSHIDA, N. VANDERPLAATS, G. N. **Structural optimization using beam elements**. AAIA Journal, Vol. 26, No. 4, pp. 454-462, 1988.

Appendix A

The Iterative Process of the Structural Optimization Code

At the beginning, the algorithm performs a reading of the input data, which emcompasse the following topics:

- Primary flags to determine the desired optimization problem, i.e. define the objective function, the design constraints and the desired optimization method (another gradient-based method is available in the code), auxiliary flags which define the method for solve the linear systems and some parameters that dictate the content of the outputs;
- Structure data: mesh, mechanical and geometric properties (both fixed and initial properties) and the boundary and load conditions to be imposed in FEA;
- Information regarding the optimization problem, such as the quantity and definition of the design variables, coefficients referring to the move limits, the quadratic variation of the additional cost of connections and limit values for design and side constraints.

After the reading data, cross-sectional properties are calculated, based on the elementary thin-wall thickness and cross-section areas, and the iterative optimization process starts. It is worth mentioning that the thickness is an input data fixed during the optimization process, while the areas are update after each iteration.

Within the optimization process, the first step is to zero out all matrices and vectors, and then calculate and store certain iterative outputs. This procedure is required not only to ensure post-processing of graphical results, but also for real-time monitoring at the prompt.

Proceeding, the assembly of the global stiffness matrix is carried out. Being the local stiffness matrix of the 3D frame element given in equation (4.22), the boundary conditions and nodal loads are imposed, and displacements, internal forces and stresses are calculated by FEA.

Concentrated or uniform distributed loads on the length of the elements can be imposed as consistent nodal loads in the vector $\boldsymbol{F}$, and multiple load cases can be considered. The condition of multiple load cases is important because a structure optimized for only one load case has the disadvantage, in safety, that the optimal solution found is not optimal if a small change in the loading condition is made.

The equilibrium equation can be solved by two methods: with a LU decomposition of the original stiffness matrix and retro-replacement or using the skyline strategy proposed by Dhatt and Touzot (1984). Since the global stiffness matrix is characterized as a band matrix and is always symmetric, the skyline strategy is more efficient than the first since it solves the equilibrium equation by storing only the elements of the main diagonal and the non-null elements above the main diagonal. Thus, the upper and lower triangles are disregarded, avoiding unnecessary operations during the solution.

According to the allowable stress, geometric properties and internal forces, the failure criterion will evaluate the mechanical strength of three cross-sections (extremities and center of the elements) through the von Mises equivalent stress. The critical point of each cross-section area and its von Mises stress are determined after a sweep of 0 to 2π, with a predetermined stepsize. Therefore, in each case study, to ensure that the sweep is efficient and effective, a previous convergence analysis of the stress calculation at the critical point of the structure is developed. Thus, the stepsize with the best cost benefit between efficacy and computational cost is defined.

When multiple load cases are considered, the amount of stress constraints increases considerably (each element has three cross-section areas of stress detection). Therefore, aiming to reduce the dimension of the optimization problems which will be investigate, and consequently the computational effort in the solver, the active set strategy demonstrated in Pedersen and Nielsen (2003) is available for the minimum element length and stress constraints. These authors also used the SLP method.

Considering this strategy, the constraint is active and need to be compute only when the length and the stress of a given element and cross-section achieve a predetermined value. Thus,

$$L_i \geq \mu L_L, \tag{A.1}$$

$$f(\theta)_{i,k}{}^{LC} \geq \mu {\sigma_e}^2, \tag{A.2}$$

where μ is the parameter that defines the predetermined value. The user should be aware of the use of this strategy, since it can easily affect the iterative process of each LP problem.

To develop the iterative optimization process, the LP routine DDLPRS of the IMSL Math/Library (1991) is used to solve each standard LP problem. Therefore, it is necessary to linearize the objective and the design constraints by the linear part of the Taylor's expansion. The linearization is performed through the calculated sensitivities, using the implemented analytical expressions, properly validated by central finite differences (CFD),

$$\frac{\partial}{\partial v_{p_j}} \approx \frac{B\left(v_{p_j} + pe\right) - B\left(v_{p_j} - pe\right)}{2pe}, \qquad pe = 10^{-8}, \tag{A.3}$$

where B represents any function and pe is the perturbation factor of the CFD. To support the development of analytic expressions, a symbolic language software was used.

After the convergence of the standard LP, the convergence criteria are calculated. These criteria are given by parameters relative to the stability of the objective function and all the design variables treated. If the convergence criteria reach the tolerances initially assumed, the optimization process is finalized and the outputs for the post-processing are computed. On the other hand, if this does not happen, the design variables and the move limits are updated and the cross-sectional properties are recalculated. Then, returned to the place where the optimization was initiated to continue the iterative process.

The side constraints of the design variables are updated externally to the LP solver, by the move limits, to ensure convergence. Based on initial percentage factors for each type of design variable, entered as input data, the move limits are updated at each iteration by percentage update factors. In the specific case of joint positions as design variables, generically represented by X^*, the initial move limits also depend on the shortest absolute distance between a given X^* and the respective joint positions that, through connectivity, form elements with X^*.

The percent update factors are fixed and the update occurs as follows: if the design variable runs successively in the same direction of the search of the optimal solution, the side constraint is relaxed by multiplying the extreme values with a percentage factor greater than the unit value, to allow larger steps. Otherwise, the step is reduced with a percentage factor less than the unit value. The computational efficiency and convergence are highly sensitive to the choice of updating parameters (VANDERPLAATS, 1999).

If desirable, the code provides the option of assuming maximum and minimum values in the side constraints of the joint positions which are design variables, constraining the design space. Also, areas and fixity factors can be organized into groups of design variables through inequality constraints, imposing symmetry at the optimal solutions. In addition, the side constraints applied to the areas and the minimum length constraints of the elements avoid poor conditioning and singularity in the stiffness matrix. Physically, it ensures that the elements of the mesh do not disappear during FEA.

The structural optimization problem is stated in Chapter 5. However, providing a variety of optimization problems and methods for the next researchers of the master's program, a complement of this research work is to make possible all the items described in the flowchart of Figs. A.1(a-d), based on flags input described at the beginning of this Appendix. It is noteworthy that some items are related to previous researchers, and some were developed with the intention of providing improvements in the optimization process and optimal solutions. Topics related to topology optimization were inserted in the previous objective of this research, were properly developed and validated (mathematically) and made available. However, due to lack of time, they were removed from the current scope.

Despite the initial option of using the SLP method, it is worth mentioning that the sequential quadratic programming (SQP) developed by Schittkowski (2001) – NLPQLP – was implemented and evaluated at the first case of layout and connections optimization (frame dome), in order to decrease processing time and improve the robustness of search for optimal solutions at the optimization process. Unfortunately, the author's implementation was not intended for problems with high number of design variables, which made the subsequent application of this method unfeasible.

Figure A.1 – Available items of the code showed by sections (a), (b), (c) and (d).

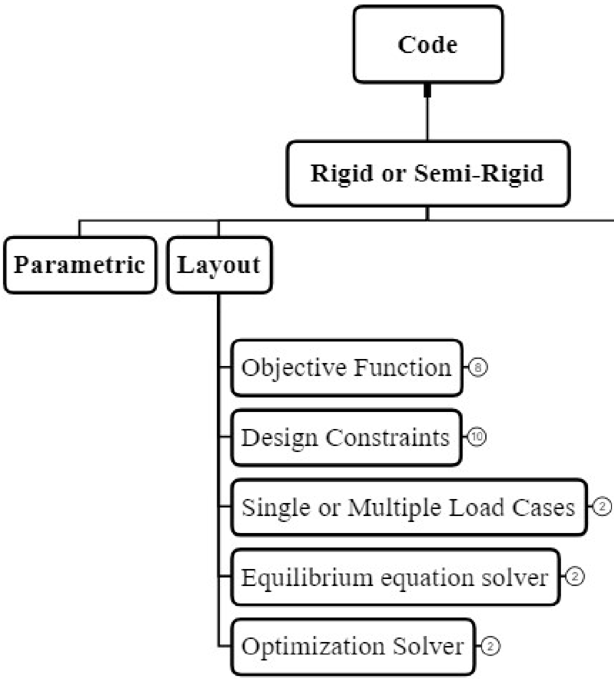

(a)

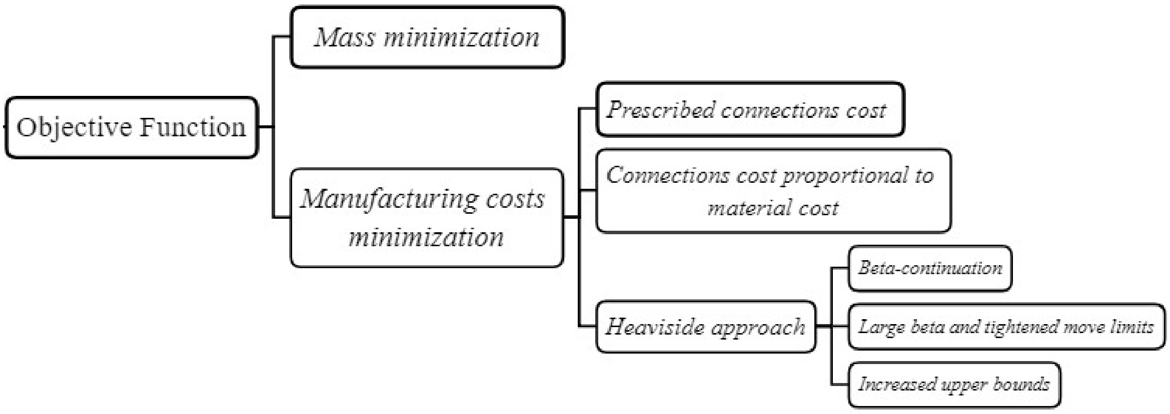

(b)

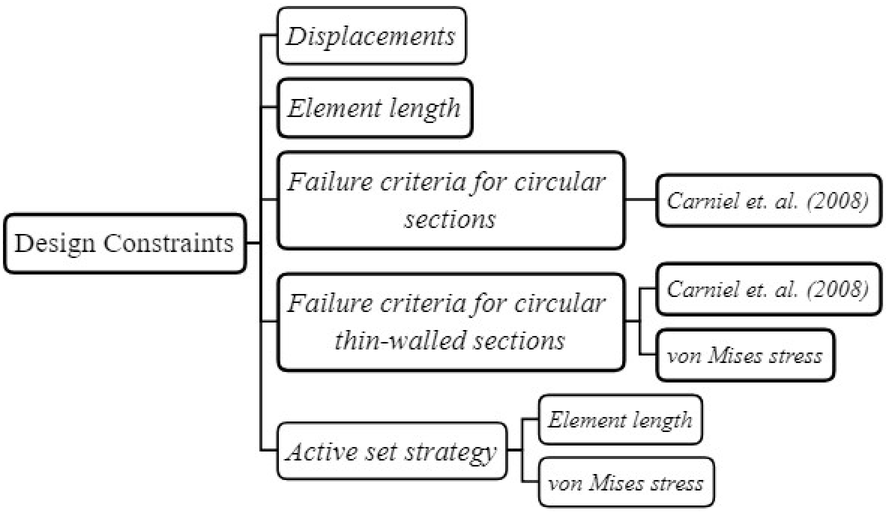

(c)

Figure A.1 (Continuation) – Available items of the code demonstrated in the sections (a), (b), (c) and (d).

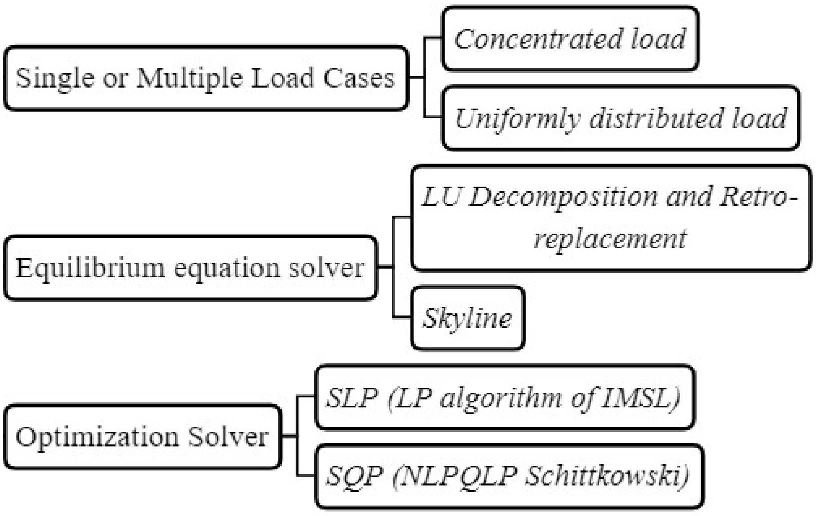

(d)

Source: Author's production.

Appendix B

The Analytical Sensitivity Analysis of the Failure Criterion with respect to the Cross-Section Areas

Analytically, the sensitivity of $f(\theta)_{i,k}$ relative to a given cross-section area can be expressed as

$$
\begin{aligned}
\frac{\partial}{\partial A_j}\left(f(\theta)_{i,k}\right) = {} & {N_{x}}_{i,k}^{\;2}\frac{\partial}{\partial A_j}\left(\frac{1}{A_i^{\,2}}\right) + \frac{1}{A_i^{\,2}}\frac{\partial}{\partial A_j}\left({N_{x}}_{i,k}^{\;2}\right) + 2\left(\frac{{N_x}_{i,k}{M_R}_{i,k}}{A_i I_i}\right)\frac{\partial}{\partial A_j}\left(\bar{c}_{i,k}\right) \\
& + 2\left(\frac{\bar{c}_{i,k}{N_x}_{i,k}{M_R}_{i,k}}{I_i}\right)\frac{\partial}{\partial A_j}\left(\frac{1}{A_i}\right) + 2\left(\frac{\bar{c}_{i,k}{N_x}_{i,k}{M_R}_{i,k}}{A_i}\right)\frac{\partial}{\partial A_j}\left(\frac{1}{I_i}\right) \\
& +2\left(\frac{\bar{c}_{i,k}{M_R}_{i,k}}{A_i I_i}\right)\frac{\partial}{\partial A_j}\left({N_x}_{i,k}\right) + 2\left(\frac{\bar{c}_{i,k}{N_x}_{i,k}}{A_i I_i}\right)\frac{\partial}{\partial A_j}\left({M_R}_{i,k}\right) + \frac{{M_R}_{i,k}^{\;2}}{I_i^{\,2}}\frac{\partial}{\partial A_j}\left(\bar{c}_{i,k}^{\,2}\right) \\
& + \bar{c}_{i,k}^{\,2}{M_R}_{i,k}^{\;2}\frac{\partial}{\partial A_j}\left(\frac{1}{I_i^{\,2}}\right) + \frac{\bar{c}_{i,k}^{\,2}}{I_i^{\,2}}\frac{\partial}{\partial A_j}\left({M_R}_{i,k}^{\;2}\right) + \frac{3}{4}\left(\frac{{M_x}_{i,k}^{\;2}}{I_i^{\,2}}\right)\frac{\partial}{\partial A_j}\left(R_i^{\,2}\right) + \frac{3}{4}\left(R_i^{\,2}{M_x}_{i,k}^{\;2}\right)\frac{\partial}{\partial A_j}\left(\frac{1}{I_i^{\,2}}\right) \\
& + \frac{3}{4}\left(\frac{R_i^{\,2}}{I_i^{\,2}}\right)\frac{\partial}{\partial A_j}\left({M_x}_{i,k}^{\;2}\right) - \frac{3}{t_i}\left(\frac{Q_i {M_x}_{i,k}{V_R^{y'}}_{i,k}}{I_i^{\,2}}\right)\frac{\partial}{\partial A_j}\left(R_i\right) \\
& - \frac{3}{t_i}\left(\frac{R_i {M_x}_{i,k}{V_R^{y'}}_{i,k}}{I_i^{\,2}}\right)\frac{\partial}{\partial A_j}\left(Q_i\right) - \frac{3}{t_i}\left(R_i Q_i {M_x}_{i,k}{V_R^{y'}}_{i,k}\right)\frac{\partial}{\partial A_j}\left(\frac{1}{I_i^{\,2}}\right) - \frac{3}{t_i}\left(\frac{R_i Q_i {V_R^{y'}}_{i,k}}{I_i^{\,2}}\right)\frac{\partial}{\partial A_j}\left({M_x}_{i,k}\right) \\
& - \frac{3}{t_i}\left(\frac{R_i Q_i {M_x}_{i,k}}{I_i^{\,2}}\right)\frac{\partial}{\partial A_j}\left({V_R^{y'}}_{i,k}\right) + \frac{3}{t_i^{\,2}}\left(\frac{{V_R^{y'}}_{i,k}^{\;2}}{I_i^{\,2}}\right)\frac{\partial}{\partial A_j}\left(Q_i^{\,2}\right) + \frac{3}{t_i^{\,2}}\left(Q_i^{\,2}{V_R^{y'}}_{i,k}^{\;2}\right)\frac{\partial}{\partial A_j}\left(\frac{1}{I_i^{\,2}}\right) \\
& + \frac{3}{t_i^{\,2}}\left(\frac{Q_i^{\,2}}{I_i^{\,2}}\right)\frac{\partial}{\partial A_j}\left({V_R^{y'}}_{i,k}^{\;2}\right).
\end{aligned}
\tag{B.1}
$$

Based on equation (B.1) and the formulation of the internal forces, explained in the Chapter 3, it is noticed that the use of the chain and product rules will be essential for some derivatives. These derivatives will be analyzed separately to present the details of each differentiation. Derivatives in relation to the six internal forces will not be presented, but can be seen in Faria and Muñoz-Rojas (2019) and follow the same procedure as Carniel *et. al.*

(2008), with some changes related to the interpolation functions and cross-sectional geometric properties.

Computation of $\frac{\partial}{\partial A_j}\left({N_{x_{i,k}}}^2\right)$ and $\frac{\partial}{\partial A_j}\left({M_{x_{i,k}}}^2\right)$

Considering p and q as

$$p = N_{x_{i,k}} \qquad and \qquad q = p^2, \tag{B.2}$$

using the chain rule

$$\frac{\partial}{\partial A_j}\left({N_{x_{i,k}}}^2\right) = \frac{dq}{dp}\frac{\partial p}{\partial A_j}, \tag{B.3}$$

and assuming that the axial internal force and its derivative are known, the sensitivity of ${N_{x_{i,k}}}^2$ is equal to

$$\frac{\partial}{\partial A_j}\left({N_{x_{i,k}}}^2\right) = 2N_{x_{i,k}}\frac{\partial}{\partial A_j}\left(N_{x_{i,k}}\right). \tag{B.4}$$

The sensitivity of ${M_{x_{i,k}}}^2$ can be defined by analogous procedure and, therefore,

$$\frac{\partial}{\partial A_j}\left({M_{x_{i,k}}}^2\right) = 2M_{x_{i,k}}\frac{\partial}{\partial A_j}\left(M_{x_{i,k}}\right). \tag{B.5}$$

Computation of $\frac{\partial}{\partial A_j}\left(M_{R_{i,k}}\right)$ and $\frac{\partial}{\partial A_j}\left({M_{R_{i,k}}}^2\right)$

Recalling that the resulting bending moment is calculated by

$$M_{R_{i,k}} = \sqrt{{M_{y_{i,k}}}^2 + {M_{z_{i,k}}}^2}, \tag{B.6}$$

and considering the chain rule

$$p = M_{y_{i,k}}{}^2 + M_{z_{i,k}}{}^2 \qquad and \qquad q = \sqrt{p}. \tag{B.7}$$

$$\frac{\partial}{\partial A_j}\left(M_{R_{i,k}}\right) = \frac{1}{2\sqrt{M_{y_{i,k}}{}^2 + M_{z_{i,k}}{}^2}} \frac{\partial}{\partial A_j}\left(M_{y_{i,k}}{}^2 + M_{z_{i,k}}{}^2\right), \tag{B.8}$$

we arrive at

$$\frac{\partial}{\partial A_j}\left(M_{R_{i,k}}\right) = \frac{1}{2M_{R_{i,k}}} \frac{\partial}{\partial A_j}\left(M_{R_{i,k}}{}^2\right), \tag{B.9}$$

that is, $\frac{\partial}{\partial A_j}\left(M_{R_{i,k}}\right)$ depends on the definition of $\frac{\partial}{\partial A_j}\left(M_{R_{i,k}}{}^2\right)$, which can be defined by the sum of two derivatives

$$\frac{\partial}{\partial A_j}\left(M_{R_{i,k}}{}^2\right) = \frac{\partial}{\partial A_j}\left(M_{y_{i,k}}{}^2\right) + \frac{\partial}{\partial A_j}\left(M_{z_{i,k}}{}^2\right). \tag{B.10}$$

Again, doing the chain rule,

$$\begin{gathered} \frac{\partial}{\partial A_j}\left(M_{y_{i,k}}{}^2\right) = 2M_{y_{i,k}} \frac{\partial}{\partial A_j}\left(M_{y_{i,k}}\right), \\ \frac{\partial}{\partial A_j}\left(M_{z_{i,k}}{}^2\right) = 2M_{z_{i,k}} \frac{\partial}{\partial A_j}\left(M_{z_{i,k}}\right), \end{gathered} \tag{B.11}$$

and returning to the previous equations (B.9) and (B.10), the sensitivities of $M_{R_{i,k}}{}^2$ and $M_{R_{i,k}}$ are given by

$$\frac{\partial}{\partial A_j}\left(M_{R_{i,k}}{}^2\right) = 2\left(M_{y_{i,k}} \frac{\partial}{\partial A_j}\left(M_{y_{i,k}}\right) + M_{z_{i,k}} \frac{\partial}{\partial A_j}\left(M_{z_{i,k}}{}^i\right)\right), \tag{B.12}$$

$$\frac{\partial}{\partial A_j}\left(M_{R_{i,k}}\right) = \frac{1}{M_{R_{i,k}}}\left(M_{y_{i,k}} \frac{\partial}{\partial A_j}\left(M_{y_{i,k}}\right) + M_{z_{i,k}} \frac{\partial}{\partial A_j}\left(M_{z_{i,k}}\right)\right). \tag{B.13}$$

Analyzing equation (B.13), it is noted that this sensitivity should be evaluated with more attention to the specific case where ${M_{R}}_{k}^{\,i}$ tends to zero, because mathematically this results in an indetermination of the type

$$\frac{\partial}{\partial A_j}\left(M_{R_{i,k}}\right) = \frac{0}{0}. \tag{B.14}$$

In order to investigate this specific case, the problem is divided into two sub-cases, which are

$$A)\;\; M_{y_{i,k}} = 0 \qquad and \qquad B)\;\; M_{z_{i,k}} = 0. \tag{B.15}$$

In both cases, replacing the respective values of null bending moments in the expression (B.13), we arrive at

$$A)\;\; \frac{\partial}{\partial A_j}\left(M_{R_{i,k}}\right) = \frac{\partial}{\partial A_j}\left(M_{z_{i,k}}\right) \qquad and \qquad B)\;\; \frac{\partial}{\partial A_j}\left(M_{R_{i,k}}\right) = \frac{\partial}{\partial A_j}\left(M_{y_{i,k}}\right), \tag{B.16}$$

and if $M_{z_{i,k}}$ tends to zero in sub-case A and $M_{y_{i,k}}$ tends to zero in sub-case B,

$$A)\;\; \frac{\partial}{\partial A_j}\left(M_{R_{i,k}}\right) = \frac{\partial}{\partial A_j}\left(M_{z_{i,k}}\right)\Big|_{M_{z_{i,k}}\to 0} \quad and \quad B)\;\; \frac{\partial}{\partial A_j}\left(M_{R_{i,k}}\right) = \frac{\partial}{\partial A_j}\left(M_{y_{i,k}}\right)\Big|_{M_{y_{i,k}}\to 0}, \tag{B.17}$$

it must comply with the following condition

$$\frac{\partial}{\partial A_j}\left(M_{R_{i,k}}\right)_{SUB-CASE\,(A)} = \frac{\partial}{\partial A_j}\left(M_{R_{i,k}}\right)_{SUB-CASE\,(B)}, \tag{B.18}$$

that is,

$$\frac{\partial}{\partial A_j}\left(M_{z_{i,k}}\right)\Big|_{M_{z_{i,k}}\to 0} = \frac{\partial}{\partial A_j}\left(M_{y_{i,k}}\right)\Big|_{M_{y_{i,k}}\to 0}. \tag{B.19}$$

By verifying equations (3.52) and (3.54), for the calculations of the bending moments $M_{z\,i,k}$ and $M_{y\,i,k}$, it is possible to note that such internal forces will be null in an element if and only if the local nodal displacements $\boldsymbol{u}_{v_{xoy}\,i}$ and $\boldsymbol{u}_{v_{xoz}\,i}$ are null because the cross-sectional area, thin-wall thickness, Young's modulus and the second derivative of the interpolation functions are parameters that do not have null values. Then, based on the previous statement,

$$\left\{\boldsymbol{u}_{v_{xoy}\,i}\right\} = 0 \;\therefore\; \left\{\frac{\partial \boldsymbol{u}_{v_{xoy}\,i}}{\partial A_j}\right\} = 0 \quad and \quad \left\{\boldsymbol{u}_{v_{xoz}\,i}\right\} = 0 \;\therefore\; \left\{\frac{\partial \boldsymbol{u}_{v_{xoz}\,i}}{\partial A_j}\right\} = 0, \tag{B.20}$$

the equality of the expression (B.18) is respected, since the derivatives of $M_{z\,i,k}$ and $M_{y\,i,k}$ will be null

$$\left.\frac{\partial}{\partial A_j}\left(M_{z\,i,k}\right)\right|_{M_{z\,i,k}\to 0} = 0 \qquad and \qquad \left.\frac{\partial}{\partial A_j}\left(M_{y\,i,k}\right)\right|_{M_{y\,i,k}\to 0} = 0, \tag{B.21}$$

and, therefore,

$$\left.\frac{\partial}{\partial A_j}\left(M_{R\,i,k}\right)\right|_{M_{R\,i,k}\to 0} = 0. \tag{B.22}$$

Computation of $\frac{\partial}{\partial A_j}\left(\boldsymbol{V_R}^{\boldsymbol{y'}}{}_{\boldsymbol{i,k}}\right)$

From the formulation of the failure criterion, it is known from equation (4.8) that

$$V_R{}^{y'}{}_{i,k} = V_{R\,i,k}\cos\left(\lambda_{i,k}\right), \tag{B.23}$$

where

$$V_{R\,i,k} = \sqrt{V_{y\,i,k}{}^2 + V_{z\,i,k}{}^2}, \qquad \lambda_{i,k} = \gamma_{V\,i,k} - \theta_{i,k} \qquad and \qquad \gamma_{V\,i,k} = \tan^{-1}\left(\frac{V_{z\,i,k}}{V_{y\,i,k}}\right). \tag{B.24}$$

Using the product rule, the derivative of $V_R{}^{y'}{}_{i,k}$ is given by

$$\frac{\partial}{\partial A_j}\left({V_R}^{y'}{}_{i,k}\right) = \cos(\lambda_{i,k})\frac{\partial}{\partial A_j}\left(V_{R_{i,k}}\right) + V_{R_{i,k}}\frac{\partial}{\partial A_j}\left(\cos(\lambda_{i,k})\right), \tag{B.25}$$

where $\frac{\partial}{\partial A_j}\left(V_{R_{i,k}}\right)$ has an analogous development to $\frac{\partial}{\partial A_j}\left(M_{R_{i,k}}\right)$ and therefore

$$\frac{\partial}{\partial A_j}\left(V_{R_{i,k}}\right) = \frac{1}{V_{R_{i,k}}}\left(V_{y_{i,k}}\frac{\partial}{\partial A_j}\left(V_{y_{i,k}}\right) + V_{z_{i,k}}\frac{\partial}{\partial A_j}\left(V_{z_{i,k}}\right)\right). \tag{B.26}$$

We need to define $\frac{\partial}{\partial A_j}\left(\cos(\lambda_{i,k})\right)$. Knowing that $\theta_{i,k}$ has no sensitivity to any design variable and making successive uses of the chain rule,

$$\begin{gathered}
p_1 = \lambda_{i,k} \qquad \mathit{and} \qquad q_1 = \cos(p_1), \\
\frac{\partial}{\partial A_j}\left(\cos(\lambda_{i,k})\right) = -\sin(\lambda_{i,k})\frac{\partial}{\partial A_j}(\lambda_{i,k}), \\
\frac{\partial}{\partial A_j}(\lambda_{i,k}) = \frac{\partial}{\partial A_j}\left(\tan^{-1}\left(\frac{V_{z_{i,k}}}{V_{y_{i,k}}}\right)\right),
\end{gathered} \tag{B.27}$$

$$\begin{gathered}
p_2 = \frac{V_{z_{i,k}}}{V_{y_{i,k}}} \qquad \mathit{and} \qquad q_2 = \tan^{-1}(p_2), \\
\frac{\partial}{\partial A_j}\left(\tan^{-1}\left(\frac{V_{z_{i,k}}}{V_{y_{i,k}}}\right)\right) = \frac{1}{\left(\frac{V_{z_{i,k}}}{V_{y_{i,k}}}\right)^2 + 1}\frac{\partial}{\partial A_j}\left(\frac{V_{z_{i,k}}}{V_{y_{i,k}}}\right), \\
\frac{\partial}{\partial A_j}\left(\frac{V_{z_{i,k}}}{V_{y_{i,k}}}\right) = \frac{1}{V_{y_{i,k}}}\frac{\partial}{\partial A_j}\left(V_{z_{i,k}}\right) + V_{z_{i,k}}\frac{\partial}{\partial A_j}\left(\frac{1}{V_{y_{i,k}}}\right),
\end{gathered} \tag{B.28}$$

$$\begin{gathered}
p_3 = V_{y_{i,k}} \qquad \mathit{and} \qquad q_3 = \frac{1}{p_3}, \\
\frac{\partial}{\partial A_j}\left(\frac{1}{V_{y_{i,k}}}\right) = -\frac{1}{{V_{y_{i,k}}}^2}\frac{\partial}{\partial A_j}\left(V_{y_{i,k}}\right),
\end{gathered} \tag{B.29}$$

replacing equation (B.29) in (B.28) and then equation (B.28) in (B.27),

$$\frac{\partial}{\partial A_j}\left(\frac{V_{z_{i,k}}}{V_{y_{i,k}}}\right)=\frac{1}{V_{y_{i,k}}}\frac{\partial}{\partial A_j}\left(V_{z_k}{}^{i}\right)-\frac{V_{z_{i,k}}}{V_{y_{i,k}}{}^{2}}\frac{\partial}{\partial A_j}\left(V_{y_{i,k}}\right), \tag{B.30}$$

$$\frac{\partial}{\partial A_j}\left(\tan^{-1}\left(\frac{V_{z_{i,k}}}{V_{y_{i,k}}}\right)\right)=\frac{1}{\left(\frac{V_{z_{i,k}}}{V_{y_{i,k}}}\right)^2+1}\left(\frac{1}{V_{y_{i,k}}}\frac{\partial}{\partial A_j}\left(V_{z_{i,k}}\right)-\frac{V_{z_{i,k}}}{V_{y_{i,k}}{}^{2}}\frac{\partial}{\partial A_j}\left(V_{y_{i,k}}\right)\right), \tag{B.31}$$

$$\frac{\partial}{\partial A_j}\left(\cos\left(\lambda_{i,k}\right)\right)=-\frac{\sin\left(\lambda_{i,k}\right)}{\left(\frac{V_{z_{i,k}}}{V_{y_{i,k}}}\right)^2+1}\left(\frac{1}{V_{y_{i,k}}}\frac{\partial}{\partial A_j}\left(V_{z_{i,k}}\right)-\frac{V_{z_{i,k}}}{V_{y_{i,k}}{}^{2}}\frac{\partial}{\partial A_j}\left(V_{y_{i,k}}\right)\right), \tag{B.32}$$

the derivative $\frac{\partial}{\partial A_j}\left(V_R{}^{y'}{}_{i,k}\right)$ is computed by

$$\begin{aligned}\frac{\partial}{\partial A_j}\left(V_R{}^{y'}{}_{i,k}\right)&=\frac{\cos\left(\lambda_{i,k}\right)}{V_{R_{i,k}}}\left(V_{y_{i,k}}\frac{\partial}{\partial A_j}\left(V_{y_{i,k}}\right)+V_{z_{i,k}}\frac{\partial}{\partial A_j}\left(V_{z_{i,k}}\right)\right)\\&-\frac{V_{R_{i,k}}\sin\left(\lambda_{i,k}\right)}{\left(\frac{V_{z_{i,k}}}{V_{y_{i,k}}}\right)^2+1}\left(\frac{1}{V_{y_{i,k}}}\frac{\partial}{\partial A_j}\left(V_{z_{i,k}}\right)-\frac{V_{z_{i,k}}}{V_{y_{i,k}}{}^{2}}\frac{\partial}{\partial A_j}\left(V_{y_{i,k}}\right)\right).\end{aligned} \tag{B.33}$$

As in equation (B.13), equation (B.33) demonstrates the same mathematical problem of division by zero in both terms of the subtraction. Then, rearranging the second term of equation (B.33)

$$\begin{aligned}\frac{\partial}{\partial A_j}\left(V_R{}^{y'}{}_{i,k}\right)&=\frac{\cos\left(\lambda_{i,k}\right)}{V_{R_{i,k}}}\left(V_{y_{i,k}}\frac{\partial}{\partial A_j}\left(V_{y_{i,k}}\right)+V_{z_{i,k}}\frac{\partial}{\partial A_j}\left(V_{z_{i,k}}\right)\right)\\&-\frac{V_{R_{i,k}}\sin\left(\lambda_{i,k}\right)}{\frac{V_{z_{i,k}}{}^{2}}{V_{y_{i,k}}{}^{2}}+\frac{V_{y_{i,k}}{}^{2}}{V_{y_{i,k}}{}^{2}}}\left(\frac{1}{V_{y_{i,k}}}\frac{\partial}{\partial A_j}\left(V_{z_{i,k}}\right)-\frac{V_{z_{i,k}}}{V_{y_{i,k}}{}^{2}}\frac{\partial}{\partial A_j}\left(V_{y_{i,k}}\right)\right),\end{aligned} \tag{B.34}$$

substituting $V_{y_{i,k}}{}^{2}+V_{z_{i,k}}{}^{2}$ for $V_{R_{i,k}}{}^{2}$ and making the product of the dividend with the inverse of the divisor

$$\frac{\partial}{\partial A_j}\left({V_R}^{y'}{}_{i,k}\right) = \frac{\cos\left(\lambda_{i,k}\right)}{V_{R\,i,k}}\left(V_{y\,i,k}\frac{\partial}{\partial A_j}\left(V_{y\,i,k}\right) + V_{z\,i,k}\frac{\partial}{\partial A_j}\left(V_{z\,i,k}\right)\right)$$
$$-\frac{{V_{y\,i,k}}^2\sin\left(\lambda_{i,k}\right)}{{V_{R\,i,k}}^2}\left(\frac{1}{V_{y\,i,k}}\frac{\partial}{\partial A_j}\left(V_{z\,i,k}\right) - \frac{V_{z\,i,k}}{{V_{y\,i,k}}^2}\frac{\partial}{\partial A_j}\left(V_{y\,i,k}\right)\right), \qquad \text{(B.35)}$$

by putting ${V_{y\,i,k}}^2$ in evidence, we arrive at the following simplification

$$\frac{\partial}{\partial A_j}\left({V_R}^{y'}{}_{i,k}\right) = \frac{\cos\left(\lambda_{i,k}\right)}{V_{R\,i,k}}\left(V_{y\,i,k}\frac{\partial}{\partial A_j}\left(V_{y\,i,k}\right) + V_{z\,i,k}\frac{\partial}{\partial A_j}\left(V_{z\,i,k}\right)\right)$$
$$-\frac{\sin\left(\lambda_{i,k}\right)}{{V_{R\,i,k}}^2}\left(V_{y\,i,k}\frac{\partial}{\partial A_j}\left(V_{z\,i,k}\right) - V_{z\,i,k}\frac{\partial}{\partial A_j}\left(V_{y\,i,k}\right)\right), \qquad \text{(B.36)}$$

and if $V_{R\,i,k}$ tends to zero, the equation continues present the same numerical error of equation (B.33). To avoid this risk, it is possible to develop more mathematical analysis.

Dividing the mathematical problem into two sub-cases A and B, where the first one encompasses $V_{y\,i,k}$ null and $V_{z\,i,k}$ tending to zero and the second one is a reciprocal case, we have

$$A)\quad \frac{\partial}{\partial A_j}\left({V_R}^{y'}{}_{i,k}\right) = \cos\left(\lambda_{i,k}\right)\frac{\partial}{\partial A_j}\left(V_{z\,i,k}\right)\Big|_{V_{z\,i,k}\to 0} + \sin\left(\lambda_{i,k}\right)\frac{\partial}{\partial A_j}\left(V_{y\,i,k}\right)\Big|_{V_{y\,i,k}=0},$$
$$B)\quad \frac{\partial}{\partial A_j}\left({V_R}^{y'}{}_{i,k}\right) = \cos\left(\lambda_{i,k}\right)\frac{\partial}{\partial A_j}\left(V_{y\,i,k}\right)\Big|_{V_{y\,i,k}\to 0} - \sin\left(\lambda_{i,k}\right)\frac{\partial}{\partial A_j}\left(V_{z\,i,k}\right)\Big|_{V_{z\,i,k}=0}. \qquad \text{(B.37)}$$

Since $\lambda_{i,k}$ is calculated by

$$\lambda_{i,k} = \tan^{-1}\left(\frac{V_{z\,i,k}}{V_{y\,i,k}}\right) - \theta_{i,k}, \qquad \text{(B.38)}$$

replacing $V_{y\,i,k}$ and $V_{z\,i,k}$ in cases A and B and using the trigonometric relations, it can be defined that

$$\begin{aligned} &A)\ \ \lambda_{i,k} = \tan^{-1}\left(\frac{V_{z_{i,k}}}{0}\right) - \theta_{i,k} \ \rightarrow \ \lambda_{i,k} = \tan^{-1}(\infty) - \theta_{i,k} \ \rightarrow \ \lambda_{i,k} = \frac{\pi}{2} - \theta_{i,k}, \\ &B)\ \ \lambda_{i,k} = \tan^{-1}\left(\frac{0}{V_{y_{i,k}}}\right) - \theta_{i,k} \ \rightarrow \ \lambda_{i,k} = \tan^{-1}(0) - \theta_{i,k} \ \rightarrow \ \lambda_{i,k} = -\theta_{i,k}. \end{aligned} \tag{B.39}$$

Substituting the expressions of $\lambda_{i,k}$ into the respective sub-cases

$$\begin{aligned} &A)\ \ \frac{\partial}{\partial A_j}\left({V_R}^{y'}{}_{i,k}\right) = \cos\left(\frac{\pi}{2} - \theta_{i,k}\right)\frac{\partial}{\partial A_j}\left(V_{z_{i,k}}\right)\Bigg|_{V_{z_{i,k}}\to 0} + \sin\left(\frac{\pi}{2} - \theta_{i,k}\right)\frac{\partial}{\partial A_j}\left(V_{y_{i,k}}\right)\Bigg|_{V_{y_{i,k}}=0}, \\ &B)\ \ \frac{\partial}{\partial A_j}\left({V_R}^{y'}{}_{i,k}\right) = -\sin\left(-\theta_{i,k}\right)\frac{\partial}{\partial A_j}\left(V_{z_{i,k}}\right)\Bigg|_{V_{z_{i,k}}=0} + \cos\left(-\theta_{i,k}\right)\frac{\partial}{\partial A_j}\left(V_{y_{i,k}}\right)\Bigg|_{V_{y_{i,k}}\to 0}, \end{aligned} \tag{B.40}$$

and identifying the following trigonometric relationships

$$\cos\left(\frac{\pi}{2} - \theta\right) = -\sin(-\theta) \quad and \quad \sin\left(\frac{\pi}{2} - \theta\right) = \cos(-\theta), \tag{B.41}$$

we notice that by going through the two paths, the expressions for the sensitivity of ${V_R}^{y'}{}_{i,k}$ when $V_{R_{i,k}}$ tends to zero are equivalent. Therefore, in this particular case, having knowledge of two more trigonometric identities

$$\cos(-\theta) = \cos(\theta) \quad and \quad -\sin(-\theta) = \sin(\theta), \tag{B.42}$$

and using the equation (B.37) of sub-case B, it is assumed that this sensitivity is given by

$$\frac{\partial}{\partial A_j}\left({V_R}^{y'}{}_{i,k}\right)\Bigg|_{V_{R_{i,k}}\to 0} = \cos\left(\theta_{i,k}\right)\frac{\partial}{\partial A_j}\left(V_{y_{i,k}}\right) + \sin\left(\theta_{i,k}\right)\frac{\partial}{\partial A_j}\left(V_{z_{i,k}}\right). \tag{B.43}$$

Moreover, it is noteworthy that the expressions of equation (B.39) are used to compute the angle $\gamma_{V_{i,k}}$ in the respective nullity occasions of $V_{y_{i,k}}$ and $V_{z_{i,k}}$. When both are null, physically the angle $\gamma_{V_{i,k}}$ does not exist, but would produce mathematical indeterminacy within the code. Therefore, through a conditional, it is considered null.

Computation of $\frac{\partial}{\partial A_j}\left({V_R^{y'}}_{i,k}^{\,2}\right)$

Since the equation for ${V_R^{y'}}_{i,k}^{\,2}$ is given by

$$ {V_R^{y'}}_{i,k}^{\,2} = {V_R}_{i,k}^{\,2}\cos^2(\lambda_{i,k}), \tag{B.44} $$

the sensitivity can be expressed by

$$ \frac{\partial}{\partial A_j}\left({V_R^{y'}}_{i,k}^{\,2}\right) = \cos^2(\lambda_{i,k})\frac{\partial}{\partial A_j}\left({V_R}_{i,k}^{\,2}\right) + {V_R}_{i,k}^{\,2}\frac{\partial}{\partial A_j}\left(\cos^2(\lambda_{i,k})\right). \tag{B.45} $$

Applying the chain rule to the two unknown derivatives,

$$ \frac{\partial}{\partial A_j}\left({V_R}_{i,k}^{\,2}\right) = 2{V_R}_{i,k}\frac{\partial}{\partial A_j}\left({V_R}_{i,k}\right), \tag{B.46} $$

$$ \frac{\partial}{\partial A_j}\left(\cos^2(\lambda_{i,k})\right) = 2\cos(\lambda_{i,k})\frac{\partial}{\partial A_j}\left(\cos(\lambda_{i,k})\right). \tag{B.47} $$

We already know $\frac{\partial}{\partial A_j}\left(\cos(\lambda_{i,k})\right)$ and $\frac{\partial}{\partial A_j}\left({V_R}_{i,k}\right)$, developed in the previous item, equations (B.26) and (B.32). Thus, the sensitivity of ${V_R^{y'}}_{i,k}^{\,2}$ is

$$ \begin{aligned} \frac{\partial}{\partial A_j}\left({V_R^{y'}}_{i,k}^{\,2}\right) = {} & 2\cos^2(\lambda_{i,k})\left({V_y}_{i,k}\frac{\partial}{\partial A_j}\left({V_y}_{i,k}\right) + {V_z}_{i,k}\frac{\partial}{\partial A_j}\left({V_z}_{i,k}\right)\right) - \\ & \frac{2{V_R}_{i,k}^{\,2}\cos(\lambda_{i,k})\sin(\lambda_{i,k})}{\left(\frac{{V_z}_{i,k}}{{V_y}_{i,k}}\right)^2 + 1}\left(\frac{1}{{V_y}_{i,k}}\frac{\partial}{\partial A_j}\left({V_z}_{i,k}\right) - \frac{{V_z}_{i,k}}{{V_y}_{i,k}^{\,2}}\frac{\partial}{\partial A_j}\left({V_y}_{i,k}\right)\right). \end{aligned} \tag{B.48} $$

To avoid mathematical indetermination, it is necessary to manipulate equation (B.48) in a similar way to that presented for equation (B.33). Therefore,

$$\frac{\partial}{\partial A_j}\left({V_R^{y'}}_{i,k}{}^2\right) = 2\cos^2(\lambda_{i,k})\left({V_y}_{i,k}\frac{\partial}{\partial A_j}\left({V_y}_{i,k}\right) + {V_z}_{i,k}\frac{\partial}{\partial A_j}\left({V_z}_{i,k}\right)\right) - \\ 2\cos(\lambda_{i,k})\sin(\lambda_{i,k})\left({V_y}_{i,k}\frac{\partial}{\partial A_j}\left({V_z}_{i,k}\right) - {V_z}_{i,k}\frac{\partial}{\partial A_j}\left({V_y}_{i,k}\right)\right), \tag{B.49}$$

and in cases where ${V_y}_{i,k}$ or ${V_z}_{i,k}$ are null, the angle $\lambda_{i,k}$ can be determined as given in equation (B.39).

Computation of $\frac{\partial}{\partial A_j}(\bar{c}_{i,k})$

The calculation of $\bar{c}_{i,k}$ is performed by

$$\bar{c}_{i,k} = R_i \sin(\varphi_{i,k}), \tag{B.50}$$

where R_i has already been informed in equation (4.11) and

$$\varphi_{i,k} = \theta_{i,k} + \frac{\pi}{2} - \gamma_{M\,i,k} \qquad and \qquad \gamma_{M\,i,k} = \tan^{-1}\left(\frac{{M_z}_{i,k}}{{M_y}_{i,k}}\right). \tag{B.51}$$

The sensitivity of $\bar{c}_{i,k}$ is conditioned in the form

$$\frac{\partial}{\partial A_j}(\bar{c}_{i,k}) = \begin{Bmatrix} \sin(\varphi_{i,k})\frac{\partial}{\partial A_j}(R_i) + R_i\frac{\partial}{\partial A_j}\left(\sin(\varphi_{i,k})\right), & if\ A_j = A_i \\ R_i\frac{\partial}{\partial A_j}\left(\sin(\varphi_{i,k})\right), & if\ A_j \neq A_i \end{Bmatrix}. \tag{B.52}$$

While the derivative of R_i is directly computed by,

$$\frac{\partial}{\partial A_j}(R_i) = \frac{\partial}{\partial A_j}\left(\frac{A_i + \pi t_i{}^2}{2\pi t_i}\right) = \frac{1}{2\pi t_i}, \tag{B.53}$$

the derivative of $\sin(\varphi_{i,k})$, by the chain rule, is given as

$$\frac{\partial}{\partial A_j}\left(\sin(\varphi_{i,k})\right) = \cos(\varphi_{i,k})\frac{\partial}{\partial A_j}(\varphi_{i,k}), \tag{B.54}$$

being that

$$\frac{\partial}{\partial A_j}(\varphi_{i,k}) = \frac{\partial}{\partial A_j}\left(-\gamma_{M\,i,k}\right) = \frac{\partial}{\partial A_j}\left(-\tan^{-1}\left(\frac{M_{z\,i,k}}{M_{y\,i,k}}\right)\right). \tag{B.55}$$

In a similar way to the development in equation (B.28) for $\frac{\partial}{\partial A_j}\left(\tan^{-1}\left(\frac{V_{z\,i,k}}{V_{y\,i,k}}\right)\right)$,

$$\frac{\partial}{\partial A_j}(\varphi_k{}^i) = -\frac{1}{\left(\frac{M_{z\,i,k}}{M_{y\,i,k}}\right)^2 + 1}\left(\frac{1}{M_{y\,i,k}}\frac{\partial}{\partial A_j}\left(M_{z\,i,k}\right) - \frac{M_{z\,i,k}}{M_{y\,i,k}{}^2}\frac{\partial}{\partial A_j}\left(M_{y\,i,k}\right)\right), \tag{B.56}$$

returning and replacing equation (B.56) in (B.54) and then equation (B.54) in (B.52), we arrive at

$$\frac{\partial}{\partial A_j}\left(\sin(\varphi_{i,k})\right) = -\frac{\cos(\varphi_{i,k})}{\left(\frac{M_{z\,i,k}}{M_{y\,i,k}}\right)^2 + 1}\left(\frac{1}{M_{y\,i,k}}\frac{\partial}{\partial A_j}\left(M_{z\,i,k}\right) - \frac{M_{z\,i,k}}{M_{y\,i,k}{}^2}\frac{\partial}{\partial A_j}\left(M_{y\,i,k}\right)\right), \tag{B.57}$$

$$\frac{\partial}{\partial A_j}(\bar{c}_{i,k}) = \left\{\begin{array}{ll} \frac{\sin(\varphi_{i,k})}{2\pi t_i} - \frac{R_i\cos(\varphi_{i,k})}{\left(\frac{M_{z\,i,k}}{M_{y\,i,k}}\right)^2 + 1}\left(\frac{1}{M_{y\,i,k}}\frac{\partial}{\partial A_j}\left(M_{z\,i,k}\right) - \frac{M_{z\,i,k}}{M_{y\,i,k}{}^2}\frac{\partial}{\partial A_j}\left(M_{y\,i,k}\right)\right), & if\ A_j = A_i \\ -\frac{R_i\cos(\varphi_{i,k})}{\left(\frac{M_{z\,i,k}}{M_{y\,i,k}}\right)^2 + 1}\left(\frac{1}{M_{y\,i,k}}\frac{\partial}{\partial A_j}\left(M_{z\,i,k}\right) - \frac{M_{z\,i,k}}{M_{y\,i,k}{}^2}\frac{\partial}{\partial A_j}\left(M_{y\,i,k}\right)\right), & if\ A_j \neq A_i \end{array}\right\}. \tag{B.58}$$

Looking at the term highlighted in a^*

$$a^* = -\frac{R_i\cos(\varphi_{i,k})}{\left(\frac{M_{z\,i,k}}{M_{y\,i,k}}\right)^2 + 1}\left(\frac{1}{M_{y\,i,k}}\frac{\partial}{\partial A_j}\left(M_{z\,i,k}\right) - \frac{M_{z\,i,k}}{M_{y\,i,k}{}^2}\frac{\partial}{\partial A_j}\left(M_{y\,i,k}\right)\right), \tag{B.59}$$

the same mathematical problem of indetermination seen in equation (B.48) is encountered.

By performing the same algebraic manipulation procedures applied in previous equations (B.34)-(B.36), the following simplification can be achieved

$$a^* = -\frac{R_i \cos(\varphi_{i,k})}{{M_{R}}_{i,k}^{\;2}}\left({M_y}_{i,k}\frac{\partial}{\partial A_j}\left({M_z}_{i,k}\right) - {M_z}_{i,k}\frac{\partial}{\partial A_j}\left({M_y}_{i,k}\right)\right), \tag{B.60}$$

where

$$\varphi_{i,k} = \theta_{i,k} - \tan^{-1}\left(\frac{{M_z}_{i,k}}{{M_y}_{i,k}}\right) + \frac{\pi}{2}. \tag{B.61}$$

If we divide the problem into sub-cases A and B, where the first one encompasses ${M_y}_{i,k}$ null and ${M_z}_{i,k}$ tending to zero and the second case is reciprocal, we have to

$$\begin{aligned} &A)\;\; a^* = R_i \cos(\varphi_{i,k})\frac{\partial}{\partial A_j}\left({M_y}_{i,k}\right)\Big|_{{M_y}_{i,k}=0} {M_z}_{i,k}\Big|_{{M_z}_{i,k}\to 0}, \\ &B)\;\; a^* = -R_i \cos(\varphi_{i,k})\frac{\partial}{\partial A_j}\left({M_z}_{i,k}\right)\Big|_{{M_z}_{i,k}=0} {M_y}_{i,k}\Big|_{{M_y}_{i,k}\to 0}, \end{aligned} \tag{B.62}$$

where

$$\begin{aligned} &A)\;\; \varphi_{i,k} = \theta_{i,k} - \tan^{-1}\left(\frac{{M_z}_{i,k}}{0}\right) + \frac{\pi}{2} \;\; \to \;\; \varphi_{i,k} = \theta_{i,k} - \tan^{-1}(\infty) + \frac{\pi}{2} \;\; \to \;\; \varphi_{i,k} = \theta_{i,k}, \\ &B)\;\; \varphi_{i,k} = \theta_{i,k} - \tan^{-1}\left(\frac{0}{{M_y}_{i,k}}\right) + \frac{\pi}{2} \;\; \to \;\; \varphi_{i,k} = \theta_{i,k} - \tan^{-1}(0) + \frac{\pi}{2} \;\; \to \;\; \varphi_{i,k} = \theta_{i,k} + \frac{\pi}{2}. \end{aligned} \tag{B.63}$$

Replacing $\varphi_{i,k}$ in the respective sub-cases,

$$\begin{aligned} &A)\;\; a^* = R_i \cos(\theta_{i,k})\frac{\partial}{\partial A_j}\left({M_y}_{i,k}\right)\Big|_{{M_y}_{i,k}=0} {M_z}_{i,k}\Big|_{{M_z}_{i,k}\to 0}, \\ &B)\;\; a^* = -R_i \cos\left(\theta_{i,k} + \frac{\pi}{2}\right)\frac{\partial}{\partial A_j}\left({M_z}_{i,k}\right)\Big|_{{M_z}_{i,k}=0} {M_y}_{i,k}\Big|_{{M_y}_{i,k}\to 0}. \end{aligned} \tag{B.64}$$

By analyzing the sub-cases A and B, due to the existence of terms $\left.M_{z_{i,k}}\right|_{M_{z_{i,k}} \to 0}$ and $\left.M_{y_{i,k}}\right|_{M_{y_{i,k}} \to 0}$, it is easy to see that in both cases a^* tends to be null. Then, since the two paths show the same result, we can assume that when $M_{R_{i,k}}$ tends to zero, the sensitivity of $\bar{c}_{i,k}$ is given by

$$\left.\frac{\partial}{\partial A_j}\left(\bar{c}_{i,k}\right)\right|_{M_{R_{i,k}} \to 0} = \left\{\begin{matrix} \dfrac{\sin\left(\varphi_{i,k}\right)}{2\pi t_i}, & if\ A_j = A_i \\ 0, & if\ A_j \neq A_i \end{matrix}\right\}, \tag{B.65}$$

being that, in this condition, the calculation of $\varphi_{i,k}$ would have mathematical indetermination due to the quotient of the term $\tan^{-1}\left(\frac{M_{z_{i,k}}}{M_{y_{i,k}}}\right)$. However, physically, if the two bending moments are null, there is no angle $\varphi_{i,k}$ and, therefore,

$$\left.\frac{\partial}{\partial A_j}\left(\bar{c}_{i,k}\right)\right|_{M_{R_{i,k}} \to 0} = \left\{\begin{matrix} \dfrac{\sin\left(\theta_{i,k} + \frac{\pi}{2}\right)}{2\pi t_i}, & if\ A_j = A_i \\ 0, & if\ A_j \neq A_i \end{matrix}\right\}. \tag{B.66}$$

In a simplified format, the generic sensitivity of $\bar{c}_{i,k}$ is computed in the form

$$\frac{\partial}{\partial A_j}\left(\bar{c}_{i,k}\right) = \left\{\begin{matrix} \dfrac{\sin\left(\varphi_{i,k}\right)}{2\pi t_i} - \dfrac{R_i \cos\left(\varphi_{i,k}\right)}{{M_{R_{i,k}}}^2}\left(M_{y_{i,k}}\dfrac{\partial}{\partial A_j}\left(M_{z_{i,k}}\right) - M_{z_{i,k}}\dfrac{\partial}{\partial A_j}\left(M_{y_{i,k}}\right)\right), & if\ A_j = A_i \\ -\dfrac{R_i \cos\left(\varphi_{i,k}\right)}{{M_{R_{i,k}}}^2}\left(M_{y_{i,k}}\dfrac{\partial}{\partial A_j}\left(M_{z_{i,k}}\right) - M_{z_{i,k}}\dfrac{\partial}{\partial A_j}\left(M_{y_{i,k}}\right)\right), & if\ A_j \neq A_i \end{matrix}\right\}. \tag{B.67}$$

Similar to the $\gamma_{V_{i,k}}$ angle computation, the expressions of equation (B.63) are used to compute the angle $\gamma_{M_{i,k}}$ in the respective nullity occasions of $M_{y_{i,k}}$ and $M_{z_{i,k}}$, and when both are null $\gamma_{M_{i,k}}$ is considered null.

Computation of $\frac{\partial}{\partial A_j}\left({\bar{c}_{i,k}}^2\right)$

Since the equation for ${\bar{c}_{i,k}}^2$ is

$$\bar{c}_{i,k}{}^2 = R_i{}^2 \sin^2(\varphi_{i,k}), \tag{B.68}$$

its sensitivity can be expressed by

$$\frac{\partial}{\partial A_j}\left(\bar{c}_{i,k}{}^2\right) = \sin^2(\varphi_{i,k}) \frac{\partial}{\partial A_j}\left(R_i{}^2\right) + R_i{}^2 \frac{\partial}{\partial A_j}\left(\sin^2(\varphi_{i,k})\right). \tag{B.69}$$

and conditioning in the form

$$\frac{\partial}{\partial A_j}\left(\bar{c}_{i,k}{}^2\right) = \left\{\begin{matrix} \sin^2(\varphi_{i,k}) \frac{\partial}{\partial A_j}\left(R_i{}^2\right) + R_i{}^2 \frac{\partial}{\partial A_j}\left(\sin^2(\varphi_{i,k})\right), & if\ A_j = A_i \\ R_i{}^2 \frac{\partial}{\partial A_j}\left(\sin^2(\varphi_{i,k})\right), & if\ A_j \neq A_i \end{matrix}\right\}. \tag{B.70}$$

While the derivative of $R_i{}^2$ is found directly,

$$\frac{\partial}{\partial A_j}\left(R_i{}^2\right) = \frac{\partial}{\partial A_j}\left(\frac{(A_i + \pi t_i{}^2)^2}{4\pi^2 t_i{}^2}\right) = \frac{A_i}{2\pi^2 t_i{}^2} + \frac{1}{2\pi} = \frac{A_i + \pi t_i{}^2}{2\pi^2 t_i{}^2}, \tag{B.71}$$

the derivative of $\sin^2(\varphi_{i,k})$, by the chain rule, is given by

$$\begin{gathered} p = \sin(\varphi_{i,k}) \qquad and \qquad q = p^2, \\ \frac{\partial}{\partial A_j}\left(\sin^2(\varphi_{i,k})\right) = 2\sin(\varphi_{i,k}) \frac{\partial}{\partial A_j}\left(\sin(\varphi_{i,k})\right). \end{gathered} \tag{B.72}$$

Recalling that the derivative of $\sin(\varphi_{i,k})$ has already been developed and presented in equation (B.57), then

$$\frac{\partial}{\partial A_j}\left(\sin^2(\varphi_{i,k})\right) = -\frac{2\sin(\varphi_{i,k})\cos(\varphi_{i,k})}{\left(\frac{M_{z_{i,k}}}{M_{y_{i,k}}}\right)^2 + 1}\left(\frac{1}{M_{y_{i,k}}} \frac{\partial}{\partial A_j}\left(M_{z_{i,k}}\right) - \frac{M_{z_{i,k}}}{M_{y_{i,k}}{}^2} \frac{\partial}{\partial A_j}\left(M_{y_{i,k}}\right)\right), \tag{B.73}$$

$$\frac{\partial}{\partial A_j}\left(\bar{c}_{i,k}{}^2\right)=\begin{Bmatrix}\frac{A_i+\pi t_i{}^2}{2\pi^2 t_i{}^2}\sin^2(\varphi_{i,k})-\frac{2R_i{}^2\sin(\varphi_{i,k})\cos(\varphi_{i,k})}{\left(\frac{M_{z_{i,k}}}{M_{y_{i,k}}}\right)^2+1}\left(\frac{1}{M_{y_{i,k}}}\frac{\partial}{\partial A_j}\left(M_{z_{i,k}}\right)-\frac{M_{z_{i,k}}}{M_{y_{i,k}}{}^2}\frac{\partial}{\partial A_j}\left(M_{y_{i,k}}\right)\right), & if\ A_j=A_i\\ -\frac{2R_i{}^2\sin(\varphi_{i,k})\cos(\varphi_{i,k})}{\left(\frac{M_{z_{i,k}}}{M_{y_{i,k}}}\right)^2+1}\left(\frac{1}{M_{y_{i,k}}}\frac{\partial}{\partial A_j}\left(M_{z_{i,k}}\right)-\frac{M_{z_{i,k}}}{M_{y_{i,k}}{}^2}\frac{\partial}{\partial A_j}\left(M_{y_{i,k}}\right)\right), & if\ A_j\neq A_i\end{Bmatrix}. \tag{B.74}$$

Observing another term highlighted in a^*

$$a^*=-\frac{2R_i{}^2\sin(\varphi_{i,k})\cos(\varphi_{i,k})}{\left(\frac{M_{z_{i,k}}}{M_{y_{i,k}}}\right)^2+1}\left(\frac{1}{M_{y_{i,k}}}\frac{\partial}{\partial A_j}\left(M_{z_{i,k}}\right)-\frac{M_{z_{i,k}}}{M_{y_{i,k}}{}^2}\frac{\partial}{\partial A_j}\left(M_{y_{i,k}}\right)\right), \tag{B.75}$$

the same adversity observed in equation (B.59) is found.

Manipulating a^*, the following simplification is defined

$$a^*=-\frac{2R_i{}^2\sin(\varphi_{i,k})\cos(\varphi_{i,k})}{M_{z_{i,k}}{}^2}\left(M_{y_{i,k}}\frac{\partial}{\partial A_j}\left(M_{z_{i,k}}\right)-M_{z_{i,k}}\frac{\partial}{\partial A_j}\left(M_{y_{i,k}}\right)\right). \tag{B.76}$$

By developing the same sub-cases A and B and the same manipulations and mathematical analyzes, the sensitivity of $\bar{c}_{i,k}{}^2$ can be computed by the following expressions

$$\left.\frac{\partial}{\partial A_j}\left(\bar{c}_{i,k}{}^2\right)\right|_{M_{R_{i,k}}\to 0}=\begin{Bmatrix}\frac{A_i+\pi t_i{}^2}{2\pi^2 t_i{}^2}\sin^2\left(\theta_{i,k}+\frac{\pi}{2}\right), & if\ A_j=A_i\\ 0, & if\ A_j\neq A_i\end{Bmatrix}, \tag{B.77}$$

$$\frac{\partial}{\partial A_j}\left(\bar{c}_{i,k}{}^2\right)=\begin{Bmatrix}\frac{A_i+\pi t_i{}^2}{2\pi^2 t_i{}^2}\sin^2(\varphi_{i,k})-\frac{2R_i{}^2\sin(\varphi_{i,k})\cos(\varphi_{i,k})}{M_{R_{i,k}}{}^2}\left(M_{y_{i,k}}\frac{\partial}{\partial A_j}\left(M_{z_{i,k}}\right)-M_{z_{i,k}}\frac{\partial}{\partial A_j}\left(M_{y_{i,k}}\right)\right), & if\ A_j=A_i\\ -\frac{2R_i{}^2\sin(\varphi_{i,k})\cos(\varphi_{i,k})}{M_{R_{i,k}}{}^2}\left(M_{y_{i,k}}\frac{\partial}{\partial A_j}\left(M_{z_{i,k}}\right)-M_{z_{i,k}}\frac{\partial}{\partial A_j}\left(M_{y_{i,k}}\right)\right), & if\ A_j\neq A_i\end{Bmatrix}. \tag{B.78}$$

Computation of $\frac{\partial}{\partial A_j}\left(\frac{1}{A_i}\right)$, $\frac{\partial}{\partial A_j}\left(\frac{1}{A_i{}^2}\right)$, $\frac{\partial}{\partial A_j}\left(\frac{1}{I_i}\right)$, $\frac{\partial}{\partial A_j}\left(\frac{1}{I_i{}^2}\right)$, $\frac{\partial}{\partial A_j}(Q_i)$ and $\frac{\partial}{\partial A_j}\left(Q_i{}^2\right)$

Directly, recalling equations (4.11) for I_i, R_{m_i} and R_i, the sensitivities of the other terms viewed in equation (B.1) are presented.

$$
\begin{aligned}
\frac{\partial}{\partial A_j}\left(\frac{1}{A_i}\right) &= -\frac{1}{{A_i}^2},\\
\frac{\partial}{\partial A_j}\left(\frac{1}{{A_i}^2}\right) &= -\frac{2}{{A_i}^3},\\
\frac{\partial}{\partial A_j}\left(\frac{1}{I_i}\right) = \frac{\partial}{\partial A_j}\left(\frac{8\pi^2{t_i}^2}{{A_i}^3}\right) &= -\frac{24\pi^2{t_i}^2}{{A_i}^4},\\
\frac{\partial}{\partial A_j}\left(\frac{1}{{I_i}^2}\right) = \frac{\partial}{\partial A_j}\left(\frac{64\pi^4{t_i}^4}{{A_i}^6}\right) &= -\frac{384\pi^4{t_i}^4}{{A_i}^7},\\
\frac{\partial}{\partial A_j}(Q_i) = \frac{\partial}{\partial A_j}\left(\frac{2t_i}{3\pi}A_i\right) &= \frac{2t_i}{3\pi},\\
\frac{\partial}{\partial A_j}\left({Q_i}^2\right) = \frac{\partial}{\partial A_j}\left(\frac{4{t_i}^2}{9\pi^2}{A_i}^2\right) &= \frac{8{t_i}^2}{9\pi^2}A_i,
\end{aligned}
\tag{B.79}
$$

valid only for when $A_j = A_i$. Otherwise, such sensitivities are null.